Corneal Tissue Engineering:

New Applications for Corneal Stromal Stem Cells

Ana Rita Gonçalves de Pinho

Supervisor: Professor Julie T Daniels

Subsidiary supervisor: Mr Steve J Tuft

Institute of Ophthalmology

University College London

Thesis submitted to UCL for the degree of Doctor of Philosophy

December 2020

‘I, Ana Rita Gonçalves de Pinho confirm that the work presented in this thesis is my own. Where information has been derived from other sources, I confirm that this has been indicated in the thesis.'

ABSTRACT

The WHO estimates 10 million people in the World are blinded by corneal disease. For many conditions, transplantation of a donor cornea may restore vision. However, there is a global shortage of suitable tissue and a high risk of rejection. The potential of stem cell therapies and tissue engineering approaches to address this significant unmet clinical need was investigated.

Limbal epithelial stem cells (LESC) maintain the epithelium, the outermost layer of the cornea, and can be successfully transplanted to restore vision. However, when scarring occurs, transplantation of corneal stroma is required. Human corneal stromal stem cells (CSSC) are involved in stroma maintenance and have previously been shown to restore transparency in cloudy mouse corneas without rejection. This study investigated the development of a surgeon friendly tissue equivalent (TE) for the therapeutic delivery of CSSC and LESCs.

For the first time, human corneal rims were rendered transparent for imaging under the iDISCO protocol. CSSC were successfully isolated and characterised with mesenchymal stem cell (MSC) properties confirmed.

RAFT-TE, a potential artificial ocular surface, has been extensively investigated by our group using research grade collagen (*First Link*; not suitable for clinical use). In this thesis, a comparative study was performed to show that *Koken* collagen (Good Manufacturing Practice compliant) is a suitable replacement for research grade collagen as it did not compromise RAFT-TE properties.

Next, co-culture conditions for LESC and CSSC in RAFT-TE were optimised. First, the idea of co-delivering CSSC together with LESCS to the surface of RAFT-TE as a mixed population was trialled. This resulted in unexpected epithelial cell peeling. To overcome this challenge, CSSC were successfully cultured for the first time inside *Koken* RAFT-TE. CSSC formed cell clusters, remodelled the matrix, and migrated to the surface of the TE. It was also shown that they can be induced to differentiate towards the keratocyte lineage inside the TE.

This work highlights the importance of considering clinical manufacturing standards early in the process of development. Overall, it provides valuable insights to develop personalised autologous therapies and off the shelf allogeneic strategies for restoring vision in patients with corneal blindness.

IMPACT STATEMENT

The cornea, on the front surface of the eye, is our window to the World. The maintenance of its transparency is crucial for vision. However, corneal transparency can be compromised by several disorders and injuries. For many conditions, transplantation of a donor cornea may restore vision for up to 5 years. However, there is a global shortage of suitable donor tissue. The WHO estimates 10 million people in the world are blinded by corneal disease and 1.5 million new cases occur annually. Stem cells and tissue engineering approaches have the power to address this unmet clinical need.

This project delves into the validation of a protocol to develop surgeon friendly tissue equivalent (TE) for the therapeutic delivery of CSSC for ocular surface reconstruction aiming to alleviate blindness worldwide by providing an alternative to donor tissue transplants. An adapted version of this therapy has been funded to proceed to clinical trials for partial thickness lamellar corneal transplantation and is now under validation in the Cells for Sight ATMP manufacturing facility.

This research has the potential to develop personalised autologous therapies and off the shelf allogeneic strategies to restore vision in patients with corneal blindness. Additionally, our experimental approach also provides valuable data to the research community regarding the interactions of stem cell populations with biomimetic materials, which could also be translated into other applications.

During my PhD I had the opportunity to raise awareness of corneal blindness, corneal donation shortage, and the potential of novel therapies to tackle this unmet clinical need. This was possible through the participation in national and international events with different audiences. A selection of the work contained in this thesis has been presented at academic conferences in the UK, Japan, and Germany, as well as at the Houses of Parliament to MPs as part of the STEM for Britain poster competition. Furthermore, this work has also been the foundation for public and patient engagement and scientific outreach events. As title of example, this includes participation both at Pint of Science festival Portugal & UK, foundation year talks, school events (Native Scientist), and science festivals (See Science and Cheltenham).

I have also developed a special interest in projects that pilot innovative processes to take patients views and concerns into account. The ‘Eating for Eye Health’ project (2016 NCCPE Engage award), for example, engaged patients suffering from dry age-related macular degeneration through a focus group and a community cookery day where patients had the opportunity to exchange insights with clinicians on how diet and nutrition can impact their eye health.

I have also shared the knowledge acquired during my PhD in numerous practical sessions with students from different programmes across UCL. Additionally, the Liberating the Curriculum Project was an enriching, and impactful experience that aimed at sharing patients’ perspectives on sight loss with medical students.

I believe that the collaborations and knowledge exchange moulded during this project were crucial to bridge the gap between a wide range of stakeholders. This was key not only to maximize research impact but also to support both my personal and professional growth.

ACKNOWLEDGEMENTS

I genuinely believe that more important than the destination, is the journey, and what a ride it has been! I am forever grateful to those who crossed my path and supported me along the way.

First, I want to take a moment to thank all the tissue donors, and their families, without whom this research would not have been possible. I am also very grateful to Fight for Sight and Moorfields Eye Charity for their financial support.

My appreciation goes to Prof Julie Daniels, my supervisor, for her guidance throughout this thesis and insightful feedback. I would also like to thank Mr Steve Tuft for facilitating access to donor tissue, and guidance during the upgrade process.

I thank my fellow labmates from the Cells for Sight Team, past and present, with whom I have learned a great deal about the cornea, and stem cells. A special mention goes to Alvena for introducing me to CSSC and RAFT, and to Louise, for all the discussions on RAFT mysteries.

I would also like to acknowledge the support and assistance received from Dr Ilaria di Napoli, and the LMCB team on the tissue clearing project. To the microscopy unit people – Peter, Matt and Diana – thanks for all the engaging discussions and for sharing this passion with me.

During my time at the Institute of Ophthalmology, I met wonderful people. I want to thank in particular the lunch club, and the third-floor crew.

There are not enough words to explain how important my research partner has been. To Carla, my twin, partner in crime, and good friend, a big thank you for being there when I most needed, and for being the best cell factory buddy I could ask for! Tiago, thanks for always being there when one needed cheering up – for suffering countless hours in buses from Liverpool to spend a relaxing evening with us, and saying it was all worth it!

Friends are the family we choose. To my Portuguese family in London, a big thank you. A special shout goes to my magic girls, Isabel, Laly and Virgínia. In Porto, Brno, or London, I would also like to thank Sofia for sharing so many

adventures with me. May this continue to be true! To my friends back home, and around the World, I now hope to have more time to reconnect with each of you.

Diogo, you have been part of this adventure from day one. London may have been our first home, but see how far we have come. Looking back, it is incredible how we have grown together. Thanks for believing in me. Your love, patience, care, and understanding were essential, and I will never be grateful enough for having a partner in life like you by my side.

Finally, I would like to thank my family. To my parents, Ângela & José, thanks for all the opportunities, care and love. For supporting me to follow my dreams even if that meant being apart. Mãe, Pai, obrigada por estarem sempre ao meu lado para celebrar as minhas conquistas, mas também para me apoiar nos momentos mais desafiantes. To my sister, Francisca, I'm sorry for missing out on such an important part of your life, you will always be my baby despite how grown-up you have become. Thanks for being my biggest fan, thanks for always wanting to know more about my research and being the best at reminding me how cool science is. Obrigada Manicla! Para a minha Titi Lourdinhas, a minha tia mais querida, o maior dos agradecimentos por todo o amor, carinho e preocupação.

Last but not least, to my grandfather Manuel who would always introduce me as a Dr, and with whom I would have long conversations explaining that biomedical engineers are not medics, so he could not refer to me as such. I'm about to be a Dr, not that type, but still, I'm sure you would be proud. I wish you were here to tell everyone about it!

TABLE OF CONTENTS

LIST OF FIGURES

LIST OF TABLES

ABBREVIATIONS

A

ABCB5 ATP-binding cassette, sub-family B, member 5
ABCG2 ATP-binding cassette transporter G2
ACTA α-smooth muscle actin gene
ALDH Aldehyde dehydrogenase
ALK Anterior lamellar keratoplasty
ATMPs Advanced therapy medicinal products

B

BM Basement membrane

C

C- Crypt region
CC Central cornea
CD73 Cluster of Differentiation 73
CD90 Cluster of Differentiation 90
Cdc42 Cell division control protein 42 homolog
CECM Corneal epithelial cell culture medium
CjE Conjunctival epithelium
CK Cytokeratin
COL Collagen
CSSC Corneal stromal stem cells

D

DALK Deep anterior lamellar keratoplasty
DAPI 4′,6-diamidino-2-phenylindole
DBE Dibasic ester
DCM Dichloromethane
DIC Differential interference contrast
DMEK Descemet's membrane endothelial keratoplasty
DMSO Dimethyl sulfoxide
DNA Deoxyribonucleic Acid
DSEK Descemet's stripping endothelial keratoplasty

E

ECM Extracellular matrix
EGF Epidermal growth factor
EMA European Medicines Agency
ESCs Embryonic Stem Cells
EVs Extracellular vesicles

F

FdA Fluorescein diacetate
FN Fibronectin
FNC Fibronectin-collagen
FSP Focal stromal projections

G

GAGs Glycosaminoglycans
GMP Good Manufacturing Practice

H

HAM Human amniotic membrane
hCECs Human corneal endothelial cells
HCFs Human corneal fibroblasts
HCK Human corneal keratocytes
HCl Hydrochloric acid
HD Hemidesmosomes
HEPES 4-(2-hydroxyethyl)-1-piperazineethanesulfonic acid
hLE Human limbal epithelium
hLF Human limbal fibroblasts
HPAs Hydrophilic porous absorbers
HSPGs Heparan sulphate proteoglycans
HTA Human Tissue Authority

I

iDISCO Immunolabeling-enabled three-Dimensional Imaging of Solvent-Cleared Organs
iHCE Immortalised human corneal epithelial cells
iPSCs Induced Pluripotent Stem Cells
ISCT International Society for Cellular Therapy

ITS Insulin-Transferrin-Selenium

K

KDM Keratocyte differentiation medium
KERA Keratocan

L

LAM Laminin
LC Limbal crypt-rich region
LESC Limbal epithelial stem cells
LSCD Limbal stem cell deficiency
LUM Lumican

M

MEM Minimum Essential Medium
MHRA Medicines and Healthcare products Regulatory Agency
MMPs Matrix metalloproteinases
MPC 2-methacryloyloxyethyl phosphorylcholine
MSC Mesenchymal stem cell

N

NA Numerical apertures
NaOH Sodium Hydroxide
NC- Non-crypt region
NS Neutralising solution

O

OC Organ culture
OCT Optical coherence tomography
Oct4 Octamer binding transcription factor-4
OP Optisol

P

p63 ΔNp63
PA Peptide Amphiphiles
PACT Passive Clarity Technique
PAX6 Paired box protein Pax-6
PBS Phosphate-buffered saline
PCL Poly-ε-caprolactone
PDGF Platelet-derived growth factor
PFA Paraformaldehyde
PK Penetrating keratoplasty
PLGA Poly-lactide-co-glycolide

Q

QMS Quality Management System

R

RA Risk Assessment
RAFT Real Architecture for 3D Tissues
RHC Recombinant human collagen
RI Refractive Index
RNA Ribonucleic acid
ROI Region of interest

S

SCs Stem cells
SEM Scanning electron microscopy
SLRPs Small leucine-rich proteoglycans
αSMA α-smooth muscle actin
SOP Standard Operation Procedures
Sox2 Sex determining region Y)-box 2

T

TACs Transient amplifying cells
TCP Tissue culture plastic
TE Tissue equivalent
TGF-β Transforming growth factor beta
THF Tetrahydrofuran
TSE Transmissible Spongiform Encephalopathies

W

WHO World Health Organisation

Chapter 1

1. INTRODUCTION

1.1. The human cornea

The cornea is the outermost layer of the eye, and its transparency is essential for vision. If the structure and function of the cornea are compromised, vision is at risk. This thesis considers some of these risks and how they may be mitigated through the development of advanced therapies such as tissue engineering.

1.1.1. Human eye development

Human eye development results from sequential events, multiple interactions between tissues, and occurs mainly between the 3rd and 10th week of gestation. PAX6 is the master regulator of this process and it is crucial for the development of a fully functional eye [1].

Ectoderm, neural crest cells, and mesenchyme are the three germ layers involved in eye development which lead to the formation of different structures:

- Neural tube ectoderm: retina, iris, ciliary body epithelia, optic nerve, iris smooth muscles, and part of the vitreous humour;
- Surface ectoderm: lens, corneal and conjunctival epithelium, eyelids, and lacrimal apparatus;
- Mesenchyme: all the remaining ocular structures.

The corneal endothelium develops from the surface ectoderm and the inner endothelium neural crest cells that migrate from the optic cup [1, 2].

In human embryos and fetuses, around the end of the 3rd week of gestation, two small optic grooves are formed on the sides of the forebrain. They will then

close to form optic vesicles that invaginate and form a double-layer structure, the optic cups: the choroid, that is pigmented and vascularised, and the sclera, that is known by its fibrous nature [2].

The developing corneal epithelium is only composed of two cell layers and is formed around the 6th week. This primitive epithelium is also responsible for the deposition of a primary acellular stroma and the Bowman's layer. Between the 8th and the 26th week of gestation, the corneal epithelium stratifies leading to four to five cell layers. However, adhesion complexes are only detectable from the 19th week of gestation. From this point onwards, a higher number of hemidesmosomes are distinguishable [2, 3].

1.1.2. The structure of the adult cornea

The cornea is the outermost layer of the eye. It is transparent and acts as the 'window' to the world. It is essential for the refraction of light, by allowing accurate focusing of incoming light to the retina. It also protects the eye from external factors such as mechanical and infectious threats [4, 5].

The human cornea is approximately 0.5mm thick and is composed of three main cellular layers: epithelium, stroma, and endothelium (Figure 1.1). Between the layers, there are two acellular interface membranes. The Bowman's layer, between the epithelium and the stroma, and the Descemet's membrane that lies between the stroma and endothelium.

The cornea is normally avascular and, in the healthy state, blood and lymphatic vessels do not enter the corneal stroma. This avascularity provides immune privilege to the cornea [6].

Interestingly, the corneal layers have different cell lineages. Both corneal stroma and endothelium are derived from mesenchymal cells, while the epithelium is formed from the overlying surface ectoderm [6, 7].

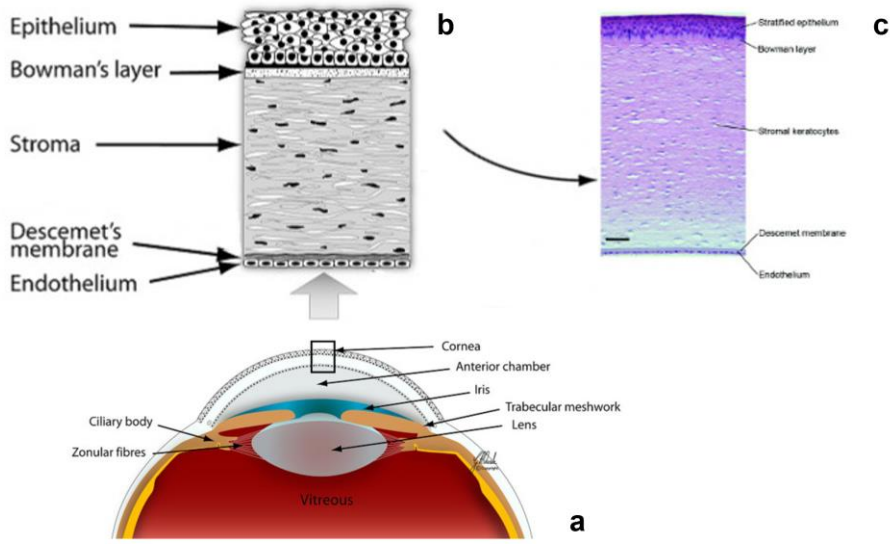

Figure 1.1 - Anatomy of the cornea. (**a**) Section of the anterior part of the eye showing the vitreous, lens, iris and the cornea; (**b**) Schematic image of human corneal layers: three cellular layers, (endothelium, stroma and epithelium), and two acellular layers (Descemet's membrane and Bowman's layer); **(c)** Histological image of a human corneal section stained with H&E. Scale bar 50 µm [4, 8].

1.1.2.1. Corneal epithelium

The corneal epithelium is the most external layer of the cornea. It consists of four to six layers of non-keratinized squamous epithelial cells. Three different cell types can be distinguished, depending on their morphology: flat, wing and basal cells (Figure 1.2) [5].

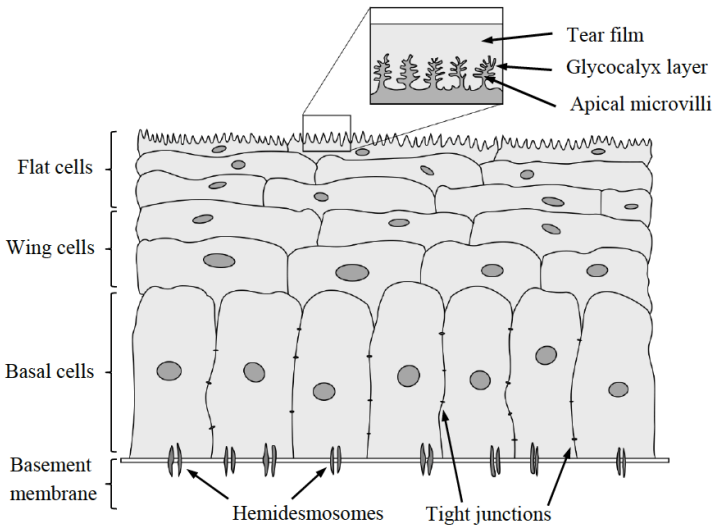

Figure 1.2 - Corneal epithelium cell types: flat or squamous cells at the surface, wing cells in between, and basal cells with columnar shape next to the basement membrane (BM) [5, 9].

The flat cells constitute two to three layers and are the most superficial cells. They are flattened and contain apical microvilli and microplicae to provide maximal surface area and attachment to the tear film. Furthermore, stable junctional complexes prevent the tear fluid from entering the intercellular space.

Just beneath the superficial layer, there are two to three layers of wing cells. These cells are not as flat and polygonal as the surface cells, but they possess similar tight junction structures.

The innermost layer consists of single 20μm tall columnar epithelial cells. These cells are responsible for renewing the epithelium by giving origin to the cells of the most superficial cell layers [5]. The basal cells are tightly attached to the epithelial basement membrane through hemidesmosomes, anchoring fibrils and filaments that create a strong complex with the stroma.

The epithelial basement membrane is primarily composed of collagen IV and several laminin isoforms [10]. Integrins are predominantly expressed in the basal epithelial layer where cells come into contact with the basement membrane. They mediate attachment to matrix proteins in the basement membrane via focal adhesions [61]. Laminins are principally responsible for the basement membrane assembly by interacting with the collagen networks [7].

1.1.2.2. Corneal stroma

The stroma is the thickest layer of the cornea (80-90% of the total depth). It is composed of dense and packed, but extremely organised, collagen fibrils and proteoglycans [11]. The arrangement of the collagen dictates the optical and tensile properties of the cornea and is critical to maintaining its transparency and mechanical stability (shape and curvature) [12].

The collagen fibrils comprise a mixture of collagen types I and V. The diameter of the fibrils varies from species to species, and in humans, it is between 25-30nm. Parallel homogeneous fibrils form a lamella [11].

The human cornea has about 200 flattened lamellae superimposed one on top of the other (Figure 1.3) [5, 13]. There is a displacement angle between each lamella, that leads to an orthogonal lattice pattern with varying spacing

between them. The space between the lamellae is higher in the central cornea and tighter closer to the limbus. The spacing is regulated by the matrix produced by a stromal cell type called keratocytes. This matrix is rich in proteoglycans such as keratocan, lumican, decorin and mimecan, and it is essential for corneal transparency [13].

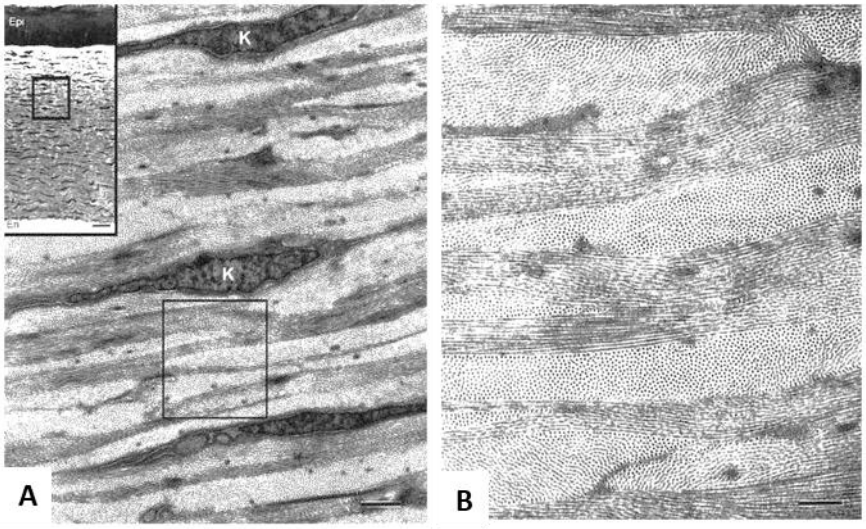

Figure 1.3 - Transmission electron micrographs of the cornea stroma structure. **(A)** Aligned collagen fibrils organised into lamellae and containing keratocytes (K). **(B)** High magnification of image A showing the regular packing of the fibrils in adjacent lamellae. The darker regions show the horizontal lamellae while the lighter areas highlight the spots of cross section of the fibrils that are perpendicularly orientated to the cut [11].

Keratocytes are quiescent cells that populate the stroma. They are found in higher density in the anterior compared to the posterior stroma, sitting in between the lamella, as shown in Figure 1.3. They maintain the stromal homeostasis by synthesising collagen and glycosaminoglycans, as well as matrix metalloproteinases (MMPs). Together with the organised extracellular matrix (ECM), the dendritic morphology and the crystalline proteins in the keratocyte cytoplasm reduce light scattering [14]. Keratocytes also express small leucine-rich proteoglycans (SLRPs) such as keratocan and lumican, and corneal crystallins such as aldehyde dehydrogenases 1A1 and 3A1 (ALDH1A1 and ALDH3A1, respectively) [15-17]. CD34 has previously been described as a keratocyte marker [18]. However, studies show that it can be lost under tissue culture conditions [19].

1.1.2.3. Corneal endothelium

The corneal endothelium is the most posterior layer of the cornea and is separated from the corneal stroma by a basement membrane called Descemet's membrane. It is formed by a single layer of hexagonal cells connected by tight junctions, usually described as having a honeycomb structure appearance [8].

Since the cornea is avascular, the nutrition of the corneal layers occurs via diffusion of glucose and other solutes from the aqueous humour, across the corneal endothelium to the stroma. Another primary function of the endothelium is the maintenance of hydration levels of the stroma at around 78%, which is essential to keep corneal transparency [20, 21]. The endothelial cells transport nutrients and water to and from the stroma preventing corneal oedema and therefore maintaining optimal hydration [22].

For this transport to happen, human corneal endothelial cells express tight junction protein ZO^{-1} [23] and sodium-potassium pump enzyme $Na^{+}K^{+}$/ATPase in the native tissue which are responsible for pumping nutrients from the aqueous humour to the corneal stroma, providing nourishment to the corneal keratocytes [24].

1.1.2.4. Bowman's layer & Descemet's membrane

The Bowman's layer is located just below the epithelial basement membrane. It is formed by a thin acellular collagenous layer, which is primarily composed of condensed type I, II and V collagen fibrils [25].

The Descemet's membrane lies between the stroma and the endothelium. It is a thick basement membrane (5-10μm), rich in collagen IV and VIII [26].

1.1.3. Mechanical properties of the cornea

Corneal biomechanics depends on the biochemical and physical nature of the components and how the fibres, cells, and other components are organised into a structure.

Cornea characteristics are not constant throughout the whole tissue, varying from central to peripheral and anterior to posterior [27]. This difference depends on the interweaving of stromal lamellae in the central anterior cornea, that does not occur in the posterior part, and increases its interlamellar cohesive strength [28]. A study found that the elastic modulus, that measures the resistance of a material being deformed elastically, was almost twice as high in the anterior than in the posterior cornea [29].

The reported values for the mechanical properties of a healthy human cornea vary and depend on the acquisition method. For example, the elastic modulus ranges from 3-16MPa [30, 31], and the tensile strength, which is the maximum stress that a material can withstand while being stretched before breaking, is around 3.81 ± 0.40 MPa [32].

Recent work from Lepert *et al.* [33] used Brillouin spectro-microscopy, a technique based on the interaction of light with spontaneous acoustic phonons, to investigate the mechanical properties of human and bovine corneas *in vitro*. Their results revealed a contrast between the stiffer inner stroma of the centre and the softer limbus.

The biomechanics of the cornea is extremely important as it affects its functional response and can have a significant impact on vision. It is decisive for diseases such as keratoconus where these properties are altered. More specifically, corneal thinning and conical protrusion are indications of keratoconus that lead to progressive visual degradation. For instance, this is caused by a disruption of the collagen organisation, and biomechanical destabilisation [34].

1.1.4. Stem Cells

Stem cells (SCs) are the foundation of every tissue of our body. They are undifferentiated cells that are not only capable of self-renewing, but also of differentiating into other cells types (potency). Based on their origin and potency, stem cells can be divided into three groups:

- Embryonic SCs (ESCs) are obtained from the inner cell mass of the blastocyst. They are pluripotent, meaning they can give rise to every

cell type in the fully formed body, but not the placenta and umbilical cord. They are also able to replicate indefinitely [35].

- Tissue-specific SCs, also known as somatic or adult SCs, are more specialised than ESCs. These cells are undifferentiated and can self-renew. Since their primary role is the maintenance and repair of the tissue in which they reside, they usually originate from the specific cells of that tissue or organ. The epidermis of the skin, blood, and the epithelial lining of the gut are good examples [36].
- Induced Pluripotent Stem Cells (iPSCs) are cells that have been engineered in the laboratory to have similar properties to ESCs. iPSCs were generated by using a combination of four reprogramming factors, Oct4 (Octamer binding transcription factor-4), Sox2 (Sex determining region Y)-box 2, Klf4 (Kruppel Like Factor-4), and c-Myc [37].

Considering their potency as the base classification, five distinct cell types of SCs (Figure 1.4) can be identified [38]:

- Unipotent: also known as a precursor cell, is a stem cell that only has the capacity to differentiate into one cell type, e.g. muscle stem cells;
- Multipotent: have the ability to differentiate into all cell types within one lineage. Most adult SCs are multipotent and are essential in tissue repair and protection, e.g. Haematopoietic stem cells and mesenchymal stem cells;
- Oligopotent: or progenitor cells, can differentiate into a few related cells, e.g. vascular stem cells;
- Pluripotent: can differentiate into other cells of the adult body, e.g. ESCs and iPS cells;
- Totipotent: can differentiate into embryonic as well as extra-embryonic tissues such as the placenta, i.e. Zygote and early morula [36].

“Mesenchymal stem cells” (MSCs) are adult multipotent SCs that were originally identified in the bone marrow stroma but are present in diverse adult organs such as the heart muscle [39], adipose tissue [40] or the corneal stroma [41]. For this reason, they are commonly referred to as “stromal cells”. They

can differentiate into cells of skeletal tissues like chondrocytes (cartilage cells), osteoblasts (bone cells) and adipocytes (fat cells) [42].

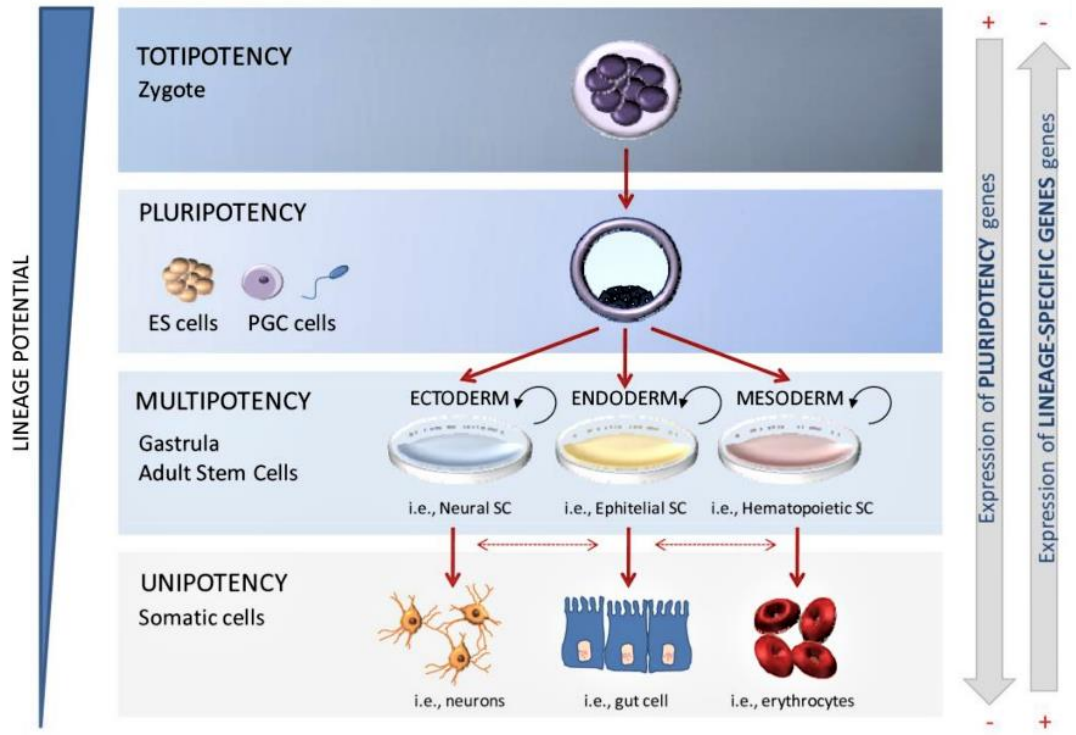

Figure 1.4 – Schematic diagram of cell potency based on lineage restriction: from the totipotent zygote to the unipotent somatic cells, and the differences in pluripotency and lineage-specific gene expression. Adapted from [43].

1.1.5. The limbus

The limbus is a transitional zone between the cornea, sclera, and the conjunctiva. It plays a vital role in the maintenance and regeneration of the corneal epithelial tissue. Moreover, it is thought that limbal epithelial stem cells (LESC) and corneal stromal stem cells (CSSC) reside within and between the limbal crypts of the palisades of Vogt, respectively (Figure 1.5).

Li and colleagues investigated the differing characteristics of limbal niche cells and limbal stromal cells, both defined as fibroblast-like cells, in the maintenance of limbal epithelial stem/progenitor cells in the cornea. Limbal niche cells were obtained from direct dissection of the human corneal limbus using dispase, and limbal stromal cells were obtained from explant cultures of limbal stromal tissue under the same culture conditions. They demonstrated that limbal niche cells of the superficial stroma were more effective at

maintaining limbal epithelial cells than limbal stromal cells from explants of the deep stroma through higher colony-forming efficiency and higher intensity of the limbal stem cell marker ΔNp63 [44]. The advantages of the co-culture based on the proximity of the limbal niche cells with the limbal epithelial cells will be explored in this thesis with a focus on corneal stromal stem cells.

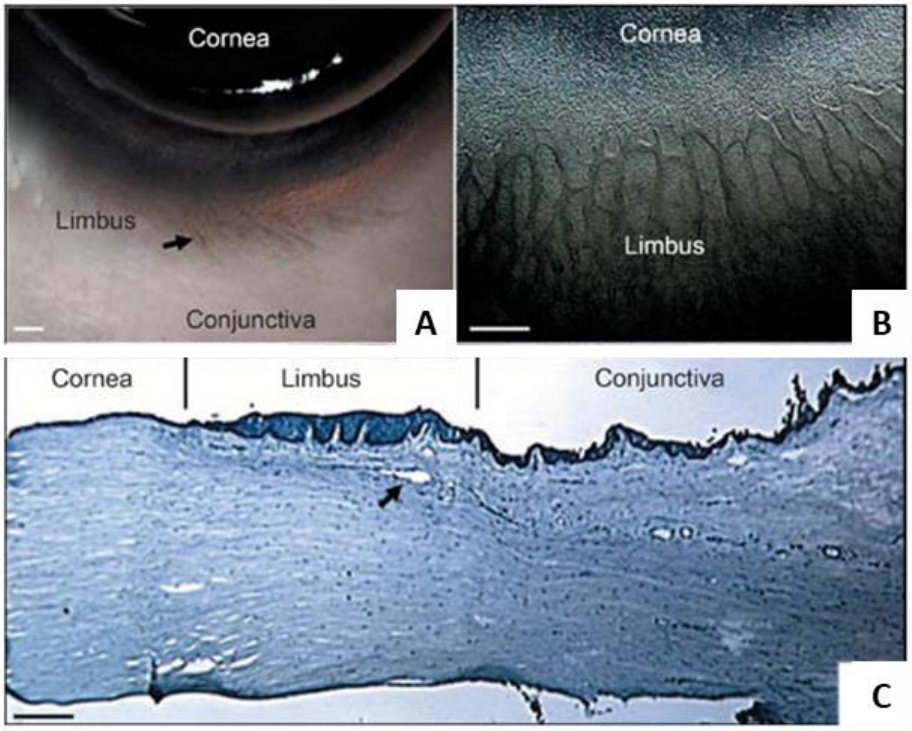

Figure 1.5 – Photograph and sections of a human eye. **(A)** The limbus is located between the cornea, the sclera and the conjunctiva (arrow); **(B)** pigmented Palisades of Vogt in the limbal region; **(C)** Haematoxylin staining of a corneal section: central cornea, limbus and conjunctiva (Bar represents 500 µm in A and B, and 200 µm in C). Adapted from Li *et al*. [45].

1.1.5.1. Limbal Epithelial Stem Cells (LESCs)

LESCs share common morphological characteristics with other adult somatic stem cells like the small size [46] and the high nucleus/cytoplasm ratio [47].

Despite efforts to find a specific marker for LESCs, this remains a challenge. LESCs and their immediate progeny may be distinguished based on a set of positive and negative markers. The putative positive markers include the transcription factor p63 [48], N-cadherin [49], integrin α9 [50], the ATP-binding cassette transporter G2 (ABCG2) [51] and more recently discovered ATP-binding cassette, sub-family B, member 5 (ABCB5) [52].

Nuclear transcription factor p63 regulates corneal epithelial cell renewal and has been shown to be of utmost importance for graft survival [53]. Different isoforms have been described. Nonetheless, the ΔNp63α isoform is the most expressed and commonly used in the field of ocular surface epithelium due to its reliability [48]. This isoform is thought to be more specific than other isoforms [53]. In general, it is considered a putative LESC marker. Despite the fact that several groups have claimed that ΔNp63α was also expressed by early transient amplifying cells (TACs) [54, 55], Di Iorio *et al.* showed that the ΔNp63α isoform is specific to LESCs using Western blotting, real time PCR, and quantitative fluorescence immunohistochemistry [56, 57].

As a human eye development marker, PAX6 remains expressed in the nuclei of all cells within the corneal, limbal, and conjunctival epithelia, and it is required for the maintenance/proliferation of corneal epithelial stem cells [58].

LESCs do not express terminal differentiation markers such as cytokeratin 12 (CK12), connexin 43 and cytokeratin 3 (CK3) that are expressed by mature corneal epithelial cells [59, 60]. Table 1.1 summarises some of the current markers used in corneal and limbal epithelial cell characterisation and their localisation.

Table 1.1 – Corneal and limbal epithelium: localisation of different associated markers.

Marker	Corneal cell type	Localisation	Reference
ABCB5	Limbal epithelium: LESC	Cell membrane	[52]
ABCG2	Limbal epithelium: LESC and basal cells	Cell membrane	[61]
Bmi1	Limbal epithelium: LESC	Nucleus	[62]
C/EBPδ	Limbal epithelium: LESC	Nucleus	[62]
Connexin 43	Corneal and limbal suprabasal epithelium	Gap junctions	[50]
Cytokeratin 12	Mature corneal epithelium	Cytoskeleton	[63]
Cytokeratin 14	Limbal epithelium: basal cells*	Cytoskeleton	[64]
Cytokeratin 15	Limbal epithelium: LESC and basal cells	Cytoskeleton	[65]
Cytokeratin 19	Limbal epithelium: basal cells*	Cytoskeleton	[66]
Cytokeratin 3	Mature corneal epithelium	Cytoskeleton	[67]
Cytokeratin 5	Limbal epithelium: basal cells*	Cytoskeleton	[64]
Desmoglein 3	Limbal epithelium: superficial	Cytoskeleton	[68]
Integrin α9	Limbal epithelium: TAC	Cell surface	[50]
Integrin β1	Limbal epithelium: TAC	Cell surface	[50]
Involucrin	Mature corneal epithelium	Cytoplasm	[50]
Ki67	Limbal epithelium	Nucleus	[69]
Nestin	Mature corneal epithelium	Cytoplasm	[50]
Notch-1	Limbal epithelium: LESC	Cell membrane and nucleus	[70]
P-cadherin	Limbal epithelium	Cell membrane	[71]
PAX6	Limbal and corneal epithelia	Nucleus	[72]
Periostin	Limbal epithelium	Cytoplasm	[73]
SOD2	Limbal epithelium	Mitochondrion	[74]
TCF4	Limbal epithelium	Cytoplasm	[75]
Vimentin	Limbal epithelium: TAC and basal	Cytoskeleton	[64]
Wnt-4	Limbal epithelium	Cell membrane (secreted)	[71]
α-enolase	Limbal epithelium: TAC	Cytoplasm	[76]
ΔNp63α	Limbal epithelium: LESC	Nucleus	[57]

** also present on mature corneal and conjunctival epithelial cells*

The importance of the mechanical properties of the cornea was addressed in an earlier section of this thesis. With regards to LESC specifically, the impact that stiffness differences have on the stem cell niche was investigated by Gouveia *et al.* The authors demonstrated that there is a correlation between corneal biomechanical properties, YAP-dependent mechanotransduction and

epithelial cell phenotype. These experiments were performed both *in vivo* and *ex-vivo* and showed that stiffer substrates promote YAP activation, which leads to cell differentiation while compliant substrates suppress YAP signalling and maintain LESCs expansion [77].

1.1.5.2. Corneal epithelial homeostasis

The corneal epithelium undergoes constant cell turnover, with the cells having an average lifespan of seven to ten days [5]. The XYZ hypothesis of Thoft *et al.* [78] in 1983 proposes that the limbus serves as a reservoir of corneal epithelial stem cells. The model "X+Y=Z" simplifies the process where "X" represents the proliferation of basal corneal epithelial cells, "Y" the centripetal migration from the limbus and "Z" the loss of cells into the tear film (desquamation) (Figure 1.6).

It is known that central corneal epithelial cells are not capable of continuous replication and enter senescence [79]. However, many studies have indicated that LESCs from the basal layer at the limbus produce daughter cells in a process called transient amplification. This is an asymmetric division of the stem cells where a stem-like daughter remains in the limbus and is considered a true LESC. At the same time, the other divides rapidly and migrates towards the centre (Transient amplifying cell – TAC). About 95% of all cells in the limbus are thought to be TACs at different levels of maturity, and only 5% are considered real LESCs [80]. Corneal TACs will ultimately replace the terminally differentiated cells that are shed continuously by the surface of the eye due to the shearing forces of the eyelid [60].

In the past decade, some human and animal studies have challenged this hypothesis. For example, patient corneal epithelial homeostasis was maintained in the absence of clinically detectable LESCs [81], and central corneal cells (from other mammals) were capable of holoclone formation [82, 83].

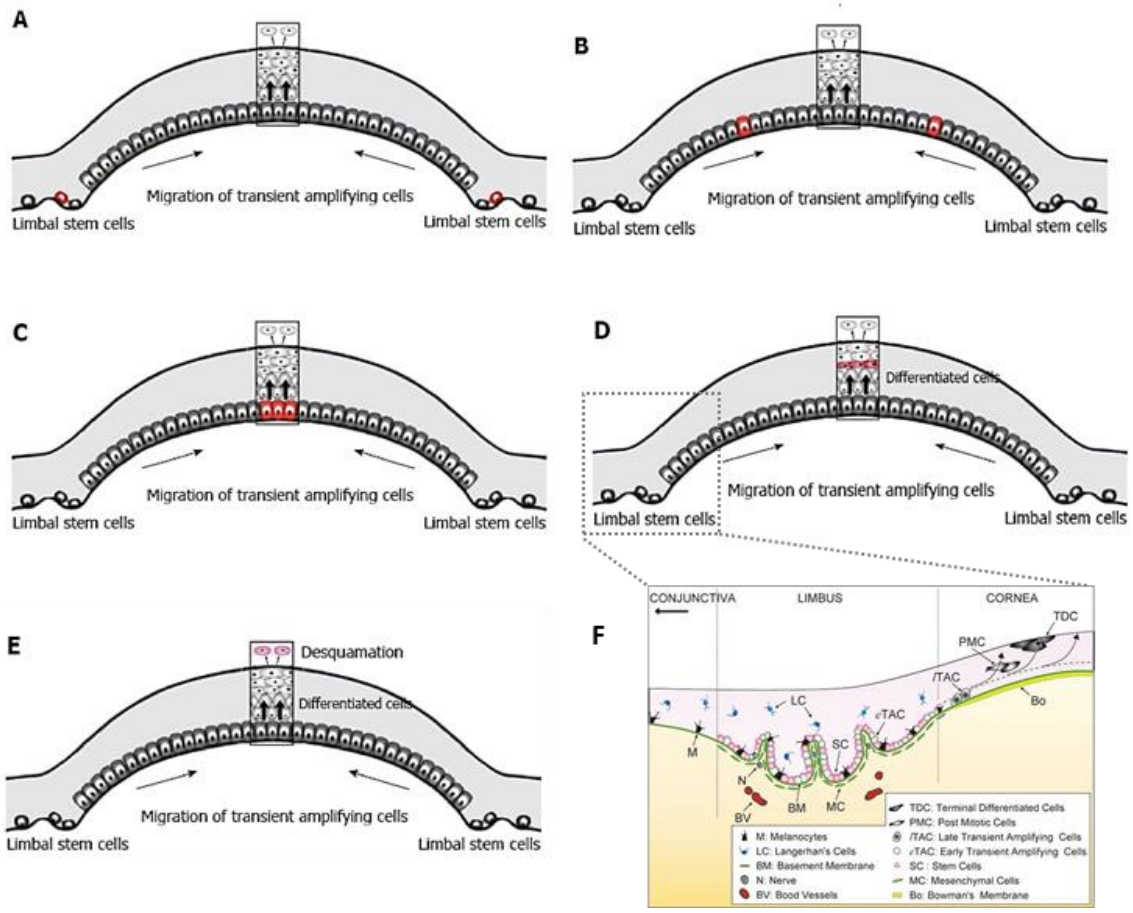

Figure 1.6 - X, Y, Z model of corneal epithelial homeostasis: **(A)** LESCs at the peripheral cornea divide and produce TACs; **(B)** TACs migrate centripetally **(C)** undergoing a few divisions on the central cornea; **(D)** The differentiated daughter cells move toward the surface to replenish the upper layers of the cornea **(E)** where they are lost due to shedding from the corneal surface [84]. **(F)** Diagram of the limbal stem cell niche highlighting the migration of TACs [45].

Majo *et al.* suggest that the stem cells within the central cornea are sufficient to maintain healthy tissue homeostasis proposing a new model where the limbus is a zone of equilibrium, but also a confrontation zone between two opposite forces generated by the expansion of stem cells from both conjunctival and central corneal epithelia (similar to tectonic plates) [82]. In this paper, they challenged the concept of limbal epithelial stem cells niche location and suggested that there is a reservoir of stem cells within the corneal epithelium. Using a murine model, they observed that the transplant of a central corneal biopsy was enough to reconstruct the corneal epithelium of recipient mice in which portions of the limbus were excised. Their study also showed that limbal stem cells were only solicited after significant corneal damage. They have also accessed porcine models and concluded that corneal

stem cells are distributed throughout the entire ocular surface in mammals [82].

More recently, Di Girolamo *et al.* [85] and Amitai-Lange *et al.* [86] investigated the cell lineages in mouse limbal and central corneal epithelium by tracking the growth of fluorescent clones from the limbus for up to 21 weeks. This method, usually referred as confetti, identified small patches of labelled epithelial cells in the corneal epithelium which supports the evidence of the existence of long-term epithelial progenitors in the central cornea as identified by Majo *et al.* [82]. However, these lineage-tracing studies demonstrated that unwounded epithelium is mainly sustained by epithelial stem cells distributed around the limbal circumference.

Although in the mouse model central corneal epithelium exhibited stem cells capable of maintaining tissue homeostasis, as yet in humans, there is no evidence to support this theory.

1.1.6. Imaging of the Limbal Niche

Stem cell niches are highly organised 3D structural units that provide an ideal microenvironment to support stem cells. The limbal stem cell niche, between the cornea and the conjunctiva, provides unique signals and extracellular matrix cues that maintain LESCs in their native, undifferentiated state [87, 88]. Even though the limbal stem cell niche has been studied for a long time, there is still a lack of understanding of its 3D architecture [89].

Over the years, different techniques have been used to explore limbal architecture. From simple slit lamp examinations [90, 91] where the palisades of Vogt were first described as “radially oriented fibrovascular ridges separated by interpalisade epithelial ridges” to histology [88, 92-94], from OCT [95-97] to confocal microscopy [68, 97], from electron microscopy [88, 92, 97, 98] to *in vivo* confocal reflectance microscopy [97, 99, 100], many researchers have looked into how to better reconstruct and understand the niche. However, none of these techniques allowed a full reconstruction of the limbal arch in 3D both at the macroscopic and microscopic level and the study of cell-cell interactions. Limitations in resolution by the technology or in-depth penetration due to the

opacity of the tissues limit these classical approaches. Therefore, they usually require the cut of physical sections of tissue samples to overcome the limited penetration of light, which is time-consuming and prone to errors [101].

Studies have reported high variability of the palisade zone in terms of shape/forms, size, orientation (mostly radial), as well as individual trabecular patterns formed by the branching and interconnection of the palisades [89].

Shortt *et al.* looked at the structural characteristics and regional distribution of the LESCs using thick sections of the limbal region (180 μm in depth). Limbal crypts were defined as “distinct invaginations of the epithelium into the underlying stroma in the peripheral cornea” and focal stromal projections (FSP) as “finger-like projections of the stroma that extend upward into the corneal limbal epithelium”. These structures were located only in the superior and inferior limbal regions with moderate extension to the nasal and temporal regions [97].

Imaging of the niche beyond LESCs has not been fully achieved yet. Further improvements in imaging technology could allow a better characterisation of the niche structure and composition. For example, innovative alternative methods using the potential of tissue clearing could be explored in order to overcome the limitations imposed by the scattering of light. Tissue clearing involves the removal of lipids, while keeping the proteins, enabling a deeper penetration of light [102]. This could create a full reconstruction of the limbal arch allowing the identification of the precise location of LESCs and CSSC [102].

The first published studies using tissue clearing techniques, focused mainly on the imagining of the brain. Since then, volume imaging of immunolabeled cleared tissues opened a new chapter in systems biology as it allows the study of connectivity and circuits, such as vascular and nervous structures [103].

Until a couple of years ago, the published clearing protocols allowed the imaging of every organ except the eye. However, recently, one piece of work looked into the clearing of the sclera in different species with a focus of imaging the back of the eye and showed that this clearing was possible although no further studies were done at the cellular or organisation level [104]. The choroid and retinal vasculature have also been recently studied using this technique

on mice eyes [103, 105]. A new clearing method that featured a whole eye reconstruction was featured in a pre-print recently, but there was no investigation at the cellular level [106]. To the extent of our knowledge, no studies have used clearing techniques to study the limbal stem cell niche.

1.1.6.1. Stem Cells in the Corneal Stroma

In 2006, the Mesenchymal and Tissue Stem Cell Committee of the International Society for Cellular Therapy wrote a paper proposing the adoption of minimal criteria to define human mesenchymal stem cells (hMSCs) internationally: (a) cells should be plastic-adherent when maintained in standard culture conditions; (b) hMSC must express CD105, CD73 and CD90, and not express CD45, CD34, CD14 or CD11b, CD79alpha or CD19 and HLA-DR surface molecules; (c) hMSC must differentiate into multiple cell lineages *in vitro*: osteoblasts, adipocytes and chondroblasts [107]. hMSCs are also known to grow clonally and exhibit asymmetric division.

Recently, there has been a call from the scientific community to revise hMSC naming. In 2017, Caplan published a paper urging the scientific community to change the name of MSCs to Medicinal Signalling Cells. In his view, this would reflect more accurately their application as a cell that secretes bioactive factors directly at the site of injury [108]. The following year Sipp *et al.* wrote a comment in Nature stating that this claim for change created even more confusion among the scientific society. One of the problems associated with this re-branding was that it incentivised the sale of unproved treatments by including ‘medicinal’ in the name leading to the assumption that MSCs have a broader therapeutic application. They asked for a concerted approach, from regulatory agencies, editors and scientists to develop and enforce rigorous methods and standards of gene expression and differentiation assays in order to address this persistent question around MSCs identity and function [109].

The idea that MSCs can be found in the corneal stroma has been explored by multiple research groups [110-117]. Funderburgh and colleagues isolated bovine stromal progenitor cells for the first time from bovine fresh corneas and showed that they exhibit clonal growth [115]. Additionally, the expression of

MSCs markers by corneal stromal stem cells (CSSCs) was also shown in cells isolated from the human corneal stroma *in vitro*. In this study, multipotency of CSSCs was not tested, but their ability to differentiate into different lineages (chondrogenic and neurogenic lineages) was demonstrated [114]. These studies provide evidence that CSSCs share some MSCs properties.

MSCs are especially promising in anti-scarring therapies due to their reported immune-modulatory capacity to delay the host rejection [114]. MSCs produce anti-inflammatory factors that participate in wound repair [118] and have the ability to migrate to the site of tissue injury and stop immune response by inhibiting T-cell proliferation [119]. Moreover, MSCs secrete growth factors and cytokines with autocrine and paracrine activities which facilitate tissue regeneration [120].

CSSCs specifically, have prevented scarring in an *in vivo* mouse model by the secretion of TDG-6 that prevented neutrophil infiltration and consequent fibrotic response [111]. A different study confirmed this anti-inflammatory effect by using an *in vitro* injury model that demonstrated that CSSC have an important role in corneal regeneration and wound healing. The use of CSSC alone and in combination with amniotic membrane showed that their presence inhibited immortalised human corneal epithelial cell line viability loss after injury. Additionally, this led to reduced production of pro-inflammatory cytokines, pro-inflammatory mRNA expression, and cytotoxicity levels [110].

CSSCs are the presumed human progenitor cells of keratocytes, which, as previously explained, reside in the central corneal stroma and maintain help maintain this tissue healthy and transparent. CSSCs reportedly exhibit multipotent differentiation potential and express MSC markers, including PAX6, CD73 and CD90 (Figure 1.7A) [121]. PAX6 is present in embryonic and developing stromal cells but not in terminally differentiated keratocytes [115] CSSCs lose PAX6 expression as they differentiate [114], and begin to expresses keratocyte markers including keratocan, lumican and ALDH1A1 (Aldehyde Dehydrogenase 1 Family Member A1) when cultured in low-mitogen, ascorbate-containing media [114, 122].

Interestingly, CSSC produce highly aligned collagen fibres similar to the native human stromal lamellae when cultured in aligned polymeric fibres *in vitro* [123].

The ability of human CSSCs to adopt a keratocyte function proved to be outstanding *in vivo*. When injected into the mouse corneal stroma, human CSSCs express keratocyte mRNA and protein, replacing the mouse ECM with human matrix components. The injected cells remain viable for months, seemingly becoming quiescent keratocytes [116].

In summary, these observations suggest that keratocyte differentiation may be the default lineage for the CSSCs. In the LESC niche, these cells seem to maintain CSSC characteristics, but *in vivo*, when in the stroma, they differentiate into keratocytes [124]. Further characterisation studies of CSSCs will be performed on this thesis prior to the development of a tissue-engineered product.

There is some evidence that CSSCs may be localised in the anterior peripheral limbal stroma close to the LESCs. More specifically, they have been found in the Palisades of Vogt subjacent to the epithelial basement membrane as it is possible to observe in Figure 1.7B [112]. Limbal melanocytes can also be observed in Figure 1.7B located in the basal epithelium of the corneoscleral limbus and observations suggest that they could play an important role in the maintenance of LESCs in the human limbal stem cell niche by interacting with the adjacent progenitor cells [125, 126].

Additionally, our group has shown that human CSSC support limbal epithelial cells when co-cultured on RAFT tissue equivalents (RAFT-TEs are collagen compressed hydrogels. For a more detailed description please see Section 4.2). It is hypothesised that mesenchymal cells also help to maintain the LESC phenotype in the limbal niche [127].

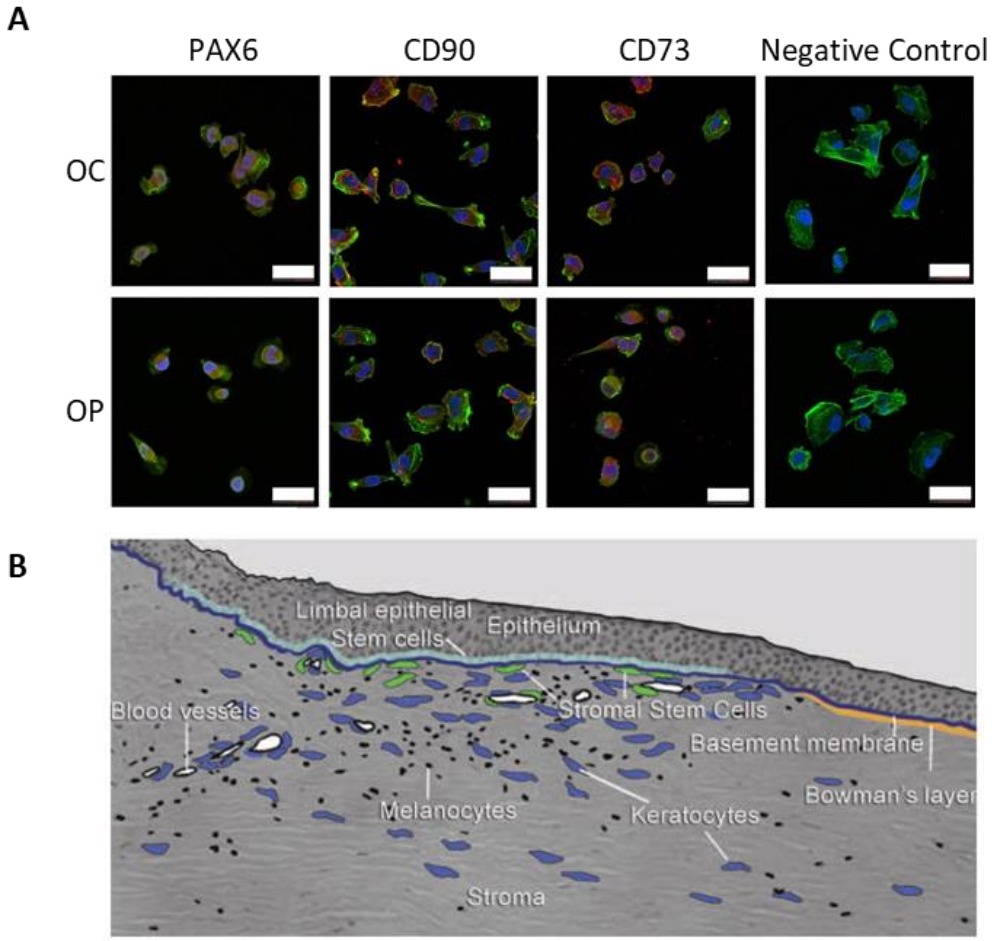

Figure 1.7 - Corneal stromal stem cells: **(A)** confocal micrographs of human CSSCs isolated from organ culture (OC) and Optisol (OP) medium. Cells have positive expression of PAX6 (eye development gene), CD73 and CD90 (MSC markers). Blue – DAPI, Green- Phalloidin, Red- Antibody; Scale bars: 40 μm [121]; **(B)** Section of the transition zone between the cornea and the sclera, known as the limbal region. Stromal cells are shown in green and are located near the limbal epithelial stem cells subjacent to the basement membrane. Melanocytes are shown in black and keratocytes in blue. Blood vessels of the limbal stroma are highlighted in white [112]

In this study, they proposed that RAFT-TEs could be used as a 3D biomimetic model to investigate the epithelial-stromal cell interactions by cultivating a mixed population of LESCs and CSSCs. Extrapolating from their *in vitro* observations, the authors hypothesised that CSSCs may also help to maintain LESCs phenotype in the native limbal niche [127]. Paracrine mediators might play an important role in this support since, at the end of this study, very few CSSCs remained on RAFT-TE. Although CSSC presence was beneficial for LESC expansion *in vitro*, it might not be necessary to transplant them in future therapeutic approaches [127]. Further studies showed that direct interaction between CSSC and the host cells is not needed for the

promotion of cornea regeneration [113]. For example, Deng *et al.* have also shown that limbal mesenchymal cells can substitute murine 3T3s fibroblasts when in co-culture with LESCs using a 3D system [128]. Tseng *et al.* were one of the first groups to report a new isolation method of human limbal epithelial progenitor cells by maintaining them in close association with their niche cells. At the time, it was not known that this might be explained by the paracrine effect of CSSC, which support the culture of LESCs [129].

In recent years, extracellular vesicles (EVs) have been studied as a potential mechanism by which MSCs communicate with their targets [130]. Shojaati, Khandaker, Funderburgh *et al*. examined the potential role for EVs in the regeneration of damaged cornea by CSSC. CSSC produce EVs that deliver miRNA that blocks scarring and promotes regeneration action [131].

In previous works, human CSSC restored transparency in cloudy lumican-deficient mice corneas without rejection. The disorganisation of the ECM in this mouse model mimics human corneal scars. The study revealed CSSC ability to prevent scarring by maintaining collagen fibril organisation and transparency when injected in the centre of the cornea [116]. Therefore, CSSCs have great potential for the development of a corneal stromal equivalent tissue in mice, but its potential application in humans still requires further studies at this point. Furthermore, there are two points of discussion: (1) mouse corneas, in comparison to human corneas, are thinner and weaker which facilitates matrix remodelling; (2) it remains unclear if this therapy would have the same benefit in pre-scarred corneas rather than corneas at earlier stages of wound healing. Nevertheless, the paper showed that co-culture of CSSCs with LESCs optimised cell-cell interactions necessary for graft function and resolved stromal haze as a one-step procedure in the murine model [116]. CSSC delivery methods and their potential will be explored in this thesis with clinical applications in mind.

1.2. Corneal disease & current treatments

According to the World Health Organisation (WHO), more than 45 million people worldwide are blinded or severely visually impaired. At least 10 million

are blind due to unilateral or bilateral corneal disease or injury, and 1.5M new cases appear per year. Yet, less than 150,000 corneal transplants are performed worldwide, mainly due to the shortage of donors [132]. Each year, corneal vascularisation and opacity are estimated to cause blindness in eight million people worldwide – roughly 10% of total cases [102].

The cornea, the outer surface of the eye, is exposed to the environment. Consequently, there is a high risk of injury, such as mechanical damage and chemical or thermal burns [5, 133]. Corneal health can also be threatened by different pathogens such as viruses, fungi, and bacteria [134]. Genetic, hereditary or congenital mutations can also cause conditions resulting in corneal opacity [135].

1.2.1. Limbal stem cell deficiency (LSCD)

Limbal stem cell deficiency (LSCD) is a disease characterised by the disruption of the LESC niche and consequent loss or dysfunction of LESCs. It affects corneal epithelium homeostasis, decreasing the rate of corneal epithelial renewal and loss of the barrier function of the limbus (invasion of conjunctival epithelium onto the cornea) [136].

The imbalance of corneal-conjunctival homeostasis often leads to conjunctivalization, which involves the re-epithelisation of the corneal surface by neighbouring conjunctival epithelial cells [137]. In more severe cases, the cornea can become covered by conjunctival substantia propria [138]. This conjunctivalization is followed by neo-vascularisation, inflammation, and opacification of the central cornea. Pain, inflammation, photophobia, and vision loss can be consequences of this process [139, 140].

The severity of LSCD depends on the extent of the injury (partial or total). It can also be unilateral or bilateral if affecting both eyes [138]. When only one part of the limbus and cornea is affected, it is known as partial or focal LSCD. When the whole circumference of the limbus and corneal epithelium is affected, it is known as total or diffuse LSCD [138].

Furthermore, the stroma is often involved in LSCD cases where the complete healing of a stromal injury may take months or even years [5]. LSCD

can be caused by different factors: genetic diseases e.g. aniridia, inflammatory disorders such as Stevens-Johnson syndrome, chemical burns, and trauma, to name a few [140]. Contact lens-associated LSCD has also been reported as result of cytotoxicity of the contact lens solution or the result of mechanical friction and inflammation of the limbus [141].

1.2.1.1. Diagnosis of limbal stem cell deficiency

LSCD can be detected based on the clinical features described above. However, some of the signs present in LSCD are also seen in other conditions, so laboratory tests are essential to confirm the diagnosis of LSCD. Impression cytology and *in vivo* confocal microscopy are two techniques available to support the diagnosis.

In corneal impression cytology, a nitrocellulose acetate filter is pressed onto the cornea under topical anaesthesia removing 1-3 cells layers of the ocular surface. The removed cells are then subjected to histological and immunohistological analysis. The presence of goblet cells on the cornea implies conjunctival epithelial invasion [142]. However, their absence does not exclude LSCD since goblet cell deficiency is also present in up to 36% of patients [143].

In vivo laser scanning confocal microscopy provides high-resolution images of the ocular surface at the cellular level. It has emerged as a promising tool for LSCD diagnosis due to the significant microstructure changes observed even in the early stage of LSCD [81, 100].

A combination of morphological changes in the corneal epithelium and a significant reduction in both basal epithelial cell density and sub-basal nerve density are signs of LSCD. The corneal epithelial cells in LSCD have less distinct borders and have prominent nuclei. The literature is controversial regarding the morphological features of goblet cells. Some authors reported that goblet cells have hyperreflective cytoplasm [144], while others proposed a hyporeflective cytoplasm [145].

1.2.1.2. Existing treatments and their drawbacks

The treatment of LSCD depends on the extent of the injury. For partial or mild disease, topical lubricants, and anti-inflammatory agents (e.g. steroid) might be sufficient to reduce discomfort. However, surgery may be required to restore function in severe disease. Corneal transplantation for LSCD has a higher failure rate as it does not reconstitute the function of the limbus, and the epithelial changes recur [80]. For unilateral disease, a limbal biopsy is taken from the contralateral healthy eye, or donor tissue can be transplanted into the injured eye [138]. Simple limbal epithelial transplantation, also known as SLET, has also been used as a surgical alternative for the treatment of unilateral limbal stem cell deficiency. This single-stage procedure consists of distributing tiny limbal explants on HAM prior to transplantation [117, 146].

As with other organs, an autologous graft has a better chance of survival. However, for patients with bilateral disease, an autograft cannot be obtained, and other approaches have been studied. New therapies are being developed using epithelium from other sources, such as oral mucosa or skin [147].

1.3. Corneal Tissue Engineering

As mentioned above, there is a global shortage of suitable corneal donor tissue and a high risk of rejection. Lack of awareness about donation, lack of facilities in some countries to remove and store corneas and the fact that not all corneas are suitable for donation also impact numbers [148-150].

The recent increase in the number of people undergoing surgery for sight correction also had a negative impact on availability [151]. It has been shown that refractive surgery significantly impacts cornea structure, weakens the stroma, and compromises its biomechanical properties [152].

Keratoprosthesis have been around for a while, but despite their success in improving vision, they have several associated complications which make them a last resort when patients are unable to sustain a corneal transplant. This device consists of replacing the cornea with a transparent polymer and a

structure that holds it in place. Boston keratoprosthesis, Alpha Cor or the osteo-odonto keratoprosthesis are all examples available in the clinic [153].

Based on the clinical history and patient needs, surgery has improved over the years, and it is now possible to replace only one of the few layers of the cornea instead of having a full-thickness transplant. This is something that also needs to be considered when exploring tissue engineering approaches for the reconstruction of the ocular surface. The more layers, the more complex the structure will be.

Cellular and acellular scaffolds have been tested over the years. Multiple materials and manufacturing approaches have been under investigation, as well as different cell sources. A few scaffolds have also entered clinical trials to investigate their potential for corneal regeneration [154].

The next sections will delve into what needs to be considered before the design of such scaffolds and the progress that has been achieved until now in the field.

1.3.1. Design considerations based on the surgical application

There are different types of surgical approaches to corneal transplantation. The same assessment needs to be done when looking for alternative tissue engineering approaches for corneal replacement.

The traditional method is known as penetrating keratoplasty (PK), and it involves the replacement of the central corneal button with a full-thickness cadaveric cornea. All three corneal layers are replaced with this method.

Alternative procedures that focus on the replacement of the specific layers of the cornea are increasingly popular [155, 156].

Anterior lamellar keratoplasty (ALK), deep anterior lamellar keratoplasty (DALK), Descemet's membrane endothelial keratoplasty (DMEK), and Descemet's stripping endothelial keratoplasty (DSEK), shown in Figure 1.8, are all examples of different surgical approaches that improved some areas of concern. The replacement of the endothelium is usually considered in cases of bullous keratopathy and Fuchs dystrophy. The strategies involving the replacement of the stroma usually involve patients with keratoconus or anterior

scarring [154].

To name a few improvements that resulted from the change from full-thickness transplants to lamellar keratoplasties: (a) DALK reduced the risk of failure due to endothelial rejection; (b) DMEK almost eliminated induced astigmatism and the problems associated with graft–host junction.

To treat limbal stem cell deficiencies, Stephen-Johnson syndrome or aniridia, the transplantation of limbal tissue has also been used as an alternative.

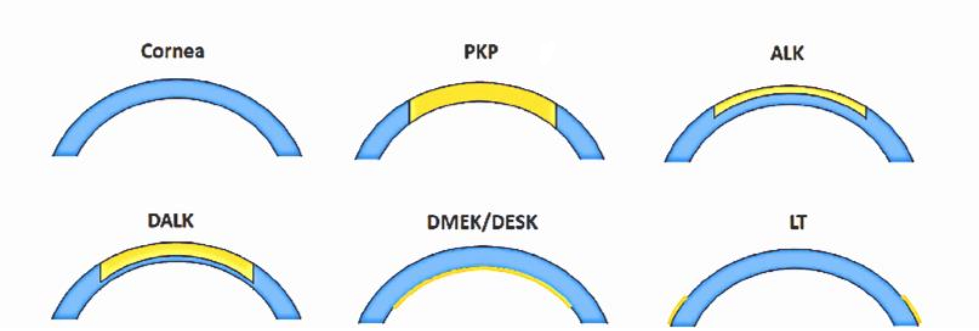

Figure 1.8 – Representation of clinical options for surgical corneal replacements. Full-thickness transplant is represented as PK; ALK indicates anterior lamellar keratoplasty, DALK highlights deep anterior lamellar keratoplasty, DMEK shows Descemet's membrane endothelial keratoplasty; Descemet's stripping endothelial keratoplasty, and LT is an example of a limbal transplant. The cornea sections are represented in blue and the tissue transplanted is highlighted in yellow [154]

In light of the different types of surgical approaches and clinical needs, the design of a scaffold needs to take these implications into account. For instance, if the surgery involves stroma replacement, a thick 3D transparent, robust scaffold needs to be designed. On the other hand, if the focus is on DMEK, a thin, permeable film to work as a carrier of the cells would be sufficient [154].

Tissue engineering aims to reproduce the natural properties of tissue in the laboratory. Research into corneal reconstruction intends to mimic the anatomy and physiology of the human cornea. In general, there is a need for producing strong, transparent, thin structures. As with the normal cornea, the structure should provide protection, be transparent and in the case of full-thickness replacement, withstand intraocular pressure. They should be biocompatible, mechanically stable and capable of promoting cell attachment and proliferation [157, 158].

As referred above, the properties of the tissue construct should be based

on the final goal. If the aim is to create a full-thickness corneal replacement, the intended thickness and biodegradability rates would be different from a structure that was only used as a temporary carrier for epithelial cell replacement.

It is imperative to understand how the chemical and biophysical properties of biomaterials, such as stiffness, biodegradation rate, topography, hydrophilicity, etc., can modify cell behaviour such as morphology, adhesion and differentiation [159].

1.3.2. Biomaterials

A range of biomaterials have been investigated for corneal tissue engineering (Table 1.2). Naturally occurring materials are generally used rather than synthetic ones due to their biocompatible, biodegradable, and bioactive properties. Some of the most studied materials in the field include many hydrogels made of alginate, collagen, and fibrin; silk fibroin and keratin films as well as electrospun fibre membranes.

Hydrogels are hydrophilic polymeric networks that can absorb and retain a thousand times their dry weight in water. They are incredibly appealing for tissue engineering of the ocular surface as their properties are exceptionally tuneable. They provide a soft tissue-like environment that allows not only the diffusion of nutrients but also the clearing of metabolic waste. However, the lack of tensile strength is a common limitation of hydrogels [160]. To improve their mechanical properties, these matrices can be crosslinked in two distinct ways: chemically, where covalent bonds form stable hydrogels and physically due to environmental changes in pH and temperature [161, 162].

1.3.2.1. Collagen-based approaches

Collagen is the major structural element of connective tissues. It contributes to the stability of the tissues and is the most abundant protein found

in the extracellular matrix (ECM). As it is the major structural component of the corneal stroma, it is commonly used as a biomaterial in ocular surface reconstruction [11, 163]. Collagen can form highly hydrated hydrogels. These hydrogels are usually fragile and often require chemical cross-linking or plastic compression to become mechanically stronger [164-166]. Table 1.3 summarises some of the latest research in corneal tissue engineering using collagen.

Table 1.2 – Corneal tissue engineering: biomaterials and cellular combinations used in an attempt to create TE for transplantation.

Biomaterial	Cell type	Clinical status	Reference
Alginate hydrogel with Collagen IV	iHCE	*In vitro*	[167]
Chitosan-gelatine membrane	iHCE or LESC	*In vitro*	[168]
Collagen-chitosan	iHCE	*In vivo* (pig)	[31]
Fibrin	LESC	Clinical trial	[169]
Genipin crosslinked chitosan membranes with, rat collagen I, elastin and hydroxypropyl cellulose	HCEs	*In vitro*	[170]
Grating patterned PDMS and chitosan membranes	HCKs	*In vitro*	[171]
Highly-aligned fibrous PEUU substrates	CSSCs & HCFs	*In vitro*	[172]
Keratin film	iHCE	*In vitro*	[173]
Laminin and fibronectin mimetic peptide -amphiphile nanofiber scaffolds	HCKs	*In vivo* (rabbit)	[174]
Patterned silk substrate with RGD surface coupling	CSSCs & HCFs	*In vitro*	[175]
PCL – electrospinning mesh	iHCE and LESC	*In vitro*	[176]
PLGA – electrospinning mesh	LESC (rabbit or human)	*In vitro*	[177]
RGD patterned and porous 3D stacked 2 µm silk films	HCKs	*In vitro*	[178]
Silicone contact lens	LESC or CjE	Clinical trial	[179]
Silk fibroin dual layer – film and fibrous mat	LESC and L-MSC	*In vitro*	[180]
Silk fibroin film	iHCE	*In vitro*	[179]

Abbreviations: HCFs, human corneal fibroblasts; CjE, conjunctival epithelium; iHCE, immortalised human corneal epithelial cell line; HCK – human corneal keratocytes, L-MSC, limbal mesenchymal stromal cells; PCL, poly-ε-caprolactone; PLGA, poly-lactide-co-glycolide.

Table 1.3 – Collagen-based approaches to corneal tissue engineering: application, collagen type, manufacturing technique, cell type and clinical status of the different approaches.

Application	Collagen Type	Technique	Cell type	Tested *in vivo*	Year	Ref
Epithelium	Collagen I (Porcine)	Crosslinking	iHCE & dorsal root ganglia	Guinea Pig	2010	[181]
	RHC I and III	Crosslinking	iHCE	Mini-pig	2007	[166]
	Collagen I (Equine)	Crosslinking	Oral mucosal cells (*in vitro*) & Acellular (*in vivo*)	Rabbit	2014	[182]
	Collagen I (Rat)	Ammonia vapor fibrillogenesis	LESC	No	2015	[183]
	Collagen I (Bovine)	Plastic compression	LESCs & CSSCs	No	2015	[184]
	Collagen I (Bovine)	Vitrification	LESC	Rabbit	2015	[185]
Epithelium & Stroma	Collagen I (Rat)	Crosslinking	LESCs and stromal cells (*in vitro*) & Acellular (*in vivo*)	Rabbit	2010	[186]
	Collagen I (Rat)	Plastic compression	LESCs & HLFs	No	2010	[164]
	Collagen I (Porcine)	Crosslinking	iHCE and stromal cells (*in vitro*) & Acellular (*in vivo*)	Rabbit	2016	[187]
Stroma	Collagen I (Bovine)	Electrochemically compacted + crosslinking	Human Keratocytes	No	2006	[188]
	Collagen I (Bovine)	Film Dehydrothermal crosslinking	Human stromal fibroblasts	No	2008	[189]
	Collagen I (Rat)	Plastic compression	Acellular	Rabbit	2014	[190]
	RHC III	Crosslinking	Acellular	Phase I clinical trial	2014	[191]
	RHC III	Crosslinking augmented with MPC	Acellular	Phase II-a clinical trial	2016	[192]
	Collagen I (Rat) + PA	Compressed Collagen	LESCs and Human corneal stromal cells	No	2019	[193]
Endothelium	Collagen I (Bovine)	Crosslinking	Human Corneal Endothelial Cells	Rabbit	2004	[194]
	Collagen I (Rat)	Plastic compression	Human Corneal Endothelial Cells	No	2012	[195]
	Collagen I (Human)	Crosslinking	Human Corneal Endothelial Cells	Rabbit	2016	[196]
	Collagen I (Rat) + COL4 or COL4+LAM layer	Compressed Collagen	Human and Bovine Corneal Endothelial Cells	No	2017	[197]
	Collagen I (Porcine)	Vitrification	Human Corneal Endothelial Cells	Rabbit	2017	[198]

Abbreviations: iHCE - Immortalised human corneal epithelial cells, RHC - Recombinant human collagen, MPC - 2-methacryloyloxyethyl phosphorylcholine, PA - Peptide Amphiphiles, COL4 - Collagen IV, LAM - Laminin

1.4. Development of an Advanced Therapy Medicinal Product for ocular surface reconstruction

Despite the fact that advanced therapy medicinal products (ATMPs) offer an opportunity to treat high-burden diseases and the expectations in the field are higher than ever, as of 2018, only ten products had received market authorisation in Europe [199].

There is a tension between science and the regulatory processes that needs to be addressed from the beginning. The next section delves into the considerations of developing a new ATMP.

Good Manufacturing Practice (GMP) is a system for ensuring that medicinal products are consistently manufactured, and according to defined quality standards to minimise the risks involved in the production and thus to ensure that the final products are as safe as possible. GMP covers all aspects, from the starting materials, manufacturing sites, and equipment to the training of staff. Sterile medicinal products must be manufactured in a cleanroom to safeguard their sterility and ensure patient safety [200].

1.4.1. A brief introduction to regulations

Within the European Union (EU), the European Medicines Agency (EMA) is the entity that regulates medicinal products manufacture. Each EU member state must select a relevant authority to oversee the licensing and inspection of GMP facilities. The Medicines and Healthcare products Regulatory Agency (MHRA) is the UK regulatory body that covers medicines, devices, blood and ATMPs for human application [201].

In 2004, the European Commission (EC) ratified the Tissues and Cells Directive, which reclassified gene therapy, somatic cell therapies (including stem cell therapy products) and tissue-engineered products as ATMPs [202]. The guidelines for human medicinal products are further described in Directive 2003/94/EC [203].

In the UK, the Human Tissue Authority (HTA) is the entity that regulates human tissue donated for transplants. However, when these tissues are

processed and become individual cells that are then used to make cell-based medicinal products, their manufacturing and quality control testing, falls under the ATMP Directive 2009/120/EC [204] and MHRA scrutiny.

1.4.1.1. Quality Management System & Risk Assessments

A Quality Management System (QMS) is an indispensable part of a GMP facility (requirement of Directive 2003/94/EC) as it oversees the manufacturing process and defines how regulations are enforced [203]. It includes policies around non-compliance reporting, validations, materials management, quality assurance procedures, complaint reporting, among others. Standard Operation Procedures (SOP) are essential in a GMP environment because they ensure the processes are clear, well defined and traceable [200].

Validations are a necessary part of the process since there is no universally accepted list of suitable materials, protocols or reagents for the manufacture of ATMPs. A Risk Assessment (RA) is performed for each reagent, piece of equipment or for the manufacturing process itself to ensure they pose the least risk for the patient and are 'fit-for-purpose'. Nowadays, most cell culture reagents are only approved for research use, and therefore, a RA addressing numerous standard tests (viruses, bacteria, fungi, mycoplasma, and endotoxins) is needed according to the regulations. Manufacturers must provide all the available quality certificates (e.g. Certificates of Analysis, Origin and Transmissible Spongiform Encephalopathies (TSE)/bovine spongiform encephalopathy compliance) whereupon a risk assessment outcome will be based [200].

1.4.2. RAFT-TE: an overview of a novel tissue engineered product

To create more robust collagen structures required for transplantation, Brown and colleagues [205] developed a method of plastic compression of type I collagen hydrogels. This method removes some of the water from a collagen hydrogel by applying a mechanical load that forces water out. Previous works from our group have demonstrated that compressed collagen

hydrogels can support not only the expansion of LESCs but also support the formation of a multi-layered epithelium [164].

RAFT-TE development is the result of an iterative process where multiple protocols have been tested. It can serve as a carrier for diverse cell types or as a structure for ocular surface replacement. Additionally, it can be used as a biomimetic 3D model for the study of cell-cell interactions and disease modelling *in vitro*. Levis *et al.* have successfully cultured primary human corneal endothelial cells (hCECs) and corneal endothelial cell lines on RAFT-TE [195]. RAFT-TE were recently successfully used as a 3D substrate for co-culturing HLE and CSSC. The incorporation of CSSC within the TE eliminates the use of animal-feeder layers that poses a risk of transfer of adventitious agents to the patient when epithelial cells are seeded directly on top of the structure [127].

1.4.2.1. The history of plastic compressed collagen

Collagen type I hydrogels have previously been used as 3D substrates for cell culture. However, their high content of water makes them extremely weak unless modified with other polymers or with the use of crosslinking approaches [206]. To overcome this problem, in 2005, Brown and colleagues established a new technic called plastic compression [205]. This method is based on the removal of unbound water from hyper-hydrated collagen gels using external mechanical loading and capillary fluid flow (Patent number WO2012004564) [205, 207]. It is an irreversible process as the thickness of the collagen structures remains stable once the fluid has been removed, meaning it will not return, recover or re-swell. Plastic compression improves TE mechanical properties; it is simple, fast, reproducible and allows individual parameter modification to tune TE properties. In the original method, hydrogels are compressed by placing the gel on top of nylon, stainless steel meshes, blotting filter paper and a load [208].

This method is also a way of getting collagen fibril densities in the order of natural tissues in a rapid and controlled manner [205, 209]. Plastic compression forces out much of the excess fluid trapped in the initial hyper-

hydrated gel, reducing the fluid content by 100–200-fold. Hyper-hydrated collagen has fibril densities 10-fold less dense than their natural equivalent, which leads to very different mechanical properties [210].

1.4.2.2. RAFT-TE evolution

RAFT-TE development is the result of several modifications to the plastic compressed method [205].

From the perspective of cell therapy, the initial protocols were not compliant to be used in a Good Manufacturing Practice (GMP) cleanroom facility [206]. While this method satisfied many of the criteria for an effective alternative to human amniotic membrane (which is not ideal due to its limited availability and biological variability), namely a simple method of preparation and good transparency, there was a significant disadvantage associated with it. Non-controlled fluid loss during compression and particle shedding as result of the manufacturing process and scalability meant this product was non-compliant with GMP standards and the production of multiple constructs at the same time was a challenge [206].

Together with TAP Biosystems, our industrial partner, a consistent method of fabrication compliant with GMP was developed [211]. The different stages of development are described in Table 4.

The original protocol from Brown and colleagues for plastic compression (Table 1.4A) was not suitable for clinical applications as the process was not tightly controlled. The compression was unconfined, which meant the final product had variable dimensions due to fluid loss in multiple directions, and it also had a high risk of aerosol and particulate production. To overcome these issues, two confined compression approaches were designed (Table 1.4B & C), where the collagen hydrogel was set and compressed using a custom-made cassette or a 12-well plate. This method reduced the risk of particle emissions and damage during handling as it was performed in a single container. It also involved a modification in the direction of fluid removal, from bottom to top, with filter paper or paper rolls. Lastly, the latest iteration (Table 1.4D) involved a change in the way the hydrogels are compressed, moving

from compression with absorbent paper and weights to hydrophilic porous absorbers (HPAs). This reduced preparation time, enhanced reproducibility and was a significant step towards GMP compliance [206].

Table 1.4– Summary of the iterations for TE production: **(A)** Original plastic compression process with application of a load for unconfined compression and downward fluid flow; **(B)** Individual cassette for upward confined compression method; **(C)** Confined compression with paper rolls in a 12-well plate with upward flow on application of a load; **(D)** Current RAFT process with hydrophilic porous absorbers (kit available from Lonza). Adapted from Levis *et al*.[206].

	Iterations	Fluid Removal Direction & Method	Confined or Unconfined	Absorbent Material	Design	Hardware
A	**Plastic Compression**	Downward Compression with load	Unconfined	Filter paper	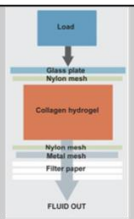	N/A
B	**Early RAFT**	Upward Compression with load	Confined	Filter paper	N/A	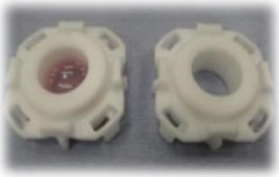
C	**Mid RAFT**	Upward Compression with load	Confined	Filter paper rolls	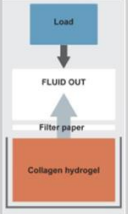	
D	**Late RAFT**	Upward Absorption	Confined	Hydrophilic porous absorber	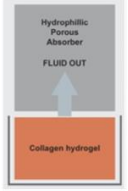	

1.4.3. RAFT-TE: focus on manufacturing changes

Previous work from our group [164] has demonstrated that compressed collagen hydrogels can support not only the expansion of LESCs but also support the formation of a multi-layered epithelium. However, from the perspective of cell therapy, this protocol was still not fully compatible to use in a Good Manufacturing Practice (GMP) cleanroom facility [206].

Some issues still need to be addressed. Modification to the protocol to achieve GMP compliance was one aims of this project, including the use of:

- Neutralising solution instead of Sodium hydroxide – a change in the manufacturing protocol towards its standardisation;
- *Koken Co. Ltd.* bovine skin collagen instead of *First Link* (UK) Ltd. rat tail collagen – a change in the protocol to comply with GMP standards for clinical applications;
- Reduction of collagen solution volume from 2.4mL to 0.6mL, which also influences the compression time – a protocol modification to achieve transplantable tissue equivalents for clinical applications rather than modelling the cornea in a dish;
- Different cell seeding methods: to avoid the use of murine 3T3 fibroblasts for *in vitro* expansion of LESC due to its associated risks, and to test the effects of co-culturing LESCs with CSSCs.

1.5. Hypotheses, Aims and Objectives

Hypothesis:

"CSSC can be used in the development of tissue engineering strategies for corneal repair."

Aims & Objectives:

The main aim of this thesis was to optimise the production of CSSC-populated RAFT-TE. To accomplish this, the work was divided into five parts with the following objectives:

i. **To identify the location of the best yield for the isolation of CSSC.** For this, novel imaging techniques based on tissue clearing methods were developed, optimised, and tested using different

microscopy units. This is of importance due to the clinical relevance to target future biopsies.

ii. **To further characterise CSSC isolated from the limbal stroma.** This was done by culturing CSSC, prompting them to differentiate towards the keratocyte phenotype and then comparing them with hMSCs and cells from the central cornea itself. It is important to understand CSSC phenotype before embedding them in RAFT-TE.

iii. **To evaluate how changes in the manufacturing process might affect RAFT-TE properties.** This work consisted of validation tests to compare RAFT-TEs manufactured with non-GMP compliant *First Link* collagen and GMP compliant *Koken* collagen. This is of importance to understand the differences in cell behaviour that might happen due to manufacturing changes.

iv. **To investigate the effect of changes on RAFT-TE production and cell seeding approaches in the development of an ATMP for ocular surface reconstruction.** Different RAFT-TEs were produced in order to independently track the effect of the manufacturing changes. LESCs alone and together with CSSCs were cultured under different conditions and seeded on top of RAFT-TE to investigate the TE capability of supporting LESCs.

v. **To investigate the feasibility of utilising CSSC, or keratocytes differentiated from CSSC, to develop an organised corneal stromal TE in compliance with GMP.** This was achieved by manipulating the genotype and phenotype of stromal cells derived from the human limbus, and by culturing them under different conditions inside RAFT-TE always with a view to optimising future therapeutic delivery.

Chapter 2

2. GENERAL MATERIALS AND METHODS

2.1. Isolation and culture of human corneal stromal stem cells in 2D

2.1.1. Corneal rim dissection

Human corneas were obtained from the Moorfields Lions Eye Bank (Research Ethics Committee – UK - reference no. 10/H0106/57-11ETR10). The tissue was washed 3 times in a mixture of Dulbecco's modified Eagle's medium - DMEM (high glucose, Sigma) and DMEM/F12 (Sigma) supplemented with 50 μg/mL gentamicin (Gibco, Life Technologies, Paisley, UK) and Penicillin-Streptomycin solution (Gibco, Life Technologies, Paisley, UK). The superficial corneal limbal region was dissected and cut into small fragments that were subsequently digested in the same media plus collagenase type L (0.5 mg/mL; Sigma-Aldrich) and incubated at 37ºC overnight.

2.1.2. Co-culture of CSSC and HLE in 2D

The digestion of limbal fragments by collagenase releases all cells from the tissue. Therefore, primary stromal cells were first seeded as a mixed population (containing LESCs and CSSCs) into T25 flasks coated with fibronectin-collagen (FNC; Athena Enzyme System, Baltimore, MD, USA). The cells were cultured in a humidified atmosphere containing 5% CO_2 in air plus CSSC medium [114] consisting of a mixture of DMEM low glucose (Gibco, 10567, Life Technologies) and MCDB-201 (Sigma-Aldrich, M6770) medium, supplemented with 2% foetal bovine serum (Invitrogen, 16000044, Life Technologies, Paisley, UK), 10 ng/mL epidermal growth factor (Sigma-Aldrich,

E9644), 10 ng/mL platelet-derived growth factor (PDGF-BB; R&D Systems, D520-BB, Abingdon, Oxford, UK), Insulin- Transferrin-Selenium (ITS) solution (Gibco, 414-045, Life Technologies), 0.1 mM ascorbic acid-2-phosphate (Sigma-Aldrich), 10-8 M dexamethasone (Sigma-Aldrich, D4902), penicillin-streptomycin solution (Corning CellGro 30-002-C1), 50 ug/mL gentamicin (Gibco, 15750-060, Life Technologies), and 100 ng/mL cholera toxin (Sigma-Aldrich, C8052,). This medium was changed every two days, and the cultures were not allowed to reach confluence. The cells were trypsinised and sub-cultured when colonies of small polygonal cells were visible.

2.1.3. Expansion of CSSCs

After 2 to 3 days in culture, Tryple express enzyme (Invitrogen, Paisley, UK) was applied to the mixed population of cultured limbal cells including LESCs and CSSCs for 2 minutes at room temperature (RT). This process selectively released CSSCs from the mixed population which were then re-plated (on pre-coated flasks with FNC Coating Mix). The CSSCs used for experiments had undergone passaging up to a maximum of six times.

2.2. Cryopreservation and recovery of CSSCs

Cells were trypsinised and centrifuged before being re-suspended in cryopreservation medium, which consisted of 70% CSSC media, 20% FBS and 10% dimethyl sulfoxide (DMSO). Directly after the transfer of the cells into the cryopreservation medium (1 million cells/ml - approximately one T225 flask in 3 vials), the samples were cooled in a controlled-rate (-1ºC per minute) freezing container (Nalgene) to -80ºC and then transferred to liquid nitrogen and stored at -196ºC. To recover the cells, vials were thawed at RT before being re-suspended in CSSC media and seeded into cell flasks pre-coated with FNC.

2.3. Differentiation of CSSCs into Keratocytes

CSSCs at passage 5 were cultured for 3 weeks in keratocyte differentiation

medium (KDM) consisting of Advanced DMEM (Sigma-Aldrich), 10 ng/mL fibroblast growth factor (Sigma-Aldrich), 0.1 mM L-ascorbic acid-2-phosphate (Sigma-Aldrich), 50 ug/mL gentamicin (Invitrogen), Penicillin-Streptomycin solution (1×; Corning) and GlutaMAX (1×; Invitrogen, Life Technologies). Media was replaced every 2 - 3 days. This cell culture condition is referred to as 'KDM' over the course of this thesis.

2.4. Spontaneous differentiation of CSSCs in CSSC media

CSSCs at passage 5 were cultured for 3 weeks in CSSC medium. Media was replaced every 2 - 3 days. This cell culture condition is referred to as 'Diff' over the course of this thesis.

2.5. Isolation and Culture of Limbal Epithelial Cells

Limbal biopsies were dissected from corneal rims and transferred separately into a solution containing 1.2 U/mL dispase II (Roche diagnostics GmbH, Mannheim, Germany) in corneal epithelial cell culture medium (CECM) containing a 1:1 ratio of DMEM:F12, 10% (v/v) fetal bovine serum, 100 U/mL penicillin, 100 µg/mL streptomycin, 0.25 µg/mL Fungizone, epidermal growth factor (EGF) 10 ng/mL (Life technologies, Paisley, UK), hydrocortisone (0.4 µg/mL), insulin (5 µg/mL), adenine (0.18 mM), transferrin (5 µg/mL), T3 (2 nM), cholera toxin (0.1 nM) (Sigma-Aldrich, Dorset, UK). The tissue was incubated o/n at 4°C. LESCs were isolated by gently scraping the epithelium using rounded forceps. LESCs were then pre-expanded in T25 flasks on a 3T3 feeder layer that had been previously growth arrested with 4 µg/mL mitomycin C (Sigma-Aldrich, Dorset, UK) for 2 hours. CECM culture medium was changed three times a week and the co-cultures maintained at 37°C in a humidified atmosphere containing 5% CO_2 in air.

2.6. Cell morphology observation

Cell morphology was monitored during cell culture at specific time points using an inverted phase-contrast microscope (Nikon Eclipse TS100 inverted phase-contrast microscope, Nikon Instruments Europe B. V., Surrey, UK). Images were taken at different magnifications over time.

2.7. Immunocytochemistry of Human CSSCs

Cells were plated onto Nun Lab-Tek II Chamber Slides, cultured for 12h in CSSC medium and fixed with 4% paraformaldehyde for 15 minutes. Cells were then washed with PBS (Invitrogen, Life Technologies) and blocked for 1 hour in goat serum (5%) prepared in 0.25% Triton-X-100 for p63α (Cell Signalling Technology, Danvers, MA, USA), CD73 (Abcam, Cambridge, UK), CD90 (Abcam), PAX6 (Covance, Princeton, NJ, USA) and CK3 (Millipore) samples. 5% goat serum without Triton-X-100 was used to block samples for the ALDH1A1 (Abcam) staining. Samples were then incubated overnight at 4 °C with the primary antibodies p63α, CK3 (both 1:100 dilution), CD73 and CD90 (both 10 µg/ml concentration), PAX6 (1:70), ALDH1A1 (1:50), and Cy3-conjugated α-SMA antibody (1:200; Sigma-Aldrich). The day after, the samples were washed three times with PBS prior to 1h (RT, in the dark) incubation with the secondary goat anti-rabbit (except CD90, anti-mouse) 594 Alexa Fluor antibody (1:500 dilution; Invitrogen) and FITC-labelled phalloidin (1:1000 concentration; Sigma-Aldrich), which binds to the actin cytoskeleton. To visualize nuclei, samples were in Vectashield mounting medium containing 4′6-diamidino-2-phenylindole (DAPI; Vector Laboratories, Inc., Burlingame, CA, USA). Samples were viewed and analysed using a confocal Zeiss LSM 710 microscope (Zeiss, Cambridge, UK).

2.8. Gene expression

2.8.1. RNA extraction from cells in 2D

The RNeasy micro kit from Qiagen was used to extract the RNA from cells cultured on tissue culture plastic (TCP). As per manufacturer instructions, the cell suspension was centrifuged for 5 min at 1000xg, the supernatant removed, and the pellet resuspended in 350µL of RLT buffer with 10µL/mL of β-mercaptoethanol (Sigma-Aldrich). Cell lysates were stored at -80°C until needed. Then, the lysates were rapidly thawed at 37°C, loaded into a Qiashredder column (Qiagen) and centrifuged 2min at 13000xg. An equal volume of 70% EtOH (Fisher Scientific) was added to the cell lysate, mixed and placed in a RNeasy column. The nucleic acids bound to the column and the flow was discarded (30s at 10000xg). The column was washed with 350µL of the RW1 buffer and centrifuged for 30s at 10000xg. The RNase free DNase kit (Qiagen) was used to ensure there was no DNA contamination. Briefly, 70µL of RDD buffer supplemented with 10µL of DNase enzyme were loaded onto the column and incubated for 10 min at room temperature to degrade the genomic DNA. The column was then washed once more with 350µL of RW1 buffer and twice with 500µL of RPE buffer. The column was then air-dried (5 min centrifugation at 13000xg) and the RNA eluted in 30µL of RNase free water.

2.8.2. RNA extraction from cells in 3D

The RNA extraction of the cells cultured inside 3D matrices was performed using a modified version of the protocol described above. The RAFT-TEs or the Gels were first placed in 500µL of Trizol, followed by a 10min incubation at RT to allow the collagen to dissolve and several ‘up and down’ cycles to disrupt the collagen matrix before moving the solution to an Eppendorf. The remaining traces of collagen were disrupted by vortexing the solution. For 500µL of Trizol, 0.1mL of chloroform was added to the Eppendorf. This was shaken vigorously by hand for 16s and then incubated for 2min at RT. The samples were then centrifuged at 12000xg for 15min. After this step, the samples displayed three distinct phases: lower red, phenol-chloroform phase (organic: proteins, lipids), an interphase (DNA), and a colourless upper aqueous phase (RNA). The aqueous phase containing the RNA was transferred to a new Eppendorf and half of its volume of 100% isopropanol added to the sample. The solutions

were mixed well and kept overnight at -20°C to allow the RNA to precipitate. The next day, the solution was placed into a RNeasy mini column, and the protocol was followed as in the 2D cell culture isolation.

2.8.3. RNA extraction from tissue

Fresh central cornea dissected from a whole eye and cut into small pieces using a scalpel. The sample was placed on ice in a 1.5 mL Eppendorf and 350 µL of lysis buffer (RNeasy mini kit, Qiagen) were added to it. The sample was sonicated for approximately 1 min to help with tissue dissociation. This process was finalized by repeated sets of up and down pipetting. The sample was then centrifuged at 13000 g for 5 min and the resulting supernatant was added to a Qiashredder column (Qiagen). The protocol was continued as described below.

2.8.4. Assessment of RNA purity and concentration

Before reverse transcription, the concentration of RNA was assessed by analysing 1 µL of RNA solution using a Nanodrop spectrophotometer (ThermoFisher Scientific). The 260/280 and 260/230 absorbance ratios indicate RNA purity. A 260/280 ratio lower than 2.0 indicates protein contamination in the sample and 260/230 ratio should be around 1.8 unless in the presence of contaminants from the isolation process, like phenols and guanodinium isothiocyanate.

2.8.5. RNA purification and concentration

RNA that was not within the standards of purification referred to above was purified using RNeasy MinElute Cleanup Kit (cat. no. 74204). Ethanol (250µL, 100%) was added to the diluted RNA and mixed well by pipetting. The sample was then transferred to a RNeasy MinElute spin column, placed in a 2mL tube, and centrifuged for 15s at 8000xg. The flow was discarded and 500µL of RPE buffer added to the spin column before it was centrifuged again for 15s at 8000xg to wash. Ethanol (80%, 500µL) was added, and the spin column was centrifuged for 2min at 8000xg. The RNeasy MinElute spin column was placed in a new collection tube and centrifuged at full speed for 5 min to dry the membrane. The column was placed in a new 1.5 ml collection tube, and 14µl

of RNase-free water added directly to the centre of the spin column membrane. Finally, the sample was centrifuged for 1 min at full speed to elute the RNA.

2.8.6. Reverse transcription

To compare different samples and donors, the RNA of all the conditions was diluted with molecular grade water to achieve the concentration of the lowest sample.

QuantiTect Reverse Transcription kit (Qiagen) was used to prepare cDNA as per manufacturer's instructions. Genomic DNA was removed by adding 2µL of gDNA wipe-out buffer to 12µL of RNA solution with a 2min incubation at 42°C. A mix of 1µL of the selected primer, 4µL buffer and 1µL of reverse transcriptase was added to the 14µL of solution. This solution was then incubated for 30 min at 42°C to activate the transcriptase and synthesize the cDNA. The reaction was stopped by raising the temperature to 95°C for 3min. The cDNA was stored at -20°C until further use.

2.8.7. Real time qPCR

qPCR was used to quantify relative gene expression. The reaction was prepared as follows: 10µL of Gene Expression Master Mix, 4 µL nuclease-free water, 1 µL of Taqman ™ assay (Table 2.1) and 5 µL of template cDNA were added to each well of a MicroAmp® Optical 96well Reaction Plate (Applied BiosystemsTM). The plate was then covered with MicroAmp® Optical Adhesive Film and centrifuged for 1 min at 1000g. A QuantStudioTM 6 Flex Real-Time PCR System was used for analysis with thermal cycling conditions set to 2 min at 50°C, 10 min at 95°C and 40 cycles of 15 s at 95°C and 1 min at 60°C. 18S ribosomal RNA was used as housekeeping gene. The fold increase was calculated using ΔΔCt method [212].

Table 2.1 - List of Taqman ™ assays used for Real time qPCR.

Taqman ™ assay ID			
CSSC Markers		***Keratocyte Markers***	
PAX6	Hs01088114_m1	KERA	Hs00559942_m1
CD90 (THY1)	Hs00174816_m1	LUM	Hs00929860_m1
CD73 (NT5E)	Hs00159686_m1	ALDH1A1	Hs00946916_m1
Epithelial Stem Cell Marker		***Differentiated Epithelial Cell Marker***	
p63 (TP63)	Hs00978338_m1	CK3 (KRT3)	Hs00365080_m1
Matrix Remodelling		***Matrix Production***	
MMP1	Hs00899658_m1	FN1	Hs01549976_m1
MMP2	Hs01548727_m1	COL1A1	Hs00164004_m1
Cell proliferation Marker		***Cell Migration Marker***	
KI67	Hs_01032443_m1	CDC42	Hs00741586_mH
Fibrosis marker		***Endogenous control***	
ASMA (ACTA2)	Hs00909449_m1	18s	Hs99999901_s1

2.9. RAFT-TE Manufacturing

2.9.1. *Koken* Collagen – Bovine Dermis

Bovine dermis type I native collagen (3 mg/mL Collagen Acidic Solution, IAC-30, *Koken*, Tokyo, Japan) was used either undiluted (3 mg/mL) or pre-diluted using 1 mM hydrochloric acid (HCl) to a final concentration of 2 mg/mL.

In a sterile specimen pot, 0.9 mL 10x Minimum Essential Medium (MEM, Invitrogen) were mixed with 7.4 mL of bovine dermis type I native collagen.

For the pre-diluted collagen samples (2 mg/mL solution), sodium hydroxide (5 M) was added dropwise to neutralise the solution to achieve a pH between 7.2 and 7.4. However, when using the collagen at the purchased

concentration, 3mg/mL, the solution was neutralised using 49 μL of neutralizing solution (Lonza RAFT™ kit – Sodium Hydroxide (NaOH) and HEPES).

Finally, 851 μL of CSSC media was carefully added, and the mixture was left on ice for 30 min to allow any air bubbles to disperse.

The collagen mixture was added into the wells of a 24 well plate (Greiner, Stonehouse, UK) in volumes of 0.6 mL, and heated to 37 °C for 30 min.

After crosslinking, hydrophilic porous absorbers (Lonza RAFT™ kit) were placed on the surface of the hydrogel for 30 min at 37 °C, as described in Figure 2.1.

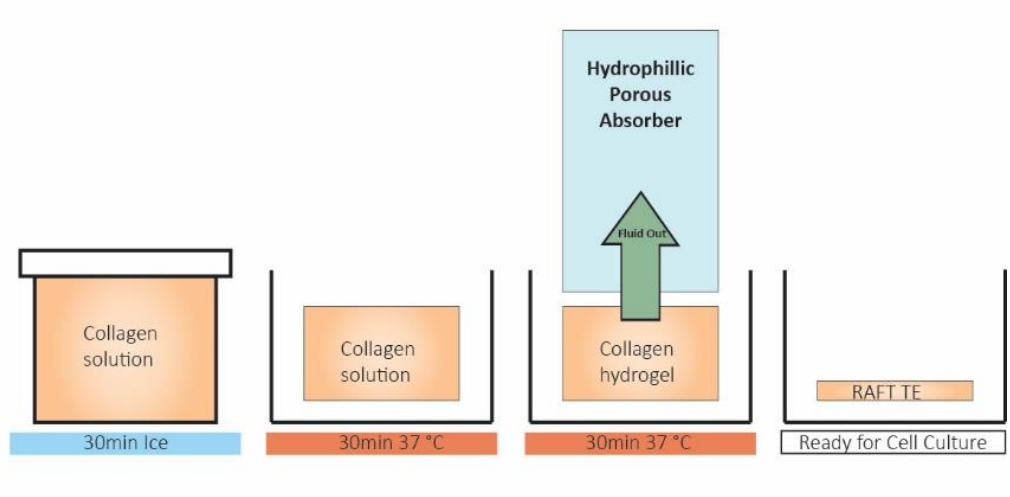

Figure 2.1 – Diagram of RAFT-TE preparation: setting and compression with HPAs

2.10. RAFT-TE Analysis

2.10.1. Scanning Electron Microscopy Analysis

RAFT-TEs were examined using scanning electron microscopy (SEM). Different protocols were tested to check which would have less impact in the TE structure, namely the use of fixative and osmium. First, different preparation protocols were tested to decide which one would affect less the structure of the TE. If cells had been present in the TE, the use of osmium would have been mandatory to promote cell contrast by lipid staining. The material properties were compared using fixed and non-fixed TEs in the

presence and absence of osmium. The RAFT-TEs containing cells were fixed with 4% paraformaldehyde for 30min and washed 3 times with PBS. Before processing, the samples were secondary fixed in 1% osmium tetroxide (FMB, Singapore), for 2 hours at room temperature and washed 3 times with PBS. Following this, samples were dehydrated in series of ethanol (50%, 70% & 90% and 2x 100%) for 10min, critical point dried (Bal-Tec CPD 030, Liechtenstein, Germany) and mounted on SEM stubs using carbon adhesive tabs. Finally, they were gold sputter coated (5 nm; Bal-Tec) and imaged with a field-emission SEM (Zeiss) at 3.5kV.

2.10.2. Light transmission measurements

Changes in the transparency of the TEs is an easy way to track the growth of HLE and of great importance when we are trying to make an artificial corneal tissue. Visible light is a portion of light in the electromagnetic spectrum. The established wavelength range of visible light is approximately 380 to 750 nm [213, 214]. The absorbance (350–900 nm) of light through RAFTs with 250 µl of PBS on top was measured using a spectrophotometer (SAFIRE, Tecan, Reading, UK). Absorbance readings were converted to percentage transmission [215] using:

$$\%\, transmission = 10^{-absorbance} \times 100$$

2.10.3. Fluorescein diacetate (FdA) staining

2.10.3.1. Fluorescein diacetate (FdA) staining to track RAFT Cell growth

The RAFT-TEs were stained with fluorescein diacetate (FdA) at different days during culture to assess the extent of epithelial cell growth on the surface. FdA is hydrolysed in live cells, and fluoresces in green under blue light excitation. With this staining, it was also possible to observe the distribution of cells entrapped within the matrix of RAFTs. RAFTs were washed with PBS prior to incubation with FdA (concentration=10µM) for 2mins in the dark at 37 °C and 5% CO_2. The solution was then removed, and the TEs were washed with PBS twice. Pictures were taken under a blue light source with a camera

previously set with a yellow filter. Next, RAFTs were washed with PBS and covered in CSSC media for further culture.

2.10.3.2. Fluorescein diacetate (FdA) quantification

The area of epithelial cell growth was calculated using Fiji image processing tools (Figure 2.2). Firstly, the background of the initial image (Figure 2.2A) was removed, and the bottom of the well selected (Figure 2.2B). Then, the region of interest (ROI) is automatically selected by the Fiji plugin, and the area of coverage (Figure 2.2C) was measured and plotted as a percentage of the well area.

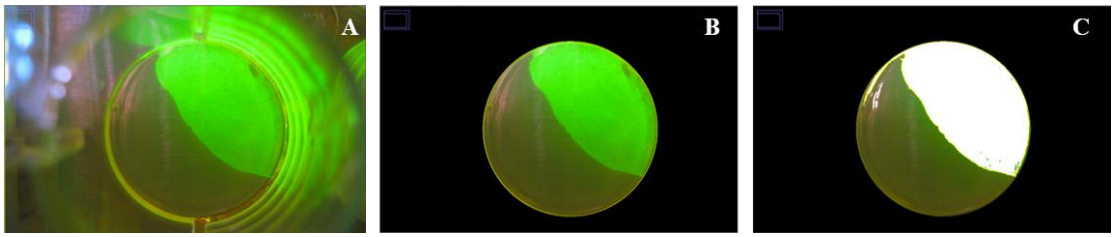

Figure 2.2 – Picture showing the Fiji steps for FdA quantification: **(A)** initial image, **(B)** background removed and **(C)** ROI selection.

2.10.4. Immunohistochemistry of RAFTs

The RAFT-TEs were analysed after 2 to 3 weeks in culture to assess the phenotype and morphology of the seeded cells. Different markers were used to track CSSCs, keratocytes and epithelial cells. RAFTs were fixed in 4% PFA for 30mins and then washed 3 times with PBS. Goat serum (5%) prepared in 0.25% Triton-X-100 was used to block samples for p63α (Cell Signalling Technology, Danvers, MA, USA), CD73 (Abcam, Cambridge, UK), CD90 (Abcam), PAX6 (Covance, Princeton, NJ, USA) and CK3 (Millipore). 5% goat serum without Triton-X-100 was used to block samples for ABCB5 (Novus Europe), anti-ALDH1A1 (Abcam) and Integrin Beta I (Millipore) staining. Samples were then incubated overnight at 4 °C with the primary antibodies p63α, ABCB5, CK3 (all 1:100 dilution), CD73 or CD90 (10 µg/ml concentration), PAX6 (1:70), Laminin (1:200) and Integrin Beta I or anti-ALDH1A1 (1:50). The primary antibodies were incubated o/n at 4 °C and then with the secondary goat anti-rabbit or anti-mouse 594 Alexa Fluor antibody (1:500 dilution; Invitrogen, UK) and FITC-labelled phalloidin (1:1000; Sigma-Aldrich, UK) for 1h at RT in the dark. Lastly, samples were mounted in

Vectashield mounting medium containing DAPI (Vector Laboratories Inc, CA) and observed using a confocal microscope (Zeiss LSM 710). For some of the experiments, the TE was cut in 8 pieces.

2.10.5. OCT# embedding and cryosectioning of RAFT-TE

RAFT-TE was cut in 8 pieces and rinsed twice with PBS before being transferred into cryomolds containing OCT# (optimal cutting temperature) compound. The samples were alternately oriented and dipped in liquid nitrogen until completely frozen. The blocks were stored at -80°C until required. They were then cut in 7.5μm thick cryosections using a Leica CM1850 cryostat (Leica microsystems, Milton Keynes, UK) and transferred onto superfrost plus microscope slides. The slides were dried at room temperature and then stored at -80°C until required for immunostaining.

2.10.6. Immunostaining of frozen tissue sections

Frozen sections were warmed for 20 min at RT, rinsed with PBS and fixed with 4% PFA (paraformaldehyde) for 10 min. Slides were washed 3x with PBS and cells were permeabilized with 0.5% TritonX-100 (to reveal intracellular antigens). Following permeabilization, slides were washed in PBS and blocked for 90 min in 5% goat serum. Sections were incubated with primary antibody - PAX6 (abcam), 10 µg/mL (abcam), 10 µg/mL CD73 (abcam), 1:20 LUM (Sigma), 1:50 KERA (Sigma), 1:500 ALDH (Abcam) - in 5% goat serum PBS (wet chamber at 4°C, o/n). Sections were washed 3x in PBS and incubated with secondary antibody and/or counterstained with FITC conjugated phalloidin (1/500) in 5% goat serum in PBS for 1 h at RT. Slides were washed 3x with PBS and mounted using Vectashield medium with DAPI (Vector laboratories Ltd. Peterborough, UK).

2.11. Statistical Analysis

Statistical analysis of results was carried out using Prism 4.0 software (GraphPad, USA). Different tests were performed according to the experiments and are detailed in the results section. Statistical significance was defined as $p<0.05$.

Chapter 3

3. LOCALISATION AND CHARACTERIZATION OF CORNEAL STROMAL STEM CELLS

3.1. Introduction

The stroma is a transparent, highly organized connective tissue that represents more than 90% of the cornea. Structurally, it is essentially a collagen matrix sparsely populated by quiescent cells, the keratocytes. Corneal stromal stem cells (CSSCs), the progenitor cells of keratocytes, were first identified in 2005 by Funderburgh JL *et al.* [114, 115]. Multiple studies have since recognized their potential for cell therapies, not only due to their immunomodulatory characteristics, but also due to their capacity to differentiate into keratocytes [112].

The overall aim of this project was to use tissue engineering approaches to develop methods for the delivery of CSSCs to patients. Therefore, the identification of the optimal anatomical location from which to harvest a limbal biopsy for CSSC isolation and expansion was of great importance. It was hypothesized that the optimal anatomical location for CSSC biopsy harvest is the limbal crypt (LC)-rich region of the human limbus due to the close proximity with LESCs. However, further analysis of this region was required to confirm this. For example, CSSC location and density can be quantified and compared by immunohistochemistry of tissue sections of LC-rich and non-LC human limbus. However, the 3D location of putative CSSC and the opportunity to observe cell-cell interactions in the human limbus is lost. Thus, part of this chapter focussed on the development and optimization of a protocol based on the iDISCO (immunolabeling-enabled three-Dimensional Imaging of Solvent-Cleared Organs) [216] and PACT (Passive Clarity Technique) [217]

techniques to allow immuno-labelling of the all structures of interest by volume imaging. This technique overcomes the limitations of light scattering by making the tissue transparent. It has been mainly applied in the study of the brain and nervous system [102]. Due to the novelty of this technique, there were very few facilities with the optimal set ups to image these samples, which proved to be an enormous challenge for this project.

A collaboration between our group and Funderburgh's group (Pittsburgh, USA) enabled knowledge transfer with regards to the culture of CSSCs *in vitro*. However, these cells required characterisation in our lab using the donor tissue available in the UK. Different policies in eye banking of research tissue at Moorfields Lions Eye bank, when compared to other sites such as the USA meant that the tissue availability was much lower and the tissue much older both in terms of age and post-mortem time. Additionally, Moorfields Eye Bank mainly uses organ culture media and not Optisol (cold storage), which is the one used in the USA. These differences in time and storage conditions might affect the phenotype of the cells populating the tissue. By the time the corneal rims were donated to the laboratory, they were three to six weeks post-mortem, which could mean that the cells obtained were already more differentiated before isolation than the ones obtained from younger and fresher tissue.

Mesenchymal stem cells (MSCs) have been extensively studied due to their potential in the development of cell therapies (e.g. corneal stromal repair), wound healing capacity and anti-inflammatory properties [218, 219]. In a nutshell, MSCs have been reported to be multipotent, self-renewing adult cells with the potential to differentiate into multiple lineages *in vitro* [107]. CSSCs have previously been defined as MSCs but no multi-lineage differentiation data was available in the literature at the time of this study. This chapter investigated CSSCs differentiation potential towards adipocytes, osteoblasts, and chondrocytes in order to confirm isolation of the population of interest.

CSSCs were also characterized by their expression of MSC markers including CD73 and CD90 (specific surface antigen markers) [107] and keratocyte lineage potential differentiation by RT-qPCR. In this study, PAX6 loss was also used to identify CSSCs differentiation since it is a transcription

factor crucial for ocular development that is present in most embryonic ocular tissues but not on keratocytes [115]. Furthermore, additional markers were chosen to assess the CSSC differentiation potential into keratocytes which are highly enriched in specific proteoglycans including lumican and keratocan [220, 221] and corneal crystallins such as aldehyde dehydrogenase A1 [16].

Taking into consideration that CSSC are isolated from a mixed population containing LESCs, within this study, p63 was used to identify LESC contamination. The p63 gene supports proliferation and regulation in epithelial cells. In 2001, Pellegrini *et al.* [53] reported p63 as a keratinocyte stem cell marker and since then it has been used as a putative stem cell marker in limbal and cultivated corneal epithelial cells. It has diverse isoforms, but ΔNp63 has proved to sustain the proliferative potential of LESCs. Previous studies have identified CK3 as a marker for differentiated corneal epithelium [50, 60]. This marker was also assessed in order to exclude any epithelial contamination from the isolated cell population.

CSSCs can differentiate into keratocytes that might become activated due to the extracellular environment. Inflammation caused by ocular injury can drive the differentiation of corneal keratocytes into activated fibroblasts, and consequently α-smooth muscle actin (αSMA)-expressing myofibroblasts through TGF-β release [222, 223]. Limbal fibroblasts (hLF) stimulated with TGF-β were used as a positive control for αSMA (ACTA) expression (Figure S3.2) as a way to check whether the cells differentiated towards the keratocyte lineage were transitioning into a corneal fibroblast or myofibroblast phenotype [224].

In summary, it was hypothesized that:

1. Tissue clearing would allow volume imaging of the corneal rim.
2. The optimal anatomical location from which to harvest a limbal biopsy for CSSC isolation and expansion is the LC-rich limbus based on the number of cells per volume.
3. CSSC yielded from LC-rich limbus would show hMSC properties, no expression of keratocyte markers (undifferentiated-like features)

and the ability to differentiate towards the keratocyte lineage under the appropriate conditions.

3.2. Aim

This chapter aimed to:

- Develop novel imaging techniques for CSSC localisation using tissue clearing methods.
- Characterize the stem cell population isolated from the limbal stroma in comparison to human mesenchymal stem cells (hMSCs), and the central cornea itself.

3.3. Materials and Methods

3.3.1. Whole globe dissection & sample preparation

The eye was oriented based on the optic nerve and ocular muscles. The globe was then placed on a Petri dish and with the help of forceps and scissors most of the conjunctiva, fat and muscle tissue was removed. Using a scalpel, a cut was performed on the top and, with a pair of sharp scissors, a cut was performed through the middle of the eye separating it in its anterior and posterior parts. The vitreous humour was then removed by tilting the side of interest (anterior). The lens and the iris were also removed by gently peeling them away from the cornea. When the orientation of the eye was impossible or dubious, microscopic analysis was performed as seen on Figure 3.1 to identify the limbal crypt-rich regions.

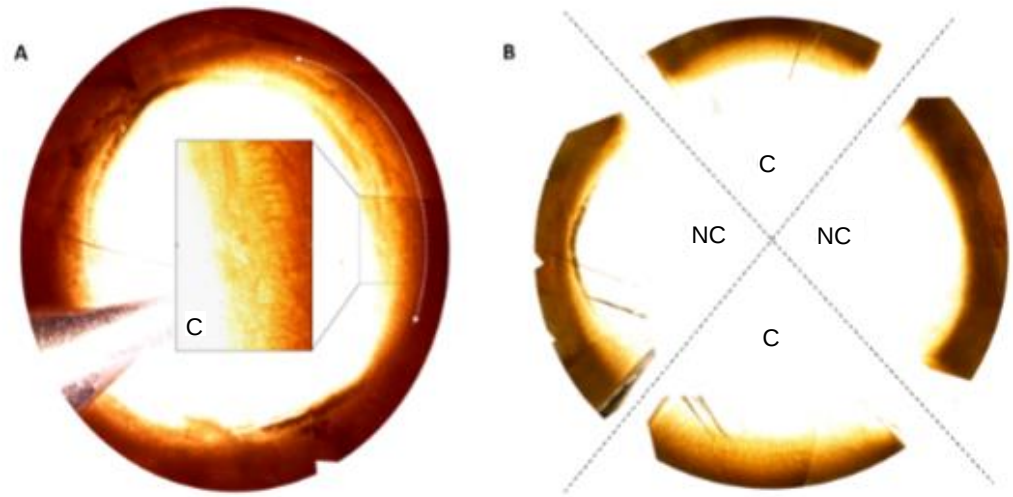

Figure 3.1 – Montage of optical microscopy tiles showing the presence of crypts. This method allows us to distinguish crypt (C) and non-crypt (NC) regions when the orientation of the rim cannot be performed. **(A)** Circular montage of the whole rim with zoom in a crypt rich area, **(B)** Example of the division of a rim based on crypt presence. Raw images in Figure S3.1.

3.3.2. Cornea tissue clearing

The two methods used to clear the corneal tissue are described below. In short, optimised versions of the iDISCO protocol, and the PACT method for corneal rim clearance.

3.3.2.1. Optimised protocol based on iDISCO [216]

The corneal rims were cut in half. After two hours of fixation overnight in 4% paraformaldehyde, the samples were washed twice in 0.2% Triton X-100 in PBS for 1 hour at room temperature. The samples were then incubated in 0.2% Triton X-100/20%DMSO in PBS at 37° C o/n, and then moved to 0.2% Triton X-100/20%DMSO with 0.1%Deoxycholate/0.1%NP40/20%DMSO o/n at 37° C. This was followed by two washes in 0.2% Triton X-100 in PBS at RT. The samples were blocked in 1xPBS/0.2%TritonX-100/10%DMSO/6% Goat Serum, at 37° C o/n, and washed twice in 1xPBS/0.2%Tween-20 with 10 μg/ml heparin (PTwH), for 1h at RT. The rims were incubated with primary antibody in PTwH/5%DMSO/3% Goat Serum, at 37° C for 4 days, where the antibody

solutions were replaced every day. This was followed by a series of washes in PTwH for 10 min, 15 min, 30 min, 1 h, and o/n. The sample was then incubated with the secondary antibody in PTwH/3% Goat Serum, at 37° C for 3 days, and the antibody solution replaced every day. The samples went through another series of washes in PTwH for 10 min, 15 min, 30 min, 1 h each, and then o/n, followed by an incubation (o/n) in 50% Tetrahydrofuran/H_2O (THF, Sigma 186562-12X100ML) in a glass vial with a silicon coated cap (Thermo Scientific C326-0020). Finally, the samples were incubated for 1 h in 80% THF, and 2h 1hin 100% THF. To end, an incubation in Dichloromethane (DCM, Sigma 270997-12X100ML) was performed until the sample sunk to the bottom, and in DiBenzyl Ether (Sigma 108014-1 KG) until the sample cleared.

Figure 3.2 highlights the main steps of the iDISCO process: solvent dehydration, solvent clearing to remove the lipids, and RI matching. A table summarising this protocol can be found in the appendix (Table S3.1).

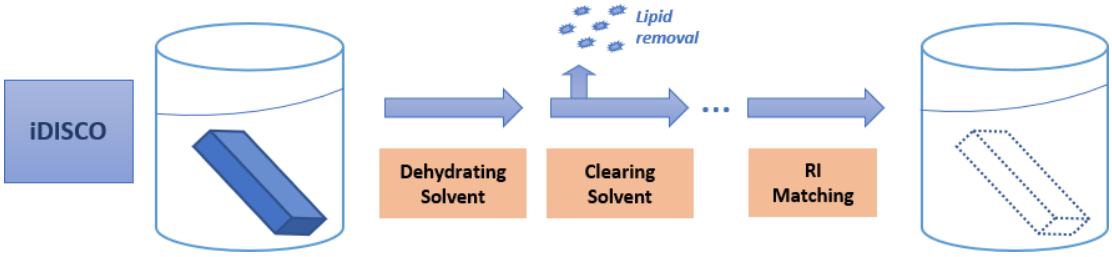

Figure 3.2 – Representative image of the main steps of the protocol for corneal tissue clearing based on iDISCO

3.3.2.2. Optimised protocol based on PACT (Passive Clarity Technique) [217]

The corneal rims were cut in half. After two hours of fixation overnight in 4% paraformaldehyde, the samples were incubated o/n at 4°C in Acrylamide - hydrogel monomer solution A4P0 (4% acrylamide in PBS) supplemented with 0.25% photoinitiator 2,2′-Azobis[2-(2-imidazolin-2-yl) propane] dihydrochloride (VA-044, Wako Chemicals USA). A4P0-infused samples were degassed with nitrogen (Rival R44, gas) for 5 min and then incubated for 2–3 h at 37°C to initiate tissue-hydrogel hybridization. The excess of hydrogel was removed via brief PBS washes, and the samples were left in PBS o/n.

Tissue-hydrogel matrices were transferred into 50 ml conical tubes containing 8% SDS (Sigma L4509) in 0.1 M PBS (pH 7.5), and depending on tissue size, were incubated for 5 days at 37°C with shaking. PACT-processed samples were washed in PBS with 4–5 buffer changes over the course of a day, and left in PBS o/n. The samples were transferred to a buffer containing primary antibodies (1:10 for 1st day and then 1:50, in PBS containing 2% goat serum, 0.1% Triton X-100 and 0.01% sodium azide) for 4 days. The antibody solutions were replaced every day, and the unbound antibody was removed via PBS washes. The rims were incubated with secondary antibodies (1:100, To-Pro 1:5000) for 3 days, with the antibody being replaced every day. The samples were washed o/n in PBS and incubated in imaging media (RIMS). Finally, the rims were placed in Histodenz, and mounted in a slide with 2 '1.0mm spacers' (Fastwell, Grace Bio-labs GBL66411350EA), dental cement and a rounded coverslip

Figure 3.3 highlights the main steps of the PACT protocol: hydrogel embedding, ionic detergent immersion to remove the lipids, and RI matching. A table summarising this protocol can be found in the appendix (Table S3.2).

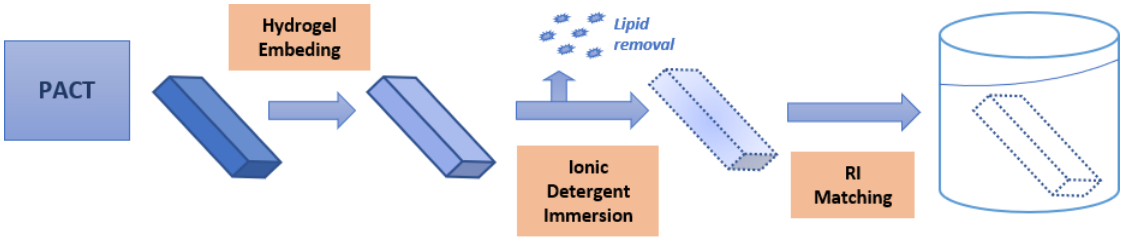

Figure 3.3 – Representative image of the main steps of the protocol for corneal tissue clearing based on PACT

3.3.2.3. 3D Imaging

The 3D whole-mounts of the corneal tissue cleared were imaged using multiple microscopes including Leica SP8 and Zeiss Z1 Lightsheet. As optimisation was required, further details regarding the tissue analysis can be found on the results section. The data acquired was rendered using Imaris software both for 3D reconstruction, stitching of tiles and video construction.

3.3.3. Isolation and culture of human corneal stromal stem cells in 2D

Corneal rim dissection, and CSSC culture was performed as described in section 2.1. in Chapter 2.

3.3.4. Immunocytochemistry of Human CSSCs

Cells were stained as described in section 2.7. in Chapter 2.

3.3.5. Culture of hMSCs

Bone marrow derived human mesenchymal stem cells (hMSCs) were purchased from Axol (ax9002, UK). The hMSCs were initially plated at a cell density of 5,000 cells/cm^2 in MSC Expansion Media for Bone Marrow Derived MSCs (Axol, ax9006) with the first media change taking place after 24h and every 2-3 days thereafter. Cells were grown in T-flasks seeded in a humidified atmosphere at 37 °C in air containing 5% CO_2 and passaged at 70-90% confluence.

3.3.6. Cell morphology observation

Cell morphology was monitored as described in section 2.6. in Chapter 2.

3.3.7. Tri-lineage Differentiation

hMSC differentiation was induced using Axol pre-prepared differentiation mediums: MSC Osteogenesis Medium (ax9010), MSC Chondrogenesis Medium (ax9009), and MSC Adipogenesis Medium (for Bone Marrow Derived and Umbilical Cord Derived MSCs, ax9019). CSSCs and hMSCs were plated at specific densities: osteogenic differentiation – 47.500 cells/well in a 6-well plate, adipogenic differentiation – 190.000 cells/well in a 6 well plate and chondrogenic differentiation – 250.000 cells per 15 mL tube (pellet culture). The cells were kept in their control media for 16h and then washed with PBS and kept in the differentiation media for 21 days. The cell monolayers media was changed every 3 days and chondrogenic pellets every other day.

After 21 days, the differentiation media was removed, and cells were processed accordingly to the different staining protocols.

3.3.8. Assessment of lineage differentiation

For the following procedures, it is important not to let the cell samples dry for more than 30s.

3.3.8.1. Adipogenic: Oil Red O staining

Oil Red O stains intracellular lipid vesicles bright red. This staining was used to access hMSC differentiation into mature adipocytes. After 21 days of differentiation in adipogenic media, the cell layer was washed in DPBS and fixed for 30 min in 10% formalin. Oil Red O stock solution was prepared by adding 150 mg of oil red powder (Sigma, O0625-25G) to 50mL of 99% isopropanol. Then, 3 parts of the stock solution were mixed with 2 parts of deionized water and allowed to sit at RT for 10min before it was filtrated (working solution). The formalin was removed from the cell culture plates and the wells were gently rinsed with sterile water. The cell monolayer was then incubated with 60% isopropanol for 3 min before the working solution of oil red was added to the samples. After 5min of incubation, the wells were rinsed with tap water until it run clear. Haematoxylin counterstain was added to each well and incubated for 1 min before the plate was rinsed again. The samples were kept in PBS until imaged.

3.3.8.2. Osteogenic

Alizarin Red S staining

Alizarin, a bright orange-red dye, is used to detect extracellular calcium deposits produced by osteoblast (differentiated hMSCs). After 3 weeks in differentiation media, the cells were carefully washed with PBS w/o Ca^{++}/Mg^{++} and fixed with formalin for 30 min. Alizarin Red S staining solution was prepared by dissolving 2 g of Alizarin Red S (Sigma, A5533-25G) in 100 mL of distilled water. This solution was filtrated and added to the cells after a wash in distilled water. The cell layer was incubated for 15 min, in the dark. The Alizarin Red S solution was then aspirated, and the cell monolayer was washed four times in distilled water. The samples were imaged in PBS using a light microscope.

BCIP/NBT staining

BCIP/NBT can be used as a substrate to stain cells blue-violet when in the presence of alkaline phosphatase (AP). Differentiated osteoblasts feature a high AP activity, therefore this test can be indicative of successful differentiation of hMSCs into the osteogenic lineage. BCIP/NBT (SigmaFast^{TM} BCIP-NBT, Sigma Aldrich) was dissolved in 10mL of distilled water. After 3weeks in differentiation media, the cells were carefully washed with PBS and fixed with 10% formalin for 1min. The monolayer was then washed with 0.05% Tween 20 in PBS w/o Ca^{++}/Mg^{++} before the BCIP/NBT substrate solution was added to cover the monolayer and incubated for 10min in the dark. The cell monolayer was then washed again with 0.05% Tween 20 in PBS w/o Ca^{++}/Mg^{++} and placed in PBS for imaging. A light microscope was used to record the results.

3.3.8.3. Chondrogenic: Alcian Blue staining

Alcian Blue, a dark-blue copper-containing dye, was used to detect a proteoglycan, aggrecan, in the cultured spheroids. The Alcian staining solution was prepared by dissolving 10mg of Alcian blue 8GX (Sigma, A5268) in a mixture of 98% ethanol (60 mL) and 98% acetic acid (40 mL). The distaining solution was prepared with 120 mL of 98% ethanol and 80mL of 98% acetic acid. The cartilage spheroids were washed twice in PBS w/o Ca^{++}/Mg^{++} and fixed for 1 h in 10% formalin. The spheroids were then washed twice in distilled water and covered in Alcian staining solution overnight, at RT, in the dark. The following day, the spheroids were washed in distaining solution for 10 min twice and kept in PBS until photographs were taken.

3.3.9. Differentiation of CSSCS Into Keratocytes.

CSSC differentiation into keratocytes was performed as described in section 2.3. in Chapter 2.

3.3.10. Isolation and Culture of Limbal Epithelial Cells

Isolation and culture of limbal epithelial cells was performed as described in section 2.5. in Chapter 2.

3.3.11. Isolation, culture and stimulation of hLF

Human limbal fibroblasts (hLF) were isolated from scleral–limbal rims. Biopsies were placed in explant culture with hLF culture medium (DMEM basal medium, 10% fetal bovine serum, 1% AA) in a humidified 5% CO_2 in air incubator at 37°C. Explant cultures were maintained until hLF outgrowth was observed before being passaged using 0.05% trypsin-EDTA. hLF were used up to passage 6. hLF were stimulated with TGF-β (10ng/mL).

3.3.12. Gene expression

Gene expression analysis was performed as described in section 2.8. in Chapter 2.

3.3.13. Statistical Analysis

Statistical analysis of results was carried out using Prism 4.0 software (GraphPad, USA). Different tests were performed according to the experiments and are detailed in the results section. Statistical significance was defined as $p<0.05$.

3.4. Results

3.4.1. Ocular Surface Tissue Clearing

3.4.1.1. Methodology and optimization of whole-tissue imaging of human limbus

Herein two methods that render intact whole corneal-tissue transparent for imaging are presented. Single-cell resolution is preserved, as well as tissue architecture.

Figure 3.4 presents the steps of sample handling through the clearing process. From the intact tissue (Figure 3.4A), to the observation of the sample at the end of the protocol in clearing media (Figure 3.4B), up to its physical appearance after the processing (Figure 3.4C). These three Figures (Figure 3.4A, B, C) show that it is possible to clear the sample without causing massive structural changes. Nevertheless, Figure 3.4C shows some shrinkage and hardening of the tissue after processing. Due to the considerable dimensions of the sample, two spacers on a coverslip were used to mount it, as shown in Figure 3.4D. Figure 3.4E shows the filling of the chamber with clearing media and Figure 3.4F the chamber closing with dental cement. Sample imaging was tested on a confocal microscope (Figure 3.4G) and imaging field tiles selected around the limbal region as seen in Figure 3.4H.

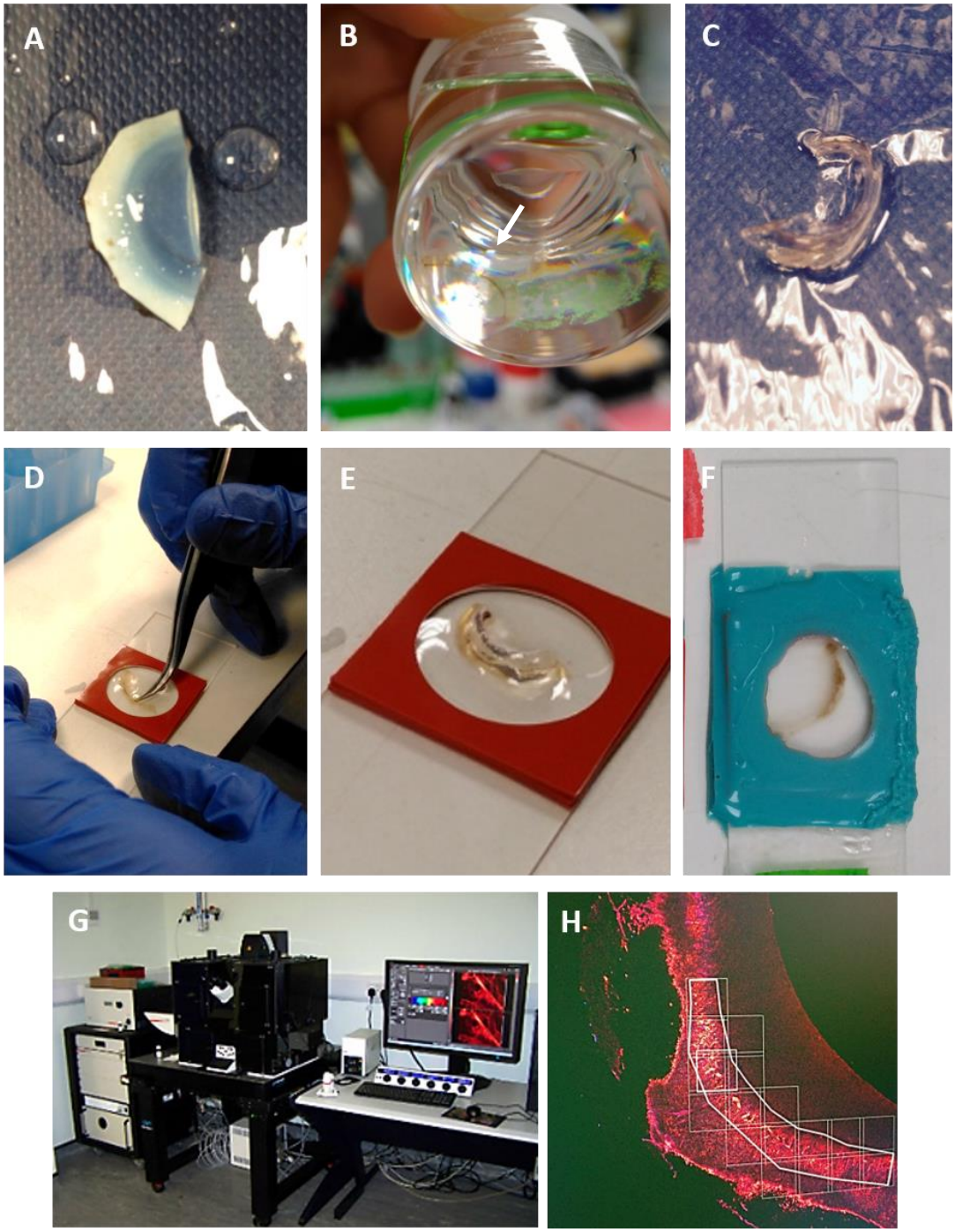

Figure 3.4 – Optimization of the protocol to clear and mount the corneal tissue: **(A)** Front surface of the eye cut in half; **(B)** Sample after processing in clearing medium; **(C)** Sample shape after processing (possible to observe some shrinkage and hardening of the tissue); **(D, E, F)** Steps towards sample mounting using spacers and dental cement to create a closed chamber, **(G)** Confocal microscope and **(H)** sample area selection for 3D imaging and tiles montage.

3.4.1.2. Preliminary results of tissue clearing protocol

A new method for 3D reconstruction of corneo-limbal wholemounts based on tissue clearing was developed as described in section 3.3.2. Initial experiments using this protocol showed it was possible to clear the tissue using both PACT and iDISCO techniques. The optimization works and challenges described below focused on the samples cleared using iDISCO.

Successfully cleared corneo-limbal samples were imaged under the confocal microscope and 3D reconstructed to check whether the process had affected tissue structure. Figure 3.5 (a) focuses on the limbal crypt region of the limbus while Figure 3.5 (b) shows a high density of focal stromal projections (FSP).

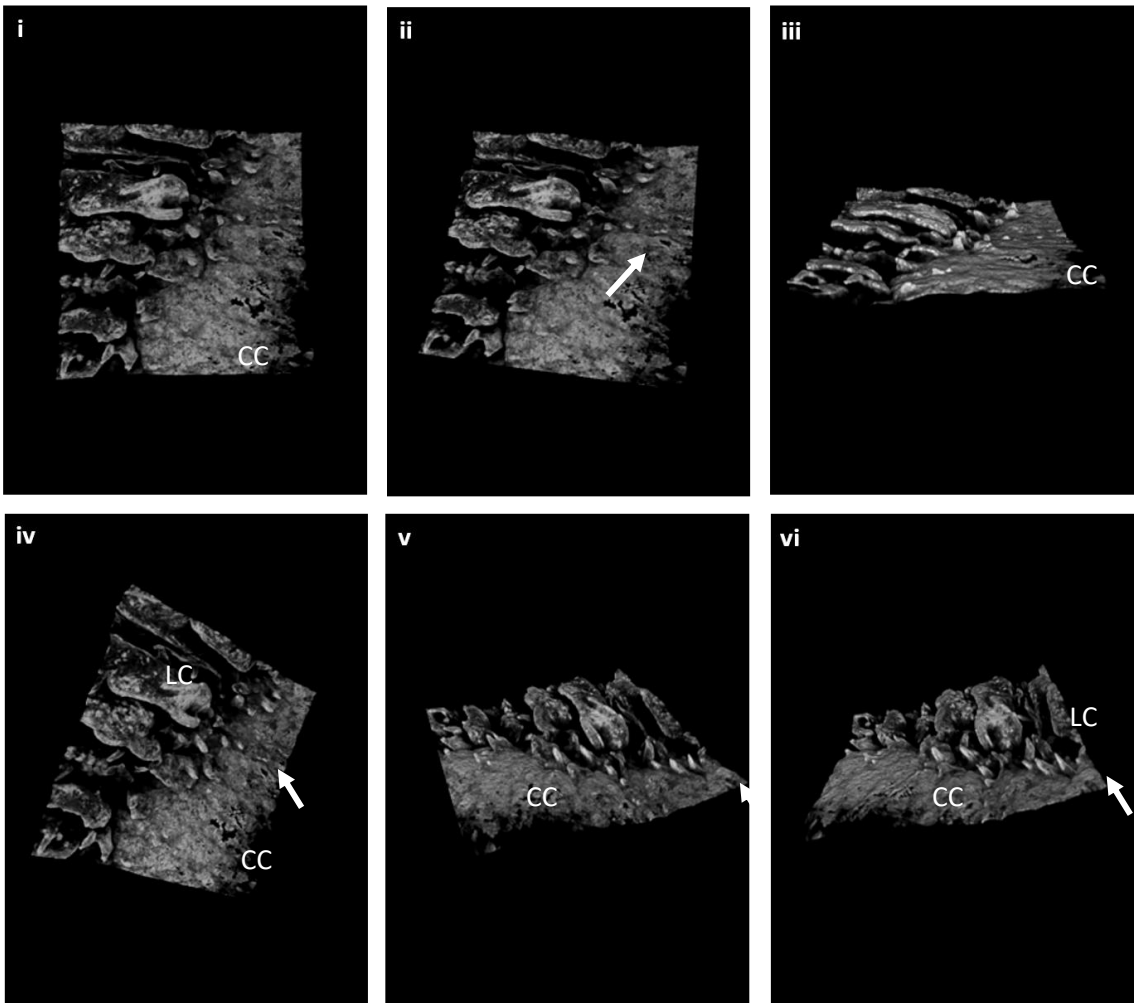

Figure 3.5 (a) – Enface view of part of a crypt-rich region of a whole-mount limbal corneal rim. Arrows on the image point at FSP. FSP are localized between the limbal crypts (LC) and the central cornea (CC). Figure i to vi are snapshots of a 3D reconstruction video.

Both Figures show six snapshots of a 3D video reconstruction (please see file Chapter 3 – VideoFig3.5). As shown in Figures 3.5 (a) & (b) the limbal niche

structures, limbal crypts (LC) and the focal stromal projections (FSP), preserved their original morphology. LCs preserved their invaginations looking into the stroma (Figure 3.5 a) and FSPs their upward finger-like projection morphology (Figure 3.5 b).

Both the LCs and the FSPs could be successfully reconstructed using Imaris software.

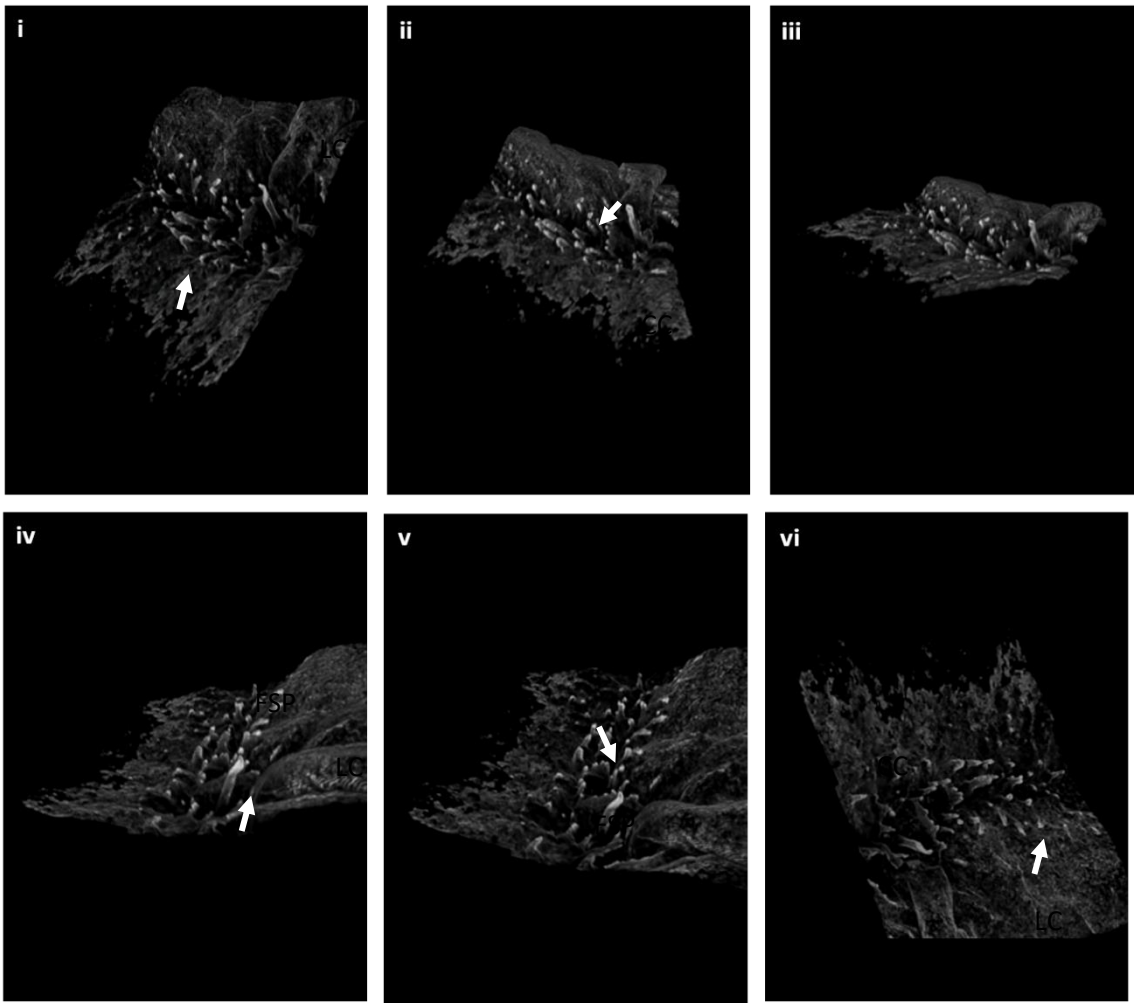

Figure 3.5 (b) –Whole-mount of corneal limbal region with focus on focal stromal projections (FSP). Arrows on the image point at a high density of focal stromal projections (FSP). For orientation purposes, the limbal crypts are marked as LC and the central cornea as CC. Figure i to vi are snapshots of a 3D reconstruction video.

Corneo-limbal tissue clearing was successfully achieved without compromising tissue architecture. However, confocal microscopy of the deceased human donor limbus demonstrated numerous technical problems: 1) as the sample is extremely big, using confocal microscopy meant it was necessary to do several z-plans as well as tile scans in order to be able to do

a 3D reconstruction. This proved to be extremely time consuming. If one wants to just scan a small area of the limbus, as in Figure 3.5, it can take between 1 to 2 h. However, larger scans like the one presented in Figure 3.6A, comprising around 1/16 of the circumferential rim, can easily surpass 6 h. This becomes problematic due to the bleaching and sample movement caused by excessive heating of the mounting solution (Figure 3.6A-D); 2). It is crucial to align the plane of optical sectioning with the tissue plane as well as carefully select the regions for tile capture. Since the samples must be kept in their respective clearing liquid, a chamber was created. However, this chamber assembly meant it was necessary to image through a very thick structure and that proved to be challenging using short working distance objectives (Figure 3.6 E & F). Some of the problems experienced can be observed on Figure 3.6 as the mismatch of the tiles after reconstruction (Figure 3.6D) or the problem faced on depth imaging and the objectives working distance and penetration (Figure 3.6 E& F).

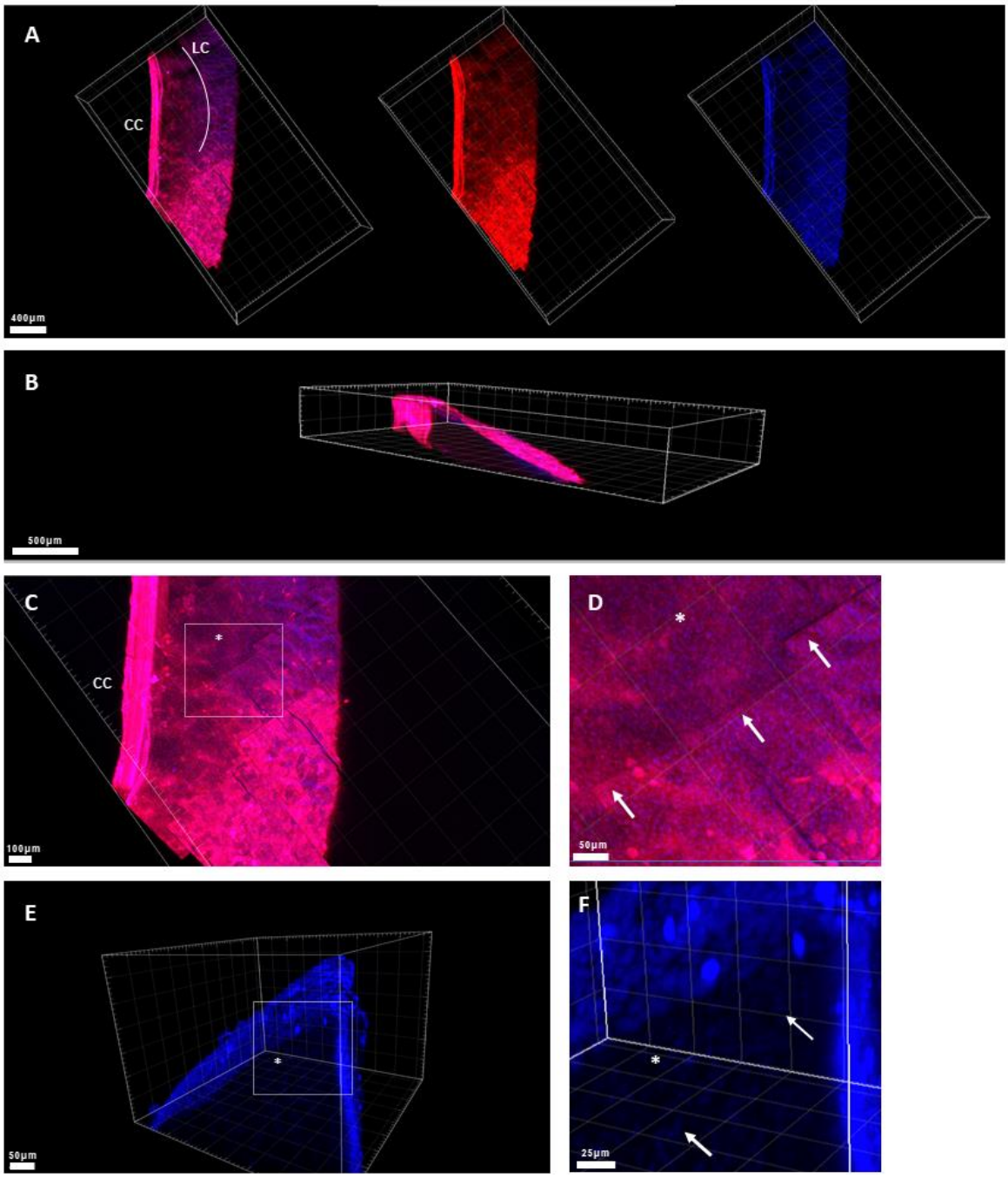

Figure 3.6 – Representative confocal images where the tissue was cleared using iDISCO technique: **(A)** 3D reconstruction of the limbal region; **(B)** Side view of corneo-limbal tissue; **(C)** Enface view showing tiles mismatch after reconstruction **(D)** Zoom in view of C; **(E)** Nuclear staining (TO-PRO) at the outer surface of the rim and **(F)** inside the sample after overexposure showing how the signal gets lost with depth.

To address these problems, multiple microscopes, objectives, mounting techniques and immersion solutions were tested. For clarity of comparison, Table 3.1 summarizes the technical challenges and how they were tackled along the process. From the several microscope facilities that were approached, three units could be used. One confocal microscope (Leica SP8)

with several objective combinations (from two different facilities) and one light sheet microscope (Zeiss Z1).

In short, regarding the Lightsheet Zeiss Z1 microscope there were challenges with the sample mounting due to the size and the immersion media. The sample size problem was successfully dealt with by mounting the specimen in different ways, as described in Table 3.1. However, the only available objective was for aqueous media which was an issue that could not be resolved due to mismatches of refractive index and to the fact that when in contact with PBS the samples will slowly go opaque.

Regarding the Leica SP8, two different units with different objectives were tested. The Biosciences unit had the advantage of offering the 25x long working distance objective with coverslip correction, which was not available at the time at the UCL Laboratory for Molecular Cell Biology (LMCB). As described in Table 3.1, different trial and error approaches were used to overcome the challenges faced in the imaging process. Different immersion media were tried in order to have a closer match of the refractive index (with the mounting solution). When possible, the resonant scanner was used to speed up the image acquisition time and, overcompensation was used when imaging larger areas to take into account sample movement due to heating.

It was also noticed that when using the oil objectives, better resolution was achieved but penetration in the sample was worse than when using the water immersion objectives. The penetration limits are imposed by the light scatter so the objectives working distance is crucial in how deep an objective can image. In this case, the 20x objective has a longer working distance (0.68mm) than the 40x objective (0.24mm) so it can better penetrate the tissue. Long working distance objectives with higher numerical apertures (NA) give the best results and that is why the 25x objective from the Biosciences facility was used for further imaging of the samples.

Table 3.1 – Summary of technical challenges based on available image acquisition hardware.

Microscope	Characteristics	Challenges	Trials
Zeiss Z1 Lightsheet Micron Advanced Imaging Facility University of Oxford	*"Commercial lightsheet microscope designed primarily for time-lapse imaging of thick specimens (...) Specimens are illuminated with one or two thin light sheets from opposite sides perpendicular to the detection objective (...) It is possible to image in single or multiview mode, the latter through rotating the sample and imaging stacks at six to eight different angles, which can then be recombined into a 360° view. Specimens are embedded in 1% low-melting agarose or similar inside glass capillaries and then extruded and imaged in buffer." This lightsheet is a very early model and was not made with clearing techniques in mind. Now the design has changed slightly so that you could fit lenses suitable for cleared samples.*	The samples are usually mounted on a capillary: ❖ Sample size is too big.	Imaging chamber is about 20mm square on the inside: ❖ Try to mount samples using: • 2.1mm Ø capillary • 1mL syringe as a capillary (but trimming more is better as you get much better images if you image through less agar and mountant) ❖ Do multi-view imaging ❖ Implant beads to assist with re-alignment (red InSpeck 2.5µm beads, 1:10000 in agarose)
		Samples have to be mounted in aqueous media since that is the only objective available: ❖ iDISCO protocol samples are mounted in DBE.	❖ Try to image samples in aqueous media. • Not optimal due to refractive index mismatches ❖ Try newer version of this microscope with the appropriate objective.
Leica SP8 (*) UCL Division of Bioscience	**25X long working distance objective with coverslip correction (water)**		This objective has a higher working distance so it improved image acquisition. However, it is still an water objective so there was a mismatch of refractive index.
Leica SP8 (STED) MRC Laboratory for Molecular Cell Biology	"The 3D STED system Leica TCS SP8 STED 3X achieves resolutions below the diffraction limit in lateral as well as axial directions (...) The system is freely adjustable for best lateral resolution, best vertical resolution and smallest confocal volume. Additionally, Leica TCS SP8 STED 3X offers multiple depletion laser choices that open up the spectrum of visible light for confocal super-resolution and gives improved capabilities for research imaging. The white light laser source of the Leica TCS SP8 X perfectly matches the wavelength of any fluorophore. (...) any dye can be optimally excited with minimum cross-excitation and specimen damage."	❖ Refractive index ❖ Sample motion ❖ Time consuming Depending on the objective, we cannot achieve enough resolution or image the all depth of the structures.	Try to immerse the objective in a solution with a closer RI to the samples than water: ❖ Sonogel ❖ Systane Eye Drops (Alcon) Correction for temperature/movement of 3D samples: ❖ Overcompensate for depth • Approx.. 10- 20µm above & 20µm below When the signal is strong, the resonant scanner can be used to increase sample acquisition speed and reduce the imaging time. 20x oil objective gives higher resolution but less penetration into the sample Water objectives - better penetration, more depth, less resolution.

Magnification	Type	Immersion	NA	Working Distance (mm)	Coverslip correction
10x	HC PL FLUOTAR	Air	0.3	11	0.17
20x	HC PL APO CS2	Oil, Glycerol & Water	0.75	0.68	0/0.17
25x (*)	HC FLUOTAR L VISIR	Water	0.95	2.4	0.17
40x	HC PL APO CS2	Oil	1.3	0.24	0.17
63x	HC PL APO CS2	Oil	1.4	0.14	0.17

** At the time this objective was only available at the UCL Division of Biosciences. After our trials LMCB also bought one (15506375 - HC FLUOTAR L 25x/0.95 W 0.17 VISIR FWD 2.40 water 0.17coverslip correction).*

3.4.1.3. Whole-Mount Immunolabeling

In Figure 3.7 it is possible to observe a 360 degrees view of part of the 3D reconstruction of the limbal niche. Apart from Figure A vii, which is a flattened tile reconstruction, all the other images are snapshots of a 3D video reconstruction performed using Imaris (please see file Chapter 3 – VideoFig3.7).

Figures 3.7A (i to vi) show several field views of CD90 immunostaining. The base of the crypts, where the CSSCs are believed to reside, presented a more intense uptake of the fluorophore. On Figure 3.7A (vii) it is possible to see a 2D image of limbal crypts with numerous finger-like projections.

Figure 3.7B shows LESCs as part of the limbal crypts stained with PAX6, an early eye development marker.

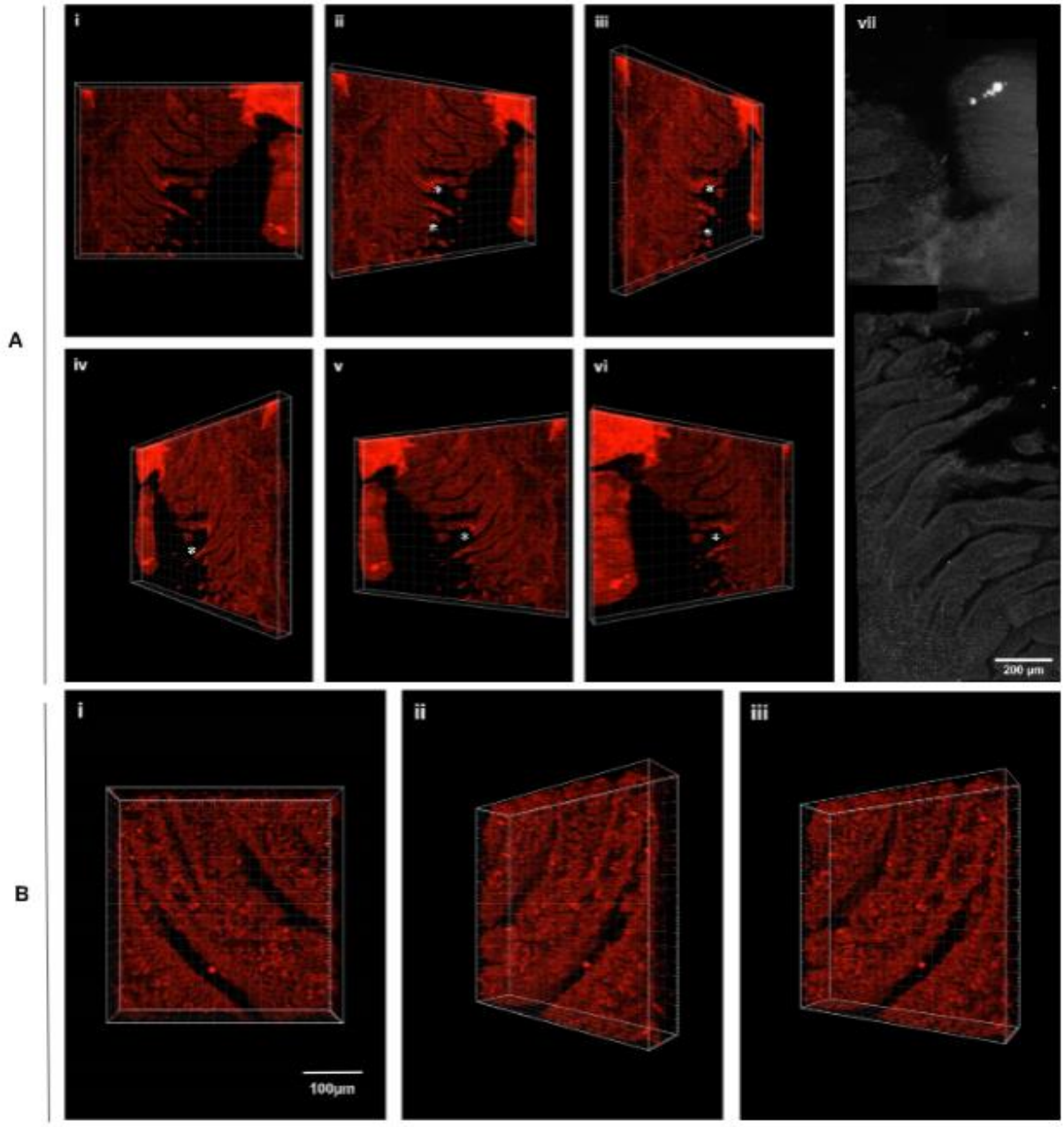

Figure 3.7 – 3D structure of the human limbal crypts using iDISCO clearing technique and immunostaining: **(A)** Multiple field views (tile stitching, CD90, red) where the asterisks * at the basis of the crypts highlight cells that have a more intense staining ;**(B)** Focused view of the limbal crypts (PAX6, red) highlighting the LESCs.

Summary of results:

Human corneo-scleral tissue clearing was successfully achieved using adapted versions of iDISCO, and PACT protocols:

- Tissue architecture was preserved
- 3D imaging of cleared tissue with confocal microscopy highlighted a diversity of challenges:
    - Time consuming
        - bleaching
        - sample movement caused by excessive heating of the mounting solution
    - Imaging chamber was too thick
    - Mismatches of refractive index caused by,
    - Objective immersion media limitations

3.4.2. Multi-lineage differentiation of CSSCs

Turning to the stromal cells isolated from the areas of the limbus imaged above, the multi-lineage differentiation potential of CSSCs towards the adipogenic, osteogenic and chondrogenic lineage was assessed.

Figure 3.8 presents light microscopy images of the morphological changes of CSSCs and hMSCs from day 1 to day 21 of differentiation. The hMSCs investigated in this study exhibited a spindle-shaped morphology (Figure 3.8A). On the other hand, CSSCs had a small square appearance in early stages (Figure 3.8B) but rapidly changed to a longer spindle-shaped morphology as cell density increased (Figure 3.8C & D). Over the time, both hMSCs and CSSCs acquired fibroblastic spindle-shape processes that extended in opposite directions from the cell body (Figure 3.8E-H). Interestingly, hMSCs after osteogenic differentiation had a flatter appearance (Figure 3.8H) than CSSCs (Figure 3.8F). In Figure 3.8E & G, it is possible to observe the fat droplets formed during adipogenic differentiation in both cell types.

Figure 3.9 shows the differential histochemical staining of the three different lineages of three donors (D1-D3) of CSSCs, hMSCs as positive control (+) and negative control (-) in basic media. All the samples were assessed in 2D TCP culture except the chondrogenic lineage that was tested in the form of a 3D pellet culture.

After adipogenic differentiation for 21 days, lipid vesicles were observed by Oil Red O staining (Figure 3.9A) with bright-field microscopy among cultures of CSSCs (population of interest) and hMSCs (positive control).

Osteogenic differentiation was observed by detecting calcium depositions with Alizarin red staining (Figure 3.9B) and confirmed by BCIP/NBT alkaline phosphatase staining (Figure 3.9C) after 21 days of differentiation. Staining of CSSCs and hMSCs with Alizarin red solution did not indicate many calcium depositions although some could be observed. Donor 1 sample showed a stronger alizarin red staining than the other samples. The differentiation was confirmed by alkaline phosphatase staining in purple (Figure 3.9C), which revealed that deposits were present.

Chondrogenic differentiation was tested by Alcian blue staining of 21-day CSSC pellets. Chondrocyte-associated extracellular proteoglycans (Figure 3.9D) can be observed in blue.

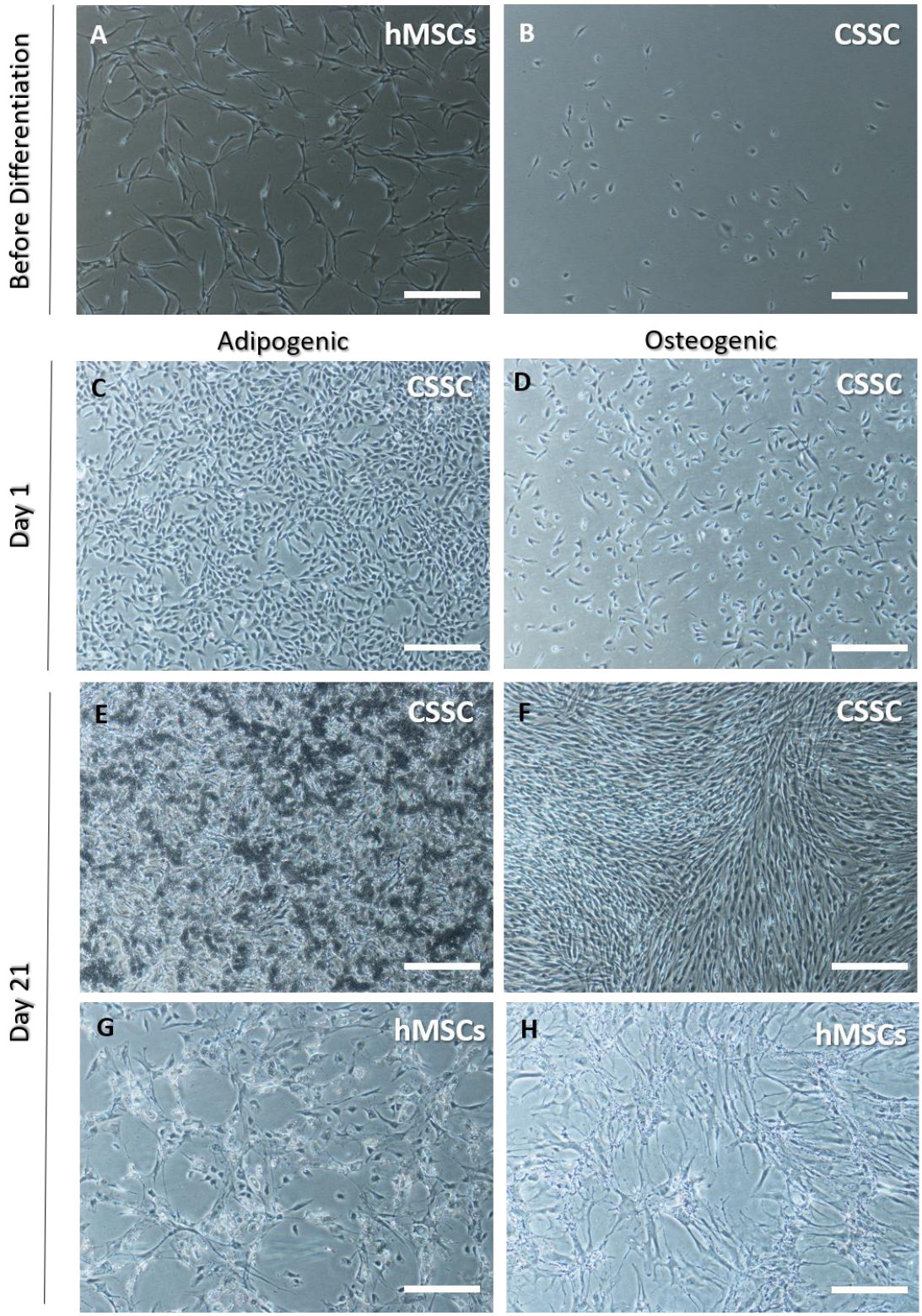

Figure 3.8 –Morphology of CSSCs and hMSCs before and after differentiation. Phase-contrast images of hMSCs **(A)** and CSSCs **(B)** at P5 before being plated for multi-lineage differentiation **(C** & **D)** show the seeding densities of CSSCs for adipogenic and osteogenic differentiation respectively. **(E)** to **(H)** show cell morphology after 3weeks in culture of CSSC **(E & F)** and hMSCs. **(G & H)** where (**E & G)** represent adipogenic lineage and **(F & H)** osteogenic differentiation. Scale bar = 400µm.

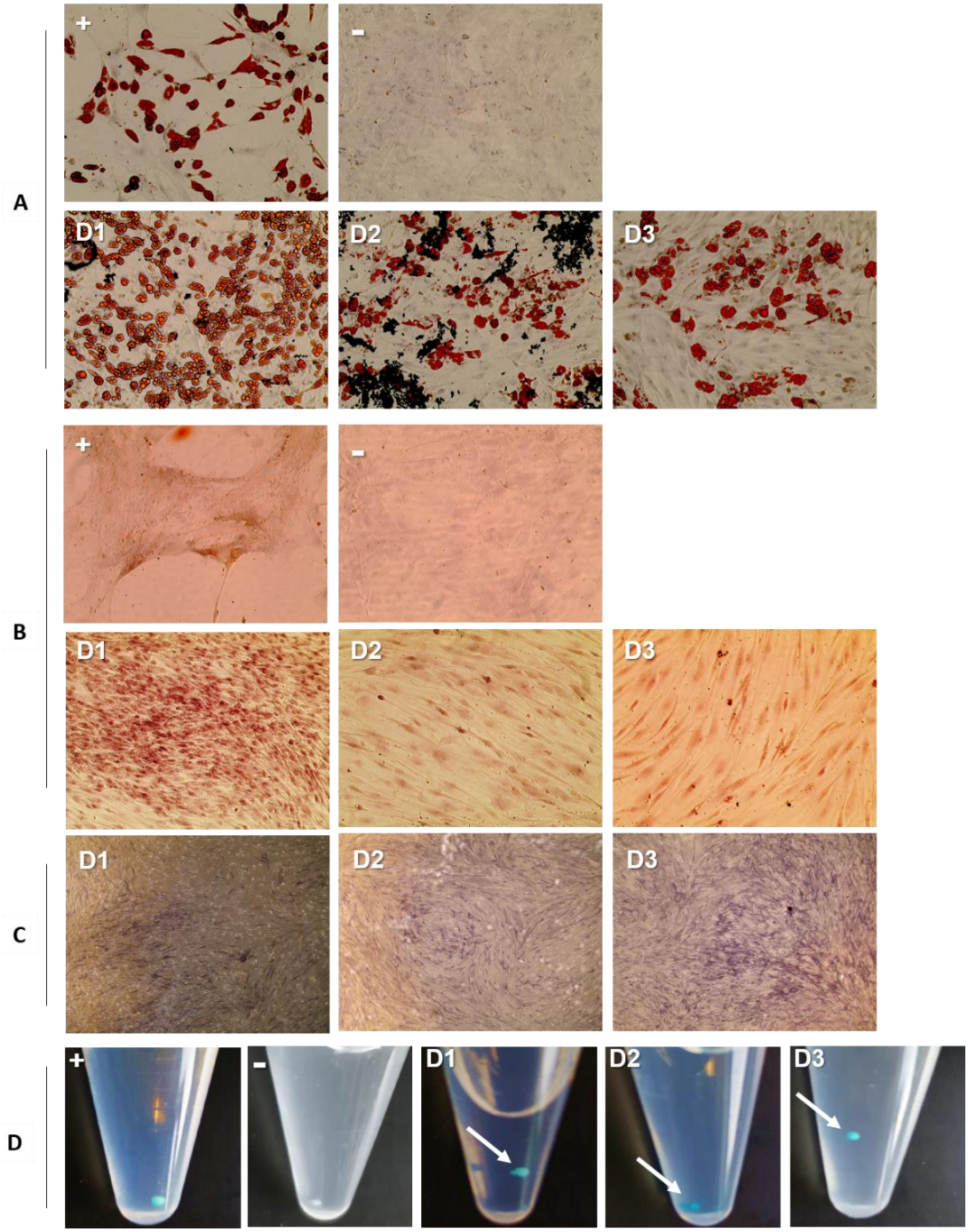

Figure 3.9 – Differentiation of CSSCs and hMSCs as positive (+) control for 3 weeks. Cells were differentiated in three different lineages, adipogenic, osteogenic and chondrogenic: **(A)** adipogenic medium, **(B & C)** osteogenic medium and **(D)** cell spheroids in chondrogenic medium (arrows point to the spheroids). **(A):** D1, D2, D3 and (+) show lipids formation (in red) within adipogenic medium by Oil red O staining. **(B):** D1, D2, D3 and (+) show small calcium deposits (in red) within induction in osteogenic medium by Alizarin Red S, **(C):** BCIP/NBT staining alkaline phosphatase in purple when in osteogenic medium and **(D):** D1, D2, D3 & (+) show glycosaminoglycans (GAGs) (in blue) within induction in chondrogenic medium by Alcian Blue staining.

3.4.3. Immunocytochemistry of CSSCs, keratocyte and epithelial cell markers in 2D

Immunocytochemistry was conducted to establish whether the putative CSSCs isolated from organ cultured tissue expressed their putative markers. Figure 3.10 shows immunostaining of CSSCs cultured in 2D on TCP by confocal microscopy for PAX6, CD90 and CD73 in red. Blue shows DAPI nuclear staining, while green represents phalloidin that stains the cytoskeleton of the CSSCs. On the right column it is possible to see a composite of all the mentioned channels. Interestingly, the small-squared morphology of CSSCs, previously described in Figure 3.8B, was also corroborated by the staining shown in Figure 3.10.

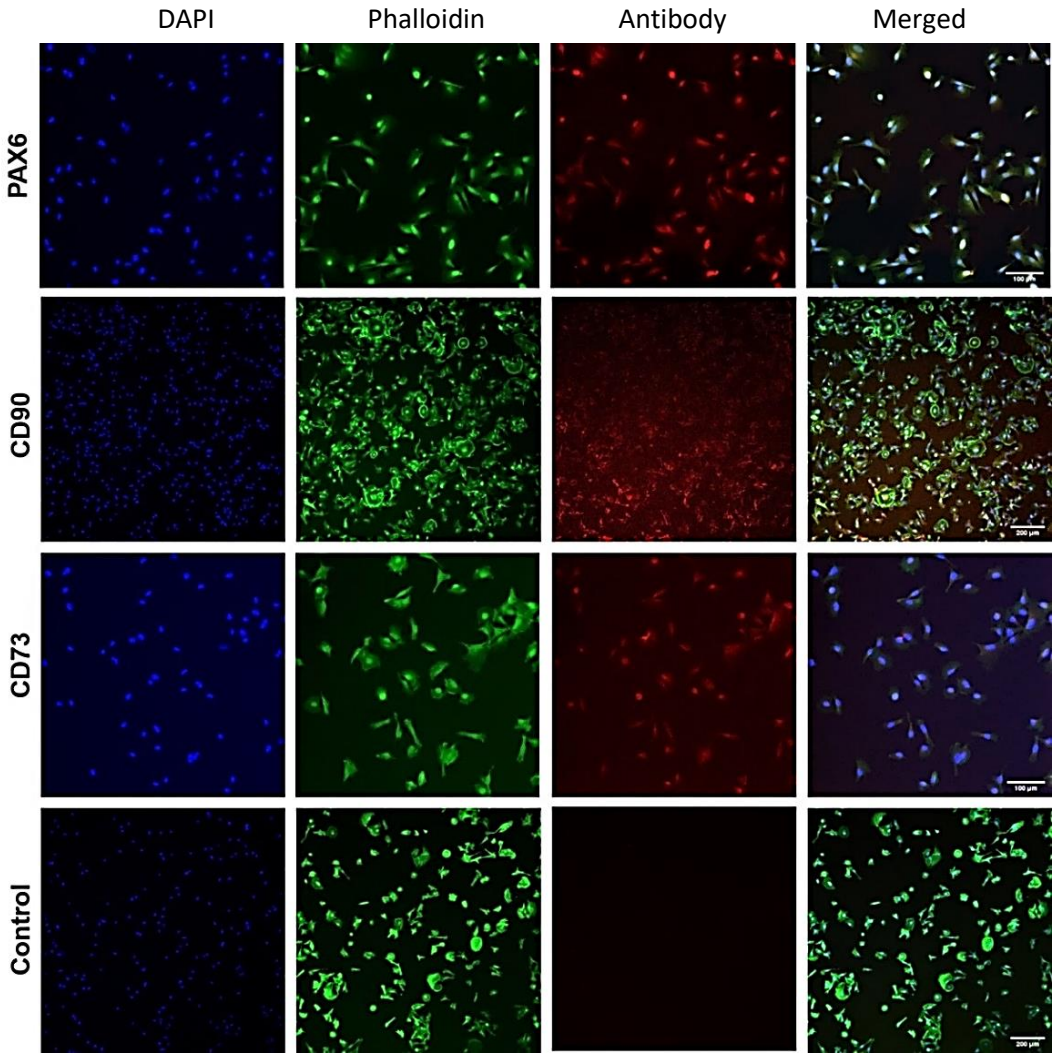

Figure 3.10 – Confocal micrographs of human CSSCs cultured in 2D. Cells display positive nuclear expression of PAX6 (gene expressed in early eye development), CD90 and CD73 (mesenchymal stem cell markers). DAPI staining nuclei in blue, FITC Phalloidin staining cytoplasm in green and differential antibody staining in red. Scale bars: 100 μm (PAX6 and CD73) & 200 μm (CD90 & Control).

Immunocytochemistry revealed that CSSCs, when cultured on CSSC media, express positive nuclear staining for PAX6, an early eye development marker. Expression of CD90 and CD73 mesenchymal stem cells markers was also positive on the isolated CSSCs as demonstrated on the second and third row of images on Figure 3.10.

CSSCs did not express ALDH1A1 (keratocyte marker), p63 (LESCs marker) or CK3 (differentiated epithelium marker), as observed in Figure 3.11.

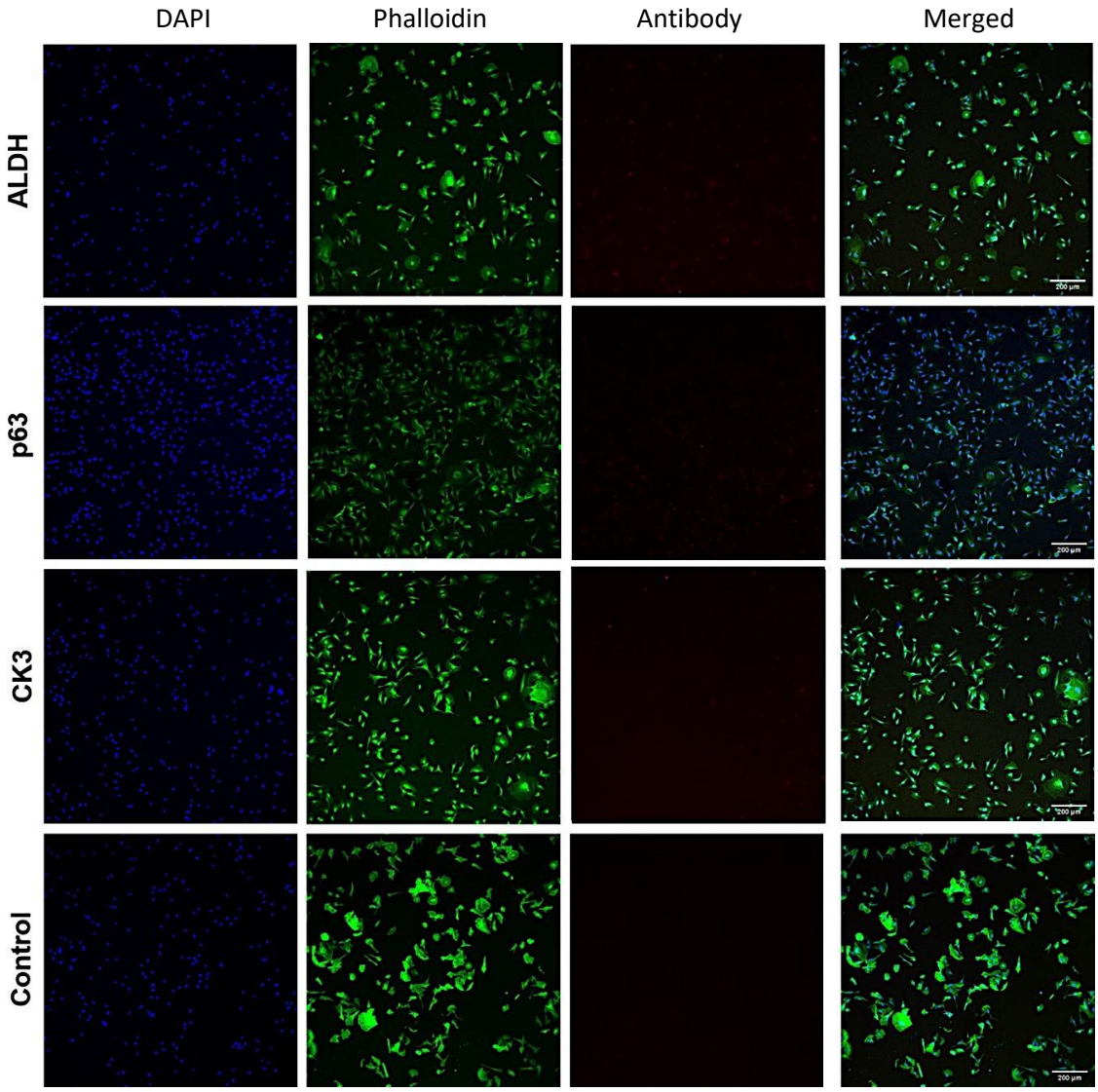

Figure 3.11 – Confocal micrographs of human CSSCs cultured in 2D. Cells are negative for ALDH1A1(Keratocyte marker), p63 (LESCs marker) and CK3 (differentiated epithelium marker). DAPI staining nuclei in blue, FITC Phalloidin staining cytoplasm in green and differential antibody staining in red. Scale bars: 200 µm.

3.4.4. Gene expression profile of CSSCs and Keratocyte-like cells

CSSCs from three different donors cultured in 2D on TCP and their respective keratocyte-lineage differentiation in KDM media were characterized by qPCR. All of the comparisons were made against baseline expression of undifferentiated CSSCs and normalised to 18S levels.

Figure 3.12 shows the gene expression of PAX6, CD90 and CD73 in three different culture conditions: CSSCs- starting population cultured in CSSC media, KDM -induction of CSSCs into keratocyte lineage differentiation using 'KDM media' and a positive control that differs depending on the target gene.

In Figure 3.12A it was possible to see a significant fold increase in PAX6 expression in LESCs (positive control) when compared to CSSCs (***$p \leq 0.001$). There was no significant difference between CSSCs and KDM with regards to PAX6 expression. PAX6 is also upregulated on LESCs when compared to KDM (**$p \leq 0.01$). CSSCs had a similar gene expression profile for both CD90 and CD73 (Figures 3.12B & C) when compared to hMSCs. The KDM condition showed a significant upregulation of both genes when compared to CSSCs (**$p \leq 0.01$) and hMSCs (***$p \leq 0.001$). Both graphs (3.12B & C) illustrate relatively small fold changes. Although they reach statistical significance, their biological relevance will be discussed later on this chapter.

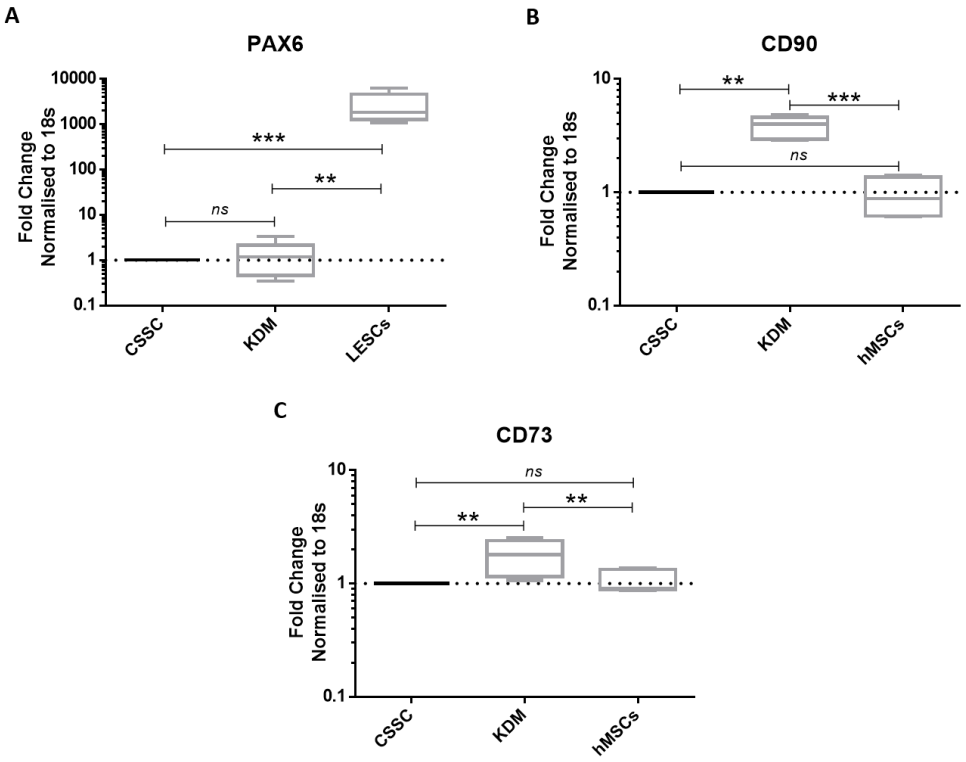

Figure 3.12 – Expression of PAX6 (gene expressed in early eye development) and mesenchymal stem cell markers CD90& CD73 by CSSCs at P6 cultured on CSSC media and when cultured on KDM (Keratocyte differentiation) media in comparison to LESCs and hMSCs (respectively) assessed by Real Time qPCR. (Data is represented in a boxplot, n=3, Kruskal-Wallis test followed by Dunn's Multiple comparison test where **p≤0.01, ***p≤0.001). Dash line represents the basal expression of the markers of interest when cells are cultured in CSSC media. Abbreviations: (A) PAX6- Paired box protein Pax-6, (B) CD90- Cluster of Differentiation 90 (also known as Thy-1) & (C) CD73 - Cluster of Differentiation 73.

Figure 3.13 shows the gene expression of LUM, KERA and ALDH1A1 in three conditions: CSSCs- starting population cultured in CSSC media, KDM - induction of CSSCs into keratocyte lineage differentiation using 'KDM media' and CC - central cornea where the native keratocytes reside as positive control.

After 21 days of differentiation of CSSCs towards the keratocyte lineage, the expression of keratocyte markers LUM, KERA and ALDH1A1 was significantly upregulated in the KDM condition when compared to CSSCs (Figures 3.13A, B & C). However, it is important to notice that the difference in LUM expression (Figure 3.11A) was much higher (****p≤ 0.0001) than KERA and ALDH1A1 (*p≤0.05), but also less consistent as seen by the amplitude of the boxplot. It is also important to recognise that LUM expression levels on KDM reached similar values to the ones of central cornea (CC – native tissue)

which is shown by a lack of statistical difference. On the other hand, cells in KDM showed lower expression of KERA and LUM than CC (*p≤0.05).

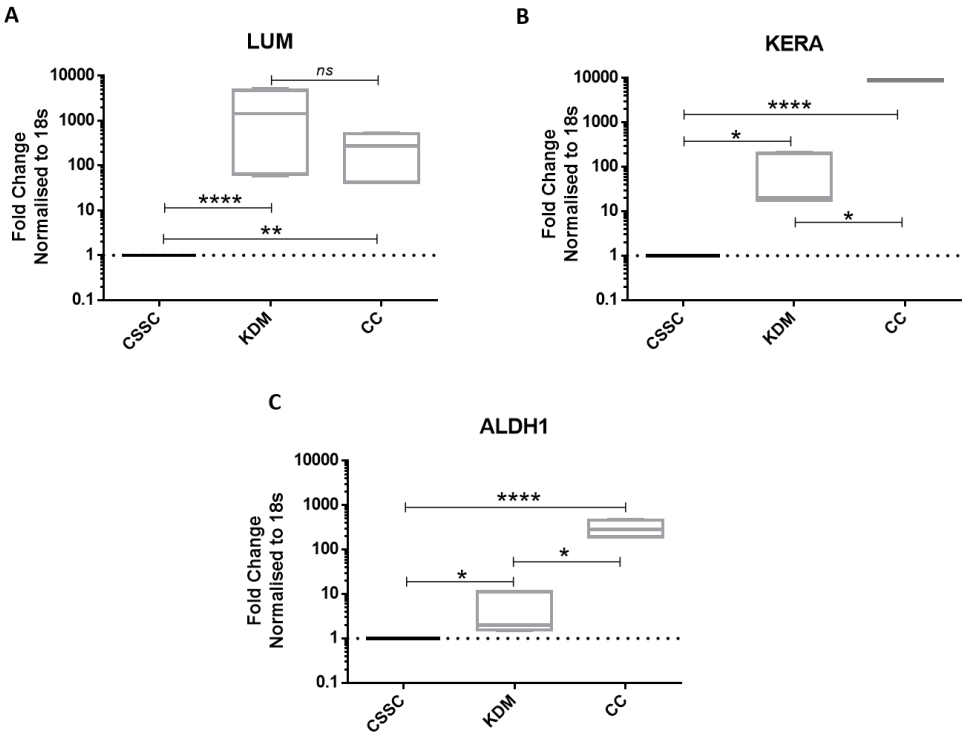

Figure 3.13 – Expression of keratocyte markers LUM, KERA & ALDH1 by CSSCs at P6 cultured on CSSC media and when cultured on KDM (Keratocyte differentiation) media in comparison to central cornea assessed by Real Time qPCR. (Data is represented in a boxplot, n=3, Kruskal-Wallis test followed by Dunn's Multiple comparison test where *p≤0.05, **p≤0.01, ***p≤0.001, ****p≤ 0.0001). Dash line represents the basal expression of the markers of interests when cells are cultured in CSSC media. Abbreviations: (A) LUM- Lumican, (B) KERA – Keratocan, (C) ALDH1 - Aldehyde Dehydrogenase 1 Family Member A1.

Lastly, Figure 3.14 focuses on the gene expression of p63, CK3 and ACTA in the same three conditions described above. The positive control condition was different for all the conditions: LESCs were used as a positive control to show p63 expression, central cornea epithelium for CK3 and activated limbal fibroblast for ACTA.

Higher p63 gene expression levels were observed in LESCs than in CSSCs and KDM, as shown in Figure 3.14A. Nevertheless, it is possible to observe a significant fold increase (*p≤0.05) when CSSCs are differentiated in KDM, compared to the initial CSSCs condition. Figure 3.14B shows that there was no significant difference with regards to CK3 expression on KDM with relation to CSSCs and that CC has a much higher expression of CK3 than CSSC and KDM samples. CSSCs have a much lower expression of ACTA

(Figure 3.14C) than hLF (**p≤0.01). However, the KDM condition shows similar gene expression levels as the positive control. Yet, when compared with CSSC, KDM condition did not show a significant difference.

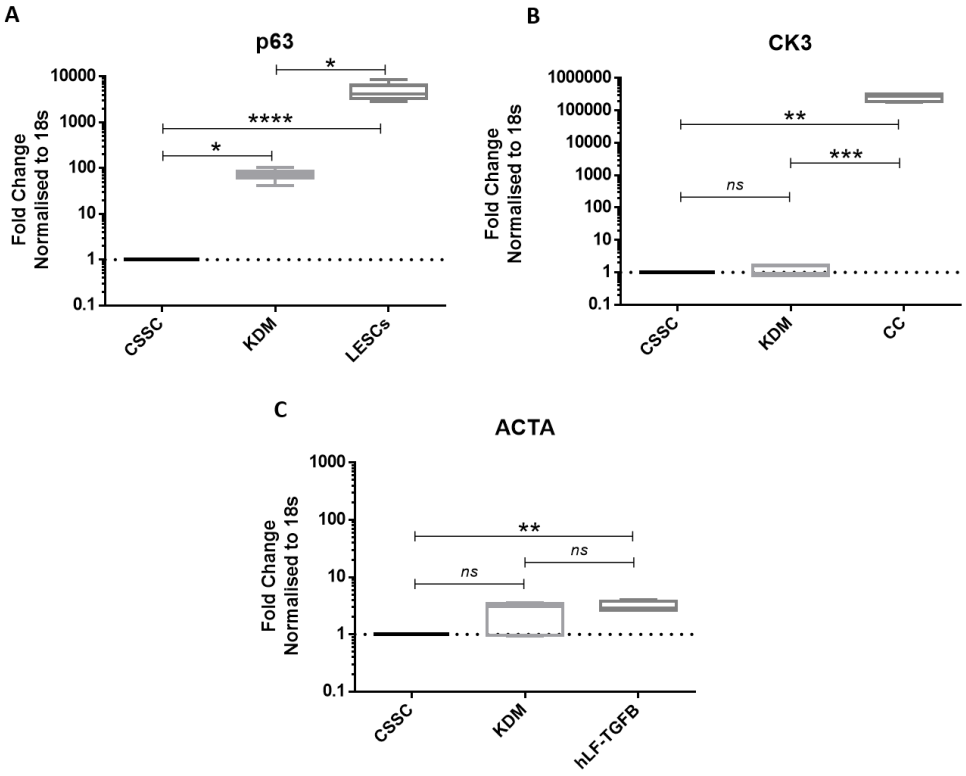

Figure 3.14 – Expression of ΔNp63, CK3 and ACTA by CSSCs at P6 cultured on CSSC media and when cultured on KDM (Keratocyte differentiation) media in comparison to LESCs (A), central cornea (B) and hLF-TGFB (C) assessed by Real Time qPCR. (Data is represented in a boxplot, n=3, Kruskal-Wallis test followed by Dunn's Multiple comparison test where *p≤0.05, **p≤0.01, ***p≤0.001, ****p≤ 0.0001). Dash line represents the basal expression of the markers of interests when cells are cultured in CSSC media. Abbreviations: (A) p63 – ΔNp63, (B) CK3- Cytokeratin 3, (C) ACTA- alpha smooth actin & hLF-TGFB – human limbal fibroblast stimulated with TGF-β.

Summary of results:

- Multi-lineage differentiation of CSSCs:
    - Successful chondrogenic differentiation
    - Successful adipogenic differentiation
    - Weak osteogenic differentiation
- CSSC confirmed the production of proteins such as: PAX6, CD90, and CD73
- The gene expression profile of CSSCs, and keratocyte-like cells in 2D was different. Taking the CSSC as the basal condition, the KDM condition experienced:
    - CSSC genes:
        - ✓ CD90– upregulation
        - ✓ CD73 - upregulation
    - Keratocyte genes:
        - ✓ ALDH1 – upregulation
        - ✓ KERA - upregulation
        - ✓ LUM – upregulation
    - Other genes:
        - ✓ p63 – upregulation

3.5. Discussion

The first question in this study wanted to determine the best anatomical location from which to isolate CSSCs using volume imaging. A tissue clearing protocol was developed and tested based on PACT and iDISCO techniques. The second question aimed to characterize the CSSCs obtained from selective trypsinization of limbal tissue dissection with regards to the markers described in the literature and their positive controls.

3.5.1. CSSCs localisation

While research has been carried out on the architecture of the limbal epithelial stem cell niche, less is known about the precise location of CSSCs. There are limited studies that reported imaging of cell-to-cell interactions between LESCs and putative CSSCs at the limbal niche [98, 225]. There have been several attempts to reconstruct the limbal niche by a variety of imaging techniques. The work of Shortt *et al.* allowed 3D imaging of smaller areas of the limbus by sampling crypt rich and non-crypt regions of the limbal circumference. The authors produced a series of tiles by confocal microscopy and SEM. However, this study was only focused on LESCs and was not able to reconstitute cell-to-cell interactions [97]. Using 3D high-resolution electron microscopy, Dziasko *et al.* suggested that putative CSSC co-localise, and are in direct contact with LESC in the limbal crypt rich superior and inferior regions of the limbus [98]. This study set out with the aim of creating a 360-degree 3D reconstruction of the corneo-limbal region to indicate the location of CSSCs.

3.5.1.1. Corneo-limbal Tissue Clearing

Corneal rims are three dimensional so imaging into a tissue can be problematic due to the scatter of light. An initial objective of the project was to identify, develop and test novel methods for tissue clearing aiming to remove light scattering lipids, while keeping the proteins, and thus allowing deep penetration of light [102].

Techniques like cryosectioning do not allow the reconstruction of large or deep tissue areas, and consequently the opportunity to observe cell-cell interactions is lost. This new method surpasses the need of making thin slices of tissue for it to become transparent, and penetrable by the antibodies, overcoming the limitations of light scattering [102].

Tissue clearing of corneo-limbal rims was successfully validated using the PACT and iDISCO adapted protocols by showing that transparency can be achieved. As described earlier, transparent samples are an advantage in relation to opaque tissue because of lower light scattering, which allows a deeper and wider imaging of the tissue in study. Since both techniques

achieved similar results, and for the sake of time and resources optimization, only iDISCO samples are shown to investigate microscope settings. In agreement with what has already been described, it was noticed that the samples slightly shrink. However, the shrinkage due to dehydration is consistent, so there is no change in projections or connective patterns [4]. One of the issues that could possibly emerge from these findings is the lack of veracity of absolute distance measurements [216].

Anatomical landmarks like the limbal crypts and focal stromal projections were clearly visible as invaginations into the epithelium and finger-like projections into the stroma respectively. The morphology observed in this study mirror the previous studies showing an excellent preservation of tissue architecture in iDISCO cleared corneal tissue [89, 97]. Hence, clearing techniques could provide an alternative to histological sectioning for volumetric studies with the added advantages of whole niche reconstruction and corneal rim reconstitution which is believed to be crucial in the understanding of cell-cell interactions in the human limbal stem cell niche [226]. However, this study has been unable to confirm the initial hypotheses that tissue clearing would support the identification of the best anatomical location from which to harvest a biopsy for CSSC isolation due to the microscopy technical difficulties explained below.

3.5.1.2. Volume imaging optimisation for cleared tissue

Tissue clearing eliminates the limitations imposed by the scattering of light [102]. Although several improved imaging platforms have been developed and tested over the last few years, the ideal collection of settings for each clearing protocol and tissue are not yet completely defined. Some of the technical challenges faced on this chapter were presented above, and the next paragraphs will discuss possible approaches to take full advantage of the development of novel microscopy technologies and components focused on tissue clearing [102].

At the time, when this project was being developed, a few optical sectioning techniques were already commercially available. Confocal, 2-Photon and

lightsheet fluorescent microscopy were all considered. However, lightsheet microscopy was still in its early days of application for cleared tissues [102, 227, 228].

In tissue clearing, the objective's working distance is then the only limiting factor for imaging deep into the tissue. By reviewing the literature, it was decided not to use 2-Photon microscopy since confocal microscopy presented better signal to noise ratios and a lower likelihood of cross-excitation between channels [102]. Following these findings, only confocal and lightsheet microscopes were tested in this chapter.

Confocal microscopy is ideal for high-resolution imaging of specific areas, yet both confocal and 2-photon microscopy have other drawbacks that make them not ideal for imaging large samples. One of the challenges described in this chapter was the time required to image multiple fields of the corneo-limbal region in 3D and how time-consuming that was. This is explained by the slow laser scanning that makes it impractical to image large fields of view [102, 229]. Resonant scanner, like the one used on the Leica SP8, can accelerate the scanning speed without compromising high-resolution and was one of the solutions implemented to improve image acquisition [217, 230].

Light-sheet microscopy is a 3D imaging technique that has emerged as an excellent alternative to image bulky cleared samples since it allows faster imaging (that are 2–3 orders of magnitude quicker than confocal and two-photon microscopy), vast fields of view and reduced sample bleaching [217, 230]. Since a whole plane is illuminated by excitation light, there is no need to map the sample with a laser as the whole plane can be captured by a single exposure [102]. However, it is essential to bear in mind that, just like the other imaging approaches, lightsheet microscopy can suffer from misalignments and refractive index mismatches.

In this study, tiling reconstruction was challenging and found to cause plane misalignment. These results match those observed in earlier studies that point to lens distortions, light fall-off and micromovements inside the imaging chamber as the leading cause for this [216]. Beads can be embedded in the mounting process to help on the alignment post-processing as this was tested on the light-sheet imaging trial [231].

All microscope optics, inherently, have some degree of spherical aberration. This occurs due to the difference in refractive index from the sample mounting media and the objective. Light has to go through numerous interfaces (glass, air and/or immersion media, etc.) between the microscopy body and the sample. Each of the materials presents a different refractive index and the mismatch in those interfaces causes blurring of the final image. The light will not focus on the right point, increasing the degree of spherical aberration. Moreover, there are also discrepancies between the physical focus movement and the focal plane [102, 232].

Microscope manufacturers and materials suppliers have been working hard to address this issue. There are three things that scientists found to be important when imaging cleared tissue for maximum imaging depth and resolution: long working distances (>5 mm), high numerical apertures (>0.9) and refractive index tunable objectives [102, 217]. This combination of findings provides the ideal setting for imaging cleared tissue under confocal microscopy. Nevertheless, this information was not known until very recently, and this kind of objective was not available commercially at the time of conducting these experiments. As described in this chapter, it was extremely challenging to image with the available objectives. The ones available at the MRC lab had, in general, very small working distance and the ones that had high numerical aperture were high magnification (40x and 63x) so would only allow restricted superficial views. Low resolution was obtained using the long working distance, small numerical aperture (10x). The UCL Division of Biosciences had a long working distance objective (yet still smaller than 5mm) and with a high numerical aperture which allows acquisition of better quality images [102].

Additionally, as mentioned above, objectives should be optimised for the refractive index of the mounting medium of the cleared samples. Air objectives have a RI equal to 1; oil immersion objectives have a refractive index of ~1.515, water of ~1.33 and glycerol (glycerine oil) of ~ 1.47 [233]. PACT protocol with 88% Histodenz results in RI = 1.46 [217] and iDISCO, has a refractive index (similar to DBE) of 1.56 [233]. In this case, glycerol objectives would be the ones with closest RI to the iDISCO and oil for the PACT protocols.

There was no ideal objective available at the time to image these samples, so a balance had to be found between the refractive index, working distance and numerical aperture. In this case, the 25x water objective proved to give the best results for the iDISCO protocol because besides having a correction collar, it also had a high numerical aperture and the highest working distance of the available immersion objectives. Nevertheless, this objective is not ideal for imaging larger areas (as initially aimed) since imaging would require capture and stitching of multiple tiles which can lead to complications (described above) and a higher risk of photobleaching [229].

Over the last years, manufacturers adapted different lensed to match scientists' requirements, and as a matter of interest now both Olympus, Zeiss and Leica have optimised lenses for cleared samples. The new 3D Leica motCORR™ objectives, for example, offer motorised correction for best optical performance by "quickly adjusting the objective lenses to varying coverglass thickness, changes in temperature, and specimen inhomogeneities."

It is also important to point out that sealed chambers were created to image the cleared tissue aiming to reduce evaporation of the imaging medium. Yet, subtle changes in the RI of the immersion media can still occur during extended imaging since the interface between the imaging chamber and the objective is open [229].

As with confocal microscope objectives, there have been considerable advancements in the light sheet setups. As referred to in this chapter, the available microscope at the time only had aqueous objectives that would not allow immersion in the imaging media, explaining why this approach did not return optimal results. Now, that appropriate objectives are available, as well as a broader range of sample holders, this would probably be a good option to get 3D rendered quality reconstructions of the corneo-limbal region [234].

3.5.1.3. Data Processing

Another major challenge in this imaging method is data storage and processing. Volume imaging generates enormous data sets, one reconstruction could have more than 20GB and if larger volumes start to be imaged (e.g. an entire corneal rim), the data can reach the order of terabytes.

Most desktops are not able to handle such big data sets due to the lack of available RAM memory. Software such as Imaris requires powerful workstations to do complex operations as full reconstructions. As suggested by the original authors of the iDISCO protocol, Fiji/Image J can only downsample the images and produce maximum projections or 2D image stacks [216]. Since big data is now a challenge in multiple fields of study, there are already computational infrastructures able to store and process this kind of data. However, access is still limited and costly [102, 114].

3.5.1.4. Future trajectory of imaging of cleared tissue

Despite all the challenges, the scientific community has been working towards the improvement of tissue clearing protocols, imaging set-ups and process software due to the ever-increasing array of biological questions that it can resolve [235].

This technique still remains inaccessible to the broader scientific community, and very much at the use of those who have designed specialized facilities and trained technical staff in this specific field.

As earlier described, there are still questions, that no other technique or system seems to be able to resolve. These questions fall into different categories, but the strength relies on the potential of having deep enough resolution inside a specimen, at the same time as spatial resolution, and, in other cases, also temporal resolution[236].

Light-sheet datasets are often too big to be shared, and tricky to process. The variety of file formats and storage methods is also a challenge. Regardless of these drawbacks, however, there are numerous ongoing efforts to uniformize and compile databases and computational tools, as well as to ensure access to the right microscope systems all over the World. The OpenSPIM project, the Janelia Advanced Imaging Center, and the Euro-BioImaging Consortium are a few examples of those [236].

3.5.2. CSSCs Characterization

Although it was not possible to image the complete limbal region in 3D due to microscopical technical limitations, the isolation and characterization of CSSC was still possible. CSSC were isolated from entire limbal arch dissections, with no targeted biopsies, because the 3D reconstruction was not possible, and thus the identification of the best location to maximize isolation yield. Having in mind the creation of a corneal tissue equivalent, CSSC were characterized *in vitro* prior to the development of a delivery strategy.

Prior studies have noted the potential of CSSCs for the advancement of cell-based therapies for corneal scarring and in the development of bioengineered stromal equivalents [116]. Since this thesis aimed to use CSSCs in the development of new therapeutic approaches, their standard characterisation is of extreme importance in order to compare the original population with the differentiated cells and their behaviour in 3D environments.

3.5.2.1. Multi-lineage differentiation

CSSC have been linked with hMSC because they can express MSCs markers and have anti-scarring properties [114]. One well-documented aspect of hMSCs is the ability to differentiate into multiple cell lineages. According to the Mesenchymal and Tissue Stem Cell Committee of the International Society for Cellular Therapy (ISCT), hMSCs must differentiate *in vitro* into: osteoblasts, adipocytes and chondroblasts [107]. When CSSCs were discovered by Funderburgh *et al*., they were only pushed towards the chondrogenic and neurogenic lineages [114]. Since the findings from that study were not enough to comply with the ISCT criteria, tri-lineage differentiation of CSSCs was performed in this chapter. This was also a necessary step to fully characterize the cells obtained from organ culture rims before embedding them in RAFT-TE in order to identify the differences in phenotype that can result from this delivery method.

Later, Deng *et al*. published a similar study where tri-lineage differentiation was performed [237]. The results presented herein also suggest that CSSCs can differentiate into the three lineages. Lipid vesicles could be observed after

21days in adipogenic differentiation media corroborating previous studies [237]. CSSCs were also able to be differentiated towards the chondrogenic lineage as has been described before and confirmed by the presence of proteoglycans [114, 237]. Contrary to expectations, this study did not find significant differentiation towards the osteogenic lineage. However, the findings match those observed later by Deng *et al.* [237].

There are, however, possible explanations for this finding. One is based on the different stages of osteogenic differentiation, BCIP/NBT staining is slightly stronger than Alizarin Red, and this can be justified by the typical sequence of events where AP is needed to initiate calcification and thus mineralisation [238]. Another interesting finding that may support the weak osteogenic differentiation of CSSCs is the work developed by Lee and colleagues where it was demonstrated that osteogenic differentiation potential correlates negatively with hMSC efficacy to reduce corneal inflammation *in vivo* [239] as well their response to pro-inflammatory cytokines [237].

3.5.2.2. Expression of CSSC markers

When looking at the immunostaining results of CSSCs, it is interesting to note that in all cases the results obtained showed a similar expression profile as had been previously described in the literature [114, 121]. CSSCs were positive for mesenchymal stem cell markers CD73 and CD90, along with PAX6, a transcription factor for ocular development [115]. As expected, they were negative for ALDH, a marker that would show differentiation towards the keratocyte lineage [16] and also for p63 and CK3 indicating that there was no contamination of epithelial cells in the isolated population [60, 240]. No direct correlation was found between the protein data, presented above, and the relative quantitative RNA analysis performed by qPCR.

PAX6 is a transcription factor with essential functions in the eye, nose, central nervous system and pancreas development. Its expression has been reported in CSSCs but not on keratocytes [115]. The results obtained in this chapter differ from previous studies where PAX6 is downregulated when CSSCs are cultured in KDM media [115]. Yet, these findings are consistent

with the work published recently by Deng *et al.* where, although not significant, a slight upregulation of PAX6 is observed straight after 7 days in KDM culture medium. In accordance with this study, the current work found that after 21 days in KDM media, there was no significant difference in relative mRNA expression of PAX6 between CSSCs and KDM conditions. On the other hand, control LESCs highly expressed PAX6 as previously reported [58].

The results presented here need to be interpreted with caution as Ct values for PAX6 in CSSCs were above 35 [241]. This indicates a low expression of the targeted gene but could also mean very low amounts of cDNA template [241]. However, a possible explanation for the differences observed is the fact that for qPCR a minimum number of cells are needed for detection within the "normal" range, and thus higher passages of CSSCs were used. This is supported by previous works where PAX6 downregulation was observed over the time from passage to passage [242].

CD90 and CD73 are specific antigen surface markers usually used in the identification of hMSCs [107]. When compared with hMSCs, CSSCs have similar levels of mRNA expression of both genes. However, contrary to what was expected, when CSSCs were directed towards the keratocyte phenotype, upregulation of both CD90 and CD73 was observed. Interestingly, Deng *et al.* reported recently that only 75% of CSSCs express CD90 as opposed to almost 100% of hMSCs. CD73 was expressed in almost 100% of both cell types [237]. Although some studies claim the loss of CD90 and CD73 expression with the differentiation of CSSCs into keratocytes [114, 121], others suggested that keratocytes are able to express CD90 and CD73 in accordance with the findings presented in this chapter [243].

3.5.2.3. Differentiation towards keratocytes

Lumican is a major keratan sulphate proteoglycan expressed by quiescent keratocytes. A significant upregulation of its expression was observed after 21days of the culture of CSSCs in keratocyte differentiation media (KDM). When compared to the central cornea lysate, where the native keratocytes reside, no significant difference was found between the differentiated cells and

the native tissue. This showed that the KDM condition reached similar levels of lumican expression as the central cornea which is supported by other authors [114, 121, 237].

An upregulation of keratocan and ALDH could be observed when the cells were pushed towards the keratocyte lineage. However, the levels of mRNA expression in the KDM condition are still significantly lower than in the central cornea tissue. The reduced upregulation of keratocan and ALDH in the KDM condition, when compared with lumican, has also been observed by other authors [237] and can be explained by the fact that lumican regulates keratocan and ALDH expression so, during the differentiation process, it is expected to see an earlier upregulation of lumican before the upregulation of the genes it regulates [244, 245].

The results of this study showed that keratocyte differentiation media (KDM) stimulates the expression of keratocyte markers such as Lumican, Keratocan and ALDH but did not downregulate the expression of hMSC markers such as CD90 and CD73. As previously described, this suggests that there was only partial differentiation of the CSSCs into the keratocyte phenotype [246].

3.5.2.4. Cell contamination

To control for epithelial cell contamination in the CSSC preparations, the same RNA samples were tested for the presence of p63 and CK3, epithelial-specific genes. The Ct value of both genes on CSSCs was above 35, which suggest it might not be expressed when compared to the high values obtained by the positive controls (LESCs and CC respectively) [241]. As expected, CK3 was also not detected in the CSSC differentiated in the KDM condition but, surprisingly, p63 was upregulated. To our knowledge, p63 expression has not been assessed in CSSCs. However, prior studies have reported expression of p63 on limbal fibroblast and hMSCs [247] which together with the initial pre-selective trypsinisation points towards a real p63 upregulation rather than an epithelial cell contamination.

In order to check whether the CSSCs differentiated towards the keratocyte lineage were transitioning into a corneal fibroblast or myofibroblast phenotype [224], the expression of alpha-smooth muscle actin (ACTA) was assessed. This is important to check whether the keratocytes were activated towards a fibrotic phenotype. There was no significant difference between CSSC and KDM conditions. Although not significant, there was a slight upregulation of ACTA on the KDM condition since its expression was not significantly different from the stimulated limbal fibroblasts.

3.6. Conclusion

This is the first study reporting the clearing of human corneal rims for volume imaging. Whilst this study did not confirm the best location for CSSC isolation, in the light of new technological advances it did provide a crucial step towards the future reconstruction of limbal cell-to-cell interactions by testing and developing the clearing protocol.

Returning to the hypothesis and aims posed at the beginning of this study, it is now possible to state that corneal rims can be successfully cleared using iDISCO and PACT techniques, but technology was not ready at the time, neither the necessary expertise to further support this project. Microscopy units, and imaging professionals were still in the process of learning, adapting, buying and experimenting with light-sheet microscopy and there were no special available confocal objectives at the time to delve into the explored settings.

The second part of this study has shown that it is crucial to perform characterization studies in each laboratory setting before embedding cells into tissue engineered therapies even when the protocol has been well described in the literature. Small things like the initial condition of the tissue supplied can impact the outcomes. The current findings add to a controversial growing body of literature on stromal stem cell characterization showing that they are not as well characterized as it was initially thought. Whereas this study did not confirm

the expected phenotype as described by Funderburgh JL *et al.* [114, 115], the results observed corroborated other authors recent findings where it was shown that osteogenic differentiation potential correlates negatively with hMSC efficacy to reduce corneal inflammation *in vivo* [239] , and that could be a possible reason for the weak differentiation of CSSC into the osteogenic lineage [237].

To conclude, this piece of work did substantiate our knowledge on CSSCs phenotype when cultured *in vitro* as well as their potential before embedding them in RAFT-TE.

Chapter 4

4. THE EFFECT OF MANUFACTURING CHANGES ON RAFT-TE PRODUCTION

4.1. Introduction

RAFT-TE has been extensively investigated by our group using research grade collagen for ocular surface reconstruction. However, it is essential that clinical manufacturing quality standards are considered prior transplantation. Together with TAP Biosystems, a new method of producing collagen compressed hydrogels was designed and named Real Architecture for 3D Tissues (RAFT). An hydrophilic porous absorber (HPA) is now used for fluid removal from the collagen rather than a mechanical load [206]. This technology has been standardised for GMP compliance. Nevertheless, some matters still need to be addressed with regards to reagents and protocol modification to achieve GMP compliance.

The manufacturing process of RAFT-TE requires collagen gelling. Gelling, or collagen fibrillogenesis, is triggered by a change of pH and temperature in the collagen solution. Gelling is responsible for the transformation of the solution into a hydrogel, or TE, which is then used as a 3D matrix for cell culture.

Among other things, the gelling capacity of RAFT-TE is dependent on the collagen extraction process that can be carried out by an acid or enzyme method [248]. To understand the differences, it is important to understand the collagen structure. Collagen I consists of a triple helix region, and telopeptide

regions at the N- and C-terminals of the molecule that are responsible for a more stable crosslinking.

The enzyme extraction methods, using pepsin, cause the cleavage of the telopeptides, which results in slower nucleation. Pepsin-solubilized collagen (or “atelo-collagen”) proteolytically digests the telopeptides resulting in weaker hydrogels [249].

In the herein project, RAFT-TE were produced from acid-extracted collagen or “telo-collagen”, in which the non-helical telopeptide regions remain intact, supporting fibrillogenesis and enhancing the mechanical properties of the TE.

The type of collagen, temperature and pH significantly impact fibrillogenesis. The self-assembly of collagen molecules is faster at higher temperatures, and 37°C is commonly used to facilitate cell seeding and viability [250]. pH also influences structural and mechanical properties of the TE [251, 252]. However, the pH of hydrogels seeded with cells is restricted to 7.4–8.4 to sustain cell viability [253].

The pH of collagen hydrogels is not only dependent on the ratio of neutralization agent to collagen solution but also dependent on the other components of the buffer. The clinically relevant protocol to manufacture RAFT-TE uses a specially-designed neutralizing solution (containing NaOH and HEPES) that enables neutralization to be carried out in a single step instead of titration with NaOH.

In addition to the physico-chemical considerations of collagen extraction, collagen source safety and product consistency must also be considered when it is to be incorporated into an advanced therapy for patients. Sourcing type I collagen from a GMP compliant supplier should minimise risks to patient safety. This is because GMP certification requires products to be manufactured using strict quality-controlled protocols. In addition, animal-derived products must be TSE compliant [206].

At the time that this PhD thesis commenced, most of the previous research and development work on RAFT-TE [127, 206, 211, 254-261] had utilised a cost-effective, acid-extracted, type I collagen from rat tail (owing to its relatively

pure collagen yield)- known as *First Link* collagen. It was therefore necessary to find an alternative type I collagen product to enable the advancement of RAFT-TE towards the clinic. Moreover, it is not sufficient, from a regulatory or scientific point of view, to simply change a component of an advanced therapy without validation to test comparability.

Koken collagen is a collagen type I extracted from bovine skin and manufactured in compliance with GMP, so it was chosen as the replacement for *First Link* rat tail collagen. *Koken* ensures the safety of their materials through strict management of the bovines they use as a source and, for this reason, they were selected as the suppliers of our clinically relevant RAFT-TE. Their criteria are as follow:

- Bovine dermis from up to 6 months calves from Australia which has a national livestock traceability system allowing the track of the bovine to their birthplace;
- Use of BSE-free safe feed;
- Use of the dermal layer of the skin, which is classified as belonging to the "no detectable infectivity" category (WHO Guidelines on Tissue Infectivity Distribution in Transmissible Spongiform Encephalopathies (TSE)).

Considering the standards mentioned above, *Koken* collagen is considered “TSE compliant”. The collagen solution is provided with all the necessary product information and quality documentation for GMP manufacture.

Human amniotic membrane (HAM) is currently the gold standard in the clinic for the transplantation of limbal epithelial stem cells on a substrate. With this in mind, Massie and colleagues designed a comparative study of RAFT-TE (manufactured with *Koken* collagen) and HAM where transparency, thickness, light transmission, tensile stress and degradation rates were assessed [184]. Different collagen concentrations and volumes were used to tune RAFT-TE properties. As expected, RAFT-TEs produced using higher amounts of collagen were thicker and stronger but had inferior optical properties than those produced using lesser amounts of collagen. The ‘optimal’

RAFT-TE protocol arose from this study and was thin, transparent but still handleable and was produced using 0.6 mL of 3 mg/mL collagen.

Although many studies have been performed by our group in the past, there is no study where both *Koken* collagen and neutralising solution are used in the production of RAFT-TE equivalents, or where *Koken* RAFT-TE is directly compared with *First Link* RAFT-TE. Kureshi *et al*. [127] have used neutralising solution in the production of RAFT-TE using *First Link* rat tail collagen, and Massie *et al*. [184] have used *Koken* collagen neutralised with sodium hydroxide (5 M).

This chapter aims to evaluate the differences caused by the replacement of research grade collagen with GMP compliant type I collagen and to track the impact of manufacturing changes, and collagen source variation on the TE properties.

RAFT-TE aims to reproduce the natural properties of tissue in the laboratory by producing strong, transparent and thin TEs. They should also be biocompatible, mechanically stable and capable of promoting cell attachment and proliferation [157, 158]. It is important to understand how the chemical and biophysical properties of RAFT-TE can modify cell behaviour such as morphology, adhesion and differentiation [159].

Whilst some progress has been made towards producing RAFT-TE with collagen matrix organization mirroring that of the cornea using *First Link* type I collagen [255], this has not yet been fully achieved. Therefore, it would be advantageous if through substitution of *First Link* with *Koken* type I collagen the RAFT-TE manufacturing process could produce fibrils of similar physical characteristics of those in the native cornea. Those fibres could subsequently be re-organised over time by incorporating stromal cells inside the RAFT-TE.

To obtain a RAFT-TE that mimics the native tissue, different parameters should be considered. The *Koken* collagen protocol should mimic the *First Link* protocol as much as possible if a like-for-like change is to be made. However, *First Link* and *Koken* collagen are supplied at different concentrations and in different acids as summarized in Table 4.1.

A head to head comparison of *First Link* and *Koken* collagen was therefore necessary because this could make a difference to the RAFT-TE manufacturing process itself.

Table 4.1 - Replacement of research grade with GMP* compliant type I collagen: *First Link* Collagen vs *Koken* Collagen.

	First Link Collagen	**Koken Collagen**
Origin	Rat Tail	Bovine Dermis
Starting Concentration	2mg/mL	3mg/mL
Type	Collagen type I (Percentage not available)	Collagen type I – 95% Collagen type III & V - 5%
Additional info	Chloroform Treated	Acid soluble collagen
Grade	Research Grade	GMP Compliant*

**As result of Risk Assessment*

This chapter puts side-by-side the last iteration of the research protocol, with the protocol we aim to use in the manufacture of RAFT-TE for clinical trials, taking into consideration the iterations in the manufacturing process. Table 4.2. highlights the differences between the compared RAFT-TE protocols.

Table 4.2 – RAFT-TE procedure modifications: research protocol vs clinically relevant protocol

RAFT TE Protocol	**Lab Based**	**Clinically Relevant**
Collagen Origin	Rat Tail	Bovine Dermis
Collagen Concentration	2mg/mL	3mg/mL
Collagen Grade	Research Grade	GMP Compliant
Neutralisation	Sodium Hydroxide	Neutralising Solution (Developed by TAP Biosystems)
Volume of Collagen Solution (24-well plate)	2.4mL per TE	0.6mL per TE
Compression Time*	30min	30min
*Although compression time was not altered, it might impact the TE due to the reduction in the solution volume		

The HPAs used to gently wick water away from the collagen hydrogels are made of porous sintered polymers and are individually wrapped and sterilised using gamma radiation [206]. This process is referred to as compression time

throughout this thesis, and the interaction between the HPA and the RAFT-TE could be altered due to the changes in the process.

It was unknown whether the *Koken* collagen would be able to substitute *First Link* collagen. To access its suitability as replacement, different parameters had to be considered.

The characteristics of the surface of the TE are of extreme importance since they affect cell attachment and behaviour. For example, collagen fibril diameter and pore size dictate the surface area available for cell attachment. Collagen fibril diameter, in general, can go from 10 to 300 nm [262]. However, in the human cornea, the diameter of the collagen fibrils is between 25-30nm [13, 263]. RAFT-TE should approximate the physical features of collagen fibrils of the cornea. However, this has not yet been studied.

The wettability of the RAFT-TE surface is directly related to its hydrophobicity. It is an important modulator of cell behaviour and by affecting conformation, concentration, and identity of adsorbed proteins [264].

RAFT-TE thickness is important due to a variety of factors. Overall, it is an important consideration in corneal tissue engineering where precise depths will be required to replace scarred tissue. The thickness can impact the surgical procedure. If thicker than needed, it might be uncomfortable for the patient. However, if too thin, it will be fragile and difficult to manipulate [184]. Thickness of the TE can also impact its mechanical and optical properties.

Since the work presented on this chapter does not aim for a full cornea replacement, the mechanical properties of the TE can differ from the cornea itself. Depending on which layer of the cornea, and the depth of the transplant, mechanical requirements will change.

Break-stress evaluates the mechanical properties of the RAFT-TE, and thus the potential to induce a different cell response if differences are found between the tested TEs [265]. For comparison, distal HAM break stress is around 0,5 MPa [184].

Transparency of RAFT-TE is relevant to improve patient's vision in short-term. However, in the long-term, TE may be absorbed or replaced by autologous tissue since it is biodegradable [184].

This chapter is novel and critical for the progress of RAFT-TE towards the clinic. It will perform for the first time a head-to-head comparison of the collagens and protocols used in the development stage of RAFT-TE with the ones aimed to be used in the clinic.

4.2. Aim

This chapter aims to:

- Validate the translation of bench to bedside RAFT-TE manufacturing modifications;
- Evaluate how changes in the manufacturing process might affect RAFT-TE properties;
- Compare head-to-head *First Link* and *Koken* collagen assessing differences in parameters such as surface topography, hydrophobicity, thickness, mechanical strength, and transparency.

4.3. Materials and Methods

4.3.1. Preparation of RAFT-TE

RAFT-TEs were prepared using different volumes and concentrations of collagen solution. The results presented in this chapter involve the comparison of different TE preparations, as shown in Figure 4.1.

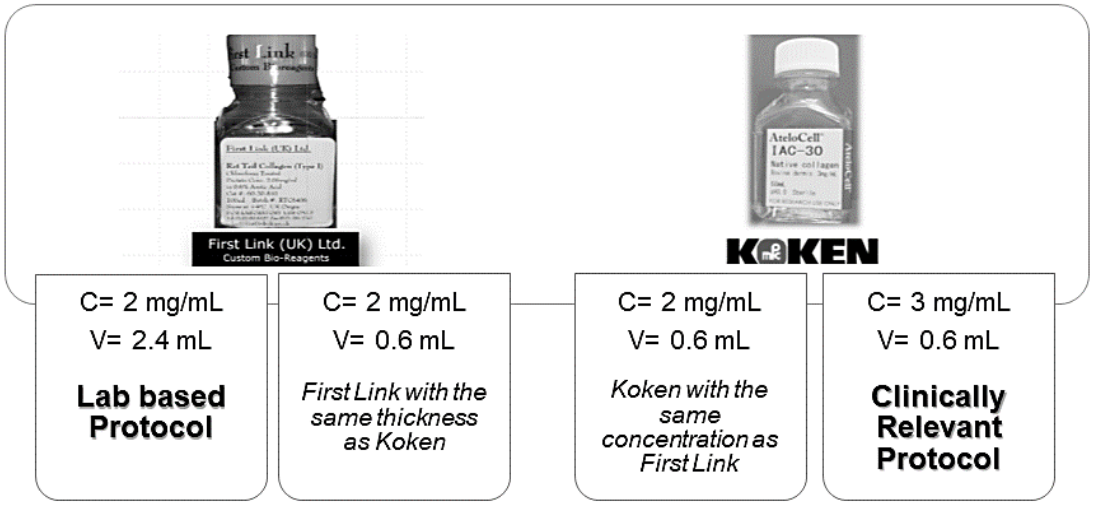

Figure 4.1. – Diagram of RAFT-TE iterations concerning volume (V) and concentration (C). Lab-based protocol leads to the production of research TEs (R TEs), and the clinically relevant protocol produces GMP compliant TEs (GMP TEs).

4.3.1.1. *Koken* Collagen – Bovine Dermis

Koken collagen RAFT-TE was prepared as described on section 2.9.1. of Chapter 2.

4.3.1.2. *First Link* Collagen - Rat tail

Rat tail collagen type I TEs were prepared as described on section 2.9.1. The mixture was prepared following the same steps but adding 9.3 mL of rat tail collagen type I (*First Link*, UK), 1.2 mL of 10x Minimum Essential Medium (MEM, Invitrogen), 0.689 mL Neutralising solution (Lonza RAFT™ kit - NaOH and HEPES) and 0.476 mL of CSSC media. These TEs are usually prepared with 2.4 mL of solution in each well of a 24-well plate. However, where noted, thinner TEs were fabricated using only 0.6 mL of collagen mixture.

4.3.2. RAFT- TE Surface Topography

4.3.2.1. Scanning Electron Microscopy Analysis

RAFT-TEs were examined as described in section 2.10.1. of Chapter 2.

The hydrophilic porous absorbers (Lonza RAFT™ kit) used in TE compression were also observed under SEM. The surface in contact with the hydrogel was gold coated (Appendix, Figure S4.2).

4.3.2.2. Collagen Fibril Organisation and Measurements

RAFTs were analysed by SEM to inspect surface topography, assess collagen fibril organisation and quantify collagen fibril diameter. The diameter of the fibres was measured using Fiji software. For each condition, three samples were tested, and 600 fibres/fibrils were measured.

4.3.3. RAFT-TE Wettability using contact angle

The wettability of the TE was verified by the measurement of the contact angle of the surface with water. All TEs were analysed following a 24h PBS soak to remove the effect of the serum present in the media.

The TEs were then blotted to remove the excess of liquid. First by moving from the well to a coverslip and then touching the surface with absorbent paper. They were let to dry at RT for 5min. The contact angle was then recorded using a camera and FTA32 software. Instant images were taken at the precise time the 10µl water drop touched the surface. Five repeats on each TE were done with n=3 for each type of TE.

4.3.4. RAFT-TE Thickness measurements by OCT

The thickness of each RAFT was measured using optical coherence tomography (OCT). An OCT machine with anterior segment adaptor (Envisu R2200, Bioptigen) was used to image individual samples (10 line scans per sample). To measure the thickness of the samples, four callipers were designed in the inbuilt software, measured and exported to an excel file (four measurements per image). All OCT measurements were performed at least four times.

4.3.5. RAFT-TE Mechanical Testing

To assess the mechanical properties of the TEs, break stress test was performed. The samples were removed from PBS and cut with a scalpel into 'dog bone' shape, approximately 4 mm wide and 10 mm long. The samples were then clamped between metal mesh grips (MeshDirect, Burslem, UK) and loaded into a custom-made tensile strength testing device. Samples were held in place, and weights applied incrementally until failure. Break stress was calculated using the following method: break stress = force/initial cross-sectional area (assuming cross sectional area did not change during the test). The last was calculated using the OCT thickness measurements previously described. This test was performed in triplicate for each TE.

4.3.6. RAFT-TE Transparency using light transmission measurements

Performed as described in section 2.10.2 of Chapter 2.

4.3.7. Statistical Analysis

Statistical analysis of results was carried out using Prism 4.0 software (GraphPad, USA). Different tests were performed according to the experiments and are detailed in the results section.

4.4. Results

4.4.1. RAFT-TE Surface Topography

Scanning electron microscopy (SEM) was performed to inspect the surface topography and to quantify collagen fibril diameter. However, looking back, it is acknowledged that transmission electron microscopy (TEM) would have been a more suitable method to assess the formation of the fibrils, and measure fibril diameter. First, different preparation protocols were tested to

decide which one least affected the structure of the TE (Figure S4.1). From this analysis, it was clear that the non-fixed TEs would fold more readily than the ones exposed to PFA, leading to poor quality structure preservation. A pattern consisting of cracks was observed across the surface of the *Koken* TEs. Additionally, to see if there was any correlation between the pattern observed in the *Koken* TEs after compression, and the plunger surface used in the manufacturing process, SEM was performed on their surface (Figure S4.2). From the pictures, it was not possible to find any relation with this phenomenon.

4.4.1.1. Morphological characterisation of TE fibrils

The following images (Figure 4.2.) and graphs (Figure 4.3.) present a comparison between RAFT-TE prepared with *First Link* Collagen (2 mg/mL- 0,6 mL and 2,4 mL) and *Koken* Collagen (2 mg/mL and 3 mg/mL - 0,6mL).

Figure 4.2. presents the fibril morphology and organisation along the different TEs. Figure 4.2 A, B, E and F show *Koken* collagen fibrils while C, D, G and H represent *First Link* collagen fibrils. Images 4.2 A-D are lower magnification and E-H high power, allowing the taking of measurements presented in Figure 4.3. It is possible to observe that *First Link* rat tail collagen forms more bundles when compared to *Koken* collagen. *Koken* collagen fibrils appear to be more aligned than the *First Link* collagen ones. *First Link* Collagen RAFT-TEs prepared with a volume of 0.6 mL were too weak and difficult to analyse. Therefore, the rest of this thesis focuses on the evaluation of the other three conditions.

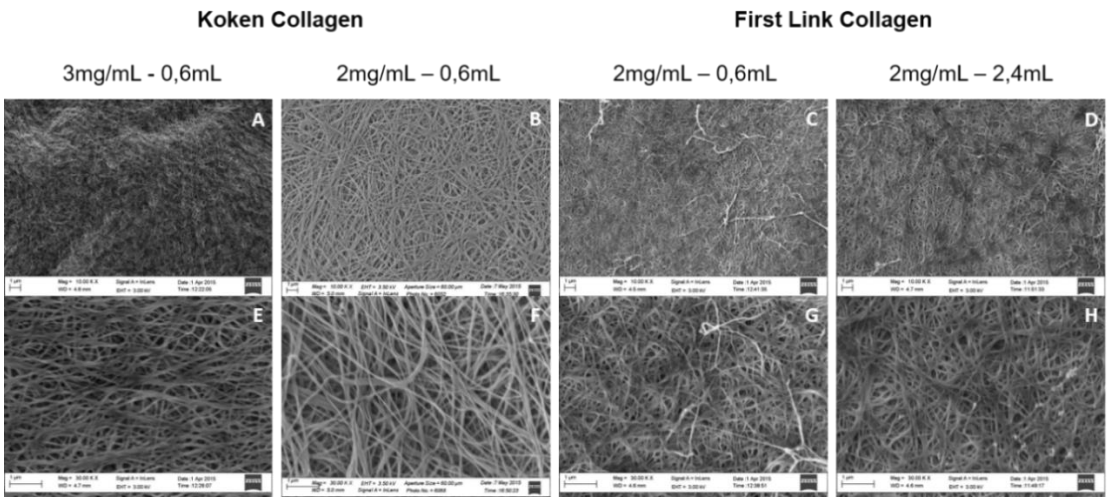

Figure 4.2 – Collagen fibril morphology characterisation of TEs by SEM: **(A, B, E & F)** Koken Collagen and **(C, D, G & H)** *First Link* Collagen. **(A & E)** *Koken* Collagen 3 mg/mL, V=0.6 mL; **(B & F)** *Koken* Collagen 2 mg/mL, V=0.6 mL; **(C & G)** *First Link* Collagen 2 mg/mL, V=0.6 mL & **(D & H)** *First Link* Collagen 2 mg/mL, V=2.4 mL. **(A-D)** Mag=10.00KX & **(E-H)** Mag=30.00KX.

Fibril diameter was measured using Fiji software, and distribution graphs are presented below (Figure 4.3). Figure 4.3 A shows a box plot of the fibril diameter of the three conditions in analysis while B, C and D are each condition respective histogram distribution. It is possible to observe that there is a higher percentage of smaller fibrils in the 2 mg/mL *First Link* collagen when compared to the 3mg/mL *Koken*. It is also clear that there is a significant difference between the two concentrations of *Koken* (Figure 4.3 A).

Figure 4.3 A is a direct comparison of the different TEs showing the median and overall distribution of the collagen fibrils. From these distribution plots, it is clear that the fibre diameter is similar for all conditions except the 3 mg/mL *Koken* TE, in which fibril diameter is larger. The averages of fibril diameters are: *Koken* 2 mg/mL – 75,56±18,58nm, *Koken* 3 mg/mL – 100,0±52,71 nm, and *First Link* 2 mg/mL – 78,62±39,93 nm

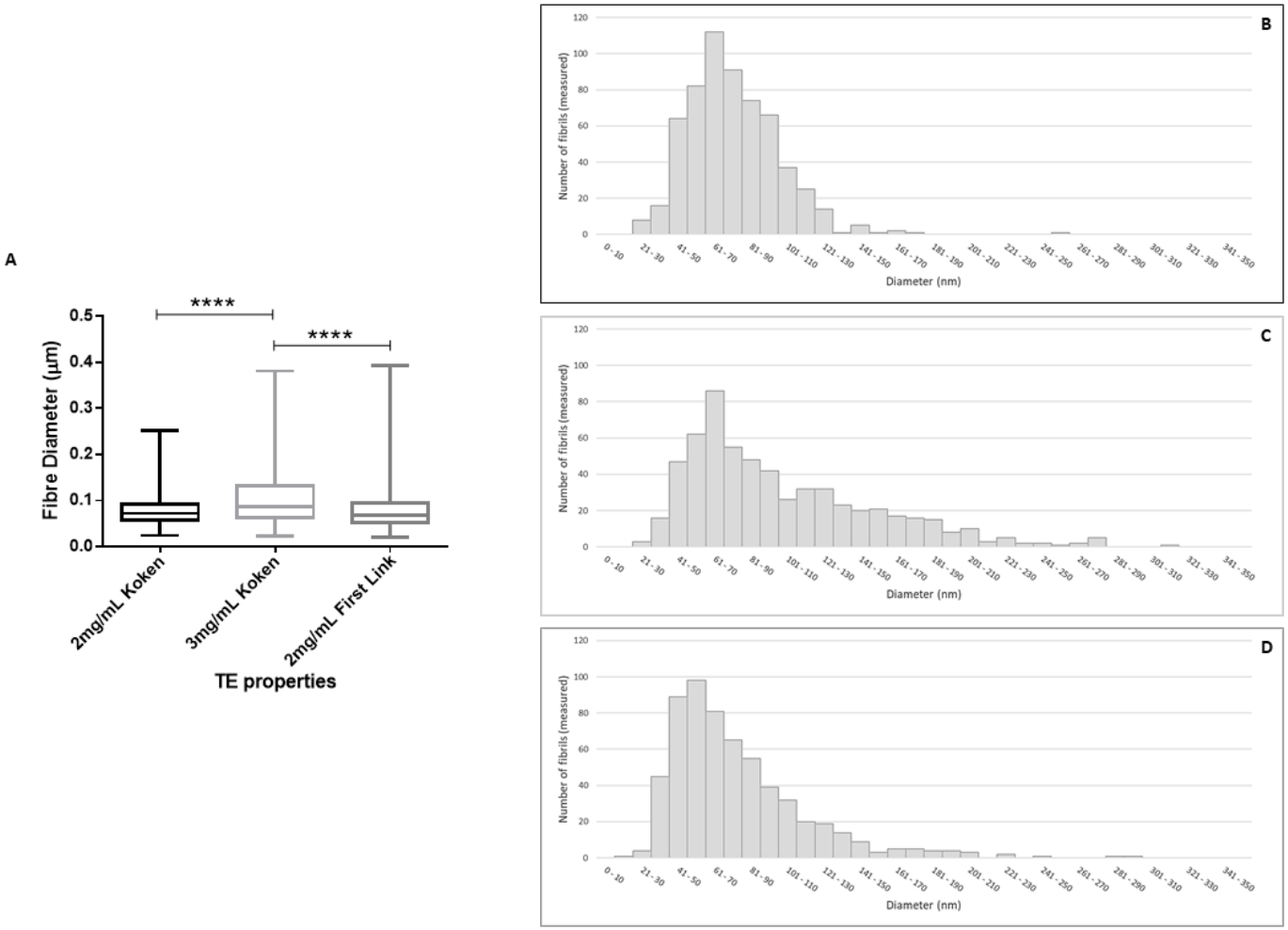

Figure 4.3 - Morphological Characterization of RAFT-TEs based on SEM. **(A)** Boxplot of collagen fibril diameter (n=600); **(B)** 2 mg/mL *Koken* Collagen, 0.6 mL; **(C)** 3 mg/mL *Koken* Collagen, 0.6 mL and **(D)** 2 mg/mL *First Link* Collagen, 2.4 mL. The diameter of the *Koken* 3 mg/mL collagen fibrils was significantly greater than 2 mg/mL *Koken* and *First Link* collagen fibrils [p<0.0001, one-way ANOVA with Tukey's multiple comparisons test].

After analysis, it is possible to say that on average, the diameter of the *Koken* (3 mg/mL) collagen fibrils was significantly higher than *First Link* fibrils and *Koken* fibrils of the lower concentration collagen solution [$p<0.0001$]. Overall, lower collagen solution concentrations produce smaller diameter fibrils. This might influence cell attachment as the surface area available for the cells to adhere is smaller.

Figure 4.3 B, C and D show the histograms of fibril diameter distribution. These histograms have eight bins and allow a more detailed comparison of fibril diameter than the boxplots of Figure 4.3 A. Comparing the two *Koken* formulations (Figure 4.3 B & C) is possible to observe that the increase on the fibril diameter comes from a decrease of the fibrils in the range of 0.061-0.100 µm and an increase of fibril distribution on the ranges from 0.101-0.340 µm. It is also important to notice that although there is no significant difference between *Koken* and *First Link* collagen of the same concentration (2 mg/mL) when accessing the median, it is clear from the histograms (Figure 4.3. B & D) that *First Link* collagen has a lot more fibrils on the range of 0.020-0.060 µm than the *Koken* collagen.

4.4.2. RAFT-TE Wettability

The wettability of the TE was verified by the measurement of the contact angle of the surface with water. Figure 4.4 A shows a bar graph of the average contact angle of the TEs with water. Figures 4.4 B, C and D are the pictures of the drop of water at the moment it reached the TE surface for the three different conditions. There was no significant difference between the contact angle of the three TE preparations as is possible to observe in Figure 4.4. All the TEs have hydrophilic surfaces with contact angle smaller than 90º [*Koken 3 mg/mL* – 81,32±2,494º < *First Link 2 mg/mL* – 84,34±1,138º < *Koken 2 mg/mL* – 87,09±2,684º].

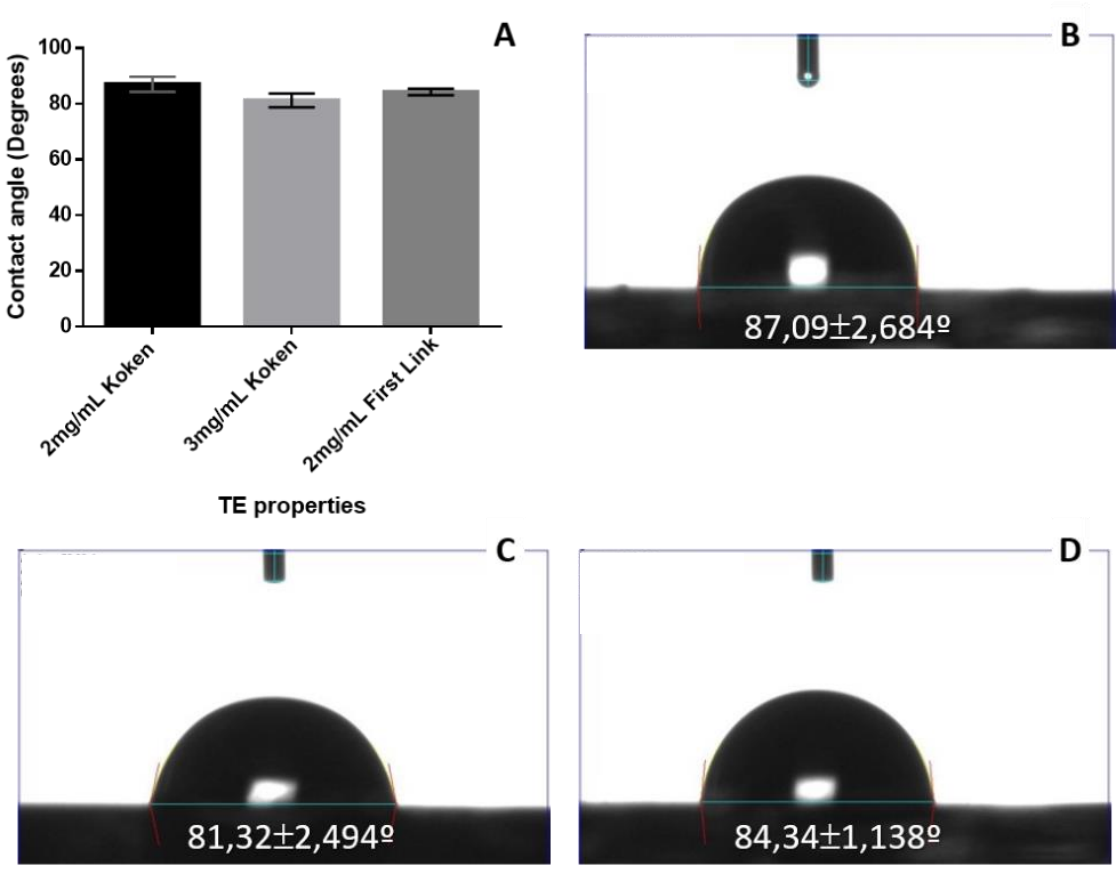

Figure 4.4 - Contact angle of the surface of the different TEs (2mg/mL Koken Collagen, 0.6 mL; 3 mg/mL Koken Collagen, 0.6 mL and 2 mg/mL First Link Collagen, 2.4 mL) with water : **(A)** Measurements graph summary and **(B-D)** Photographs of the drop in the exact moment that it reached the sample surface **(B)** 2 mg/mL Koken Collagen, **(C)** 3 mg/mL Koken Collagen and **(D)** 2 mg/mL First Link Collagen. There was no significant difference between the contact angle of the three TE preparations.

4.4.3. RAFT-TE Thickness

The thickness of the RAFT-TE was assessed by optical coherence tomography (OCT). Figure 4.5. A is a graph bar with an average of TE thickness. Figures 4.5 B, C and D are OCT images of each sample. As expected, RAFT-TE thickness varied with the change of volume of collagen and not within TEs of the same concentration. *Koken* RAFT-TEs were thinner than *First Link* TE due to the volume difference. The thickest RAFT-TEs were produced using 2.4 mL of 2 mg/mL *First Link* collagen (Figure 4.5). A one-way ANOVA test showed that there is no statistically significant difference between the two concentrations of *Koken* collagen. However, the other comparisons

were significant [*First Link* (2 mg/mL) vs. *Koken* (3 mg/mL) [p=0,0037] and *First Link* (2 mg/mL) vs. *Koken* (2 mg/mL) [p =0,0030].

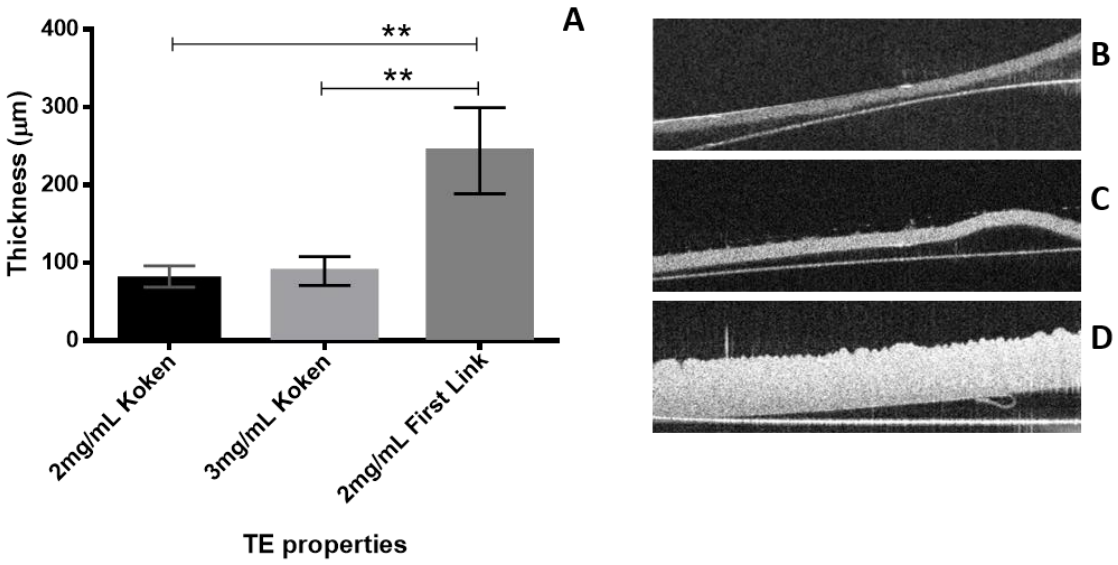

Figure 4.5 . – RAFT-TEs thickness assessment. **(A)** Graph with average thickness for different TE conditions and **(B, C, D)** OCT pictures for the different properties of RAFT-TE **(B)** 2 mg/mL Koken Collagen, 0.6 mL; **(C)** 3 mg/mL Koken Collagen, 0.6 mL and **(D)** 2 mg/mL First Link Collagen, 2.4 mL. First Link TE is significantly thicker than Koken TEs [p =0.0030]. Koken 2 mg/mL – 82,57±13,59 μm < Koken 3 mg/mL – 89,55±18,58 μm < First Link 2 mg/mL – 244,2±55,26 μm].

4.4.4. RAFT-TE Mechanical properties

Break-stress tests were performed to evaluate the mechanical properties of the RAFT-TEs. Figure 4.6 A shows a bar graph with TEs break stress average for the samples in analysis while B is a picture of the apparatus with one of the samples in place in dog bone shape. They showed that *Koken* TE (3 mg/mL) were significantly stronger than *First Link* and *Koken* TE (2 mg/mL) [$p < 0.05$, one-way ANOVA with Tukey's multiple comparisons test] (Figure 4.6) [*First Link 2 mg/mL* – 400±56 KPa < *Koken 2 mg/mL* – 405±21 KPa < *Koken 3 mg/mL* – 660±20 KPa]. The average break stress for RAFT-TEs was affected by both collagen volume and concentration.

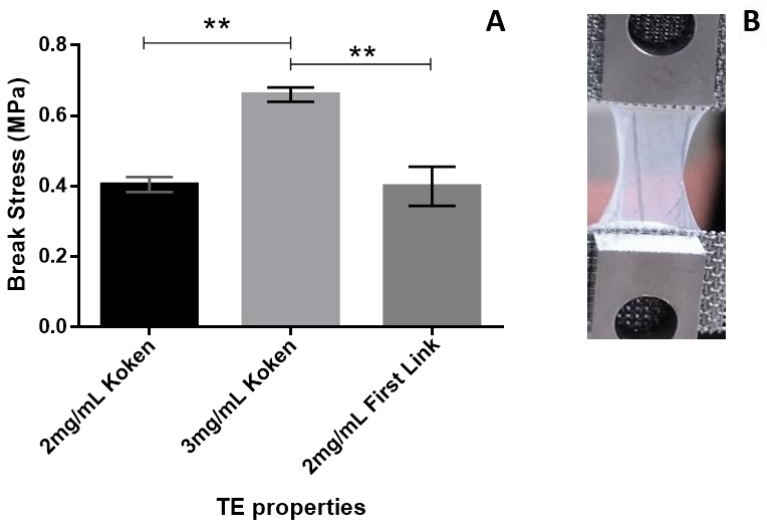

Figure 4.6 – Mechanical properties of the different RAFT-TE ((2 mg/mL Koken Collagen, 0.6 mL; 3 mg/mL Koken Collagen, 0.6 mL and 2 mg/mL First Link Collagen, 2.4 mL)): **(A)** Break stress in MPa of the different TEs and **(B)** picture of the apparatus with the TE in dog-bone shape. Koken TE 3 mg/mL is significantly stronger [$p<0.05$] than First Link 2 mg/mL and Koken TE 2 mg/mL.

4.4.5. RAFT-TE Transparency

Transparency was assessed through light transmission by absorbance readings using a spectrophotometer. Different collagen concentrations were evaluated to optimise strength without affecting transparency.

Figure 4.7 A shows the subjective assessment of transparency of the 'optimal' TE protocol (*Koken*, 3 mg/mL, 0.6 mL). Figure 4.7 B presents the transmission of light through the different TEs across the spectrum (visible light 380-740 nm) while C displays the average transmission of light at 550 nm since the maximum sensitivity of the eye is around this wavelength.

Figure 4.7 shows that there was a clear difference between the *First Link* TE (much thicker) and the other two conditions [*First Link 2 mg/mL* ≅ 24% < *Koken 3 mg/mL* ≅ 65% < *Koken 2 mg/mL* ≅ 72%; $p<0,0001$, one-way ANOVA with Tukey's multiple comparisons test]. There was also a significant difference in transparency between the two concentrations of *Koken* collagen, even though the same volume of solution was used; lower concentrations of collagen lead to more transparent TEs. *Koken* 2 mg/mL was more transparent than the *Koken* 3 mg/mL [$p=0,0116$].

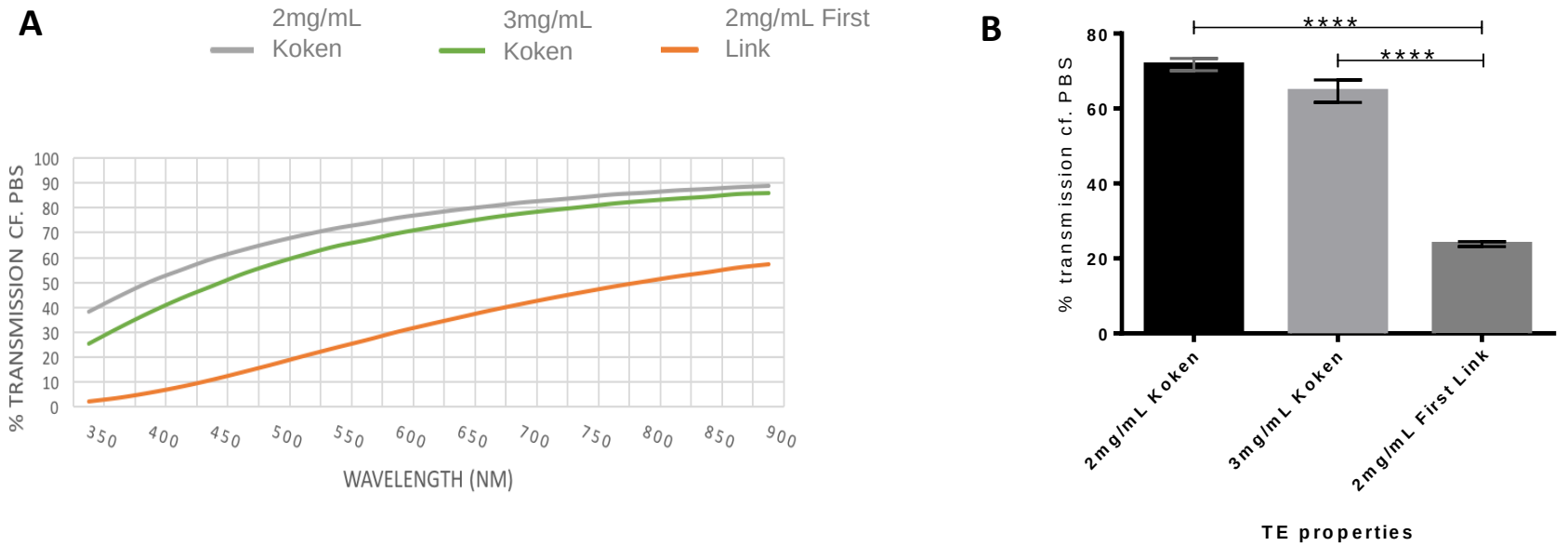

Figure 4.7 – RAFT-TE transparency of the three different structures in analysis: 2 mg/mL Koken Collagen, 0.6 mL; 3 mg/mL Koken Collagen, 0.6 mL and 2 mg/mL First Link Collagen, 2.4 mL. Transmission of light through RAFT-TEs: **(A)** spectrum screening from 350 to 900 nm wavelength and **(B)** average at 550 nm. First Link TE is the least transparent [p<0,0001]. The 2 mg/mL Koken TE is more transparent than that made with Koken collagen at 3 mg/mL [p=0,0116].

Summary of results:

The comparison of clinically relevant TE (0.6 mL of *Koken* collagen 3 mg/mL) with research TE (2.4 mL of *First Link* collagen 2 mg/mL) highlighted that:

- TE fibril diameter is higher in *Koken* TE than in *First Link* TE;
- TE wettability is similar in both TEs;
- *Koken* TE is stronger than *First Link* TE;
- *Koken* TE is more transparent than *First Link* TE.

4.5. Discussion

This chapter aimed to make a direct comparison of two type I collagen sources to establish if a GMP compliant product could be used to replace a research grade only material without compromising the desired characteristics of RAFT-TE.

For Good Manufacturing Practices and from a clinical point of view, it is vital to demonstrate that the RAFT-TE production process is reproducible and tuneable. For ocular surface reconstruction, there is a need for producing strong, transparent, thin structures. However, this study might also be relevant for other tissue regeneration approaches where different properties are prioritised.

The suitability of *Koken* collagen to produce TEs for ocular surface reconstruction was assessed based on multiple parameters, and in direct comparison with the previous lab tested *First Link* collagen TE.

4.5.1. RAFT-TE Surface Topography

The surface structure of a biomaterial is very important as it can affect cell behaviour. In this study, SEM protocols were optimised to assess the surface properties of the TE. Looking at the different protocols of TE preparation for SEM, it is possible to conclude that fixation with PFA helps in the maintenance of the 3D structure.

It was not possible to find a correlation between the plunger surface and the cracks observed in the surface of the *Koken* TEs. There is no obvious explanation for this phenomenon in the literature. However, an analogy can be made with a phenomenon that was observed by Casares *et al.* [266] when testing the different substrates for the culture of epithelial cell sheets under different mechanical conditions. They demonstrated that the formation of epithelium is hydraulic, resulting from a transient pressure build-up in the substrate during stretch and compression. An analogy can be made with the compression process of TEs. The flow of water from the hydrogel network to the hydrophilic porous absorber might build pressure at the surface of the 3 mg/mL *Koken* TEs, which was not experienced so often with the *First Link* TEs. This might be explained by the poroelastic theory that predicts that stiffer hydrogels, as 3mg/mL *Koken* when compared to *First Link*, build up higher pressure and thereby increase the cracked area.

4.5.2. Morphological characterisation of TE fibrils

The surface area available for cell attachment depends on variables such as fibril diameter and pore size. The SEM images reveal that the collagen matrices were composed of long thin filaments. The fibril diameter is within the usual range of collagen, that can go from 10 to 300 nm [262]. Fibril structure in collagen TEs is variable and affected by parameters like density, diameter, pore size and orientation.

There are several methods available for the measurement of hydrogel fibre structure. SEM had been previously used for semi-quantitative analysis of the fibril network. Still, it is recognised that the manipulation of the TEs before imaging can lead to shrinkage and collapse of the structure [267]. The data presented allows a comparison between the different TEs as they go through the same protocol but does not allow the determination of the exact fibril diameter value due to artefacts (like reduction in size due to dehydration) created by the preparation of the samples itself. An increase in fibril diameter is seen when the collagen concentration of the TE increases. Published results on this matter showed inconclusive results. Some authors claim that at lower

concentrations fibril diameter should remain constant, others report an increase or even a decrease in diameter [268-270].

Fibre shape may also depend on the neutralising solution [271], so it would be incorrect to compare the 2 mg/mL *Koken* prepared with NaOH, with the neutralising solution containing HEPES used for the 3 mg/mL *Koken* and *First Link* collagen. Another possible parameter influencing fibril diameter is the percentage of different collagen types in solution. Previous work by Linsenmayer and colleagues has shown that collagen V forms smaller fibrils than collagen I [272]. This raises a question on whether First Link contains a higher percentage of Collagen V than Koken collagen as the concentration of the different collagen type is not disclosed by the manufacturing company.

When in the presence of the same volume of solution per TE, aggregation of fibrils is higher in high concentration leading to a higher diameter and to an increase in opacity as was possible to observe when the two *Koken* TE collagen concentrations were assessed (2 mg/mL vs 3 mg/mL) by transmission [273]. These results show that differences in the concentration of collagen are the primary trigger of fibril diameter changes. Lower concentrations lead to smaller fibril diameters.

In conclusion, RAFT-TE prepared under the same conditions but with different types of collagen, presented different morphological characteristics, especially differences in the diameter of the collagen fibrils.

4.5.3. RAFT-TE Wettability

Contact angle measurements are directly related to the wettability of the surface. Hydrogel hydrophobicity is an important modulator of cell behaviour being primarily critical in the determination of the conformation, concentration, and identity of adsorbed proteins [264].

There was no significant difference between the TEs, so this is not a variable that might affect cell behaviour.

4.5.4. RAFT-TE Thickness

As previously reported, the thickness of the RAFT-TE measured by OCT is important due to a variety of factors. If too thick, it can disturb the surgical

procedure and be uncomfortable to the patient. Conversely, if too thin, it can be extremely fragile and difficult to handle [184].

First Link collagen (2 mg/mL, 2,4 mL) tested in this section has a similar thickness to the *Koken* TE under the same conditions tested in previous reports [184]. Both RAFT-TE of 2 mg/mL and 3 mg/mL *Koken* collagen showed similar thickness to the ones produced by Masie *et al.* using NaOH instead of neutralising solution [184].

This technique requires the assumption of similar refractive indices for the materials in comparison. Human cornea and RAFT-TEs are identified to have similar refractive indices [184]. In conclusion, collagen volume increased RAFT-TE thickness and decreased light transmission and transparency.

4.5.5. RAFT-TE Mechanical properties

Mechanical properties have the potential to evoke considerable cell responses. The micro-environment should be well understood in order to explain cell behaviour [265]. This is true not only at the TE surface but also at the environment that cells experience when embedded in the TE.

When looking at the mechanical properties of RAFT-TEs, we found that the RAFT-TEs produced using 0,6 mL of 3 mg/mL *Koken* collagen were stronger than the others, withstanding the stress of 0,66±0,020 MPa while the others stayed around 0,4 MPa.

All the TEs were much weaker than the cornea itself. However, these are much thinner structures than the full thickness cornea. Nevertheless, as stated by Massie and colleagues [184], these values are still comparable to distal HAM break stress that is around 0,5 MPa.

It is also important to point out that the break stress of the RAFT-TEs produced with the new protocol (using neutralising solution instead of NaOH) are stronger than what has been previously reported for *Koken* collagen. Specifically, 3 mg/mL *Koken* RAFT-TE has break stress around 0.66 MPa instead of the 0.4 MPa previously reported. If we aim to compare *Koken* and *First Link* collagen RAFT-TE under the same conditions, *First Link* proved to be much weaker (around 0.4 MPa, on this study) than *Koken* collagen (around

0.65 MPa, on Massie *et al.* study [184]).

The differences in the *Koken* collagen could be due to a batch-to-batch variation. However, since the processing of this collagen is tightly controlled by the suppliers, we might attribute the variance to the use of a different neutralising solution.

4.5.6. RAFT-TE Transparency

As expected, TE transparency was higher in thinner gels with lower collagen concentrations. Aggregation of fibrils is higher in high concentration, increasing the opacity of the TEs [273]. These results corroborate the previous study of our group using a different collagen neutralising approach [184]. This is mainly relevant to improve patient's vision in short-term because, in the long-term, the biodegradable TE may be absorbed or replaced by autologous tissue.

4.5.7. Summary

The head-to-head comparison of *First Link* and *Koken* Collagen TE showed that *Koken* TEs have the potential to be used as an advanced therapy for ocular surface reconstruction due to the improved characteristics in comparison to *First Link* TE.

Although *Koken* TE fibril diameter has increased from an average of 78,62±39,93 nm to 100,0±52,71 nm, more than 60% of *Koken* fibrils are smaller, and closer to the average corneal fibril diameter that is between 25 and 30 nm [13, 263].

TE wettability suffered no significant changes, which means the change in collagen used to prepare the TEs should not directly affect protein or cell attachment.

Even though *Koken* TE thickness was reduced to allow surgical implantation, its strength increased, as shown by the higher breaking stress. The reduction of TE thickness also improved *Koken* TE transparency in comparison to the *First Link* TE.

4.6. Conclusion

Translation from bench to clinics is always a challenge, and this work highlights the importance of considering clinically accepted reagents early in the process of development. This study provides quantitative comparative data against which other collagens could be compared if required.

The *Koken* RAFT-TE shows similar or improved properties to what has been described before. However, the change in neutralising solution affected its mechanical properties. Although not directly measured in this experiment, the TEs produced now with NS instead of NaOH are considerably stronger.

The future chapters of this thesis will delve into cell culture work and how the TE properties analysed in this chapter might explain different cell behaviours when compared to previous investigations.

Chapter 5

5. AN INVESTIGATION OF THE EFFECT OF MANUFACTURING AND CELL SEEDING MODIFICATIONS ON RAFT-TE PRODUCTION FOR OCULAR SURFACE RECONSTRUCTION

5.1. Introduction

The transparency and homeostasis of the cornea are essential for the maintenance of normal vision. The outer layer of the cornea, the epithelium, is easily exposed to injuries and insults from the surrounding environment [274]. Thus, LESCs are of extreme importance because they are responsible for the physiological renewal of the corneal epithelium. Adult corneal epithelial cells have a short lifespan of 7 to 10 days before undergoing apoptosis and desquamation. To replace them, LESCs divide to produce daughter cells which differentiate and migrate centripetally from the limbus to the central cornea [275].

Patients with LESC deficiency rely on the transplantation of autologous or allogenic LESCs. The current gold standard is the use of HAM as a carrier [276], but results can still be inconsistent [277].

Previous chapters of this thesis have presented Real Architecture for 3D Tissue (RAFT) as an alternative to HAM with regards to its properties. Studies have been done by our group on the potential for RAFT to support the growth of LESCs, and it has been previously reported that LESCs preserve a stem-like cell phenotype when cultured on top of RAFT. For example, by expressing high levels of the putative stem cell marker p63α, maintaining a small cell size

and high nucleus/cytoplasm ratio as well as the ability to stratify and differentiate into terminally differentiated cells [206, 211, 258].

Most of the work done so far expanding corneal epithelial cells involved a growth-arrested 3T3 fibroblast feeder layer [278, 279]. However, this is now seen to be sub-optimal, as murine cells pose a risk of transferring adventitious agents to the patient [127]; hence alternative methods have been developed to eliminate the use of a murine 3T3s feeder layers.

In the search for replacements, it has been found that human limbal fibroblasts support LESC growth in RAFT and lead to a higher organisation of the matrix and an increase of basement membrane production [164, 257]. More recently, a population of putative MSCs, now known as CSSC, has also been identified in the limbal niche in close proximity with LESCs [98, 114].

To mimic this arrangement, RAFT has been used as a 3D substrate for co-culturing LESCs and CSSC [127]. This method is referred to as mixed population and involves the dissection of the superficial corneal limbal region, and collagenase dissociation before seeding of the mix of cells obtained in a flask coated with FNC. It is likely that there is a synergic interaction between these cells [280], which could be exploited to eliminate the need for murine 3T3 feeder layers [127]. Furthermore, as it is a one-step procedure, it would simplify production in the GMP environment. Initially, this seemed to be the best cell seeding option [127]. However, over time, it became clear that this protocol did not meet expectations. Specifically, when the RAFT-TE were moved out of the well prior to *in vivo* transplantation in a pre-clinical study, the epithelial cell layer unexpectedly detached from the carriers.

In this chapter, different hypotheses were tested to attempt to identify why epithelial detachment occurred. Interestingly, the cell detachment phenomenon was not experienced prior to the change of collagen source for a clinically acceptable GMP grade material. Therefore, all the changes implemented in the clinical RAFT-TE manufacturing protocol were explored in this study. These were the use of neutralising solution (NS) instead of Sodium hydroxide (NaOH), the change to *Koken* collagen (bovine dermis) instead of *First Link* collagen (rat tail), and the fact that the compression time was not

reduced to account for the decrease in the final volume of collagen mix solution.

The conditions of donor cornea storage, prior to RAFT-TE manufacture, varied during the course of this thesis. Therefore, this chapter also investigated to what extent different corneal donor storage media and RAFT-TE cell seeding methods, e.g. the new mixed population protocol, might be contributing to the cell detachment. The worldwide shortage of donor corneas for transplantation also impacts tissue availability for research. This problem is aggravated by the different storage methods used around the world [281, 282]. European eye banks tend to utilise long-term storage (3-4weeks, at 37°C) of the donor corneas in organ culture media (OC). However, most US eye banks use short-term storage [283] under hypothermic conditions (up to 7 days, between 2°C and 8°C) in medium such as Optisol (OP)-GS (Bausch and Lomb, Rochester, NY, USA) [282].

Although hypothermic storage is the most common worldwide, Moorfields Lions Eye Bank (London, UK), the supplier of most of the tissue for this piece of research, stores the majority of corneas under OC conditions. A healthy endothelium is a major requirement for a successful corneal transplant. OC storage facilitates the monitoring of endothelium stability, allows more time to schedule in surgical procedures, match tissue types and consequently minimise waste of donor tissue [274]. This was probably the reason why OC was the preferred corneal tissue storage medium in Moorfields Lions Eye bank.

Over the course of this work, there was a reduction in OP tissue availability, until eventually the Moorfields Lions Eye Bank stopped using OP media altogether. Therefore, OP stored corneas had to be obtained from the USA to enable experimental comparison of epithelial cell detachment from RAFT-TE with cells isolated from OP versus OC conditions.

The revised aim of this chapter was to investigate the best way to deliver LESCs using the clinically relevant RAFT. This was accomplished by evaluating the impact of manufacturing changes of RAFT, as well as the different cell seeding techniques, on LESC behaviour.

5.2. Aim & Hypotheses

The previous chapter focused on the effect of manufacturing changes on RAFT production from the material characterisation perspective. It was shown that RAFT-TE made using the clinically relevant protocol differs from the lab-based protocol in terms of fibril diameter and break stress.

This chapter aims to investigate whether it is still possible to manufacture TEs using the new parameters of the clinically relevant RAFT-TE protocol while maintaining similar results. Preliminary studies showed that the new manufacturing protocol and the mixed population cell seeding approach led to the growth of healthy epithelial cells layers [184]. However, when removing the TE from the well before fixation in follow up studies, it was observed that the cells started to peel from the surface of the RAFT.

It was hypothesised that one of the manufacturing or cell seeding steps was introducing structural changes to the RAFT-TE that caused the epithelial cell peeling. This led to the review of the manufacturing process step-by-step in order to identify what could be impacting epithelial cell attachment. Therefore, the aims were to:

- Evaluate the impact of RAFT-TE manufacturing changes on cell behaviour:
    - Compare RAFT-TEs prepared with different collagen sources and neutralising solutions;
    - Compare RAFT-TEs prepared with different compression times;
- Compare different tissue storage media on the performance of mixed population seeding on top of RAFT-TEs
- Evaluate different cell seeding strategies on top of RAFT-TEs
    - Mixed population isolated from OP corneal rims on top on RAFT-TE;
    - LESCs expanded on 3T3s on top on RAFT-TE;
    - LESCs isolated with dispase directly cultured on top on RAFT-TE

The general hypothesis was that RAFT-TE would be able to support LESCs. Therefore, the aim of this chapter is to identify which step in the manufacturing process the cell peeling problem arose and to design an alternative that allows the LESCs culture on RAFT-TE.

5.3. Materials & Methods

5.3.1. Preparation of RAFT tissue equivalents (TE)

RAFT-TE were prepared as described in Chapter 2 (section 2.9). Table 5.1 summarises the different combinations of manufacturing procedures with different collagens, neutralisers and compression times. Symatese was used as an alternative GMP-compliant type I collagen for comparison purposes.

Table 5.1 – RAFT manufacturing combinations: collagen supplier, pH modifier and compression time.

Collagen	Concentration	pH Modifier	Compression Time (min)		
Symatese	3mg/mL (pre-diluted from original solution of 5mg/ml)	NaOH	30		
		NS			
Koken	3mg/mL	NaOH	30		
		NS	30	15	7.5

5.3.2. Cell seeding strategies

Table 5.2 presents a summary of the various methods used in the isolation and seeding of cells on top of RAFT. A detailed description of each method can be found below.

Table 5.2– Cell seeding strategies used to deliver cells to the surface of RAFT: tissue origin, isolation reagent, culture and seeding method.

Tissue	Isolation	Culture Method	Seeding Strategy	
OC/ OP Corneal Rims	Collagenase	Mixed Population	Direct Seeding	(A)
			Pre-expansion	(B)
Fresh Corneal Rim* * Obtained from cadaveric donors - Moorfields Lions Eye Bank.	Dispase	LESCs on growth-arrested 3T3s	Pre-expansion	(C)
		LESCs	Direct Seeding	(D)
			Pre-dissociated	(E)

5.3.2.1. (A) Direct seeding of mixed population on top of RAFT-TE

The limbus was dissected as previously described in section 2.1.1. and digested in collagenase overnight. Then, the mixed population, containing both epithelial (hLE) and stromal (CSSC) cells, was centrifuged and the pellet was washed in PBS. The cell suspension of each donor was divided into 4 equal parts, and 1 part added to each RAFT-TE in CSSC media.

5.3.2.2. (B) Pre-expansion of mixed population before seeding on top of RAFT-TE

Same procedure as described on 2.1.1 but instead of adding the cell suspension to RAFT-TE, 1 part was added to a well of a 6-well plate pre-coated with fibronectin-collagen (FNC; Athena Enzyme System, Baltimore, MD, USA). Cells were cultured at 37 °C, and 5% CO_2, and CSSC media was replaced three times a week.

When colonies of small polygonal cells were visible, Tryple express enzyme (Invitrogen, Paisley, UK) was applied to the mixed population of cultured limbal cells including LESCs and CSSCs for 2 minutes at room temperature (RT). This process selectively released some of the CSSCs from the mixed population which were discarded. The LESCs were then trypsinised, the colonies dissociated, and 100,000 cells were plated on top of RAFT.

5.3.2.3. (C) Seeding of LESCs pre-expanded on 3T3s on top of RAFT

The process of isolation and expansion of LESCs with dispase and growth-arrested 3T3s has already been described in Chapter 2 (section 2.5).

In this strategy, LESCs which had previously been expanded on 3T3 cells were seeded onto the surface of the RAFT-TE (100 000 cells/RAFT) and maintained in CECM culture medium in a humidified 5% CO_2 incubator at 37 °C, with three medium changes per week until confluency.

5.3.2.4. (D) LESCs directly seeded on top of RAFT

LESCs were isolated from fresh corneal rims using dispase as described in Chapter 2 (section 2.5). Part of the cell suspension (1/9, as there were too few cells to be counted) obtained from each corneal rim was added to the surface of RAFT and maintained in CECM culture medium in a humidified 5% CO_2 incubator at 37 °C, with three medium changes per week until confluency.

5.3.2.5. (E) LESCs pre-dissociated with TE before seeding on top of RAFT

Same procedure as described in 5.3.2.4. but with a 2min dissociation of the cells in Tryple express enzyme (Invitrogen, Paisley, UK) before being added to the surface of RAFT. This was performed to ensure that singe cells were obtained.

5.3.3. RAFT Cell Confluency and Attachment Analysis

The light transmission measurement protocol (section 2.10.2) and FdA staining (section 2.10.3) have already been described in Chapter 2. Below, an automated analysis algorithm to increase the efficiency of FdA quantification, and consequently cell confluency measurements, is presented.

5.3.3.1. Automatic Fluorescein diacetate (FdA) quantification

To optimise the process of FdA quantification, an algorithm for automatic detection was designed. Raw images were cropped to centre and enable a single well containing a RAFT-TE to be analysed at a time. Single well figures were resized to 256*256 pixel to ensure uniformity of size. Contrast Limited Adaptive Histogram Equalization (CLAHE) was used to improve the overall

contrast and intensity levels. The mean intensity of blue and red pixels (background) was subtracted to the intensity of the green (FdA) pixels to reduce noise. Final pixels with an intensity higher than a predefined threshold were labelled positive while others were labelled negative. The relative number of labelled pixels, in relation to the total number of pixels, was evaluated in a circle centred in the figures with a radius equal to 45% of the figure width. This number corresponded to the area covered. These routines were performed in python and OpenCV libraries.

Manual visual inspection was performed to confirm the correct labelling of the automated algorithm. In cases in which the automatic labelling was not satisfactory, manual labelling was conducted. Manual labelling was performed using ImageJ as described in Chapter 2 (section 2.10.3.2).

5.3.3.2. Evaluation of mixed population layer attachment

Once the cultures were confluent, the TEs were removed from the well where they were cultured and placed in a petri dish.

Aiming to mimic the stress the TE might be exposed to when moving from the manufacturing unit to the place of clinical implantation, the TEs where exposed to agitation in L15medium in an orbital shaker for 15min.

Light microscopy and macroscopical assessments were performed before and after the TE was placed in L15medium, and subject to movement by an orbital shaker. Videos and photos were recorded at the endpoint to assess whether the epithelial cell layer was peeling from the surface of RAFT.

5.4. Results

In order to understand the effect of manufacturing and cell seeding changes on RAFT-TE outcomes, all the steps of modification of the process were taken as a parameter of study. This chapter goes through an iterative

process of understanding why the epithelial cell layer started to detach from the surface of RAFT-TE after handling when using the clinically relevant protocol described in previous chapters.

5.4.1. Impact of RAFT-TE manufacturing changes on cell behaviour

5.4.1.1. Comparison of RAFT-TEs prepared with different collagen sources and neutralising solutions

Based on the literature, it was hypothesised that the HEPES present in the neutralising solution (NS) might affect epithelial cell attachment [284]. Previously, NaOH had been used as the standard neutraliser. Therefore, the behaviour of hLE cells (isolated from the same donor) expanded on TEs prepared with the different solutions was assessed. Additionally, collagen type I provided by a different company (*Symatese*) was also used to test whether the change in cell behaviour could be due to the modification of *First Link* to *Koken* collagen. *Symatese* is an alternative GMP collagen that could work as a replacement for *Koken* in case it failed.

Figure 5.1 summarises hLE growth and RAFT-TE transmission overtime when a cell suspension obtained from the mixed population isolation method was seeded on top of RAFT-TE. hLE growth on the surface of RAFT TE was tracked using FdA.

Photographs were taken at days 8, 11 and 13 in culture, and the mean area of coverage is plotted in Figure 5.1A. This graph shows an increase in hLE coverage overtime for all the different conditions. Nevertheless, after 13 days in culture, not all the RAFTs were confluent.

Figure 5.1B presents the transmission through RAFT-TE at 550nm. It can be observed that there are differences in transmission depending on the RAFT manufacturing conditions and, over time, there is a slight decrease in transparency as RAFT is populated by hLE.

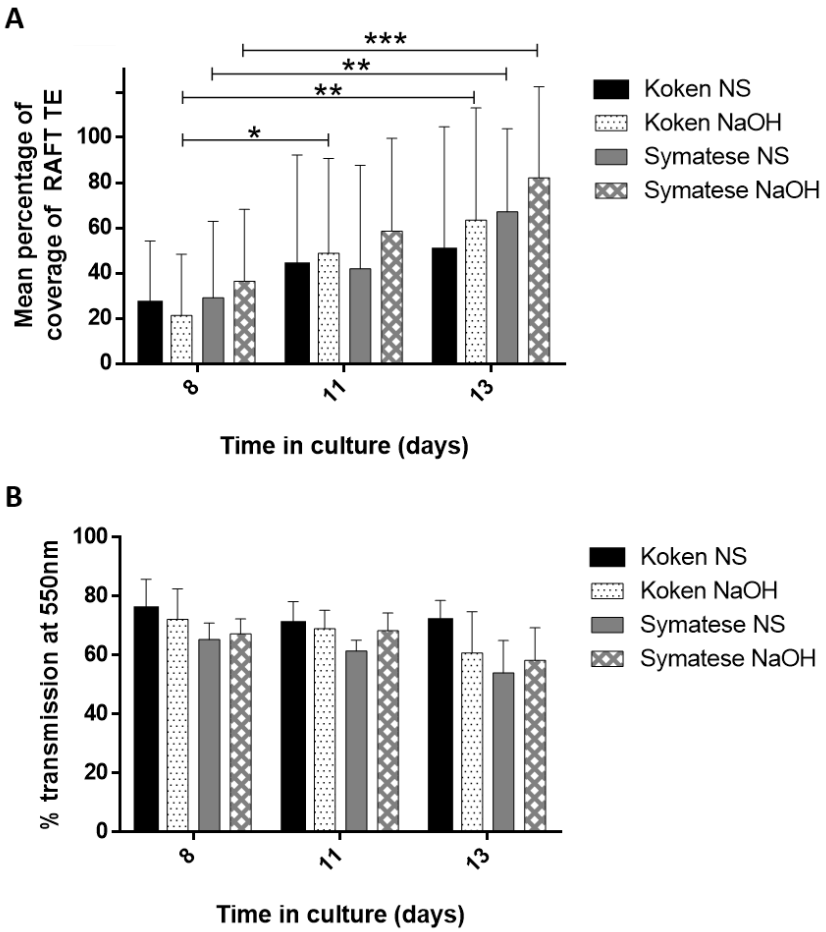

Figure 5.1 – Characterisation of hLE growth on RAFT-TE (n = 4 donors) prepared with either Koken or Symatese collagen, and with two different neutralisers, NaOH or NS. **(A)** Mean area of hLE growth over 13 days of culture (two-way ANOVA test followed by Sidak's multiple comparison test where *p≤0.05, **p≤0.01, ***p≤0.001). RAFT-TEs were stained with FdA and images taken at different time points during culture. **(B)** The % transmission at 550 nm through RAFT-TE was measured before culture and after 13 days in culture.

After 13 days in culture, the RAFT-TEs were removed from the well. Using light microscopy, the TEs were evaluated after being moved from the cell culture well to a petri dish, cut in six pieces and shaken. All the RAFTs that were confluent started to peel from the border or near the cut (Figure S5.1). Despite the apparent peeling from the borders of the RAFT-TE, confocal imaging was performed using different markers. Basement membrane protein laminin (data not shown) and its associated ligand β1 integrin were detected in both types of TE, as well as eye development marker PAX6 (Figure 5.2, 5.3 and 5.4).

To assess hLE morphology, marker expression, attachment and integrity of the cell layer, confocal microscopy was performed. Cells detachment can be identified in the following figures by cell layer disruption and folding.

Confocal assessment of the cell layer morphology on top of RAFT-TE by phalloidin staining showed that most of the cells present a small cobblestone morphology. Nevertheless, in some cases, it was possible to observe the stratification and differentiation of the epithelial cells by their large appearance (e.g. Figure 5.2N and 5.3B).

Figure 5.2 shows that all the conditions, *Koken* (NS and NaOH) and *Symatese* (NS and NaOH) have positive expression of early eye development PAX6 marker (Figure 5.2C, G, K, O). On this image, it is also shown that cell layer detachment can occur in different bandwidths. Although in some cases (as Figure 5.2L) the whole cell layer detaches and folds, in others the detachment is much smaller and could even be due to the cut of the sample (Figure 5.2H). In some cases, as Figure 5.2P demonstrates, the epithelial cell layer looks healthy and attached to the TE.

Integrin β1 is one of the main adhesion molecules responsible for the attachment of cells to collagen, as well as for the integrity of the epithelial cells layer. It is also a putative progenitor and proliferative cell marker usually expressed in the basal cell membranes of the central corneal. For this reason, its expression was assessed on RAFT-TEs in order to understand epithelial cell layer detachment and disintegration observed in some of the samples (Figure 5.3 and 5.4).

Figure 5.3D & 3P highlight cases where only the superficial cell layer detached, but the basal cell layer remained attached to the TE. Although expression of Integrin β1 was positive in all the cases, it seems to be more patchy and less uniform in the cell layers that remain attached to the TE in comparison to the cell layer that detached from the surface of the TE (Figure 5.3C, G, K & O).

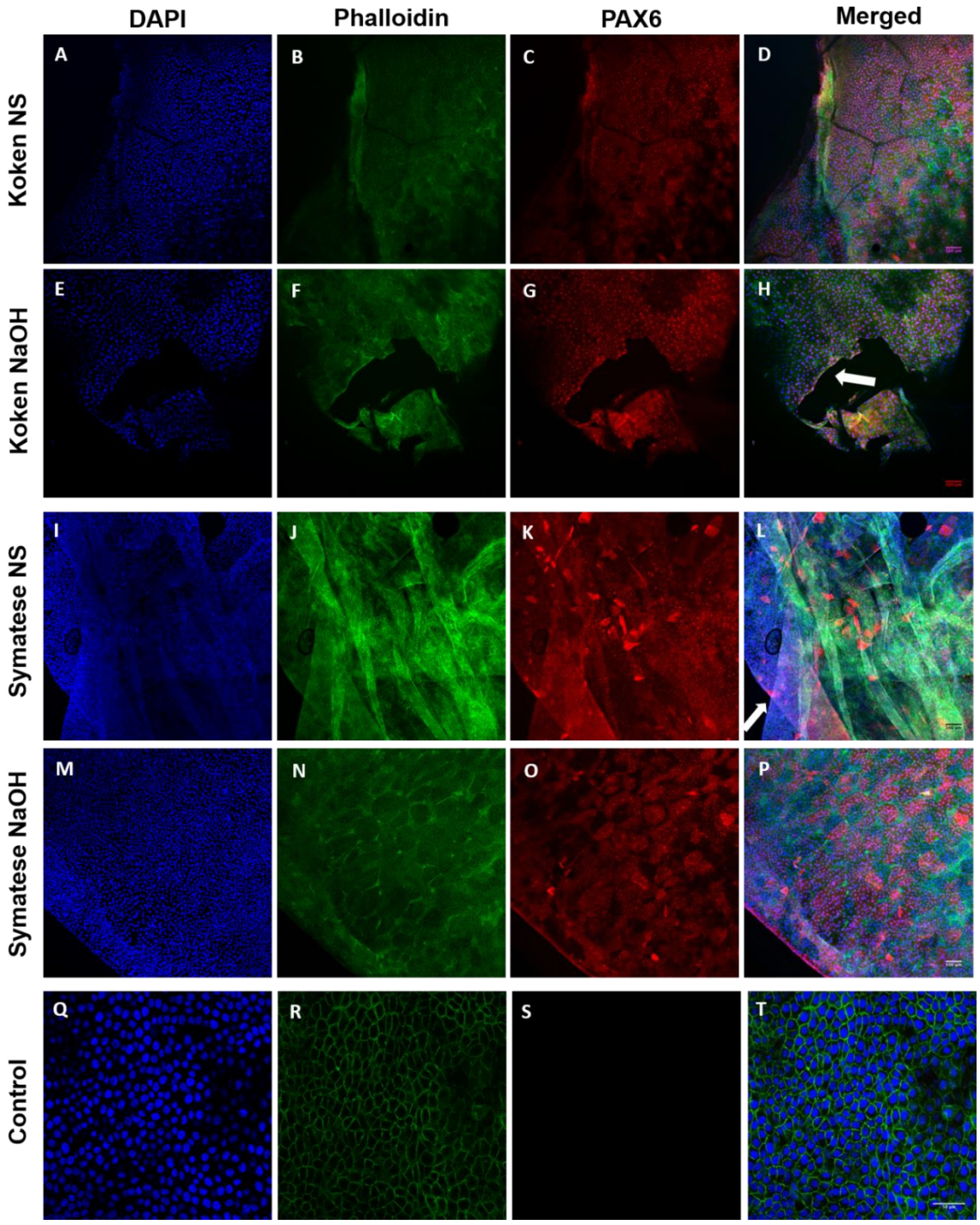

Figure 5.2 – Mixed population on top of *Koken* and *Symatese* RAFT-TE prepared with NaOH and NS. Positive staining of early eye development marker (PAX6) in red, nucleus staining (DAPI) in blue and cell cytoskeleton (phalloidin) in green. The column on the right shows the merged images of the three channels. **(A - D)** *Koken* NS, **(E – H)** - *Koken* NaOH, **(I – L)** *Symatese* NS, **(M – P)** *Symatese* NaOH, and **(Q – T)** Negative Control. White arrow highlights areas of hLE detachment and obvious folding of the cellular layer. Scale bars = 100 µm **(A - P)** & 50 µm **(Q – T).**

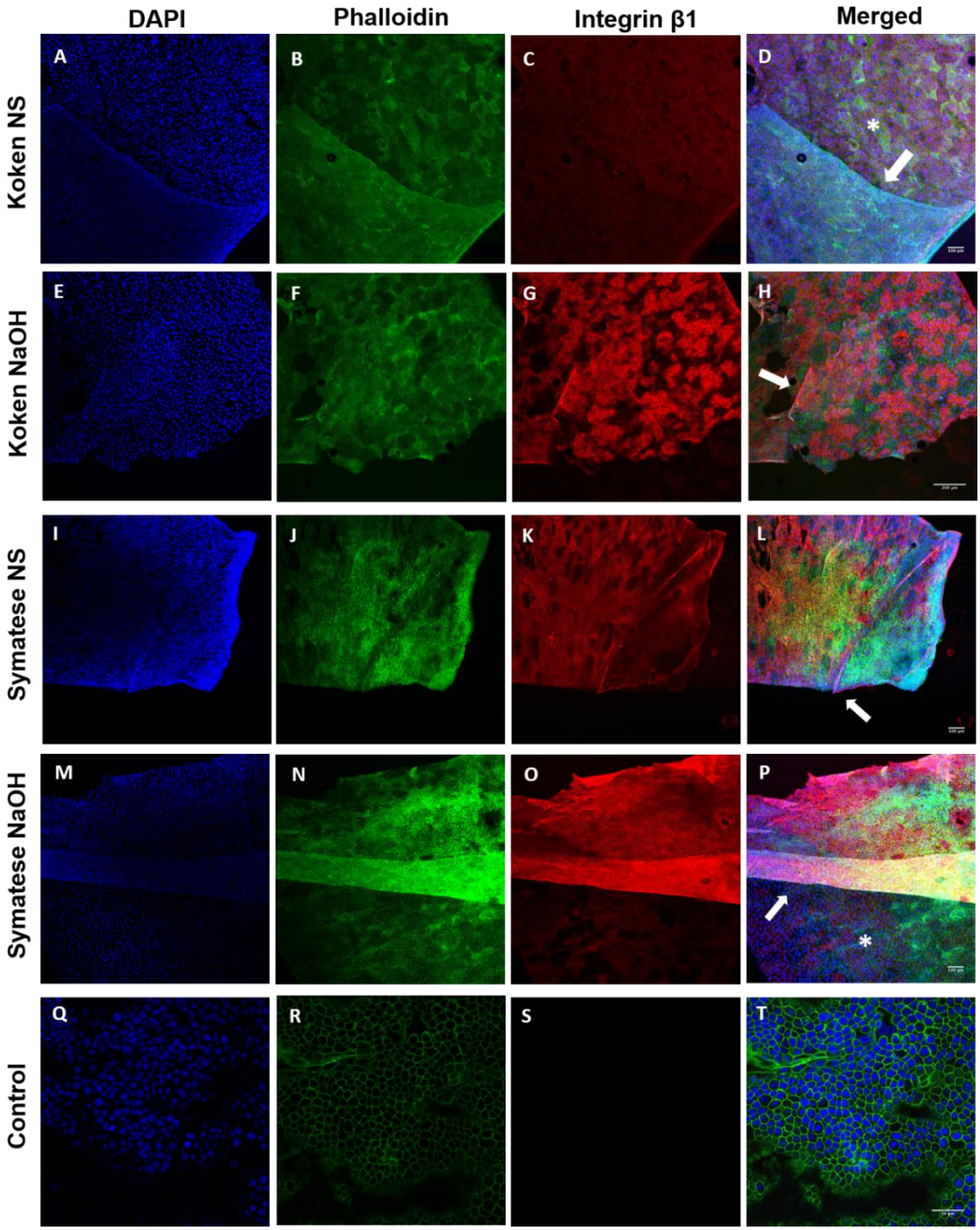

Figure 5.3 – Mixed population on top of Koken and Symatese RAFT-TE prepared with NaOH and NS. Positive staining of integrin β1 in red, nucleus staining (DAPI) in blue and cell cytoskeleton (phalloidin) in green. The column on the right shows the merged images of the three channels. **(A - D)** Koken NS, **(E – H)** - Koken NaOH, **(I – L)** Symatese NS, **(M – P)** Symatese NaOH, and **(Q – T)** Negative Control. White arrow highlights areas of hLE detachment. The asterisks (*) point regions where some of the cells detached while others remained attached to the TE based on the different intensity of the signal and plane of focus. Scale bars = 200 µm **(E - H),** 100 µm **(A – D + I - P)** & 50 µm **(Q – T).**

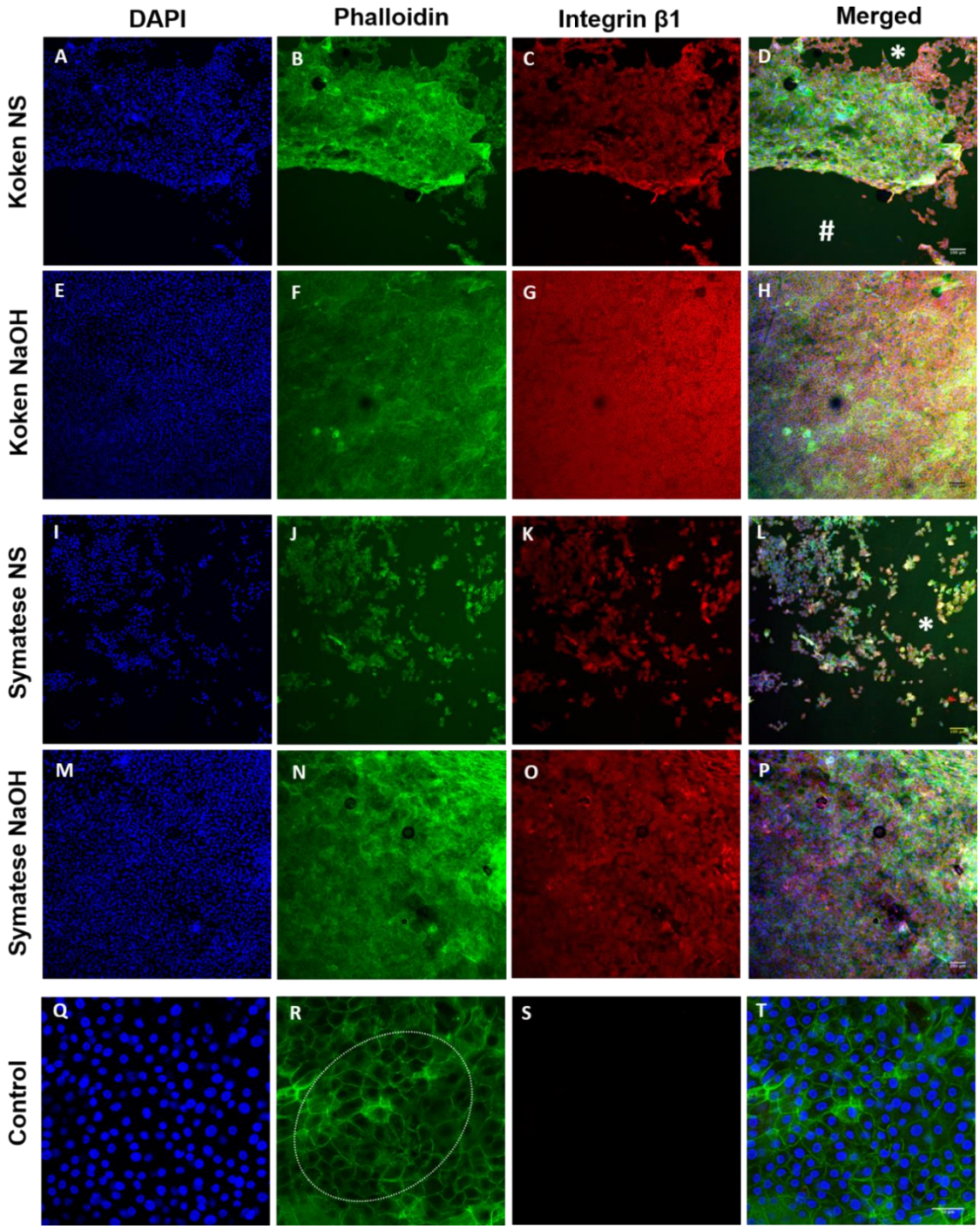

Figure 5.4 – Mixed population on top of *Koken* and *Symatese* RAFT-TE prepared with NaOH and NS. Positive staining of integrin β1 in red, nucleus staining (DAPI) in blue and cell cytoskeleton (phalloidin) in green. The column on the right shows the merged images of the three channels. **(A - D)** *Koken* NS, **(E – H)** - *Koken* NaOH, **(I – L)** *Symatese* NS, **(M – P)** *Symatese* NaOH, and **(Q – T)** Negative Control. The asterisks (*) highlight regions where some of the cells detached while others remained attached to the TE. The white ellipsis encases cells that have stratified - larger and more flattened morphology. The cardinal (#) highlights regions of the TE where all the cells have detached. Scale bars = 100 µm **(A - P)** & 50 µm **(Q – T).**

Figure 5.4 also presents the immunostaining of Integrin β1, but in cases where the whole RAFT-TE was stained and not cut in different samples before microscopical evaluation. Although this did not stop cell detachment, from this point, in order to avoid this variable, staining was subsequently performed using wholemounts.

Epithelial cell layer disintegration and detachment can be seen in Figure 5.4D & 4E after 13 days of culture. Both TEs were prepared with NS.

In general, the RAFT-TEs prepared with NS peeled more than the ones prepared with NaOH. The new collagen (*Symatese*) behaved similarly to *Koken*. There was no noticeable improvement in cell attachment.

Tile reconstructions presented in Figure 5.5 give an overview of the cell layer condition of the top of the RAFT-TE. In Figure 5.5A patchy disintegration is obvious with emphasis on the border of the TE. Figure 5.5B shows superficial cell layer detachment in some regions, while in others, the cell layer is inexistent.

As everything in the protocol was optimised for the use of *Koken* collagen, it was decided to continue using *Koken* collagen in future experiments and do further investigations on the effect of the neutralising solution. Previous results seemed to give a slight advantage to the use of NaOH, with higher cell coverage and less peeling.

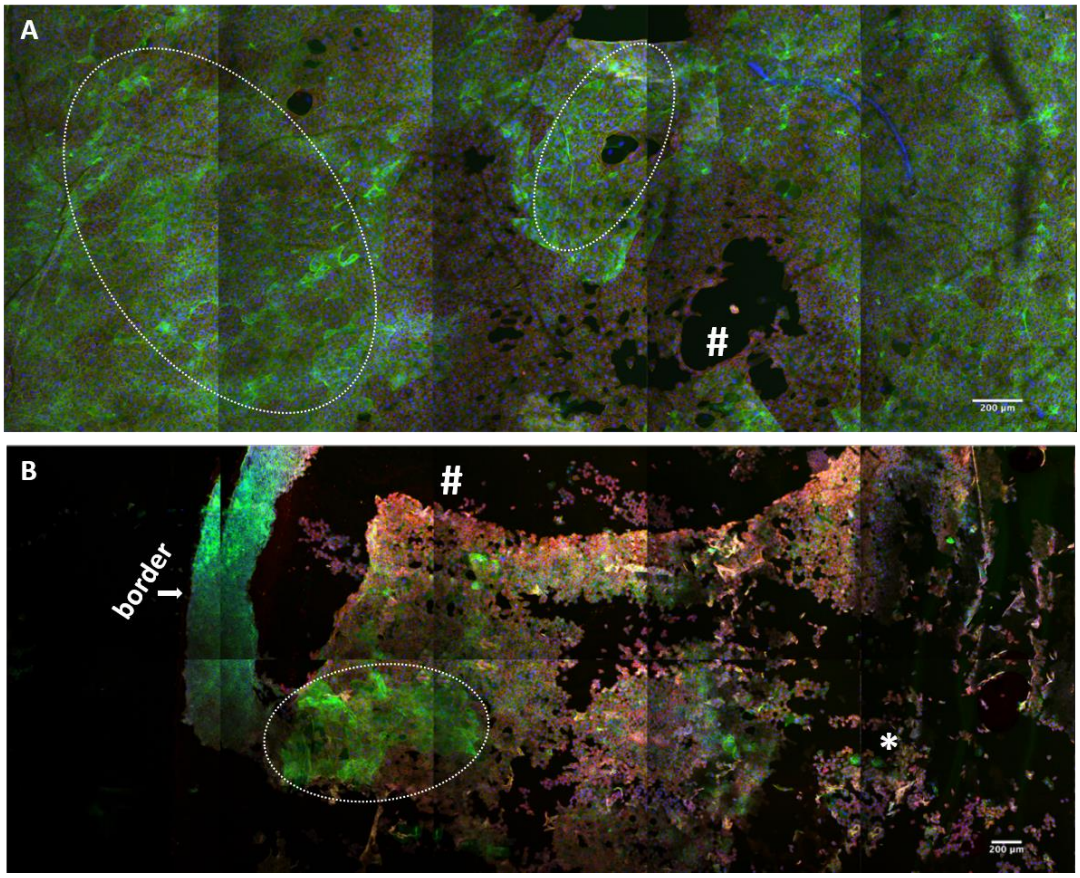

Figure 5.5 – Confocal images of RAFT-TEs cultured with a mixed population of CSSC and HLE for 13 days in CSSC media. Tile reconstruction of multiple fields of view: **(A)** *Koken* NaOH, **(B)** *Symatese* NS. Border – RAFT-TE border. The asterisks (*) highlight regions where some there is visible cell dissociation, the ellipsis highlight regions where the cells have stratified and started to differentiate, and cardinal (#) marks a region where all the cells have detached. Scale bars = 200µm.

5.4.1.2. Comparison of *Koken* RAFT-TEs prepared with different neutralising solutions

Although not significant, in the previous section, the experiments showed that in general, the *Koken* RAFTs prepared with NaOH had a higher percentage of epithelial coverage than the ones prepared with NS (Figure 5.1A). It was also observed that complete epithelial disintegration would only happen when RAFT was prepared with NS. Nevertheless, the TEs prepared with NaOH also led to cell detachment (Figures 5.2, 5.3 & 5.4).

A direct comparison between *Koken* NS and *Koken* NaOH TEs was performed with three additional donors and more replicates per condition. In addition to FdA staining to track hLE growth and transmission measurements over time, a macroscopic evaluation was also performed after 13 days in culture and 15min of shaking.

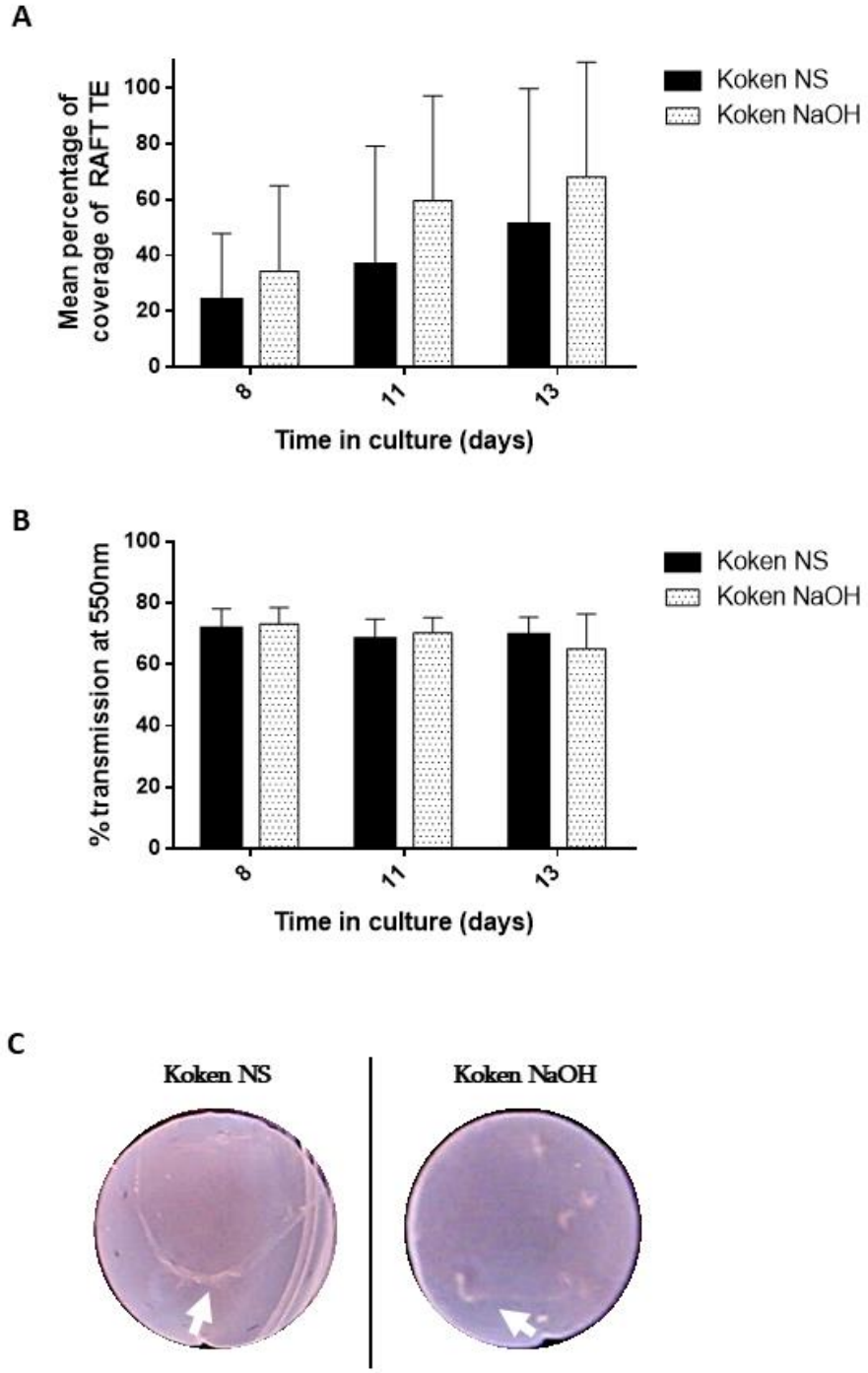

Figure 5.6 – Characterisation of hLE growth and behaviour on RAFT-TE (n = 3 donors) prepared with *Koken* collagen, and with two different neutralisers, NaOH or NS. **(A)** Mean area of hLE growth over 13 days of culture. RAFT-TEs were stained with FdA and images taken at different time points during culture. **(B)** The % transmission at 550 nm through RAFT-TE was measured before culture and after 13 days in culture. **(C)** Images highlighting the epithelial cell layer peeling from the surface of RAFT-TE in both conditions.

Figure 5.6A presents the mean coverage of RAFT-TE over time, but no significant differences between RAFT NS and NaOH could be observed.

Figure 5.6B shows the transmission at 550nm through RAFT-TE, but no significant differences were observed.

Figure 5.6C illustrates the epithelial cell layer detachment from RAFT in both conditions.

5.4.1.3. Comparison of RAFT-TEs prepared with different compression times

As described in Chapter 4, the original protocol for the production of RAFT-TE used a higher volume of collagen (*First Link*, 2.4mL) than the current one that only uses 0.6mL of *Koken* collagen. The compression time of 30min was kept the same for all the RAFT-TEs. It is, therefore, possible that the TE prepared with a smaller volume of collagen is denser and less hydrated than the previous one, thus affecting epithelial cell behaviour.

RAFT-TEs compression by porous absorbers is used to improve mechanical properties. The original protocol used a higher volume of collagen solution and a compression time that was iterated to obtain optimal results with regards to TE stability. As the volume of the solution was reduced, the compression time was also proportionally reduced to approximately 7minutes and 30 seconds (calculations presented below), but the cells still peeled from the TE (Figure S5.2). $Equivalent\ compression\ time = \frac{30min \times 0.6mL}{2.4mL} = 7{,}5min$

Aiming for a compression time between the equivalent of 7.5 min and the 30 min, a compression time in between both values was tested. A direct comparison between cell behaviour on RAFT compressed by 30 and 15 min is presented below.

Figure 5.7A shows the mean coverage of RAFT-TE by hLE, and it can be observed that there is no significant difference in FdA coverage between the two methodologies. The RAFT-TEs compressed for 30min were more transparent than the ones compressed only for 15min (Figure 5.7B). The transmission of light through the TEs that had 15min of compression reduced from day 8 to 11 but has a slight increase on day 13. The same was observed for the 30min compression TEs.

When the RAFT-TEs were removed from the culture well and shaken, they started to peel from the edge in both conditions as seen in Figure 5.7C.

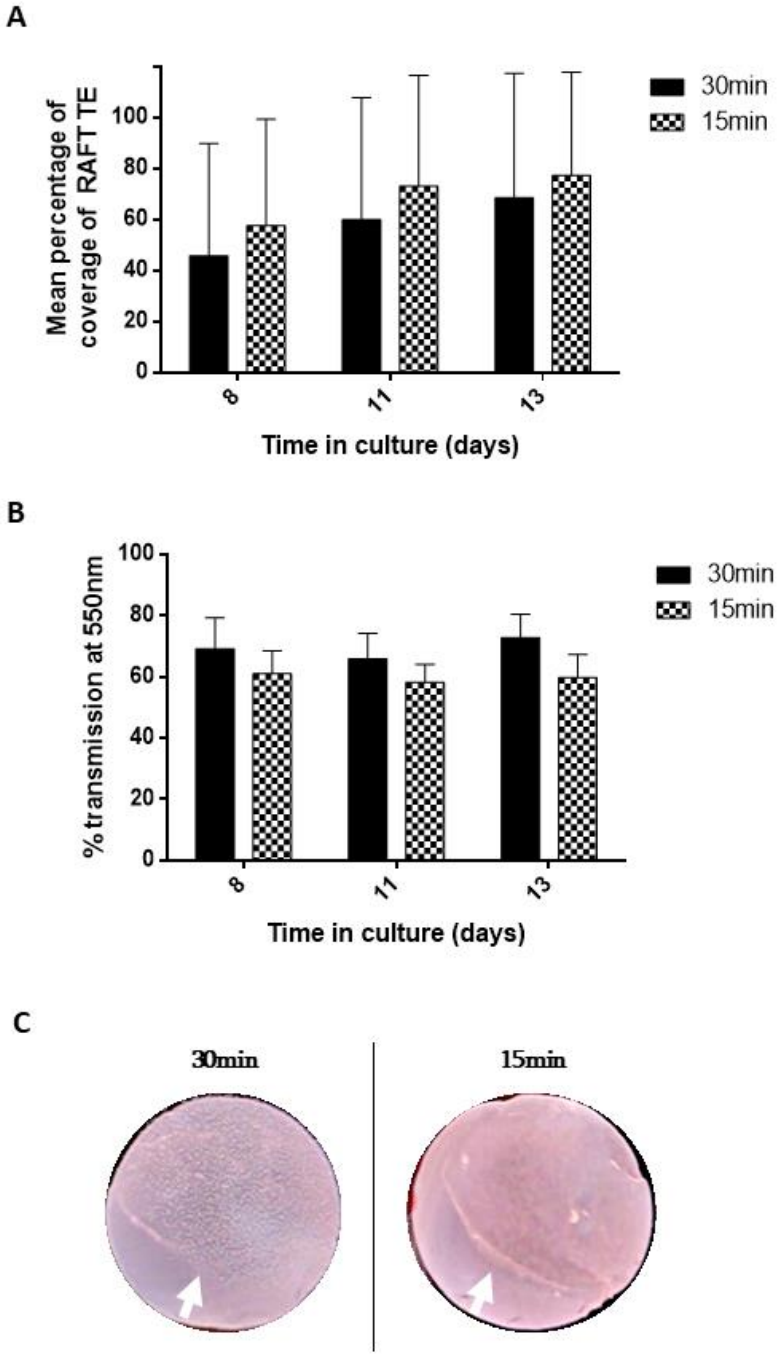

Figure 5.7 – Characterisation of hLE growth and behaviour on RAFT-TE (n = 3 donors) prepared with *Koken* collagen, and two different compression times, 30 and 15min. **(A)** Mean area of hLE growth over 13 days of culture. RAFT-TEs were stained with FdA and images taken at different time points during culture. **(B)** The % transmission at 550 nm through RAFT-TE was measured before culture and after 13 days in culture. **(C)** Images highlighting the epithelial cell layer peeling from the surface of RAFT-TE in both conditions.

Summary of results:

- Mixed population cultured on top of RAFT-TE demonstrated cell peeling in RAFT-TEs manufactured with:
  - *Koken* and *Symatese* collagen;
  - NaOH and NS;
  - 30 and 15min compression times;
- Mixed population cultured on top of RAFT-TEs still express:
  - PAX6
  - Integrin B1

5.4.2. Tissue Storage

5.4.2.1. Comparison of different tissue storage media on the performance of mixed population seeding on top of RAFT-TEs

Although the mixed population technique was initially used to isolate CSSCs, researchers have claimed that it is also a good method for hLE isolation [127, 274].

Mixed population obtained from corneal rims stored in two different culture media, both OP and OC, were cultured side-by-side as a starting comparative point for future experiments depending on tissue availability.

When cultured on top of RAFT-TE, multiple small colonies of hLE, with the characteristic cobblestone morphology, appeared in both conditions (Figure 5.8). CSSC were also visible and quickly changed morphology from small square appearance to elongated spindle-shaped cells as highlighted by the white arrows in Figure 5.8.

Although initially, most of the CSSC appeared to be pushed away as the hLE colonies were expanding (Figure 5.8A & 5.8D), it was then observed that they were also present within the epithelial colonies (Figure 5.8B, 5.8C, 5.8E and 5.8F).

The mean percentage coverage of RAFT-TE by hLE over 13 days is presented in Figure 5.9A. The hLE colonies significantly expand over time in both cases, but there is never a significant difference in area between the mixed population isolated from OP and OC corneal rims.

Figure 5.9B presents a summary table of the epithelial cell behaviour on top of RAFT-TE after being removed from the well, stored in L15 media and shaken for 15 min. The macroscopical observation (video records and pictures not presented) showed that the epithelial cell layer peeled more when isolated from OC rims than OP corneal rims.

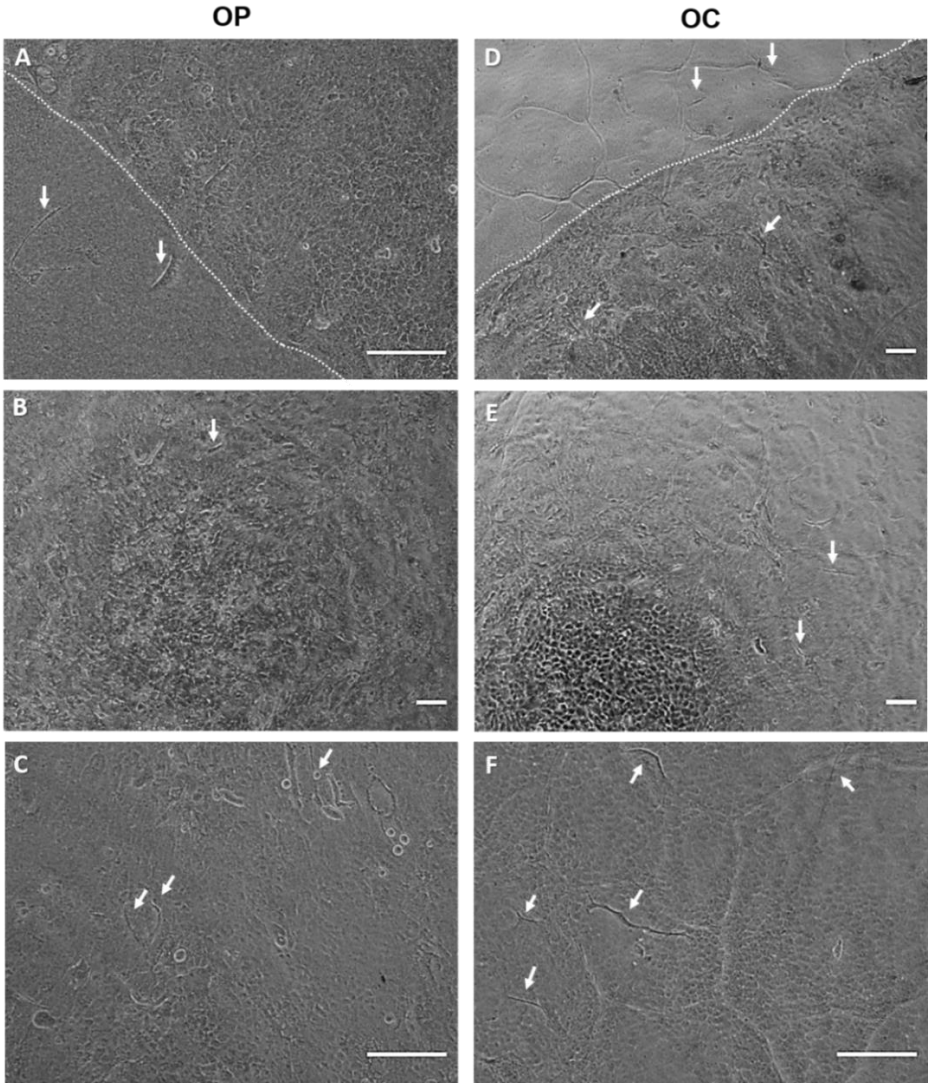

Figure 5.8 – Light microscopy image of a primary culture of mixed population of human LESCs and CSSCs isolated from OP **(A-C)** and OC **(D-F)** corneal rims growing on the top of RAFT-TE. Images of the border of the epithelial colonies are presented on (**A & D)**. The characteristic cobblestone morphology of LESCS is visible on all the images. Stromal cells can be seen not only in the periphery of the colonies **(A & D)** but also in between the epithelial cells **(B, C, E & F)** as pointed by the white arrows. Scale bar = 150µm.

A

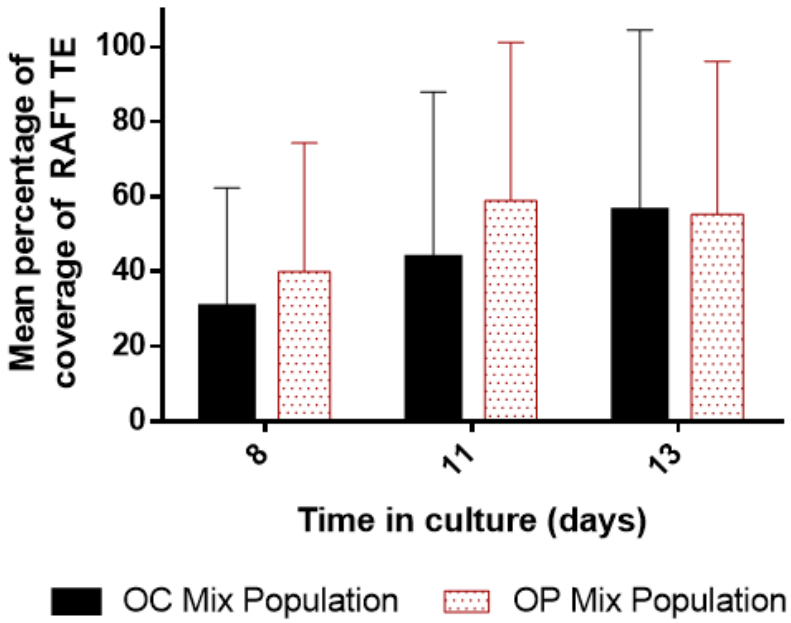

B

Storage Media	Peeling	Attached
OC	12 in 14 TE	2 in 14 TE
OP	14 in 20 TE	6 in 20 TE

Figure 5.9 – Characterisation of hLE growth and epithelial cells layer behaviour on top of Koken RAFT-TE prepared with NS. A mixed population of CSSC and LESCs isolated from OC or OP corneal rims (OC n = 4 donors & OP n = 8 donors) was cultured on RAFT-TE for 13 days. **(A)** Mean area of hLE growth over 13 days of culture. RAFT-TEs were stained with FdA and images taken at different time points during culture. **(B)** Table summarising the behaviour of the epithelial layer post handling with regards to cell attachment to the TE.

RAFT-TEs with mixed population cultured for 13 days were assessed using immunohistochemistry for expression of hLE markers (Figure 5.10). LESC marker p63α was observed in all the basal hLE of both conditions (Figure 5.10C, 5.10G, 5.10K, 5.10O, 5.10S & 5.10W), with only a few more differentiated cells at the surface of the RAFT-TE proving to be negative (highlighted by white arrows of Figure 5.10D).

Figure 5.11 and 5.12 show the expression of CSSC markers on RAFT-TEs. MSC marker CD73 is presented in Figure 5.11, while marker CD90 is shown in Figure 5.12. The images show that a few CSSC remained under or within

the hLE layer (Figure 5.11C, 5.11G, 5.12C & 5.12G). CSSC present a small, irregular shape in comparison to hLE. The z-stack galley images presented on Figure 5.11I and Figure 5.12I, show the localisation of CD73 and CD90 respectively within the stratified epithelial cell layer on top of RAFT-TE. There is no noticeable difference with regards to hLE and CSSC marker expression in OC and OP mixed population methods.

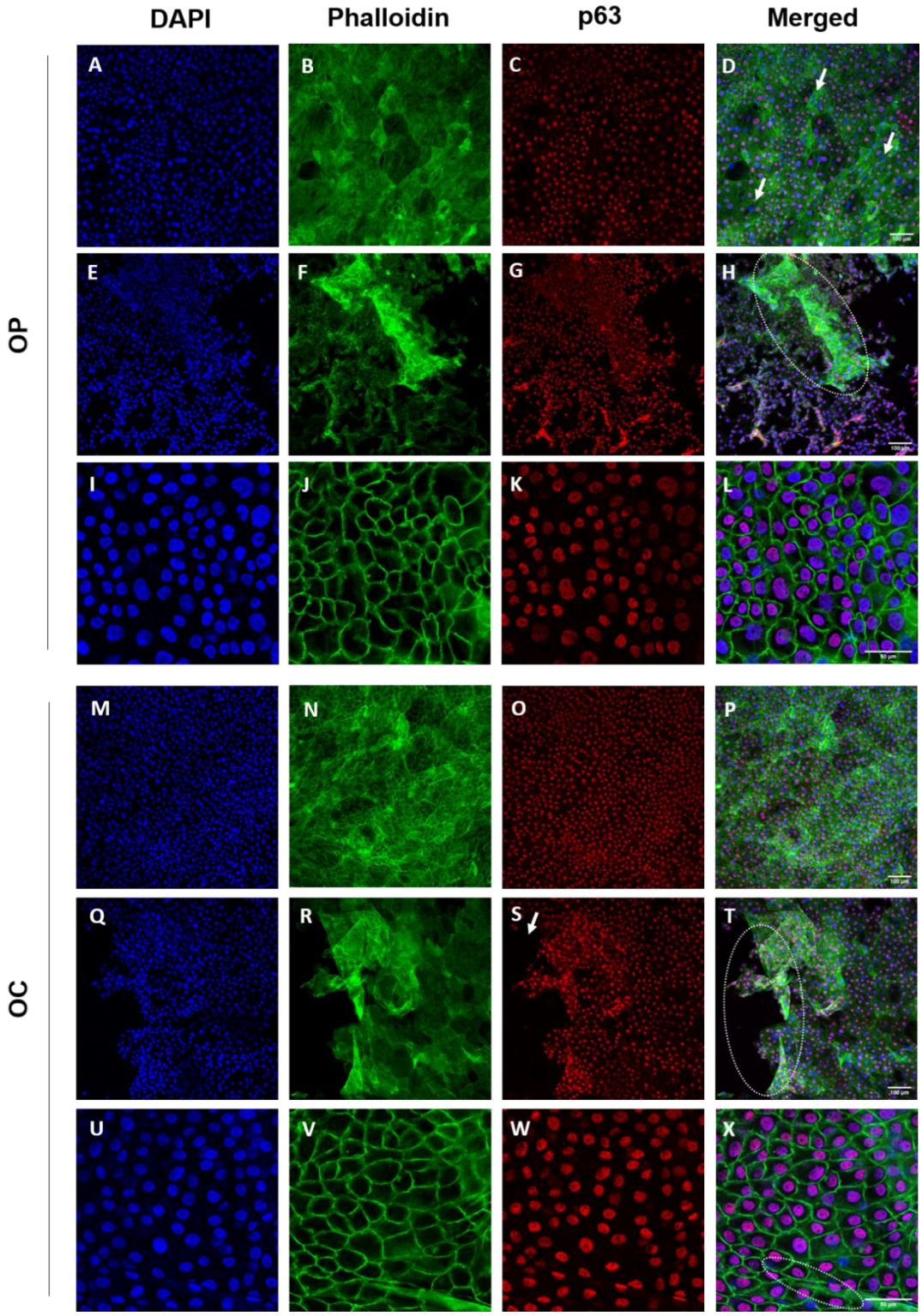

Figure 5.10 – Mixed population on top of *Koken* RAFT-TE prepared with NS. A mixed population of CSSC and LESCs isolated from OC or OP corneal rims was cultured on top of RAFT-TE for 13 days. Positive staining of corneal epithelial stem cell marker p63α in red, nucleus staining (DAPI) in blue and cell cytoskeleton (phalloidin) in green. The column on the right shows the merged images of the three channels. **(A - L)** OP Mixed population, **(M – X)** OC mixed population. White arrow highlights areas of cell differentiation and stratification. The ellipsis highlights regions of the TE where the cells have detached as shown by the disruption of the cell layer. Scale bars = 100 µm (A – H & M-T) & 50 µm (I – L & U-X).

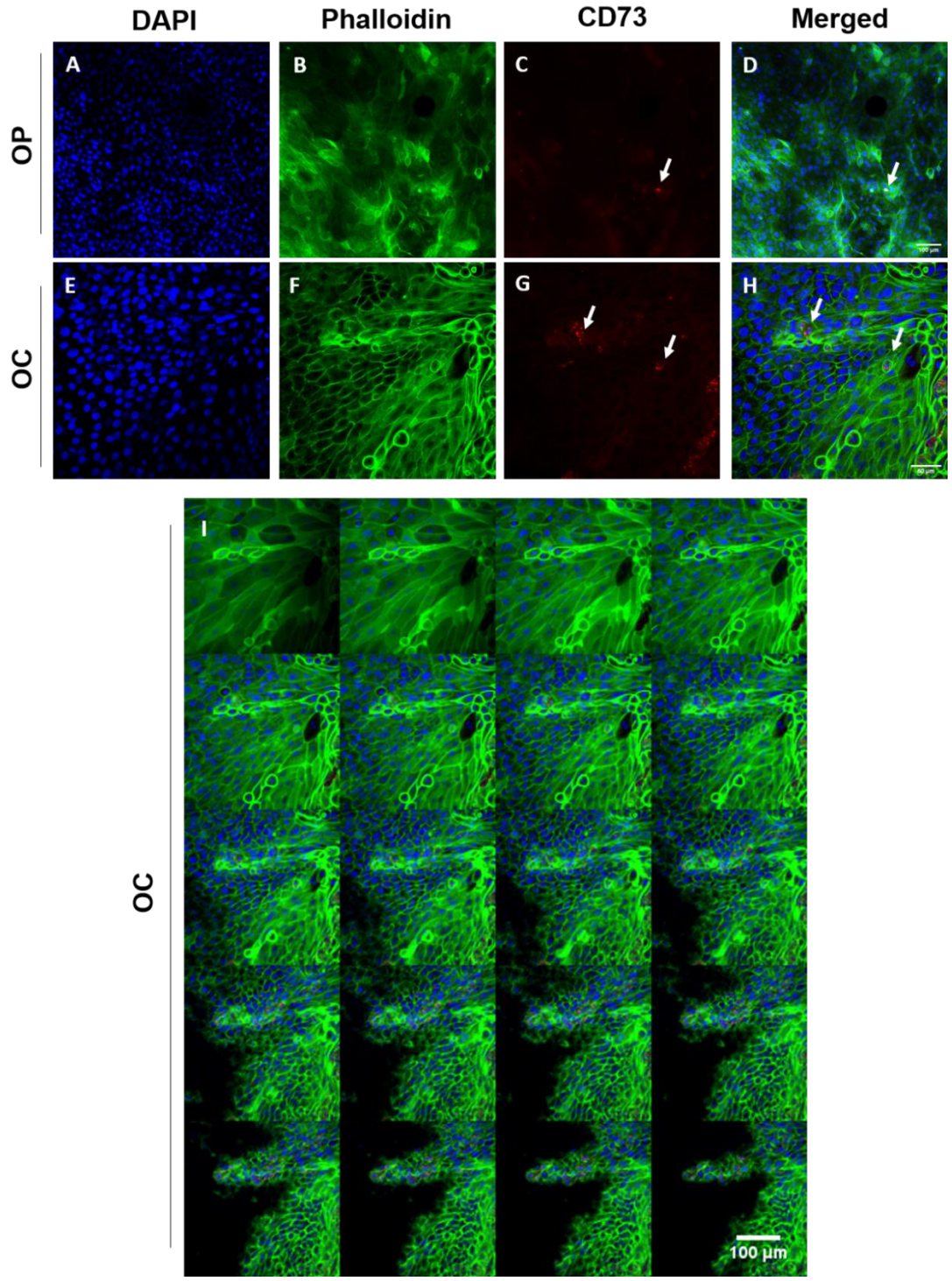

Figure 5.11 – Mixed population on top of *Koken* RAFT-TE prepared with NS. A mixed population of CSSC and LESCs isolated from OC or OP corneal rims was cultured on top of RAFT-TE for 13 days. Positive staining of corneal stromal stem cell marker CD73 in red, nucleus staining (DAPI) in blue and cell cytoskeleton (phalloidin) in green. **(A - H)** The column on the right shows the merged images of the three channels. **(A - D)** OP Mixed population, **(E – H)** OC mixed population; **(I)** gallery view of z-stack images showing the different morphologies of the mixed population of cells (isolated from OC corneal rims) from top to bottom of the TE. White arrow highlights areas where a few cells are positive for CD73. Scale bars = 100 µm (A – D & I) & 50 µm (E – H).

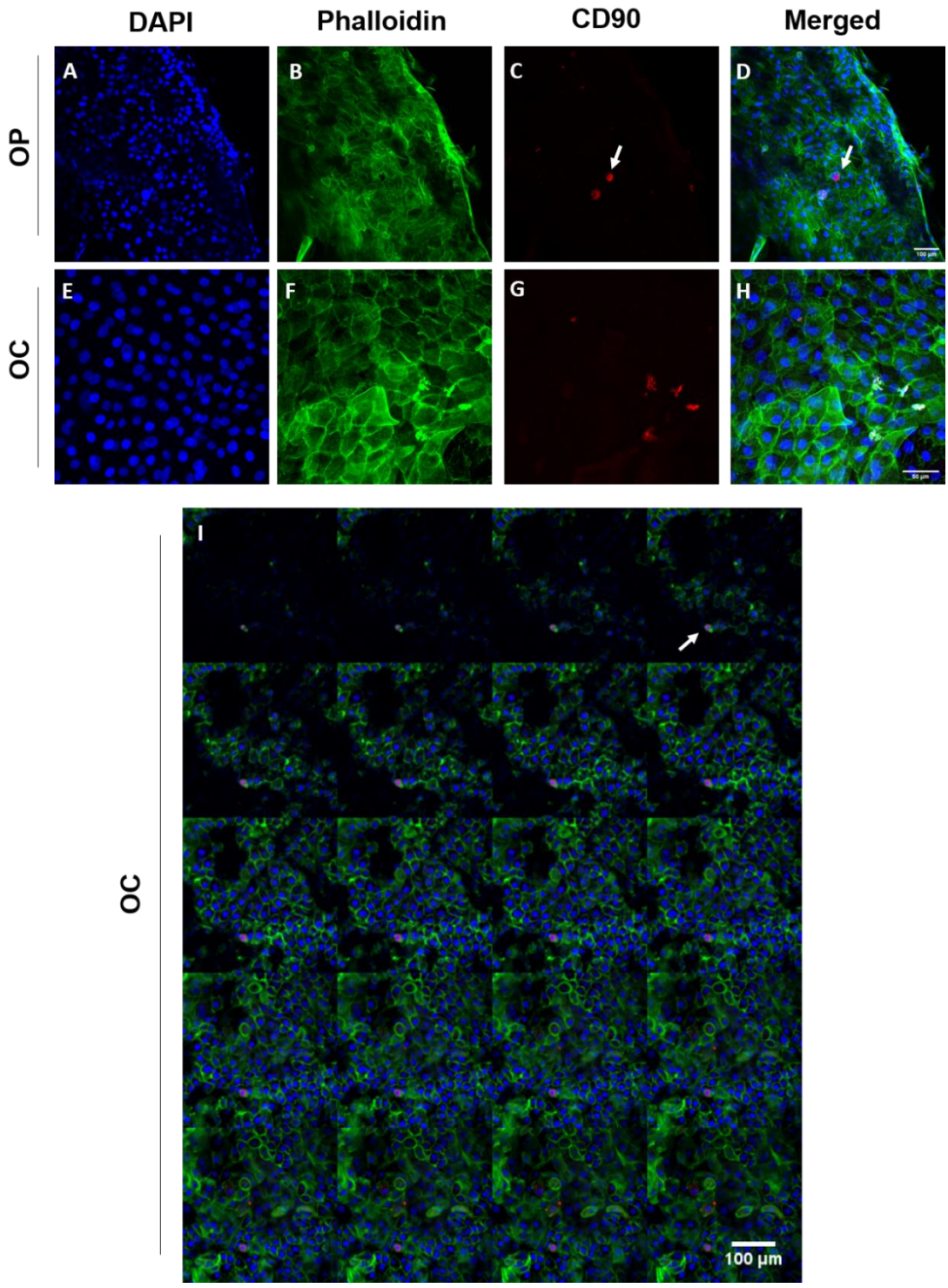

Figure 5.12 – Mixed population on top of *Koken* RAFT-TE prepared with NS. A mixed population of CSSC and LESCs isolated from OC or OP corneal rims was cultured on top of RAFT-TE for 13 days. Positive staining of corneal stromal stem cell marker CD90 in red, nucleus staining (DAPI) in blue and cell cytoskeleton (phalloidin) in green. **(A - H)** The column on the right shows the merged images of the three channels. **(A - D)** OP Mixed population, **(E – H)** OC mixed population, **(I)** gallery view of z-stack images showing the different morphologies of the mixed population of cells (isolated from OC corneal rims) from top to bottom of the TE. White arrow highlights areas where a few cells are positive for CD90. Scale bars = 100 µm (A – D & I) & 50 µm (E – H).

Summary of results:

- Mixed population cultured on top of RAFT-TE isolated from OP rims peeled less than those isolated from OC corneal rims.
- Mixed population isolated both from OP and OC rims displayed positive immunostaining of p63 when cultured on top of RAFT-TE
- A few cells underlying the epithelial cell layer were positive for CD73 and CD90

5.4.3. Comparison of different cell seeding strategies on top of RAFT-TEs

Different cell seeding strategies on top of RAFT-TE were compared in order to assess whether cell attachment could be optimised during the manufacturing protocol.

The cells were either seeded directly on top of the RAFT-TE as a mixed population or pre-expanded on tissue culture plastic for some days until large, defined colonies of LESCs were observed and selected before transfer to RAFT. As the gold standard, LESCs expanded on 3T3s were also tested. A new seeding method, using a cell suspension isolated with dispase and then directly seeded on top of RAFT-TE was also tried.

5.4.3.1. Mixed population isolated from OP corneal rims on top of RAFT-TE

With the rationale that the stromal cells might be having a negative impact on epithelial cell layer attachment, the mixed population was first expanded in 2D culture. The hLE were then selected for cell seeding on the surface of RAFT-TE.

A mixed population isolated from OP corneal rims was directly seeded on top of RAFT or pre-expanded in TCP before transferring to RAFT. Figure 5.13 shows the appearance and quantification of the hLE colonies in 2D (TCP) and RAFT-TE by FdA staining. In some cases, the colonies had defined borders and looked healthy (Figure 5.13A), while Figure 5.13B showcases a less healthy culture.

Figure 5.13C shows a direct comparison where one-fourth of the isolated mixed population cell suspension was pre-expanded in 2D (TCP) and the other three-fourths of the suspension were divided between three RAFTs for direct seeding without pre-expansion. The maximum area of each RAFT-TE is $2cm^2$, while the pre-expansion occurred in plates with a maximum area of $9cm^2$. Although the area of coverage was always bigger in the 2D (TCP) condition, it is not possible to say what would have happened if the RAFT-TEs were bigger and thus allowing further expansion of the hLE. Nevertheless, looking at Figure 5.9 or 5.14, for example, it is possible to see that the percentage of coverage even within the same condition can be very different from experiment to experiment due to donor variability.

Figure 5.14 emphasises this inter-experiment variability. Figure 5.14A presents the results of a set of four biological donors where two RAFT-TEs were prepared directly from the mixed population method (half of the cell suspension divided by two) and four with the cells that were pre-expanded (from the other half of the cell suspension). Figure 5.14B is a repeat of the same experiment, but with four additional biological donors, where ¼ of the cell suspension was pre-expanded and then seeded on three RAFTs and the ¾ of the sell suspension where directly seeded on three RAFTs

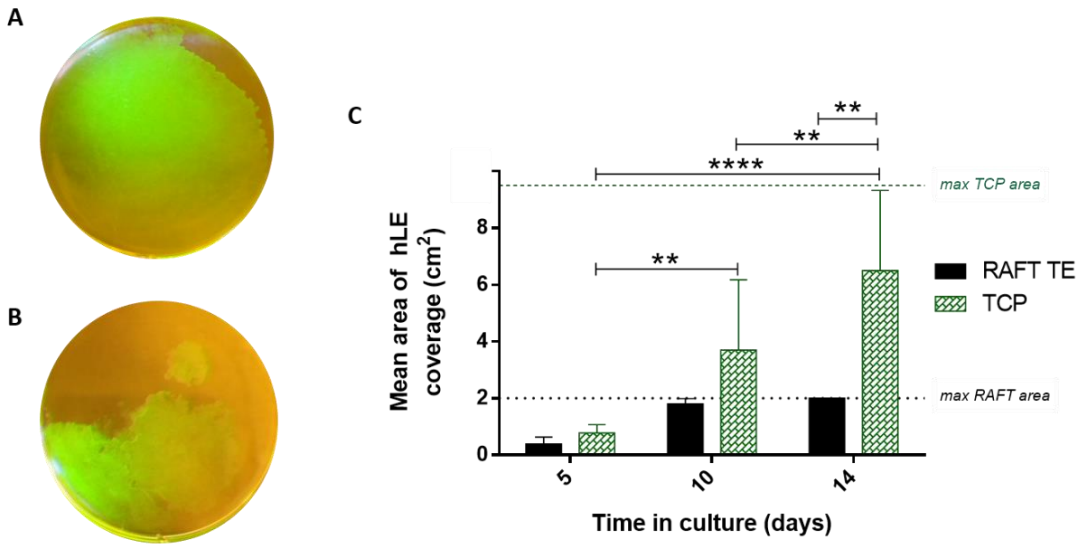

Figure 5.13 – Characterisation of hLE growth on top of Koken RAFT-TE prepared with NS and on TCP. A mixed population of CSSC and LESCs isolated from OP corneal rims was directly seeded on RAFT or pre-expanded on TCP for 14 days. RAFT-TEs were stained with FdA and images taken at different time points during culture. FdA representative images of the cells cultured in TCP **(A)** healthy colonies, **(B)** irregular colonies. **(C)** Mean area of hLE growth (n = 4 donors) over 14 days of culture on TCP and RAFT-TE (two-way ANOVA test followed by Sidak's multiple comparison test where **p≤0.01, ****p≤ 0.0001).

For each of the set of experiments referred above, the mean percentage area of coverage by FdA on top of RAFT-TE, as well as a summary of the cell layer behaviour at the end of culture is presented on both Figures 5.14A and B.

Figure 5.14A graph shows that the coverage of RAFT-TEs was higher when the cells were pre-expanded, and that difference was significant over time with the pre-expanded cells at day 11 covering more of the RAFT-TE than the direct mixed population at day 13 (**p≤0.01). Nevertheless, the pre-expanded cells had a higher rate of detachment from the TE.

A

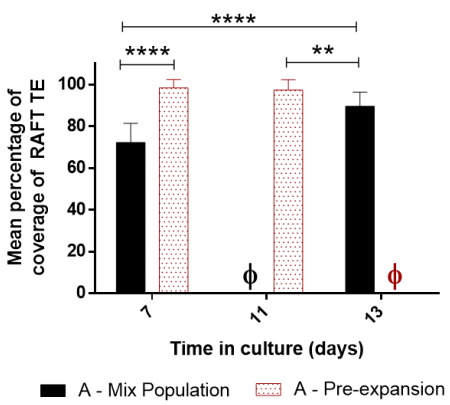

A	Peeling	Attached
Mix Population	4 in 8 TE	4 in 8 TE
Pre-expansion	12 in 15 TE	3 in 15 TE

B

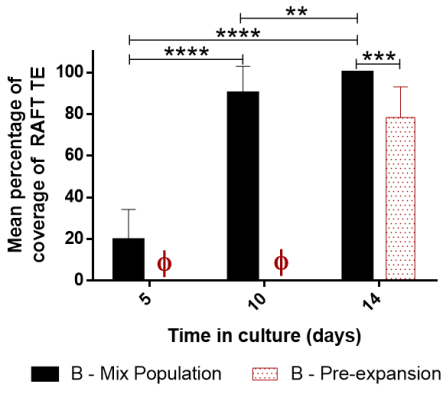

B	Peeling	Attached
Mix Population	10 in 12 TE	2 in 12 TE
Pre-expansion	5 in 11 TE	6 in 11 TE

C

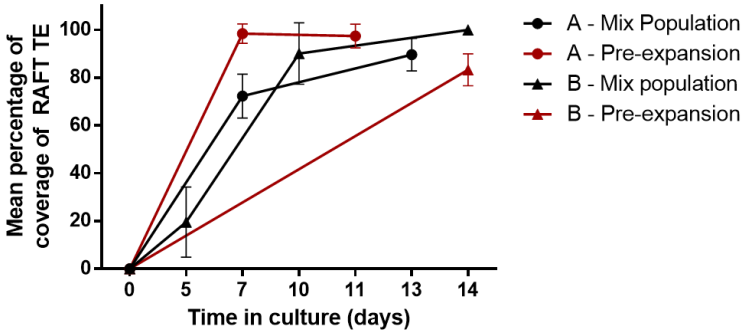

A + B	Peeling	Attached
Mix Population	14 in 20 TE	6 in 20 TE
Pre-expansion	17 in 26 TE	9 in 26 TE

D

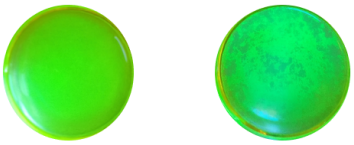

Figure 5.14 – Characterisation of hLE growth and epithelial cells layer behaviour on top of *Koken* RAFT-TE prepared with NS. A mixed population of CSSC and LESCs isolated from OP corneal rims was directly seeded or pre-expanded before being cultured on top of RAFT-TE for up to 14 days. **(A)** Mean area of hLE growth ($n_A = 4$ donors) over 13 days of culture. **(B)** Mean area of hLE growth (nB = 4 donors) over 14 days of culture. RAFT-TEs were stained with FdA and images taken at different time points during culture (two-way ANOVA test followed by Sidak's multiple comparison test where **p≤0.01, ***p≤0.001, ****p≤ 0.0001, ϕ - data not available.). The RAFT-TEs were shaken in order to test the cell layer attachment to the TE. **(C)** Table summarising the behaviour of the epithelial layer (n = 8 donors) post handling with regards to cell attachment to the TE in case of direct cells seeding or pre-expansion of the mixed population. **(D)** Example of FdA image of the cells cultured on top of RAFT-TE.

Figure 5.14B shows an opposite trend than Figure 5.14A, with mixed population showing a higher rate of coverage after 14 days of culture (***p≤0.001) and the RAFT-TEs that were seeded with pre-expanded cell showing a lower rate of detachment.

The graph and table presented on Figure 5.14C summarise the experiments and, overall, the RAFTs seeded with pre-expanded cells have a lower rate of detachment (65%) when compared with the directly seeded mixed population (70%). The percentages are too close to infer any impact of the pre-expansion method on the reduction of epithelial cell layer detachment.

Although the rate of detachment was lower on the pre-expanded condition, the hLE morphology and colony appearance was better in the mixed population strategy, as showed in Figure 5.14D. Taking into account the appearance of the colonies and the fact that the pre-expansion did not show outstanding improvements with regards to cell attachment, only the RAFTs using the direct mixed population approach were sectioned and observed under confocal microscopy.

Figure 5.15 shows the negative control for both the mouse and rabbit secondary antibodies. Figure 5.15A shows that there is no background staining when in the presence of the mouse control; however, there is a slight signal of green when looking at the rabbit control presented in Figure 5.15B. It is possible to observe that the cells stratified by the location of multiple nuclei (Figure 5.15C) on top of RAFT-TE as shown in Figure 5.15E.

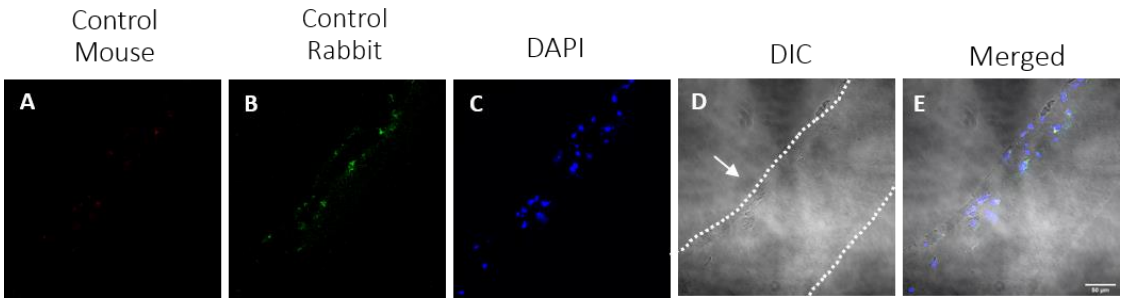

Figure 5.15 – Representative confocal micrographs of frozen sections of RAFT-TEs showing immunochemical control staining of mixed population seeding method grown on the surface of RAFT-TE for 13 days: **(A)** mouse control in red, **(B)** rabbit control in green, **(C)** nuclei counterstained with DAPI in blue, **(D)** differential interference contrast (DIC) microscopy in grey showing the TE and **(E)** merged image of all the previous channels. White arrow points at which side the cells were seeded on. Scale bars = 50 μm.

Basement membrane protein and putative stem cell marker expression profiles were assessed using immunohistochemistry, and the results are presented in Figures 5.16, 5.17 and 5.18. Sections of RAFT-TEs where there was no noticeable cell peeling are highlighted with number 1, while sections of RAFT-TEs where macroscopic cell peeling was observed are marked as 2.

Representative sections of the expression pattern of corneal epithelial putative stem cell marker p63α (in green) and basement membrane protein Perlecan (in red) on top of RAFT-TE can be observed in Figure 5.16.

Perlecan (Figure 5.16A, F, K, P & U) is a major heparan sulphate proteoglycan usually strongly expressed in the central cornea, but its expression was weak in the sections of RAFT-TE. Putative stem cell marker, p63α, was expressed in the nuclei of most of the cells cultured at the surface of RAFT-TE. However, a few cases do not display p63α in all the cells, as Figure 5.16B or present the signal outside the nucleus as highlighted on Figure 5.16Q where multiple cell layers can be observed stratified on the top of RAFT-TE.

Figure 5.16 also shows that there are different patterns of cell peeling, a partial detachment as shown in Figure 5.16O or the break of the stratified cell layers, as shown in Figure 5.16T.

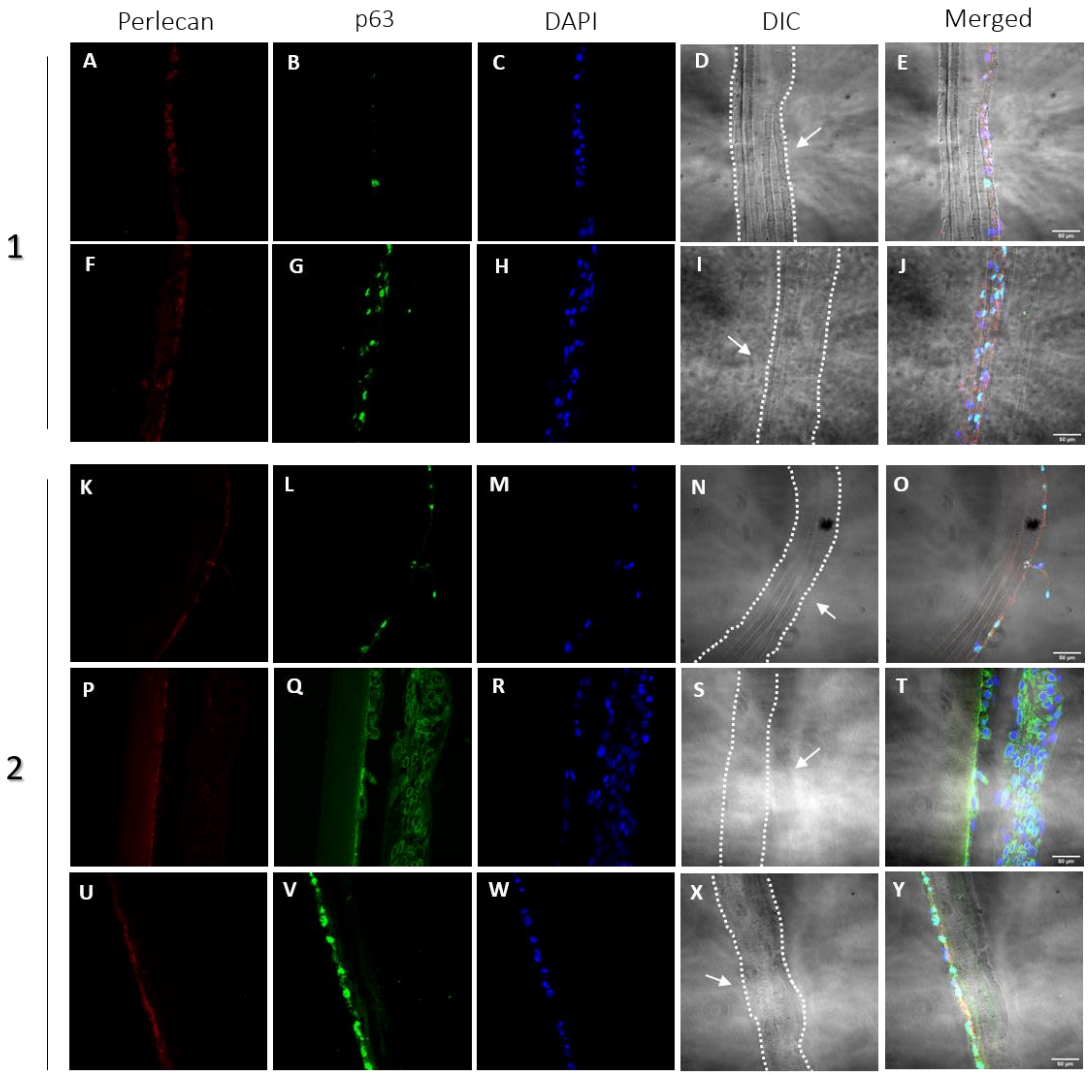

Figure 5.16 – Representative confocal micrographs of frozen sections of RAFT-TEs showing immunochemical staining of mixed population seeding method grown on the surface of RAFT-TE for 13 days. Extracellular matrix marker perlecan in red (first column), epithelial stem cell marker p63α in green (second column), and nuclei counterstained with DAPI in blue (third column). Most of the cells displayed positive expression of p63α and very weak staining of perlecan. Differential interference contrast (DIC) microscopy (in grey, fourth column)) shows the TE, while the latest column displays the merged of all the channels. White arrow points at which side the cells were seeded on. **(1)** Sections of RAFT-TEs where there was no obvious cell peeling and **(2)** sections of RAFT-TEs were macroscopic cell peeling was observed. Scale bars = 50 μm.

Figure 5.17 presents collagen VII (in green), a key structural component of anchoring fibrils, and PAX6 (in red) an early eye development marker expressed in stem cells from the cornea. Collagen VII staining is very weak in all the samples. PAX6 is positive in most of the cells cultured on the surface of RAFT-TE with exceptions like the one presented in Figure 5.17(a) A-E.

In Figures 5.17 (a) J and O is possible to observe single cells shedding from the surface of the TE. Figure 5.17 (a) J did not show any evident cell detachment macroscopically on the contrary to Figure 5.17 (a) O.

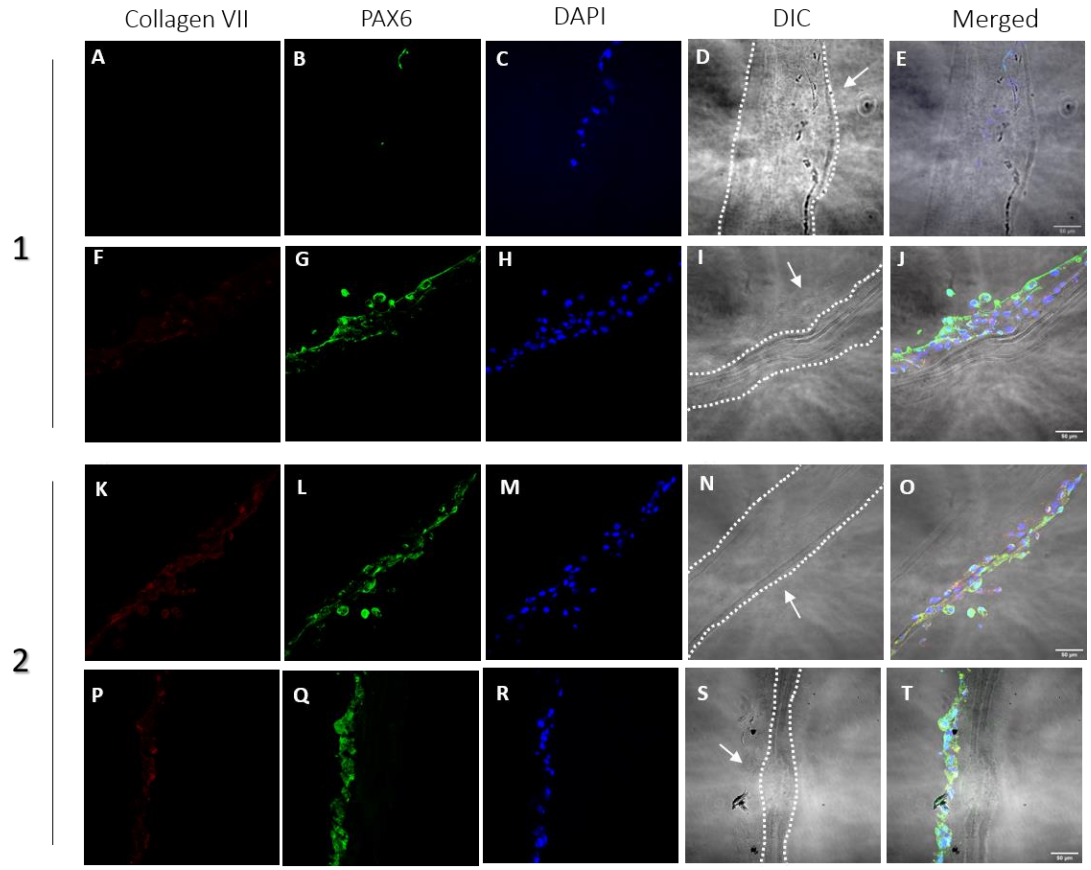

Figure 5.17 (a) – Representative confocal micrographs of frozen sections of RAFT-TEs showing immunochemical staining of mixed population seeding method grown on the surface of RAFT-TE for 13 days. Extracellular matrix marker collagen VII in red (first column), early eye development marker PAX6 in green (second column), and nuclei counterstained with DAPI in blue (third column). Cells displayed positive expression of PAX6 and almost no staining of collagen VII. Differential interference contrast (DIC) microscopy (in grey, fourth column)) shows the TE, while the latest column displays the merged of all the channels. White arrow points at which side the cells were seeded on. **(1)** Sections of RAFT-TEs where there was no obvious cell peeling, and **(2)** sections of RAFT-TEs were macroscopic cell peeling was observed. Scale bars = 50 µm.

Figure 5.17 (b) is a composition of low and high magnification images of sections of RAFT-TE. It highlights a case where the cell layer detachment was complete in some regions of RAFT-TE (A-J), and another case where the stratified cells detached from a basal cell layer which itself remained attached to the TE (K-T). There were no apparent differences with regards to both cases in terms of marker expression.

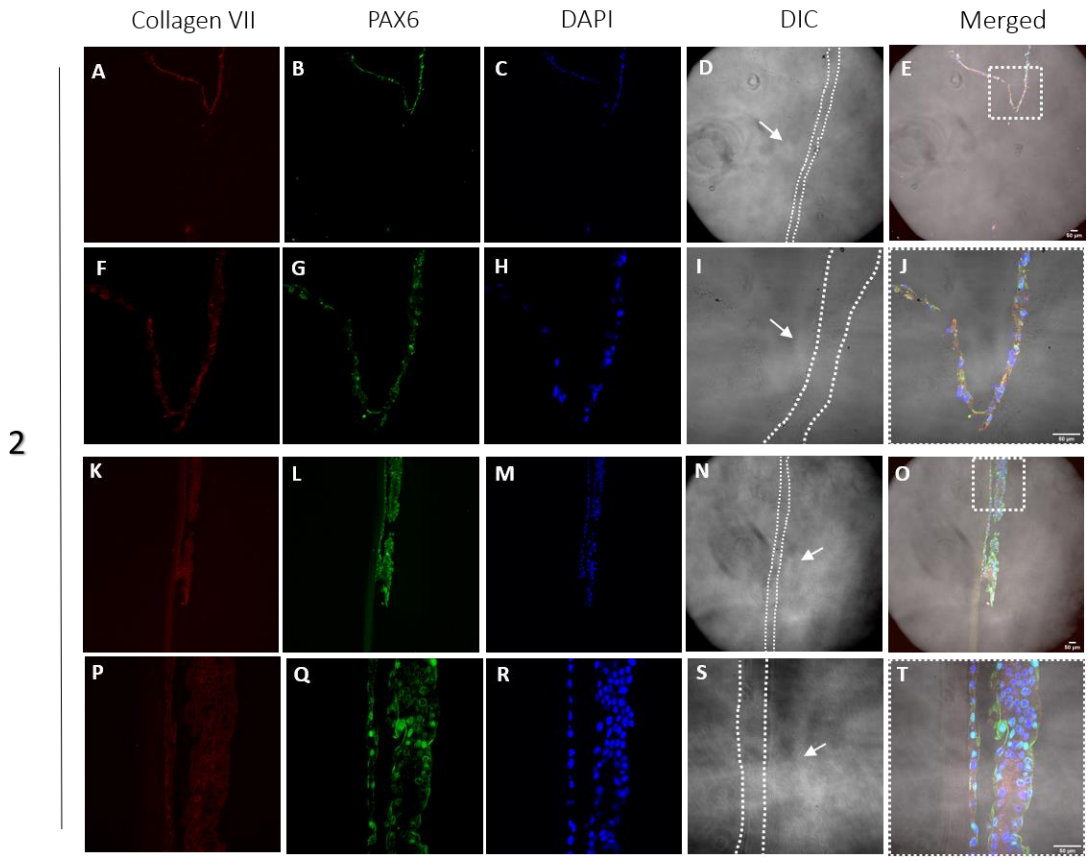

Figure 5.17 (b) – Representative confocal micrographs of frozen sections of RAFT-TEs showing immunochemical staining of mixed population seeding method grown on the surface of RAFT-TE for 13 days. Extracellular matrix marker collagen VII in red (first column), early eye development marker PAX6 in green (second column), and nuclei counterstained with DAPI in blue (third column). Cells displayed strong expression of PAX6 and faint expression of collagen VII. Differential interference contrast (DIC) microscopy (in grey, fourth column)) shows the TE, while the latest column displays the merged of all the channels. White arrow points at which side the cells were seeded on. Only sections of RAFT-TEs were macroscopic cell peeling was observed redisplayed. **(F-J)** are a zoom-in of **(A-E)** and show a case where the entire cell layer peels from the TE. **(P – T)** are a zoom-in of **(K-O)** and display a case where the cells have stratified, and only part of the cells detach from the basal layer. Scale bars = 50 µm.

Laminin was assessed on Figure 5.18 (in red, Figure 18A, F, K, P & U). It is a main non-collagenous basement membrane constituent of the central cornea but was only expressed in some areas of the TE, and in some of the samples, it was almost undetectable.

Collagen IV is strongly expressed in the central cornea, and it is considered one of the major structural basement membrane proteins. It was more strongly expressed than laminin, but only in some regions of the TE (in green, Figure 5.18B, G, L, Q & V).

Figure 5.18 shows all the cases of epithelial cell layer detachment described above: superficial hLE detachment with a remaining basal layer attached (Figure 5.18O), complete cell layer detachment (Figure 5.18T) and partial cell layer detachment (Figure 5.18Y).

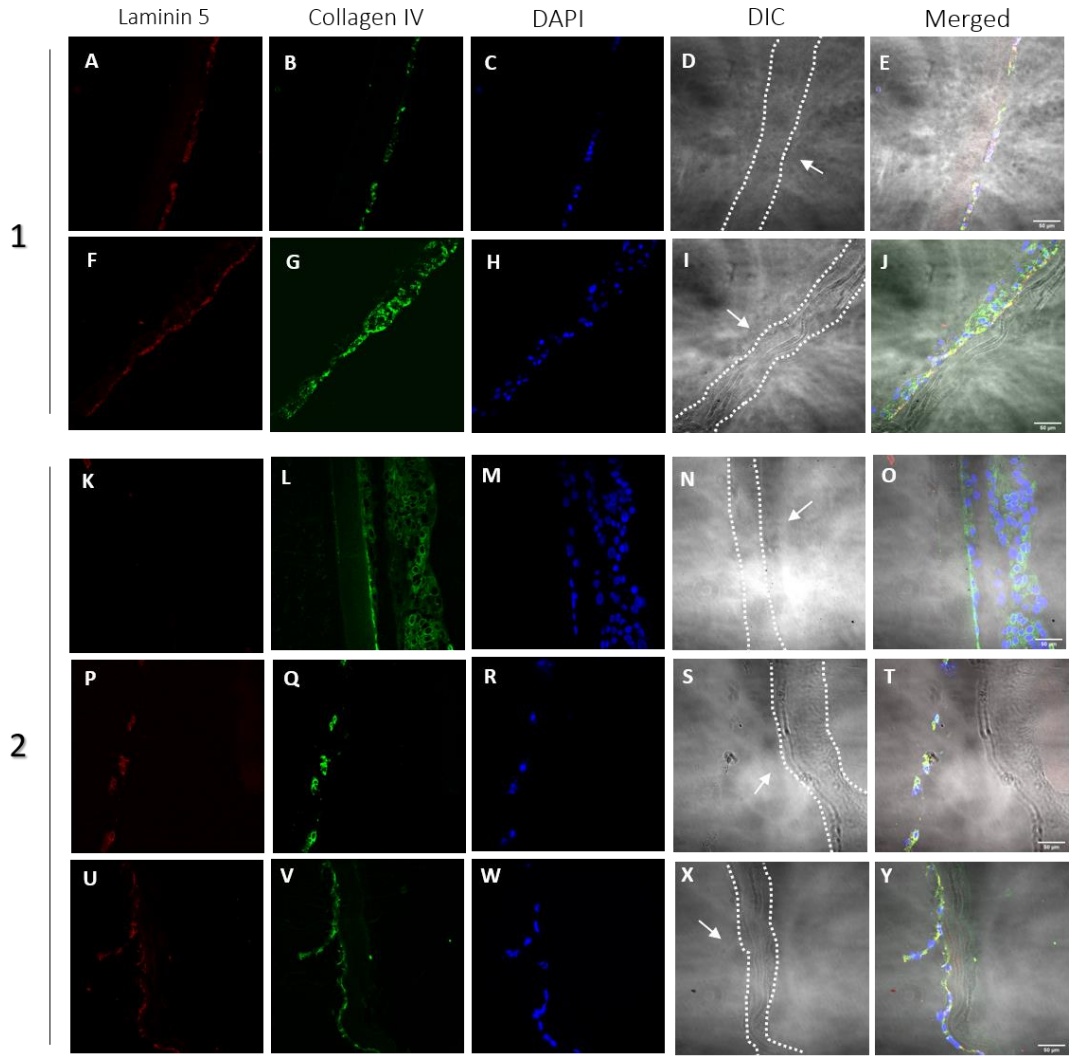

Figure 5.18 – Representative confocal micrographs of frozen sections of RAFT-TEs showing immunochemical staining of mixed population seeding method grown on the surface of RAFT-TE for 13 days. Extracellular matrix markers laminin 5 in red (first column) and collagen IV in green (second column), and nuclei counterstained with DAPI in blue (third column). Cells displayed positive expression of collagen IV and very weak staining of laminin 5. Differential interference contrast (DIC) microscopy (in grey, fourth column)) shows the TE, while the latest column displays the merged of all the channels. White arrow points at which side the cells were seeded on. **(1)** Sections of RAFT-TEs were there was no obvious cell peeling, and **(2)** sections of RAFT-TEs were macroscopic cell peeling was observed. Scale bars = 50 μm.

No apparent differences could be identified between samples of group 1 (where there was no macroscopic cell peeling) and group 2 (where there was obvious cell detachment) with regards to marker expression.

Aiming to identify any stromal cells that might have expanded under the epithelial cell layer and differentiated towards a large cell phenotype occupying, and potentially blocking epithelial cell access to collagen attachment sites, alpha-smooth actin (sma) staining was performed. The results are shown in Figure 5.19, and SMA could be detected in some of the samples (Figure 5.19 A-D and Figure 5.19 M-P as an example).

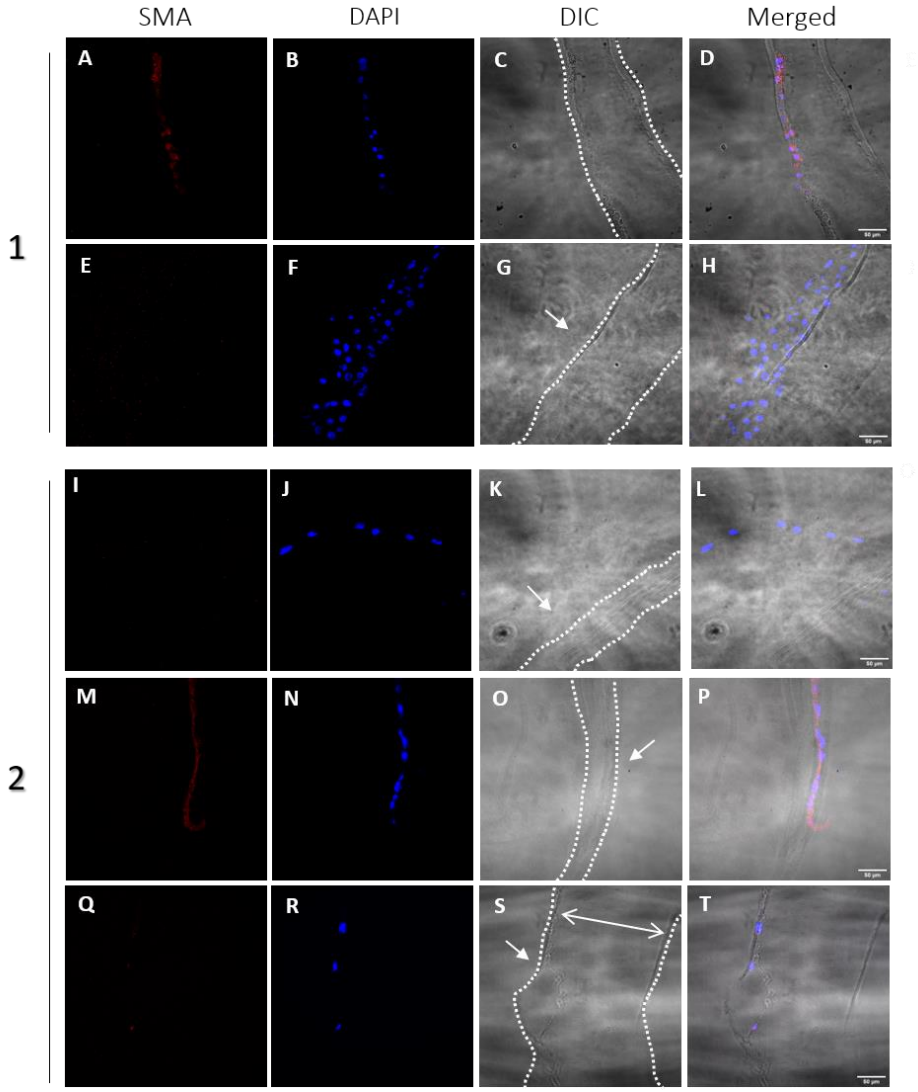

Figure 5.19 – Representative confocal micrographs of frozen sections of RAFT-TEs showing immunochemical staining of mixed population seeding method grown on the surface of RAFT-TE for 13 days. Alpha-smooth muscle actin in red (first column), nuclei counterstained with DAPI in blue (second column) and DIC microscopy in grey (third column)) shows the TE, while the latest column displays the merged of all the channels. Come areas displayed positive expression of SMA. White arrow points at which side the cells were seeded on. **(1)** Sections of RAFT-TEs were there was no obvious cell peeling, and **(2)** sections of RAFT-TEs were macroscopic cell peeling was observed. Scale bars = 50 µm.

5.4.3.2. LESCs expanded on 3T3s on top on RAFT-TE

The gold-standard method of isolation of LESCs using dispase and then expanding on 3T3 feeders was also tested in the clinically relevant RAFT-TE. Representative photomicrographs of the colonies in TCP can be observed in Figure 5.20 (a), while the morphology of the cells after seeding on RAFT-TE can be seen in Figure 5.20 (b).

Epithelial colony size and coverage was different from donor to donor depending on the quality of the available tissue. While some colonies presented regular borders and a small cobblestone morphology (Figure 5.20 (a) A & B), others had irregular borders (Figure 5.20 (a) C) and cells growing within the colonies of different appearances. Although some cells still exhibited a small cobblestone morphology, some were bigger and more disorganised, and others elongated (Figure 5.20 (a) E & F).

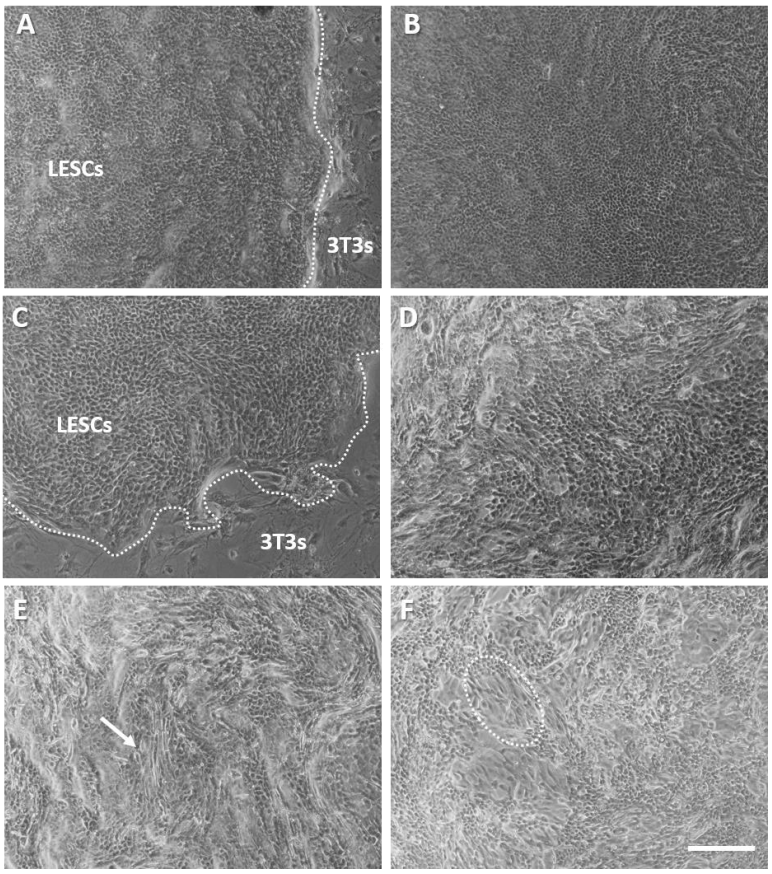

Figure 5.20 (a) – Morphology of LESCs on 3T3 feeders in TCP. Representative photomicrographs of the colonies during the expansion in TCP previous to RAFT cell seeding. **(A)** Border of a healthy epithelial colony, **(B)** LESCs with small cobblestone appearance, **(C)** less defined border of a LESC colony, **(D)** region of the colony where the cells started to differentiate and thus the bigger appearance, **(E)** and **(F)** highlight areas where the cells have a more elongated morphology. Scale bar = 150µm.

Figure 5.20 (b) presents the cell morphology and behaviour when the LESCs pre-expanded on 3T3s were transferred to the surface of RAFT-TE. Although in some cases the LESCs expanded on RAFT-TE maintained their initial cobblestone morphology (Figure 5.20 (b) A), in other occasions the cells started to differentiate and stratify as shown in Figure 5.20 (b) B & C.

Despite the fact that the 3T3 have been growth arrested with mitomycin C, previously selectively trypsinised and ideally, only a cell suspension containing LESCs transferred to RAFT-TE, in some samples, cells with a fibroblast morphology could be observed (Figure 5.20 (b) E &F).

In some of the samples, the quality of the obtained epithelial layer was not consistent. The morphology of the cells was uneven, and the cells started to die, creating holes of coverage on the surface of RAFT-TE (Figures 5.20 (b) F and Figure 5.21B).

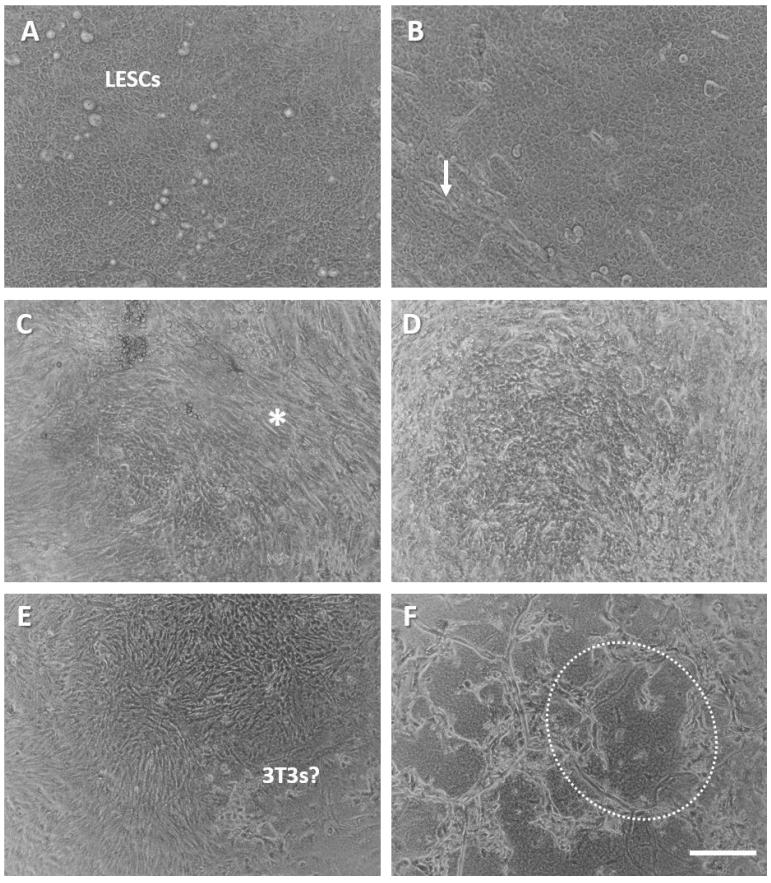

Figure 5.20 (b) –Morphology of LESCs pre-expanded on 3T3 feeders and seeded on RAFT-TE. **(A)** LESCs with small cobblestone appearance, **(B)** highlights a region with elongated cells, **(C)** showcases epithelial cell differentiation with *, **(D)** area showing irregular cell morphology, **(E)** and **(F)** highlight areas of possible contamination with 3T3s. Scale bar = 150µm.

Next, in order to highlight the dependence of this method on the availability of fresh corneal rims for the isolation of LESCs, two different sets of experiments are presented in Figure 5.21. Each set comprises two different donors and three samples per donor. While in group A, the FdA staining showed a healthy epithelium and a confluent RAFT-TE after 10 days of culture (Figure 5.21A and C), the Group B displayed poor epithelium growth (Figure 5.21B) and high variability between samples as observed by the larger error bars of the graph presented in Figure 5.21C.

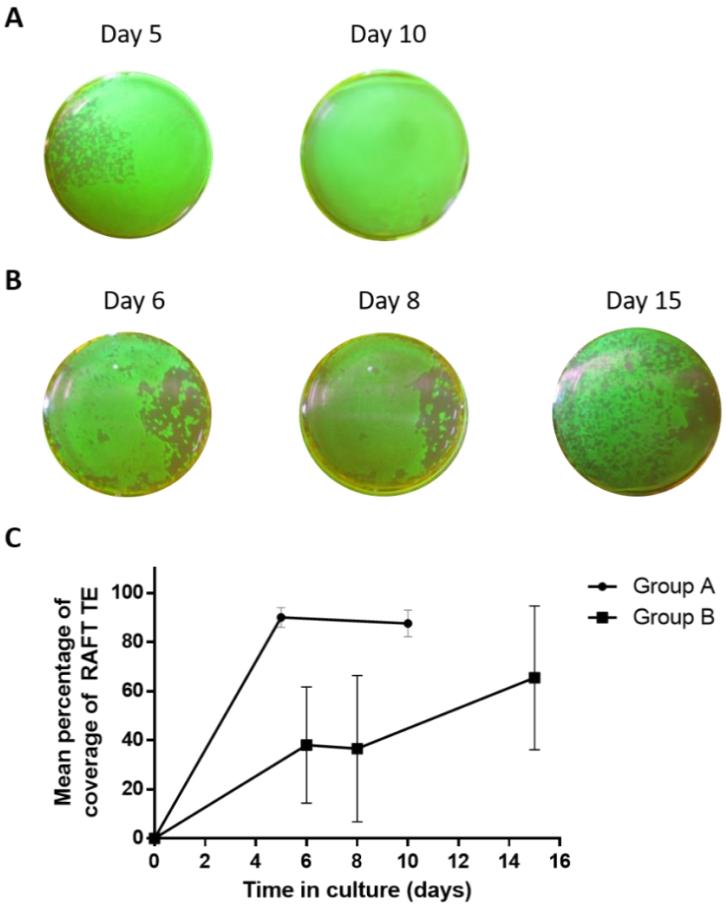

Figure 5.21 – Characterisation of hLE growth on top of Koken RAFT-TE prepared with NS. LESCs pre-expanded on 3T3 feeders and seeded on RAFT-TE being cultured on top of RAFT-TE for up to 15days. RAFT-TEs were stained with FdA and images taken at different time points to access the growth and appearance of the colonies **(A)** Example of FdA image of the cells cultured on top of RAFT-TE up to 10 days (nA = 2 donors) and **(B)** up to 15 days (nB = 2 donors). **(C)** Summary of mean area of hLE growth quantification over time.

5.4.3.3. LESCs isolated with dispase directly cultured on top on RAFT-TE

Since the isolation with dispase and culture in CECM medium is still the gold-standard, a new seeding method aiming to remove the adventitious risk of the pre-expansion on 3T3s was tested.

The cell suspension obtained after the dispase isolation of the corneal rim was directly seeded on top of the RAFT-TE (1/9 of a rim to each TE). An initial trial only with one donor was performed in order to test if the cells would survive, and the FdA staining over time is presented in Figure S5.3 (appendix).

This initial test showed that samples were not seeded with similar cell concentrations, highlighting the issues that results from a non-uniform cell suspension. Aiming to reduce this, an additional step of cell dissociation with Tryple Express was added to the protocol.

Figure 5.22 shows the summary of a comparative experiment between the Direct Dispase and Direct Dispase + TrypExp (3 biological donors, 3 TEs per donor) cell seeding methods with regards to hLE coverage and epithelial cell detachment after 19 days in culture.

Figure 5.22 A presents the FdA staining over time of the Direct Dispase Method. It is possible to observe that a few colonies start to form and then merge into a bigger one. One the other hand, Figure 5.22B presents the coverage of the seeding method where the cells were pre-dissociated with Tryple Express. At day 5, only single cells can be observed on the top of the TE. Over time, many small colonies start to form and join until confluency.

The graph presented in Figure 5.22C shows that there is a significant expansion of the hLE colonies over time. However, there is no significant difference, at any point from day 10 to day 19 of the two conditions in analysis. Unfortunately, the coverage measurements at day 5 of the condition Direct Dispase + Tryple Express were not possible due to the low contrast and presence of only single cells on the RAFT-TE.

In both cases, most of the RAFT-TEs remained intact after being removed from the well and subject to stress under shaking. A summary is presented in Figure 5.22D, and although not substantially different, the condition of Direct Dispase+ Tryple Express is the one that detaches the least from the RAFT surface.

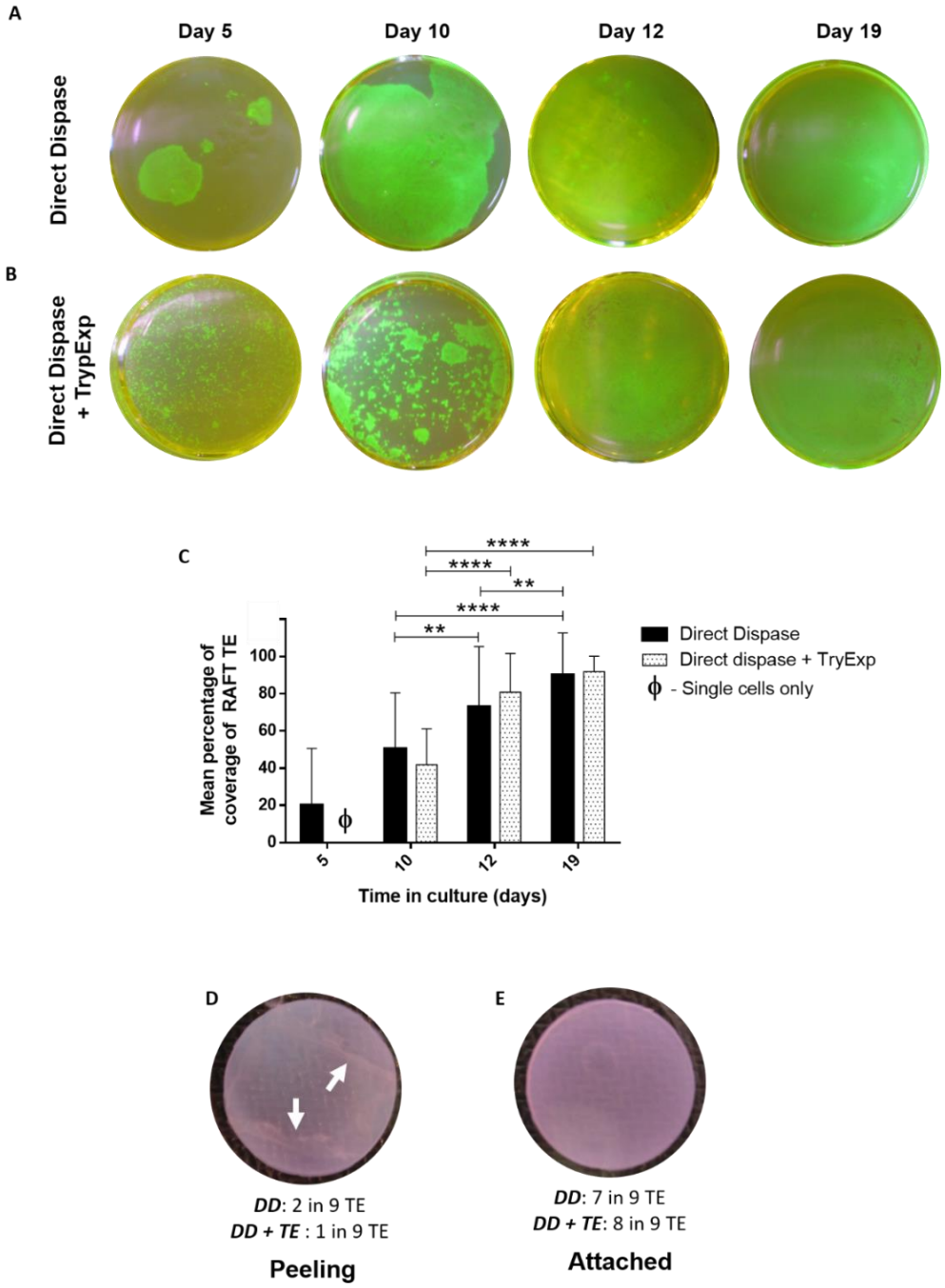

Figure 5.22 – Characterisation of hLE growth and epithelial cells layer behaviour on top of *Koken* RAFT-TE prepared with NS. LESCs were isolated from corneal fresh corneal rims using dispase, and 1/9 of the cell suspension obtained from each corneal rim was added to the surface of RAFT (before or after dissociation with Tryple Express). The cells were cultured on top of RAFT-TE for 19 days. **(A)** hLE growth (n = 3 donors) over 19 days of culture - cell suspension directly added to the surface of RAFT. **(B)** hLE growth (n = 3 donors) over 19 days of culture - pre-dissociated cell suspension with Tryple Express. **(C)** Mean area of hLE growth (n = 3 donors) over 19 days of culture in both conditions. RAFT-TEs were stained with FdA and images taken at different time points during culture (two-way ANOVA test followed by Sidak's multiple comparison test where **p≤0.01, ****p≤ 0.0001). **(D)** The RAFT-TEs were shaken in order to test the cell layer attachment to the TE. Images highlighting the epithelial cell layer appearance on the surface of RAFT-TE post handling with regards to cell attachment and summary of the epithelial cell layer behaviour in terms of attachment to the TE.

Summary of results:

- Both mixed population directly seeded on top of RAFT-TE, and pre-expanded in 2D (TCP) resulted in cell peeling.
- Stratification was visible by cryosectioning, and expression of markers such as p63 and PAX6 was positive;
- Despite the cell peeling, there was expression of basement membrane markers such as perlecan, Collagen IV, VII and laminin 5 in most cases.
- Sometimes part of the epithelial cell layer remains attached to the TE;
- There was a weak expression of SMA at the interface of the RAFT and the cellular part of the TE in some cases;
- Direct dispase seeding method significantly reduces cell peeling.
    - This was even more evident in the cases were the cells were pre-dissociated with Tryple Express.

5.4.3.4. Summary

Table 5.3 summarises epithelial cell layer attachment, in percentage, of all the seeding methods tested on RAFT-TE prepared with the clinically relevant protocol (*Koken* NS).

The RAFT-TEs were removed from the well after cultured and subject to stress by shaking in L15. The condition that had most cell detachment from the surface of RAFT-TE was the direct mixed population isolated from OC rims. The mixed population isolated from OP rims also had a very poor rate of intact RAFT-TEs (30%), but still twice better than the OC one.

OC mixed population pre-expansion resulted in poor growth, and the LESCs expanded on 3T3 resulted in poor quality epithelium so were not shaken at the end of culture.

OP pre-expanded seeding method was slightly better than the direct OP mixed population. Nevertheless, there is an obvious improvement from the mixed population methods using the direct dispase technique.

The RAFT-TE seeded with a cell suspension prepared directly from the dispased corneal rim proved to detach less than all the other conditions. The condition where cell peeling was less frequent was the Direct Dispase + Tryple express.

Table 5.3 – Summary of epithelial cell layer behaviour on top of RAFT-TE with the different cell seeding methods. *Really bad quality epithelium, not worth shaking, # Really poor growth. Irregular colonies.

Seeding Method	Epithelial Cell Layer attachment
DD+TE	89%
DD	78%
LESCs expanded on 3T3s	NA*
OP Pre-expansion	35%
OC Pre-expansion	#
OP Mix population	30%
OC Mix population	14%

5.5. Discussion

The aim of this chapter was to design a safe and efficient strategy to deliver LESCs and CSSCs for ocular surface reconstruction.

The first part of this chapter presents a comparative study of collagen sources, as well as two different ways of neutralising the collagen solution, to test whether the changes in the manufacturing protocol affected cell behaviour.

The second part of this chapter assesses different storage medias, isolation methods and seeding strategies of cells on top of RAFT-TE.

5.5.1. Impact of RAFT-TE manufacturing changes on cell behaviour

First Link rat tail collagen has been used in our laboratory to model corneal diseases *in vitro* for a long time but cannot be used in clinics. *Koken* bovine skin collagen is clinically acceptable and an option for RAFT-TE production for human transplantation.

This change in protocol led to unexpected changes in cell behaviour. The mixed-population direct cell seeding had been used as an easy, fast and feeders-free way for seeding cells on the surface of RAFT-TE. This approach proved to be unreliable in terms of initial cell growth and subsequent epithelial cell peeling. This phenomenon was first observed prior to transplantation during our rabbit study (not published) when the RAFT-TEs were released from the dish but was not previously observed using the *First Link* rat tail collagen.

5.5.1.1. Comparison of RAFT-TEs prepared with different collagen sources and neutralising solutions

Koken collagen was compared with another clinically approved collagen source, *Symatese*. As expected, significant differences with regards to the mean area of coverage of RAFT-TE could be observed over time [127]. However, no significant difference could be detected between the two collagen sources. As observed by the large error bars, it is also possible to note the considerable variability between samples

HEPES containing media has been previously reported as toxic when exposed to light due to the formation of hydrogen peroxide [284]. As the new neutralising solution used for RAFT-TE preparation contains HEPES, a comparison with NaOH was made. NaOH was the research protocol reagent used in the lab previous to GMP optimisation and standardisation. Although the mean area of coverage was higher when RAFT-TE were manufactured with NaOH, no significant differences could be observed. Nonetheless, both the RAFT-TE prepared with NS (containing HEPES) and the ones prepared with NaOH peeled. For the subsequent experiments presented, the

neutralizing solution was covered with aluminium foil during storage and particularly during use in laminar flow hoods [285].

Although not directly impacting cell peeling, light transmission was assessed as an indicator of RAFT-TE transparency. In the short term, RAFT TE transparency is necessary to allow vision to the patients, post-surgery. Transmission over 50% of all RAFT-TE was maintained in all the conditions. It is anticipated that, in the long term, RAFT-TE will be remodelled in the recipient's cornea.

Hydrogels are extremely attractive as platforms for 2D and 3D cell culture. RAFT-TE is a 3D collagen compressed hydrogel that allows the culture of cells in 3D, when inside the TE or in 2D, when cultured on top. In the native environment, epithelial cells are subject to a 2D environment. Factors such as substrate stiffness and the presentation of adhesive ligands are crucial [286]. For example, it is suggested that substrate stiffness affects the morphology, division and differentiation of stem cells, as well as corneal epithelial cells [287]. As observed by confocal microscopy, manufacturing changes did not prevent cell peeling. Previous papers from our group showed that epithelial cells on top of RAFT-TE express similar markers to the native corneal tissue. Nevertheless, as the protocol for the TE evolved, and the cell isolation method was changed, a new investigation was performed. Likewise, the expression of β1-integrin, PAX6 remained positive on the TE despite cell peeling and individual cell dissociation.

To understand the response of cells to substrate stiffness, cell–material mechano-interactions have been studied. Cell surface receptors, such as integrins, bind to ligands within the hydrogel if such adhesion sites exist. The cell adhesion spots to the substrate are called focal adhesions. Integrins are directly associated with cell attachment, migration and ECM remodelling. They attach to the actin filaments on one side and to ECM ligands on the other [287].

β1-integrin is a putative progenitor and proliferative cell marker. It is strongly expressed in the basal cell membranes of the central corneal epithelial layer and was highly expressed in the cells membrane on RAFT-TE both in this study and in previous works [164]. Integrin β1 staining was performed to

test the presence of this important intermediary of cell-hydrogel attachment. Nevertheless, even in its presence, cell detachment and peeling still occurred. Other proteoglycans, such as syndecans and cadherin molecules, could be studied to understand cell-cell adhesions and its influence on ECM interaction and production in this model [288].

LESC populating the RAFT-TE expressed PAX6 and Integrin β1. However, the expression of these two markers presented varied intensities across the RAFT-TE. PAX6 is an early differentiation marker expressed by corneal epithelial cells [289]. Integrin β1 plays a role in mediating cell attachment to proteins on the BM, and has also been used to identify basal limbal epithelial cells [290, 291]. The varied expression of PAX6 and Integrin β1 across the sample might reflect different stages of cell differentiation. The mixed population method relies on the expansion of LESCs from a small number of colonies. These colonies start to expand at different time points, and rates on the TE, which might be the reason behind the non-uniform cell differentiation across the epithelial cell layer.

5.5.1.2. Comparison of RAFT-TEs prepared with different compression times

The amount of time that the hydrogel is exposed to the hydrophilic porous absorber, to remove most of the water, is defined as compression time. The first RAFT prepared with 2.4mL of the solution containing *First Link* collagen, was compressed for 30min. However, when the protocol was adjusted to 0.6m/L of solution with *Koken* collagen, this compression time was not adjusted. This could have an impact on the RAFT-TE properties like water content and the density of the collagen or stiffness. This could then affect cell attachment.

Interestingly, no significant improvements were observed in terms of epithelial cell layer coverage or attachment when manufacturing RAFT-TE using different compression times. A high rate of variability due to the quality of the tissue and the method itself was also observed.

5.5.2. Comparison of different tissue storage media on the performance of mixed population seeding on top of RAFT-TEs

A new method to isolate a mixed population of HLE and CSSC using collagenase digestion has been reported by Chen and colleagues [292]. This is important because it has been previously shown by different groups that mesenchymal stromal cells play an important role in maintaining epithelial stem cell phenotype and in promoting its clonal growth both *in vivo* and *in vitro* [98, 112, 127, 293, 294].

Levis *et al.* have previously revealed the beneficial effect of fibroblast co-cultured inside RAFT-TE in epithelial cell differentiation and layering. Specifically, more intercellular junctions and higher levels of basement membrane proteins such as laminin, collagen IV and β1 integrin were reported [164]. However, this traditional approach was a longer process and required the use of murine 3T3 fibroblasts for *in vitro* expansion of HLE, which had an associated risk for the patients.

From a GMP perspective, the new cell isolation and seeding protocol on top of RAFT-TE (direct mixed population) would make the process easier and faster when compared to the pre-expansion of the epithelial cells using feeder cells (3T3s). As shown by Kureshi *et al.* [127], this is a technique that only requires 15 days to promote HLE layering and differentiation. The delivery of the cells as a mixed population, a co-culture of HLE and CSSC abolishes the use of animal-derived feeder cells and the risks associated with it.

LESCs and CSSCs can be isolated from fresh corneas, but also from Optisol and organ cultures stored rims [121, 274]. Since the experiments were dependent on tissue availability and storage conditions, a side by side comparison was initially made between OC and OP corneal rims with regards to the success of its mixed population protocol outcomes.

As expected, epithelial stem cells cultured from a mixed population on top of RAFT-TE showed a healthy small cobblestone morphology and were p63 positive [127, 184, 274]. Despite the fact that CSSC seems to support HLE

growth, after two weeks in culture, only a few cells could be detected beneath the epithelial cell layer, which corroborates previous studies [127].

Even though OC rims were older than OP rims, with differences between time of death and cell isolation being up to six weeks and up to a week, respectively, no significant differences could be detected in terms of HLE coverage. Nevertheless, high variability could be detected in both OP and OC cell suspensions. Differences in terms of epithelial cell stratification were also observed in different areas of the surface of the RAFT-TE. This supports the idea that a few colonies expansion results in full coverage of RAFT-TE, which might lead to differences in cell differentiation across the surface of the TE.

Cell peeling was two times more frequent when the mixed population was isolated from OC corneal rims. Yet, only 30% of the RAFT-TEs prepared with OP mixed cell suspension did not peel. Decisively, this new approach, that requires less manipulation and decreases the time of production was not leading to a consistent outcome in terms of HLE growth in RAFT-TE. The idea of streamlining this protocol with a therapy in mind needed to be rethought.

5.5.3. Comparison of different cell seeding strategies on top of RAFT-TEs

This section delves into different hypotheses to explain HLE cell peeling from RAFT-TE. This phenomenon was first observed when the cells on top of RAFT-TE had to be released from the dish before transplantation during an animal study (not yet published). To the extent of our knowledge, this had never been observed in previous studies.

5.5.3.1. Mixed population isolated from OP corneal rims on top on RAFT-TE

Notara *et al.* proposed that the culture ratio of 1 HLF for 3 HLE cells was ideal for enhancing the expression of putative stem cell markers in HLE [280]. This balance might be needed to support HLE, and the direct mixed population

cell seeding strategy used in this study does not give a consistent proportion of CSSC vs HLE in the cell suspension.

Pre-expansion of HLE as a mixed population was tested in comparison with the direct mixed population cell seeding as a way to increase HLE numbers in culture. The cells were then selectively trypsinised and the cell suspension seeded on the surface of RAFT-TE had a higher number of HLE. While the ideal ratio of HLE vs CSSC was not known, this lead to a much higher number of HLE vs CSSC, which was closer to the fibroblast proportion referred previously [280].

Although the previous experiment showed a better performance of the cells isolated from OP corneal rims when compared to OC corneal rims, this pre-expansion protocol was also tested on OC isolated cells. This occurred because OP stored rims stopped being available from our local eye bank due to changes in regulations. Despite the efforts to pre-expand the mixed population isolated from OC rims, the quality of the epithelium was inferior, and thus this option was not pursued (results not shown).

Corneal rims stored in Optisol were imported from an American Eye Bank, and the experiment was repeated with eight donors in total.

Previous to the cell seeding of the pre-expanded mixed cell population, a comparison between culture in TCP (coated with FNC) and onto RAFT was made. When comparing the expansion of the epithelium on RAFT-TE from the direct mixed population on top of RAFT-TE with its expansion on TCP, it was clear that the expansion is faster on TCP. However, it is not possible to say if it would achieve similar coverage after more time in culture since the maximum area of RAFT-TE ($2cm^2$) was reached.

There are many possible explanations for the differences observed between the two conditions. The matrices were different, not only in terms of composition but also of dimension. It is known that cells cultured on 2D and 3D matrices show significantly different behaviours with regards to cell proliferation, differentiation, mechano-response, and cell survival [295, 296]. For example, studies with cancer cells have shown higher proliferation rates

in 2D when comparing with 3D [297], which corroborates the results presented here. Cell migration rates also tend to differ between the two dimensions, which can be explained by the more complex interactions with a 3D substrate [295, 298, 299] being also a possible explanation for the different rates of growth.

Looking at the two cell seeding methods, it was possible to conclude that although the RAFT-TEs that were seeded with pre-expanded cells peeled in less 5% of cases, in comparison to those cultured with a direct mixed population, the cell morphology was not as healthy. Based on this, the direct mixed population method was selected for further study.

Cell-cell and cell-matrix interactions play a crucial role in the maintenance of the corneal epithelium. More specifically, the interaction between the epithelial cells and the underlying basement membrane has proven to be critical in wound healing and in the preservation of a healthy epithelium. It is also known that epithelial cell migration requires cycles of de-adhesion and re-adhesion, which has an impact on intercellular junctions [300].

Since the epithelial cells, in this case, were peeling as an intact layer, the problem seemed to reside in the cell-matrix interactions. Nevertheless, in some cases, detachment of the superficial epithelial layer was also observed, leaving only the basal cell layer behind when the epithelium had stratified. The expression patterns of putative stem cell marker p63α and eye development marker PAX6 enabled investigation of the extent of differentiation of the cells.

Most of the basal cells attached to the RAFT surface were p63α and PAX6 positive, indicating that most of these cells remained in a non-differentiated state with LESC characteristics. The small cell size observed corroborates previous studies, but the expression of these early markers was not consistent with previous observations in an earlier version of RAFT-TE using First Link collagen and a load for plastic compression [46, 164, 301]. Colleagues have reported the loss of p63α expression as expected. They claimed that more differentiated structures better mimic the native central cornea, where there is no evidence of the presence of LESCs in humans [164, 302]. Some groups claim that p63α expression described in the central cornea is a result of post

mortem changes [303]. The cells cultured on top of RAFT-TE were not as differentiated as the ones cultured by colleagues in earlier versions RAFT-TE [164].

Cell-matrix interactions, in this case, epithelial-stromal interactions rely on the basement membrane formed between the two cellular layers and structures called hemidesmosomes (HD) [304]. These are mainly composed of collagens, laminins, heparan sulphate proteoglycans (HSPGs) and nidogens [305]. The extracellular matrix basement membrane (BM) proteins collagen IV, collagen VII, laminin 5 and perlecan (that is an HSPG) were evaluated on cryosections of the collagen constructs to understand why the cells were so loosely attached to the surface of RAFT-TE.

There were no obvious differences in perlecan expression in the RAFT-TEs that peeled and that did not peel. However, surprisingly, it was possible to see weak staining of this BM marker while in previous studies this was not present [164]. Some authors showed that in HAM cultures this is only possible to observe after three weeks in culture [306]. Nevertheless, its expression might be related to its mediation function in migration, cell proliferation and differentiation that are important in epithelial cell expansion and differentiation [304].

Collagen VII staining was almost not perceptible, which is corroborated by previous studies. This was expected since the epithelial cells were in an early stage of differentiation [164]. It is known that Collagen VII is a primary structural element of anchoring fibrils that play a crucial role in cell-matrix interactions. The lack of this BM component might be related to the epithelial cell detachment [307].

Laminins are the most abundant non-collagenous protein of the BM and are essential for the BM assembly due to their interaction with collagens via nidogens and other ECM molecules [308, 309]. Laminin 5 staining was more uniform in the RAFT-TEs that did not peel. In the samples that peeled, the staining was patchier or non-existent. A previous study showed that laminin was expressed with the presence of fibroblasts inside RAFT-TE (and HLE on top), in comparison to the same setup without the cells inside. Taking this into

consideration, it was expected that the stromal cells in the mixed population would potentiate laminin expression as it was observed before [164]. *In vivo* and *in vitro* studies have shown that laminins are responsible for the initial BM self-assembly without the contribution of other components [304, 310]. This might explain its presence in comparison to other BM molecules.

Collagen IV presence in the cornea has always been questioned. This has been explained by its spatial variability and multiple chains that can assemble into different heterotrimers [304]. In this study, Collagen IV was highly expressed in the BM, similarly to what has been shown by Levis *et al*. in a previous RAFT-TE study [164]. No relevant differences could be observed between the samples that peeled and the ones that did not.

In a few samples, it was possible to detect SMA staining. This may point towards cell contamination of the mixed population or the differentiation of CSSC into fibroblast. This could be a reason for the impaired attachment of the epithelial cell layers due to the high remodelling capacity of collagen by fibroblast [298]. Yet, no obvious differences, or strong SMA staining, could be observed in either of the conditions.

5.5.3.2. LESCs expanded on 3T3s on top on RAFT-TE

Despite the fact that 3T3s can already be banked according to GMP standards, they still pose a risk associated with xenotoxicity [274]. Regardless of the recent scientific advances, LESCs expanded on 3T3s remain the gold-standard of epithelial cell expansion [311, 312].

This method of cell isolation and seeding was tried on the clinically relevant version of RAFT-TE. However, the quality of the tissue had a great impact on the outcomes of the cultures.

LESCs expanded on 3T3s are usually isolated from fresh cadaveric eyes. Despite our efforts, the eye bank could not provide eyes in less than 24h post-mortem. In a study that compared the yield and viability of human limbal stem cells from fresh and stored tissue, it was shown that this reduces both cell numbers and expression of ΔNp63 and TrkA [313]. The high variability in tissue

quality, post-death time and age of the donors led to high variability and poor-quality epithelium. Thus, a fair comparison with previous studies that had access to good quality tissue for LESC isolation and expansion prior to seeding on RAFT-TE was not possible.

5.5.3.3. LESCs isolated with dispase directly cultured on top on RAFT-TE

The cell isolation method with dispase that is currently used prior to LESC expansion in 3T3s was used in a novel seeding strategy. The isolation procedure was followed as previously described, but instead of seeding the cell suspension on top of 3T3s, the cells were directly seeded on top of RAFT-TE, replicating the direct mixed population cell seeding method. However, instead of digestion in collagenase of the superficial limbal tissue, the cells were isolated by scraping the limbal region after being exposed to dispase.

The isolation with dispase and the superficial scraping of the limbus ensured a lower percentage of stromal cells in the cell suspension when compared to the collagenase method that involved the dissection of the superficial corneal limbal region. The direct cell seeding avoided the use of 3T3s.

Surprisingly, with this method, 1/9 of the cell suspension of each corneal rim was enough to ensure RAFT-TE confluency in 12 to 19 days. In the direct mixed population ¼ of the cell suspension from a corneal rim was added to each RAFT-TE.

Early in the experiment, it was observed that, as with mixed population, colonies of HLE would start to expand from a single or few colonies until achieving RAFT confluency. This also led to poor distribution, and high variability between RAFT-TE seeded with a cell suspension from the same donor. To try to achieve an even cell distribution, previous to cell seeding, the cell suspension was subject to Triple Express to ensure cell dissociation. This was a way to ensure the cells had similar differentiation stages. Dispersed cells were the origin of independent colonies that expanded until RAFT-TE

confluency, contrarily to other strategies where the cells within one big colony might already display different stages of differentiation.

Regarding mean percentage coverage of RAFT-TE over time, no significant differences were observed between the RAFT-TE culture with the pre-dissociated cell suspension (DD+TE) and the ones that were seeded with the non-uniform cell suspension (DD).

This direct dispase method was the one that ensured a higher percentage of epithelial cell attachment, with differences of more than 40%. The RAFT-TEs culture with the pre-dissociated cell suspension peeled less (89% of cell attachment) than the ones with the direct cell suspension (78% of cell attachment) which supports the theory that cell differentiation stages might play a role in epithelial cell detachment.

It has been demonstrated by colony-forming efficient analysis that the further the cells are from an explant or the centre of their colony, the lower their proliferative potential is [314]. It has been reported that LESCs properties and consequently, putative marker expression is reduced towards the periphery of the outgrowth in explant cultures. The same study also pointed to the fact that the cells on the periphery divide more quickly and become more differentiated due to the extensive number of divisions [314]. This quick division also reduces attachment to the basement membrane [315]. Another study has also highlighted the different adhesion capacity of the limbal cells when compared to the rest of the epithelium both in terms of adhesion structures and surface topography. It emphasised the higher capacity of limbal stem cells to adhere to rougher surfaces [316].

5.6. Conclusion

This chapter focused on investigating the manufacturing and cell seeding steps that might have introduced structural changes to the RAFT-TE.

Cell peeling represents an issue to the development of a therapy. To address this problem, a thorough approach targeting every major modification of the protocol was performed. It was analysed whether the storage medium of the corneal rims, the manufacturing changes of RAFT-TE, or the different cell seeding approaches had an impact on cell attachment.

It was found that the mixed population cell seeding method was the major cause of cell detachment. During this work, it became clear that the mixed population isolation protocol is not consistent. As expected, there is vast variability between donors, but surprisingly also between samples prepared with the same cell suspension and TE conditions.

The direct dispase method with pre-dissociation in Tryple expressed was the one that resulted in the smallest percentage of cell peeling, and improved cell adhesion. It is hypothesized that this was due to remodelling of the matrix by CSSC, and possible competition for adhesion sites.

Although the best achieved protocol is still not acceptable for clinical translation, the work presented in this chapter presents a great improvement over the initial protocol, improving adhesion from 14% to 89% of RAFT-TEs.

For clinical translation, reproducibility needs to be ensured from the first step. As a group, a step back was taken, and one of the first methods is now being used for the clinical validations. Corneal limbal explants are being seeded on top of RAFT-TE with outstanding results, and no cell peeling has been observed.

Chapter 6

6. MANIPULATION OF THE PHENOTYPE OF STROMAL CELLS DERIVED FROM THE HUMAN LIMBUS TO OPTIMIZE FUTURE THERAPEUTIC DELIVERY

6.1. Introduction

MSCs are especially promising in tissue engineering due to their reported immunomodulatory capacity to delay the host rejection of allogeneic tissue in human recipients [317]. A population of MSC-like cells, called CSSC, has been identified in the stroma at the corneal limbus and can be made to differentiate into keratocytes [114]. Promisingly, human CSSC were not rejected when transplanted into murine corneas and were able to reduce haze [113].

Investigations in our laboratory suggest that CSSC reside in close proximity to LESC in the LC-rich superior and inferior regions of limbus [98]. The importance of epithelial/stromal cell interactions in the maintenance of LESC holoclones and epithelium *in vitro* was showed by Tovell *et al.* [274]. Co-culture and transplantation of CSSC with autologous LESC could restore important cell-cell interactions that may be required for optimal function post-transplantation and resolve haze in a one-step procedure.

Currently, the gold-standard for the delivery of stem cell therapies to the cornea is still human amniotic membrane (HAM) [278]. Although different attempts have been made to create tissue engineering alternatives for the delivery of these cell therapies, no ideal formulation has yet been achieved. It is important to highlight that HAM does not allow the incorporation of cells inside its structure but only at the surface. On the other hand, RAFT-TE

(presented in previous chapters), was designed as an alternative approach that can be engineered to produce corneal tissue equivalents and allows cell culture both inside the collagen hydrogel and on its surface.

First attempts to use RAFT-TE as an alternative to HAM include the culture of HLE on top and the inclusion of limbal fibroblasts inside the TE to support epithelial cell stratification [164, 258, 318]. RAFT-TE has also been used to culture a mixed population of HLE with CSSC, without the use of animal-derived feeder cells, thus avoiding the regulatory issues described earlier on this thesis [127]. Additionally, Mukhey *et al.* created a biomimetic version of the TE by tethering the gels in order to resemble the alignment of the collagen fibrils in the native cornea. Ideally, this structure would be populated by keratocytes but, as they are difficult to culture *in vitro* (do not proliferate), CSSCs were used instead because of their rapid proliferation *in vitro*, and ability to differentiate into keratocytes [255].

Recently, Funderburgh's group has demonstrated that CSSCs promote the regeneration of healthy stromal tissue by avoiding deposition of scar tissue, therefore, increasing corneal transparency and stromal lamellar organisation when applied to the injury in a fibrinogen solution [111, 113]. Based on this, a clinical trial using CSSC to treat individuals with existing corneal scars is ongoing (NCT02948023).

Inspired by the previous work of our lab, where CSSCs have successfully been embedded in different iterative protocols of RAFT-TE [255], Funderburgh's group has also effectively embedded CSSCs in compressed gels using rat-tendon collagen and the commercially available Lonza kit as a vehicle for delivery of CSSC to wounded corneas [319]. This study reported increased potency of the treatment by the CSSCs embedded in the compressed collagen hydrogels when compared to the fibrinogen solution, as well as improved handling and off-the-shelf storage capacity (supported by successful cryopreservation). This study also reported that CSSCs arrange in flattened disk-like spheroids (50–100 μm aggregates in the gels) which, after 48h of implantation, cannot be observed inside the collagen gels. This loss is

believed to be correlated with an increase in MMPs and the consequent digestion of the collagen gel by the CSSCs. These are important findings that were not known when the work presented in this chapter was performed and will be further discussed in light of our findings (CSSC cultured inside RAFT-TE form cell clusters).

MMPs play a crucial role in cell migration, wound healing and tissue/matrix remodelling, thus affecting cell cluster formation [320]. MMP1 (interstitial collagenase) and MMP2 (gelatinase A) contribute to epithelial repair and stromal remodelling in the cornea [321, 322], and for this reason will be investigated throughout this chapter.

PDGF promotes cell migration and matrix remodelling [323-325] which could also impact cell cluster dispersal in collagen matrices [326]. Therefore, it was studied as a potential candidate influencing CSSC clustering inside RAFT-TE.

A comparison between compressed, (referred as RAFT-TE) and non-compressed (referred as Gel) hydrogels as a matrix for cell delivery was also performed to investigate the impact of the compression process in cell-matrix interaction and remodelling which is crucial for cluster formation.

The following experiments were an initial step towards the creation of a tissue equivalent for the delivery of CSSC to patients. The hypothesis was that RAFT-TE would be able to support CSSC and CSSC-derived keratocytes.

6.2. Aim

This chapter aimed to:

- Investigate the feasibility of utilizing CSSC, or keratocytes differentiated from CSSC to develop an organized corneal stromal

tissue equivalent using RAFT-TE protocol made of GMP-acceptable bovine skin collagen.

This was divided into four sub-goals:

(1) Assess the feasibility of embedding CSSC in RAFT-TE;

(2) Track phenotypic changes in CSSCs when embedded in RAFT-TE;

(3) Culture quiescent keratocytes on RAFT-TE;

(4) Understand the role of a growth factor known to influence keratocyte differentiation (PDGF) on CSSC behaviour inside RAFT-TE.

6.3. Materials & Methods

6.3.1. Isolation and culture of human corneal stromal stem cells in 2D

Performed as described in section 2.1 of Chapter 2.

6.3.2. Differentiation of CSSCs into Keratocytes.

Performed as described in section 2.3 of Chapter 2.

6.3.3. Spontaneous differentiation of CSSCs in CSSC media

Performed as described in section 2.4 of Chapter 2.

6.3.4. Cell morphology observation

Performed as described in section 2.6 of Chapter 2.

6.3.5. Live Cell tracking

In some experiments, namely when the influence of PDGF on keratocyte differentiation was investigated, cell behaviour inside the RAFT-TE was

tracked using a CytoSMART (Lonza) live cell imaging microscope. Images were taken every 15min and gathered in time-lapse videos of two days, over two weeks, from the same samples in order to track cell cluster formation and growth as well as cell migration towards the surface of RAFT-TE (termed 'hatching').

6.3.6. Preparation of RAFT tissue equivalents (TE)

RAFT-TEs were prepared using *Koken* Collagen as described on Chapter 2, section 2.9.

6.3.7. Cell culture inside and on top of RAFT

6.3.7.1. Direct seeding - mixed population on top of RAFT-TE

The limbus was dissected as previously described in section 2.1 and digested in collagenase overnight. Then, the mixed population was centrifuged, and the pellet was washed in PBS. The cell suspension of each donor was divided into 4 RAFTs in CSSC media.

6.3.7.2. Stromal-cell populated RAFT or Gel

Stromal-cell populated RAFTs were prepared as described before in section 2.9 (Chapter 2). However, CSSC or keratocytes were added as a cell suspension in the CSSC media step at different concentrations. Cells were not used beyond passage 6 to avoid significant alterations to their characteristics. The cultures were usually kept for 2 to 3 weeks in CSSC or KDM media, respectively.

The term Gel refers to non-compressed hydrogels. Gels were produced using the same protocol as RAFT-TE, but without being subject to the HPAs step of fluid removal.

6.3.8. Cell culture experiment set-up summary

In order to help the reader, schematic representations of the experimental set-ups were created. The schematic diagrams for the different experiments are presented in Figures 6.1 to 6.4.

6.3.8.1. Identification of the optimum CSSC seeding density inside RAFT-TE

Figure 6.1 represents the cell culture design towards the identification of the optimum CSSC seeding density inside RAFT-TE (CSSC incorporated into RAFT-TEs before compression). Different CSSC concentrations were cultured inside RAFT-TE, and their behaviour analysed. The 30k per RAFT-TE CSSC concentration was selected as the one closest to the native environment, and a mixed population of cells (as described in 6.3.7.1.) was cultured on top to establish an epithelial layer at the surface.

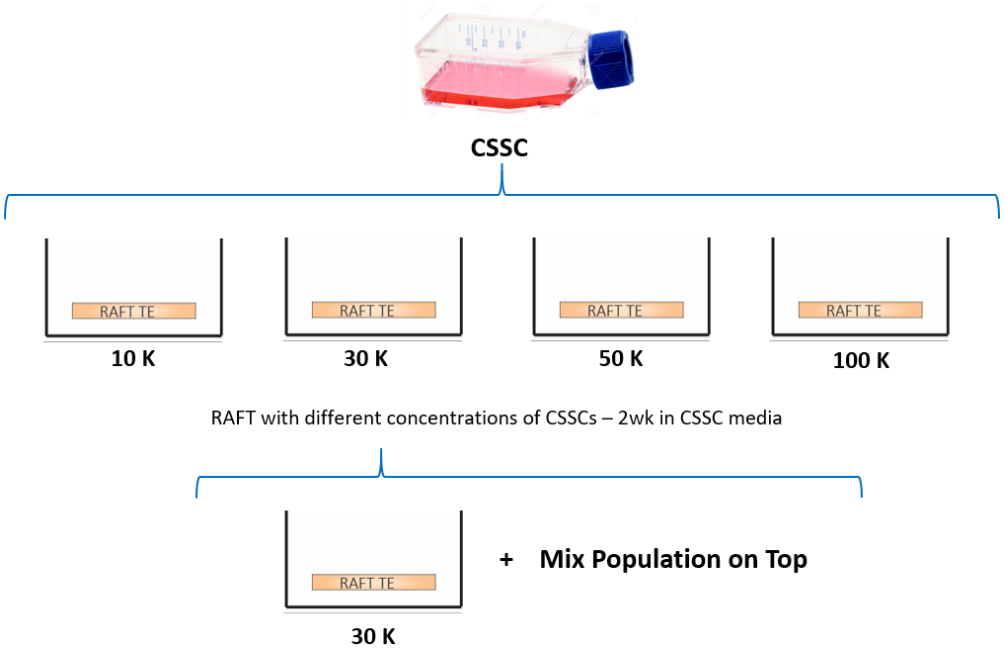

Figure 6.1 – Diagram of the experiment presented in section 6.4.1: RAFT-TE with different cell densities of CSSC cultured inside and with mixed population on top for 2 weeks.

6.3.8.2. The effect of culture conditions and spatial arrangement of cells on CSSC behaviour

Figure 6.2 guides the reader through the cultures performed to assess the effect of the culture conditions and spatial arrangement on CSSC behaviour.

This set of experiments were also designed to expand our knowledge on the phenotype the CSSC were acquiring when cultured inside RAFT-TE by direct compassion with the other conditions in study. CSSC cultured in 2D in CSSC media were used as the baseline, and compared with:

- Group 1 (KDM): CSSCs were cultured in 2D in CSSC media and differentiated (in 2D) into keratocytes using KDM media for 3 weeks.
- Group 2 (Diff): CSSC were allowed to spontaneously differentiate (prompted by naturally increasing cell density) in CSSC medium for 3 weeks.
- Group 3 (RAFT): CSSCs were cultured in 2D in CSSC media, and cultured inside RAFT-TE for 3 weeks in CSSC media.
- Group 4 (Gel): CSSCs were cultured in 2D in CSSC media, and cultured inside Gel (non-compressed RAFT-TE) for 3 weeks in CSSC media.

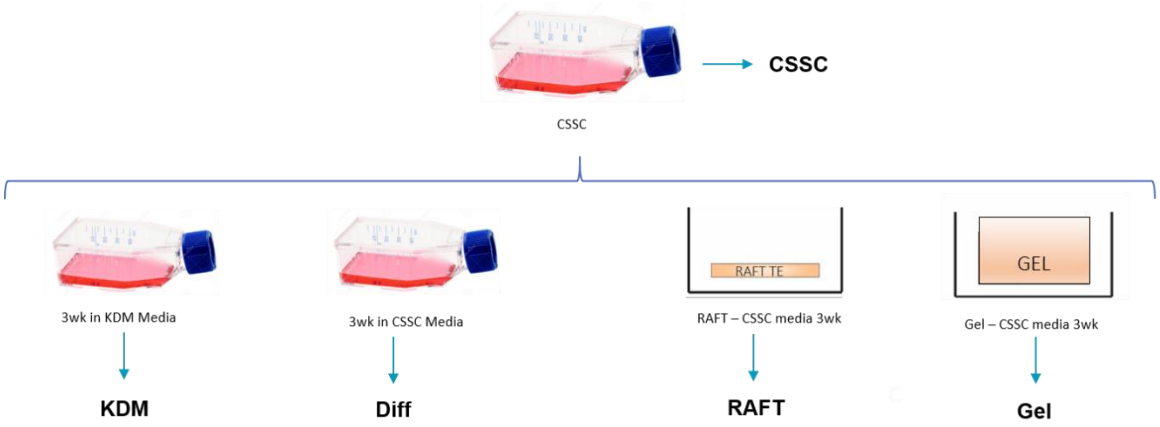

Figure 6.2 – Diagram of the different culture conditions presented in section 6.4.2: CSSCs culture in 2D using different cell culture mediums (CSSC and KDM media) and inside 3D matrices (RAFT-TE & Gel) for 3 weeks.

6.3.8.3. The effect of culture conditions and spatial arrangement of cells on keratocyte behaviour

Figure 6.3 represents the setup used to test the effect of cell culture conditions and spatial arrangement on keratocyte behaviour. CSSCs were first pre-expanded in 2D in CSSC media and then differentiated in 2D and in 3D using KDM media. This experiment was designed to test whether it was

possible to culture pre-differentiated keratocytes inside RAFT-TE, or differentiate them onsite.

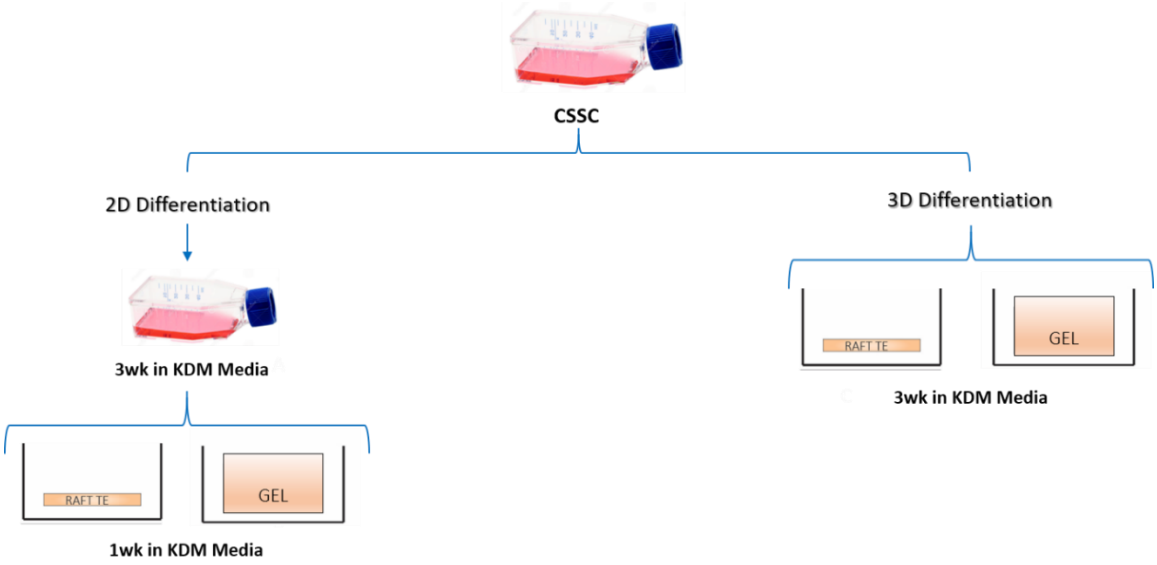

Figure 6.3 – Diagram of the different culture conditions presented in section 6.4.3: CSSCs differentiated in KDM media in 2D (3wks) and posteriorly cultured in 3D (1wk) and CSSCs directly differentiated inside 3D matrices (RAFT-TE & Gel) using KDM media (3wks).

6.3.8.4. The role of PDGF on cluster formation

Finally, Figure 6.4 summarizes the experiments designed to test the effect of PDGF on CSSC in RAFT-TE. CSSCs were cultured inside RAFT-TE for 2wks either in the standard CSSC media containing PDGF (PDGF+) or without PDGF (PDGF-) to investigate the role of PDGF on cluster formation inside RAFT-TE.

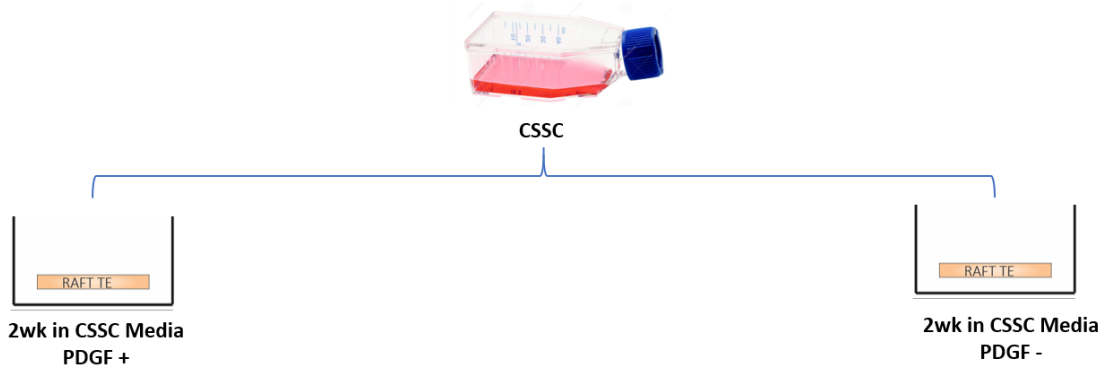

Figure 6.4 – Diagram of the experiment presented in section 6.4.4: RAFT-TE with CSSCs cultured in CSSC media with (PDGF +) and without (PDGF-) PDGF for 2 weeks.

6.3.9. RAFT Analysis

6.3.9.1. Scanning Electron Microscopy Analysis

Performed as described in section 2.10.1 of Chapter 2.

6.3.9.2. Light transmission measurements

Performed as described in section 2.10.2 of Chapter 2.

6.3.9.3. Fluorescein diacetate (FdA) staining

Performed as described in section 2.10.3 of Chapter 2.

6.3.9.4. Immunohistochemistry of RAFTs

Performed as described in section 2.10.4 of Chapter 2.

6.3.9.5. OCT# embedding and cryosectioning of RAFT-TE

Performed as described in section 2.10.5 of Chapter 2.

6.3.9.6. Immunostaining of frozen tissue sections

Performed as described in section 2.10.6 of Chapter 2.

6.3.9.7. Gene expression

Performed as described in section 2.8 of Chapter 2.

6.3.9.8. Whole Transcriptome Amplification

For the preparation of cDNA from total RNA of the samples that were purified (as described in Chapter 2) by whole transcriptome amplification, the QuantiTect Whole Transcriptome Kit (car. No. 207043, Qiagen) was used as per manufacturer's instructions. Briefly, 5µL of RT (reverse transcription) mix was added to each sample, vortexed and centrifuge briefly before incubation at 37°C for 30min, followed by 5min at 95°C. After cooling the samples down to 22°C, 10µL of ligation mix were added to each sample, vortexed and incubated for 2h at 22°C. Finally, 30µL of amplification mix was added to the samples, vortexed and incubated for 4h at 30°C and 5min at 95°C. The amplified cDNA was stored undiluted at -20°C until required.

6.3.10. Statistical Analysis

Statistical analysis of results was carried out using Prism 4.0 software (GraphPad, USA). Different tests were performed according to the experiments and are detailed in the results section. Statistical significance was defined as $p<0.05$.

6.4. Results

6.4.1. Identification of the optimum CSSC seeding density inside RAFT-TE

The first set of results aimed to investigate if it was possible to embed CSSC in RAFT-TE. For that, the behaviour of different concentrations of CSSC inside RAFT-TE was evaluated.

6.4.1.1. CSSC morphology in RAFT-TE

CSSC morphology inside RAFT-TE can be observed in Figure 6.5. Different cell seeding concentrations, namely 10 000, 30 000, 50 000 and 100 00 cells/RAFT, were tracked over time for up to two weeks in culture. In Figure 6.5 it is possible to observe that CSSC proliferate *in situ* and form cell clusters (as highlighted by the dashed line). Initially, all the cells were uniformly distributed through the TE. After a few days, cell clustering started to be visible. The cell clusters became more prominent over time, with their formation starting as early as day four at the higher cell seeding concentrations. At day 14, the final day of this experiment, large individual clusters can be clearly visualized.

In order to better understand CSSC behaviour inside RAFT-TE and to evaluate cell behaviour in the z-axis plane (thickness in the order of 100 µm), confocal microscopy was performed as shown in Figure 6.6. The z-stack series (Figure 6.6A) showed that some of the CSSC seeded inside the RAFT-TE migrate towards the surface and acquire an elongated aligned morphology. The orthogonal view presented in Figure 6.6B aims to show that cluster formation inside RAFT-TE occurs at different depths of the RAFT-TE. It is also important to note that the cells within the clusters also appear to be aligned.

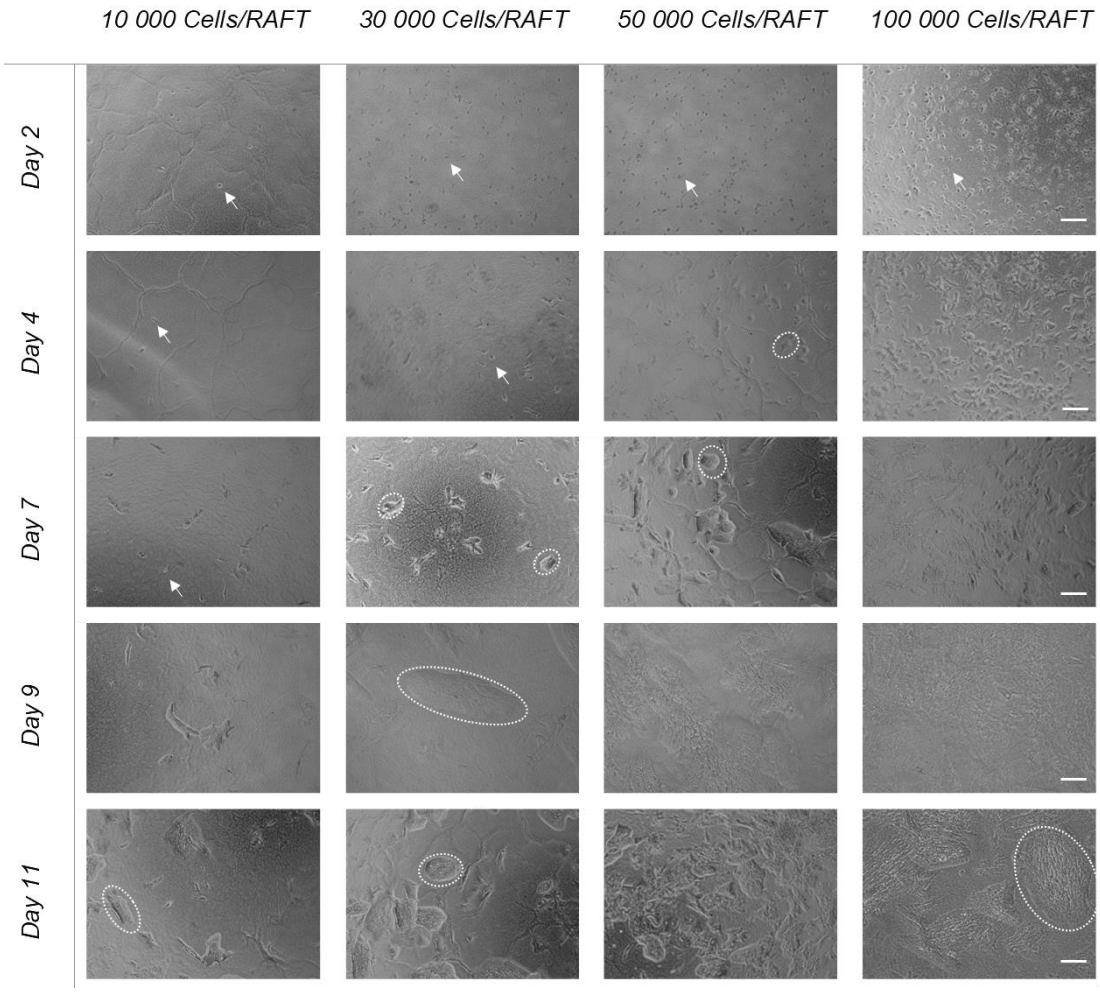

Figure 6.5 – Light microscopy images of CSSC growth inside RAFT-TE over time for different seeding concentrations (10 000, 30 000, 50 000 and 100 000cells/RAFT). Depending on the cell concentration, cell clustering can be observed as early as day 4 and clusters get bigger over time. Cell clusters are highlighted with dashed ellipses and single cells with an arrow. Scale bar = 200µm.

Supporting videos of confocal 3D projections and z-stack reconstructions can be found in the attached multimedia support (please check folder Chapter 6 - Cell clustering confocal videos).

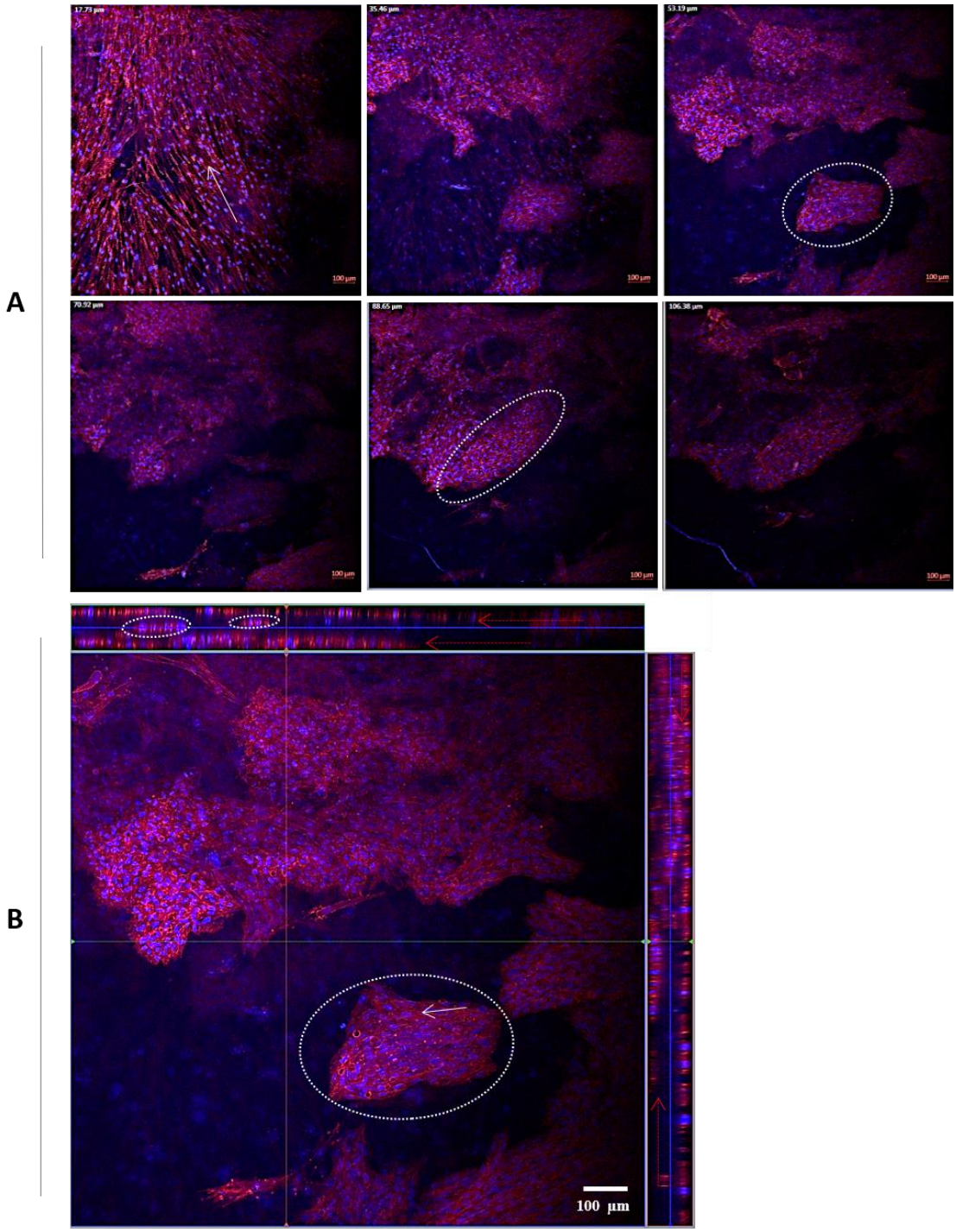

Figure 6.6 – Confocal images of 100 000 CSSC cultured inside RAFT-TEs for 13 days: **(A)** gallery view of z-stack images showing the different morphologies from top to bottom of the TEs; **(B)** representative orthogonal view of a z-stack pointing towards the cluster sparsity (Phalloidin – red, DAPI – blue). The white arrows point cells direction and/or polarisation within the cell clusters. The ellipses highlight cell clusters within RAFT-TE Scale bars = 100 µm.

6.4.1.2. CSSC marker expression when cultured inside RAFT-TE

The ‘clustering’ of CSSCs inside RAFT-TE was observed consistently over the course of the experiments. Also, depending on the proximity to the surface of the TE, different morphologies were observed (as shown above).

RAFT-TEs with 30 000 CSSCs were prepared and stained after 13 days with a range of CSSC (PAX6, CD90 & CD73), epithelial (p63 & CK3) and keratocyte markers (ALDH) in order to characterize CSSC phenotype inside RAFT-TE (Figure 6.7). Most of the cells remained PAX6 positive (Figure 6.7A), especially within the cell clusters, but CD90 negative (Figure 6.7B) and with very weak CD73 signal (Figure 6.7C).

CSSCs were initially isolated and cultured as a mixed population of CSSCs and LESCs. Bearing in mind the possibility of ‘cell contamination’, the CSSCs were stained with p63 (Figure 6.7D) and CK3 (Figure 6.7E). The cells appeared to be p63 negative, but some signal was still detected. CK3 is an epithelium differentiation marker and was used to test the possible onset of ‘trans-differentiation’ of CSSC into terminally differentiated epithelial cells. As shown in Figure 6.7E, no cells exhibited positive expression of CK3. Indeed, the keratocyte marker ALDH1A1 (Figure 6.7F) showed positive expression in the cells present at the surface of RAFT-TE.

To test whether PAX6 and p63 staining were constant throughout the RAFT-TEs cultures, further analysis of RAFT-TEs seeded with multiple CSSC densities were tested for these markers since they were an indicator of the presence of CSSC, and possible LESC contamination respectively. Figure 6.8 shows the positive expression of p63 (Figure 6.8 A-D) and PAX6 (Figure 6.8 E-H) across the range of CSSC densities. However, it is noteworthy to mention that PAX6 positive expression was again mainly observed within the cluster, while p63 expression was found only in some of the cells present at the surface.

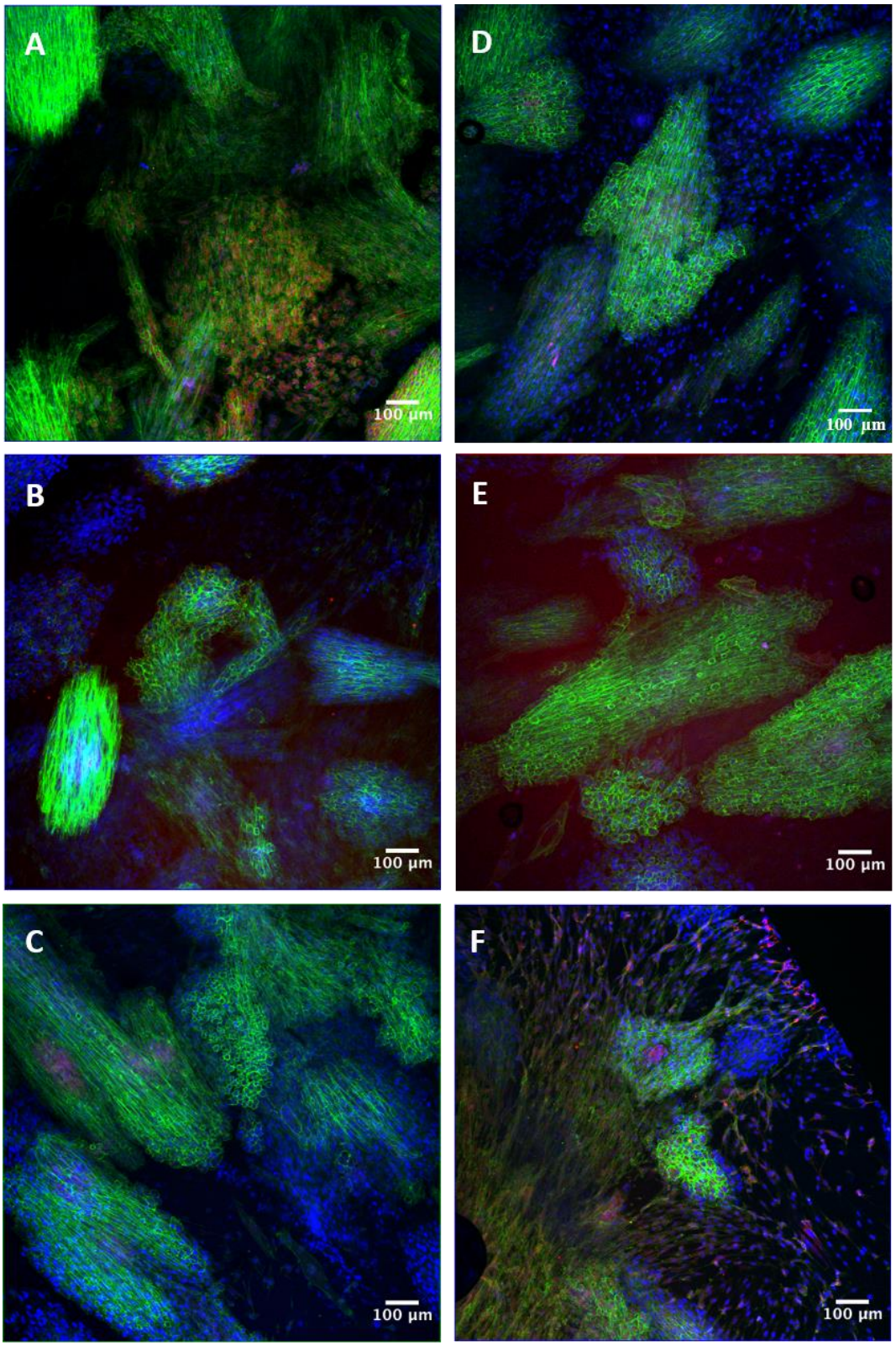

Figure 6.7 – Confocal micrographs of 30 000 human CSSCs cultured in 3D RAFT-TE. **(A)** PAX6 (gene expressed in early eye development), **(B)** CD90, **(C)** CD73 (mesenchymal stem cell markers), **(D)** p63, **(E)** CK3 (epithelial markers) and **(F)** ALDH (keratocyte marker). DAPI staining nuclei in blue, FITC Phalloidin staining cytoplasm in green and differential antibody staining in red. Scale bars: 100 µm.

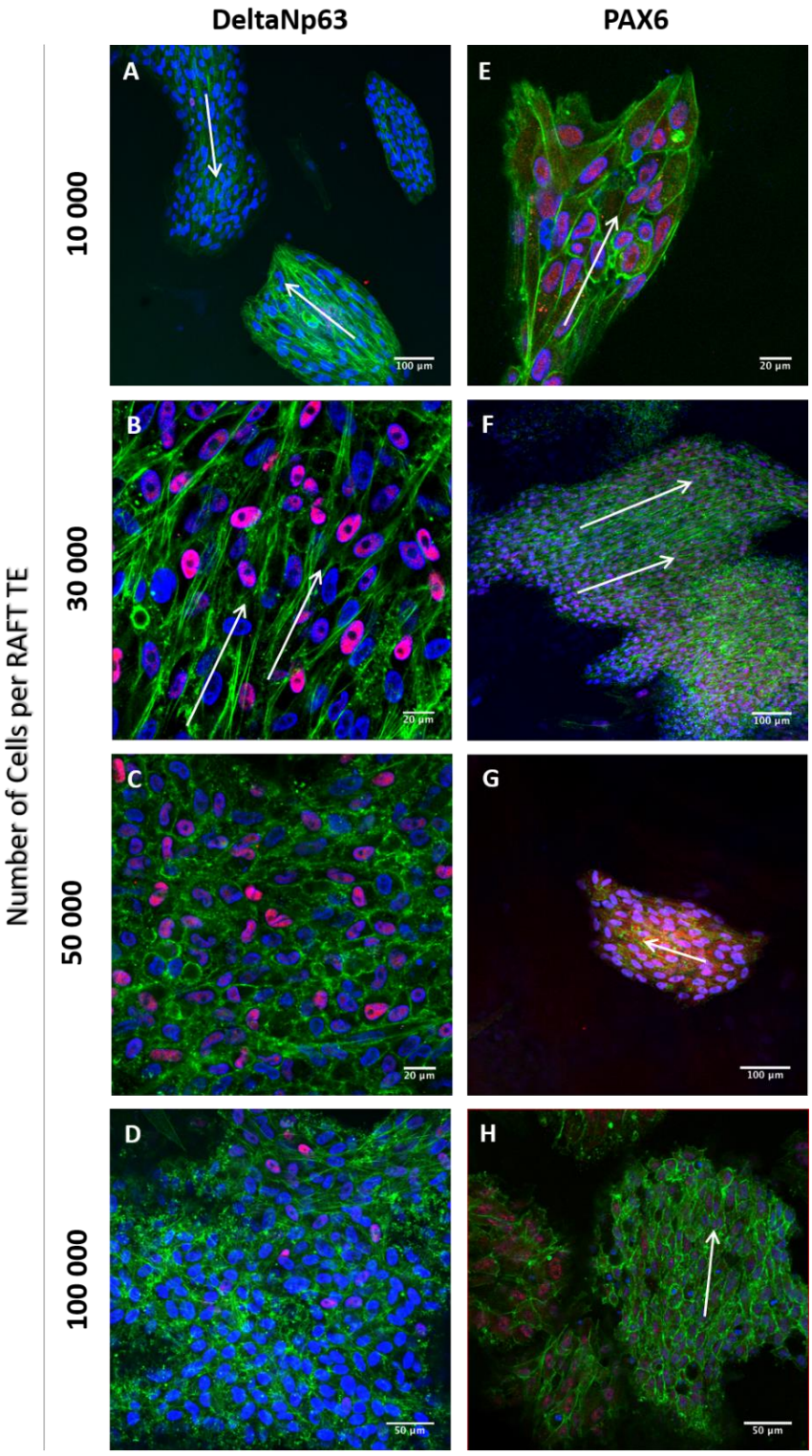

Figure 6.8 – Confocal micrographs of human CSSC cultured in RAFT-TEs for 13 days. **(A – D)**: immunostaining of DeltaNp63 (LESCs marker) of RAFT-TEs with 10 000, 30 000, 50 000 and 100 000 cells /RAFT respectively. **(E – H):** PAX6 (gene expressed in early eye development) staining of RAFT-TEs with 10 000, 30 000, 50 000 and 100 000 cells /RAFT respectively DAPI staining nuclei in blue, FITC Phalloidin staining cytoplasm in green and differential antibody staining in red. The white arrows point cells direction and/or polarisation within the cell clusters. Scale bars = 20 µm (B, C, E), 50 µm (D, H) & 100 µm (A, F, G).

6.4.1.3. Morphological analysis of cells cultured in RAFT-TE

SEM was used to examine the surface morphology and ECM of 30 000 (Figure 6.9 A-F) and 100 000 (Figure 6.9 G-L) CSSCs in RAFT-TE. With both concentrations, it was possible to see elongated, and uniformly oriented cells as well as deposited ECM.

The cells secreted high amounts of ECM and, although some regional fibril alignment was observed at the higher cell concentration (Figure 6.9 J-L), the degree and direction of the alignment was not consistent at lower cell density (Figure 6.9 A, B, E). In both cases, it was possible to observe the 'hatching of cells' from inside of RAFT-TE onto its surface. These cells presented mainly an elongated spindle morphology. As highlighted in Figures 6.9 F & L, the cells seemed to be extremely active due to the presence of numerous villi.

While in some places the cells were sparse, possibly indicating points of cell hatching (Figure 6.9 I), other areas of the RAFT-TEs were covered entirely with tightly aligned spindle cells at the surface, with circumferential arrangement at the borders of the wells.

The SEM images also show the extracellular matrix fibrils (Figure 6.9 K) laid down by stromal cells when cultured on RAFT-TE within both individual fibrils and mesh-like areas.

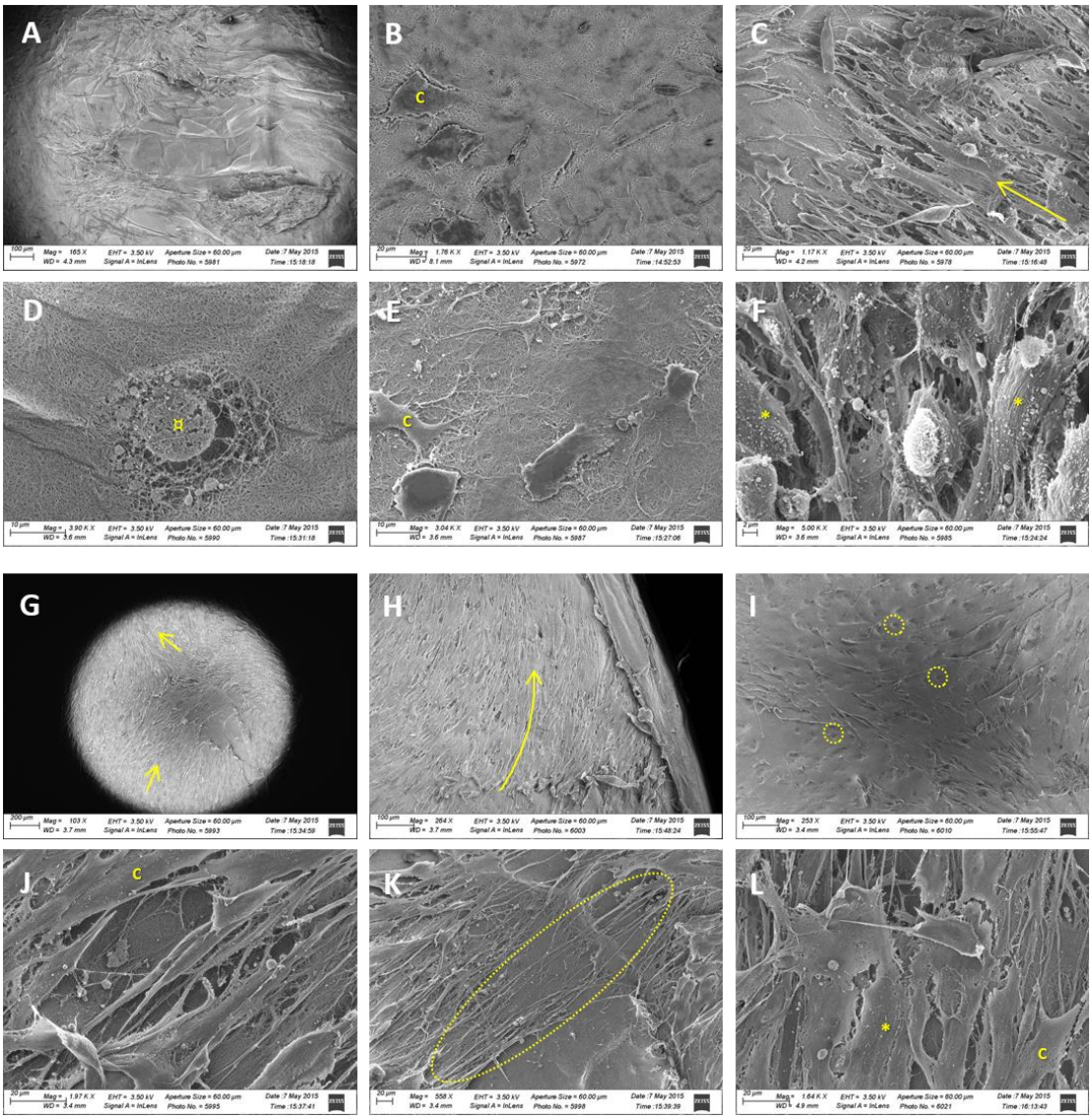

Figure 6.9 – Morphology observation of CSSC inside RAFT-TE after 13 days in culture by SEM: **(A - F)** 30.000 CSSC/RAFT-TE and **(G - L)** 100.000 CSSC/RAFT-TE (C- cell, Arrow – cell alignment, ¤ - disruption of collagen fibrils, *- villi on the cell surface, circle – hatching points, ellipses – fibrils matrix produced by the cells).

6.4.1.4. Transmission of light through RAFT-TE after seeding with CSSCs

The transparency of the RAFT-TEs was assessed by spectroscopy based on light transmission methods. As shown in Figure 6.10, transparency decreased over time. There was a significant reduction of transparency of the TE in all the conditions from day 1 to days 11 and 13. However, there was no significant difference in the transmission between the different concentrations of CSSCs added to the TE.

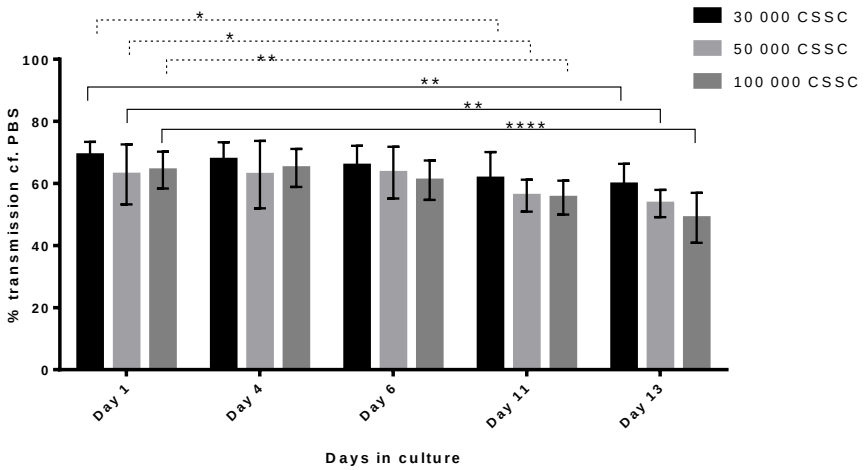

Figure 6.10 –Transmission of light over 13 days through RAFT-TEs cultured with different concentrations of CSSCs (10 000, 30 000, 50 000 and 100 000cells/RAFT). Average at 550nm (n=3, Tukey's with multiple comparisons test *p≤0.05, **p≤0.01, ****p≤ 0.0001).

6.4.1.5. Co-culture of CSSC inside RAFT-TE with a mixed-population on the surface

To check whether the incorporation of CSSCs into the RAFT-TE impacted limbal epithelial cell growth, the mixed-population cell seeding method was used to add cells to the surface of RAFT-TEs previously populated with 30 000 CSSCs inside.

Photographs of fluorescein diacetate-stained RAFT-TEs were taken at day 8, 11 and 13 in culture (Figure 6.11A) and analysed using Image J software to assess the extent of HLE growth over the days as shown on Figure 6.11B. The epithelial cell growth was continuous over time (Figure 6.11 A & B), suggesting that clustering of the stromal cells does not hinder the mixed population outgrowth.

HLE colonies were only visible after a few days of culture. Cells with cobblestone appearance (Figure 6.11C) covered the surface of RAFT-TEs as a monolayer within 13 days of culture. RAFT-TEs at day 13 of culture were assessed using immunohistochemistry for expression of p63, a putative epithelial stem cell marker. Positive expression of p63 was observed in a large proportion of basal HLE (Figure 6.11C), confirming that most of the cells retained their progenitor potential throughout the culture. It is also possible to observe some larger cells stratifying on the top, which were p63 negative.

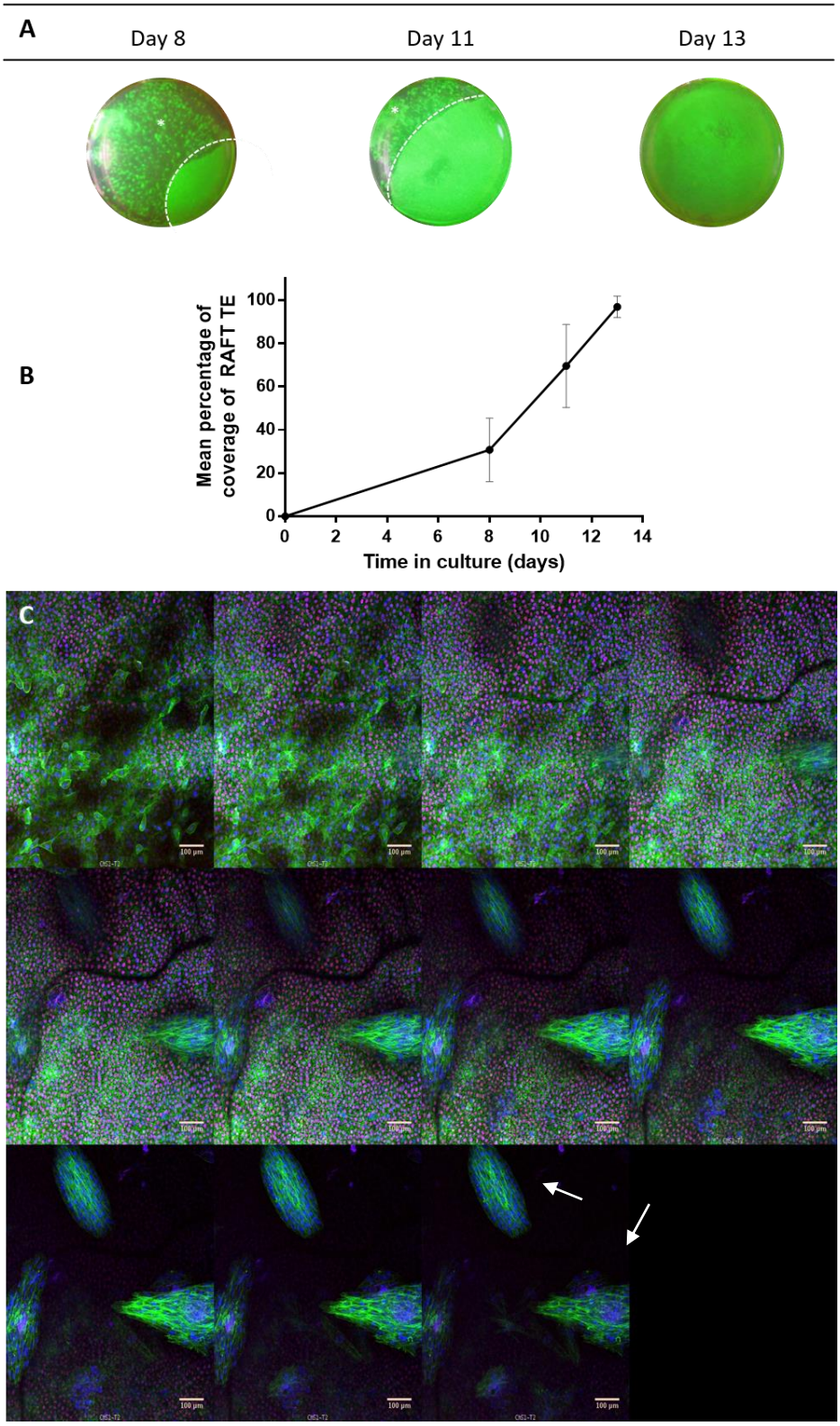

Figure 6.11 - RAFT-TE with 30 000 CSSCs cultured inside and mixed population cultured on the top (n=3): **(A)** Photographs of FdA-staining of RAFT-TE (at days 8, 11 and 13) using a camera and a yellow lens under a blue light; **(B)** Graph illustrating percentage of coverage of a 24-well plate RAFT-TE by HLE growth over 13 days of culture; **(C)** Confocal series of z-stack images of RAFT-TEs cultured with CSSC inside and mixed population on top for 13 days in CSSC media. HLE with positive p63 expression (seen in red). Arrows point at the cell clusters. (Blue - DAPI; Green - phalloidin). Scale bar = 100µm.

Summary of Results:

- CSSC were successfully embedded into clinically relevant RAFT-TE at multiple cell seeding densities (from 10 to 100 k).
- CSSC cultured inside RAFT-TE displayed different behaviours including:
    - formation of cell clusters inside the matrix;
    - migration of cells to the surface, and subsequent alignment;
    - extensive cell matrix remodelling.
- After 2 weeks, CSSC cultured inside RAFT-TE changed their protein expression profile:
    - PAX6 remained present within cell clusters;
    - MSC markers CD90 and CD73 were almost absent;
    - Keratocyte marker ALDH1A1 was positive at the surface;
    - p63 expression was present in some cells at the surface.
- There was a significant reduction in transparency over time, but no significant difference was observed between the different cell seeding densities.
- CSSC cultured inside RAFT-TE did not prevent mixed population expansion at the surface.

6.4.2. The effect of culture conditions and spatial arrangement of cells on CSSC behaviour

Based on the previous results that showed that it is possible to successfully culture CSSC inside the RAFT-TE produced using the clinically-relevant protocol, further investigations were performed to understand cell clustering and differentiation.

The second set of results here presented aimed to track phenotypic changes in CSSCs when embedded in RAFT-TE. This was possible through a comparison of the cells cultured 3 weeks inside RAFT-TE in CSSC media (RAFT), with the starting cell (CSSC), the keratocyte-like cells differentiated

from CSSC for 3 weeks in KDM media (KDM), and the CSSC that were allowed to spontaneously differentiate (prompted by naturally increasing cell density) in CSSC medium for 3 weeks (named as Diff).

6.4.2.1. Gene expression profile of CSSCs when cultured under different conditions

The gene expression profile of CSSC cultured under different conditions both in 2D (on TCP) and 3D (inside RAFT-TE) was characterized by q-PCR. All the comparisons were made against baseline expression of CSSC (in 2D) and normalised to 18s levels. RNA quality (A260/280) can be found in Appendix Figure S6.1.

Figure 6.12 shows the gene expression of CSSC markers (PAX6, CD90 and CD73) in multiple culture conditions: KDM - CSSCs differentiated for 3 weeks in KDM (Keratocyte differentiation media); Diff- cells spontaneously differentiated for 3 weeks in CSSC media; RAFT – CSSCs cultured inside RAFT-TE for 3 weeks in CSSC media; and Gel - CSSCs cultured inside non-compressed TE for 3 weeks in CSSC media; against the baseline defined as CSSC- CSSCs at P6 cultured on CSSC media (on TCP). The results for each individual donor can be found in Figure S6.2 of Appendix.

There was no significant fold change in PAX6 expression in any of the conditions, as shown in Figure 6.12A. Figure 6.12B also shows that CSSCs cultured under 3D conditions (RAFT-TE and Gel) had similar expression levels of CD90 as when cultured in 2D in CSSC media (sparse in TCP). However, CSSCs showed an upregulation of CD90 when cultured in 2D in KDM medium (**$p \leq 0.01$), and when allowed to spontaneously differentiate and grow on the same TCP flask (reaching confluency) in CSSC media (Diff condition, *$p \leq 0.05$). Figure 6.12C shows upregulation of CD73 on the KDM condition (**$p \leq 0.01$) while all the other conditions did not present significant differences with regards to CD73 expression in comparison to the baseline of CSSC.

Figure 6.13 illustrates the gene expression of keratocyte markers (LUM, KERA and ALDH1A1) in multiple culture conditions: KDM- CSSCs

differentiated for 3 weeks in KDM (Keratocyte differentiation media); Diff- cells spontaneously differentiated for 3 weeks in CSSC media; RAFT – CSSCs cultured inside RAFT-TEs for 3 weeks in CSSC media; and Gel - CSSCs cultured inside non-compressed RAFT-TEs for 3 weeks in CSSC media; against the baseline defined as CSSC- CSSCs at P6 cultured on CSSC media.

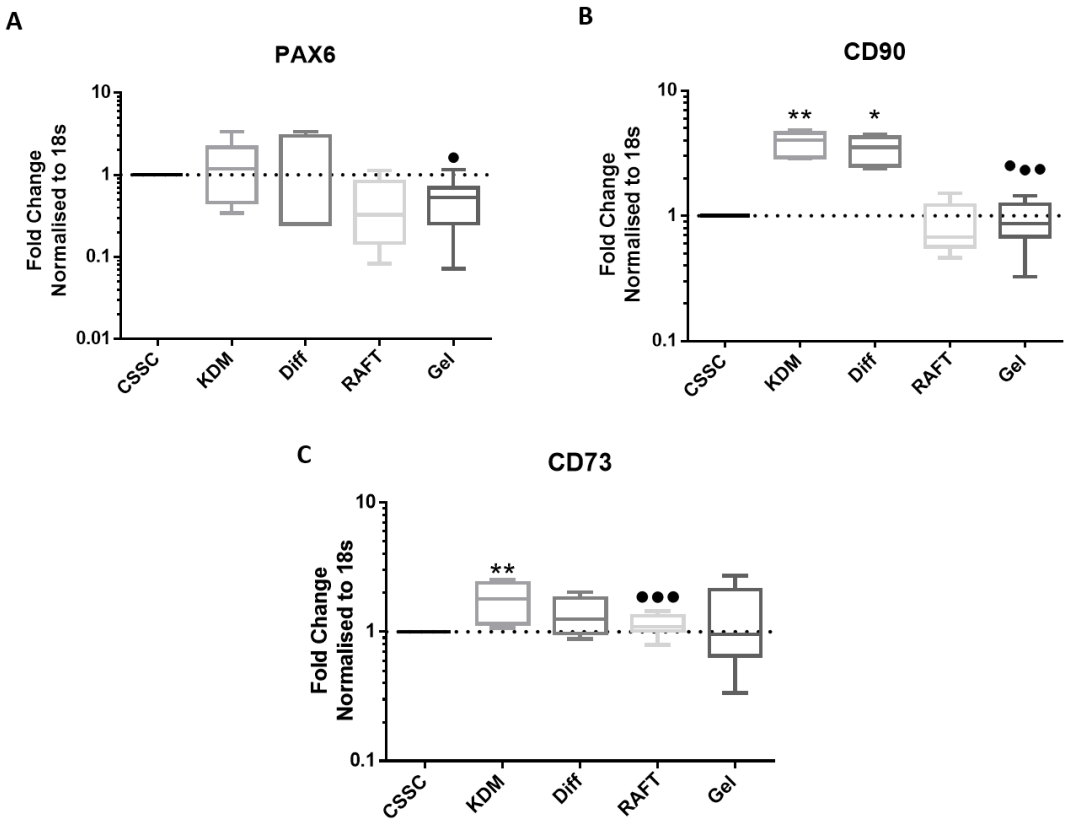

Figure 6.12 – Expression of PAX6 (gene expressed in early eye development) and mesenchymal stem cell markers CD90 and CD73 by: **KDM**- CSSCs differentiated for 3 weeks in KDM (Keratocyte differentiation media), **Diff**- cells spontaneously differentiated for 3 weeks in CSSC media, **RAFT** – CSSCs cultured inside RAFT-TEs for 3 weeks in CSSC media and **Gel** - CSSCs cultured inside gel (non-compressed RAFT- TE) for 3 weeks in CSSC media in comparison to **CSSC**- CSSCs at P6 cultured on CSSC media assessed by Real-Time qPCR. (Data is represented in a boxplot, n=3, Kruskal-Wallis test followed by Dunn's multiple comparison test where *p≤0.05, **p≤0.01). Dash line represents the basal expression of the markers of interests when cells are cultured in CSSC media. Abbreviations: (A) PAX6- Paired box protein Pax-6, (B) CD90- Cluster of Differentiation 90 (also known as Thy-1) & (C) CD73 - Cluster of Differentiation 73.

After 3 weeks of culture of CSSCs under the different conditions, the expression of keratocyte markers lumican and ALDH1A1 was significantly upregulated in all the conditions except the Gel (Figure 6.13 A & C). Lumican expression was higher in the KDM condition (****p≤ 0.0001), while ALDH1 increase was more significant in the Diff and RAFT conditions (****p≤ 0.0001).

Keratocan was only upregulated in the KDM condition (****p≤ 0.0001) when compared to the CSSCs baseline. The results for each individual donor can be found in Figure S6.3 of Appendix.

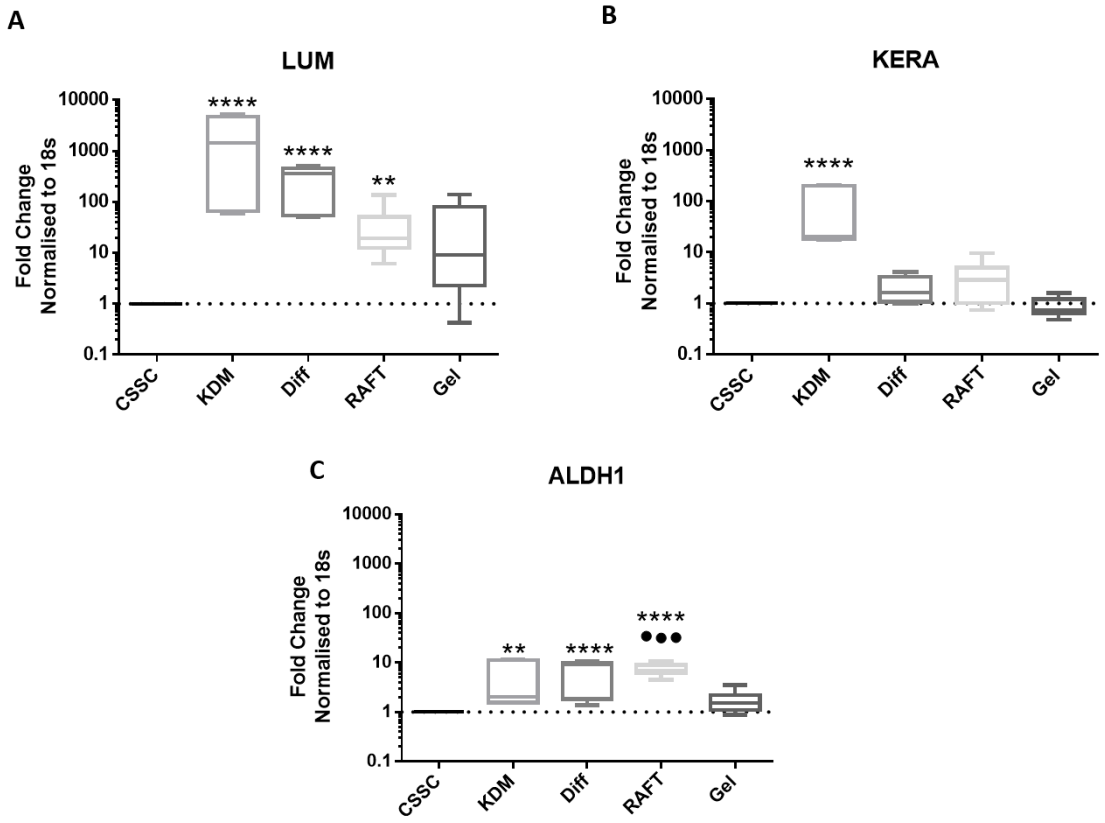

Figure 6.13 – Expression of keratocyte markers LUM, KERA and ALDH1 by: **KDM**- CSSCs differentiated for 3 weeks in KDM (Keratocyte differentiation media), **Diff**- cells spontaneously differentiated for 3 weeks in CSSC media, **RAFT** – CSSCs cultured inside RAFT-TEs for 3 weeks in CSSC media and **Gel** - CSSCs cultured inside gel (non-compressed RAFT-TEs) for 3 weeks in CSSC media in comparison to **CSSC**- CSSCs at P6 cultured on CSSC media assessed by Real-Time qPCR. (Data is represented in a boxplot, n=3, Kruskal-Wallis test followed by Dunn's multiple comparison test where **p≤0.01, ****p≤ 0.0001). Dash line represents the basal expression of the markers of interests when cells are cultured in CSSC media. Abbreviations: (A) LUM- Lumican, (B) KERA – Keratocan, (C) ALDH1 - Aldehyde Dehydrogenase 1 Family Member A1.

Finally, Figure 6.14 demonstrates the gene expression of p63, CK3 and ACTA in the same multiple culture conditions described above: KDM- CSSCs differentiated for 3 weeks in KDM (Keratocyte differentiation media); Diff- cells spontaneously differentiated for 3 weeks in CSSC media; RAFT – CSSCs cultured inside RAFT-TEs for 3 weeks in CSSC media; and Gel - CSSCs cultured inside non-compressed RAFT-TEs for 3 weeks in CSSC media

against the baseline defined as CSSC- CSSCs at P6 cultured on CSSC media. The results for each individual donor can be found in Figure S6.4 of Appendix.

With regards to p63 and ACTA, all the conditions presented a higher expression of these genes than the CSSC baseline, as shown in Figure 6.14A & C. The 2D conditions, KDM and Diff have a much higher expression (****p≤ 0.0001) than the 3D conditions (RAFT & Gel) when compared to the baseline (CSSC). ACTA was highly expressed in the spontaneous differentiation condition, Diff (****p≤ 0.0001) while the difference in the other conditions was less evident (**p≤0.01). Yet, it was not possible to observe a significant difference in CK3 expression in comparison to the baseline (Figure 6.14B).

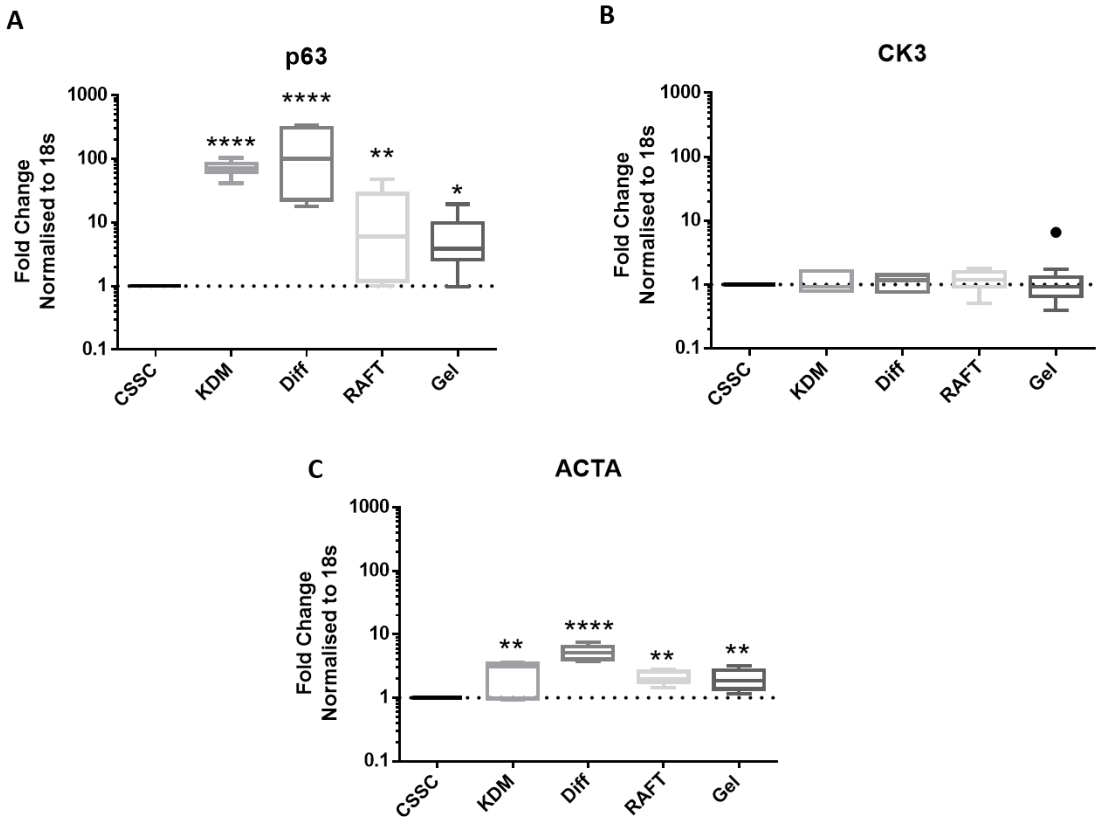

Figure 6.14 – Expression of ΔNp63, CK3 and ACTA by: **KDM**- CSSCs differentiated for 3 weeks in KDM (Keratocyte differentiation media), **Diff**- cells spontaneously differentiated for 3 weeks in CSSC media, **RAFT** – CSSCs cultured inside RAFT-TEs for 3 weeks in CSSC media and **Gel** - CSSCs cultured inside gel (non-compressed RAFT-TEs) for 3 weeks in CSSC media in comparison to **CSSC**- CSSCs at P6 cultured on CSSC media assessed by Real-Time qPCR. (Data is represented in a boxplot, n=3, Kruskal-Wallis test followed by Dunn's multiple comparison test where *p≤0.05, **p≤0.01, ****p≤ 0.0001). Dash line represents the basal expression of the markers of interests when cells are cultured in CSSC media. Abbreviations: (A) p63 – ΔNp63, (B) CK3- Cytokeratin 3, (C) ACTA- alpha-smooth actin.

Table 6.1 presents a summary of gene expression as analysed by qPCR. Here, all culture conditions were compared against each other. The green stars indicate upregulation of a gene, while the red stars indicate downregulation of a gene. The higher the number of stars, the more significant the gene expression. No statistical difference is represented as ns.

The results indicate similarities in CSSC gene expression in 2D KDM and Diff conditions, despite the use of different culture media. However, when Diff is compared to RAFT (2D vs 3D, both in CSSC media), CSSC exhibit upregulation of CD90, p63 and ACTA under Diff conditions. Interestingly, when comparing RAFT and Gel matrices, where the difference is the compression of the hydrogel, the only significant difference is the upregulation of ALDH in the RAFT condition.

Table 6.1 – Summary of the statistical analysis of the qPCR analysis presented in Figures 12, 13 and 14. Kruskal-Wallis test followed by Dunn's multiple comparison test where *p≤0.05, **p≤0.01, ***p≤0.001, ****p≤ 0.0001. The stars (*) in green represent gene upregulation, while the stars in red represent gene downregulation. Non-significant differences are represented as ns. Gene expression changes are plotted in relation to the top variable in the upper row of the table. Conditions: KDM- CSSCs differentiated for 3 weeks in KDM (Keratocyte differentiation media), Diff- cells spontaneously differentiated for 3 weeks in CSSC media, RAFT – CSSCs cultured inside RAFT-TEs for 3 weeks in CSSC media and Gel - CSSCs cultured inside non-compressed RAFT-TEs for 3 weeks in CSSC media in comparison to CSSC- CSSCs at P6 cultured on CSSC media. Genes: PAX6- Paired box protein Pax-6, CD90- Cluster of Differentiation 90 (also known as Thy-1), CD73 - Cluster of Differentiation 73, LUM- Lumican, KERA – Keratocan, ALDH1 - Aldehyde Dehydrogenase 1 Family Member A1, p63 – ΔNp63, CK3- Cytokeratin 3, and ACTA- alpha-smooth actin.

	CSSC vs KDM	CSSC vs Diff	CSSC vs RAFT	CSSC vs Gel	KDM vs Diff	KDM vs RAFT	KDM vs Gel	Diff vs RAFT	Diff vs Gel	RAFT vs Gel
PAX6	*ns*	*ns*	*ns*	*ns*	*ns*	*ns*	*ns*	*ns*	*ns*	*ns*
CD90	*	*	*ns*	*ns*	*ns*	****	****	****	***	*ns*
CD73	*	*ns*	*ns*	*ns*	*ns*	*ns*	*	*ns*	*ns*	*ns*
LUM	****	****	**	*ns*	*ns*	*	***	*ns*	**	*ns*
KERA	***	*ns*	*ns*	*ns*	*ns*	*	****	*ns*	*ns*	*ns*
ALDH	**	***	****	*ns*	*ns*	*ns*	*ns*	*ns*	**	****
P63	****	****	*	*ns*	*ns*	**	**	**	**	*ns*
CK3	*ns*	*ns*	*ns*	*ns*	*ns*	*ns*	*ns*	*ns*	*ns*	*ns*
ACTA	**	****	**	**	*ns*	*ns*	*ns*	***	***	*ns*

6.4.2.2. Immunocytochemistry of CSSCs when cultured in RAFT-TE with CSSC media

Figure 6.15 and 6.16 show the immunostaining of frozen sections of CSSCs cultured for 3 weeks in RAFT-TE by confocal microscopy for CSSC markers (PAX6, CD90 and CD73) and keratocyte markers (LUM, KERA, ALDHA1). Blue shows DAPI nuclear staining, while green represents phalloidin staining of the cytoskeleton of the CSSCs. Red represents the different antibodies, and DIC, Differential interference contrast, microscopy is shown in grey and allows identification of the positioning of the cells within the collagen structure. On the right, it is possible to see the merged image generated from all the channels.

Immunocytochemistry revealed that CSSCs cultured in RAFT-TE in CSSC media maintain expression of PAX6 (Figure 6.15 A-E), an early eye development marker and CD90 (Figure 6.15 F-J), a mesenchymal stem cell marker. However, it was not possible to observe any staining of CD73 (Figure 6.15 K-O).

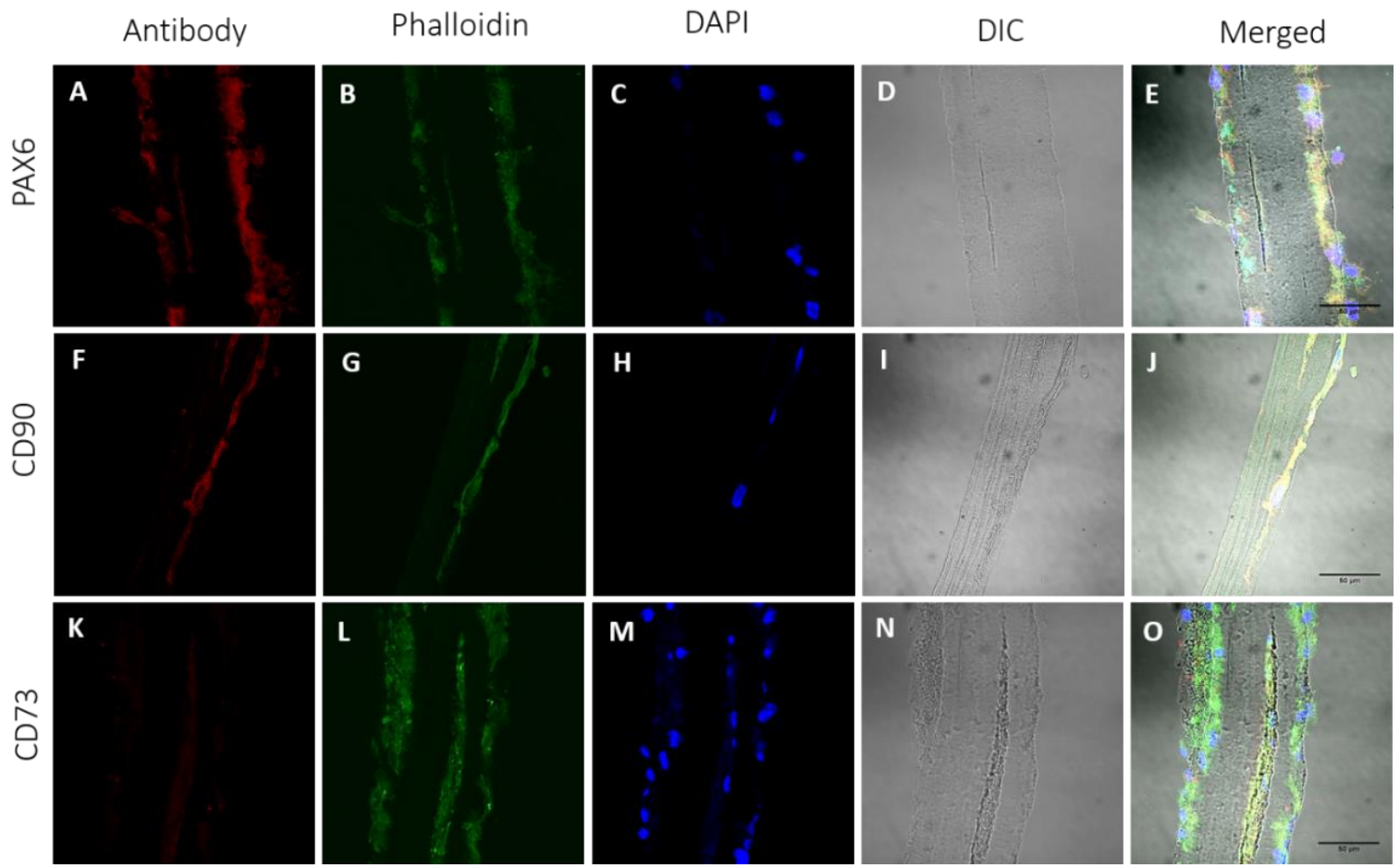

Figure 6.15 – Confocal micrographs of frozen sections of RAFT-TEs cultured with human CSSCs in CSSC media for 3 weeks. Cells displayed positive expression of PAX6 (gene expressed in early eye development), CD90 (mesenchymal stem cell marker) and CD73 expression was negative (mesenchymal stem cell markers). DAPI staining nuclei in blue, FITC Phalloidin staining cytoplasm in green and differential antibody staining in red. Differential interference contrast (DIC) microscopy (in grey) shows the collagen structure. Arrow points at cell clusters. Scale bars = 50 μm.

Figure 6.16 presents the immunostaining of LUM, KERA and ALDH. As described above, the first column (in red) presents the antibody of interest, the second (in green) the cytoskeleton, the third column (in blue) displays the nucleus with DAPI staining and the fourth column the collagen structure. The last column shows the merge of the different channels. Figure 6.16 A, F and K present positive staining for all the keratocyte markers. It is important to notice that keratocan (Figure 6.16F) staining is much weaker than Lumican (Figure 6.16A) and ALDH (Figure 6.16K).

From Figure 6.15 and 6.16 is also possible to observe that most of the cells have escaped the collagen matrix and are now residing on the upper and lower surfaces of the RAFT-TE structure. Nevertheless, it is still possible to observe multiple cells inside RAFT-TE that likely represent the cluster areas (Figure 6.15L, 6.16B 6.16L).

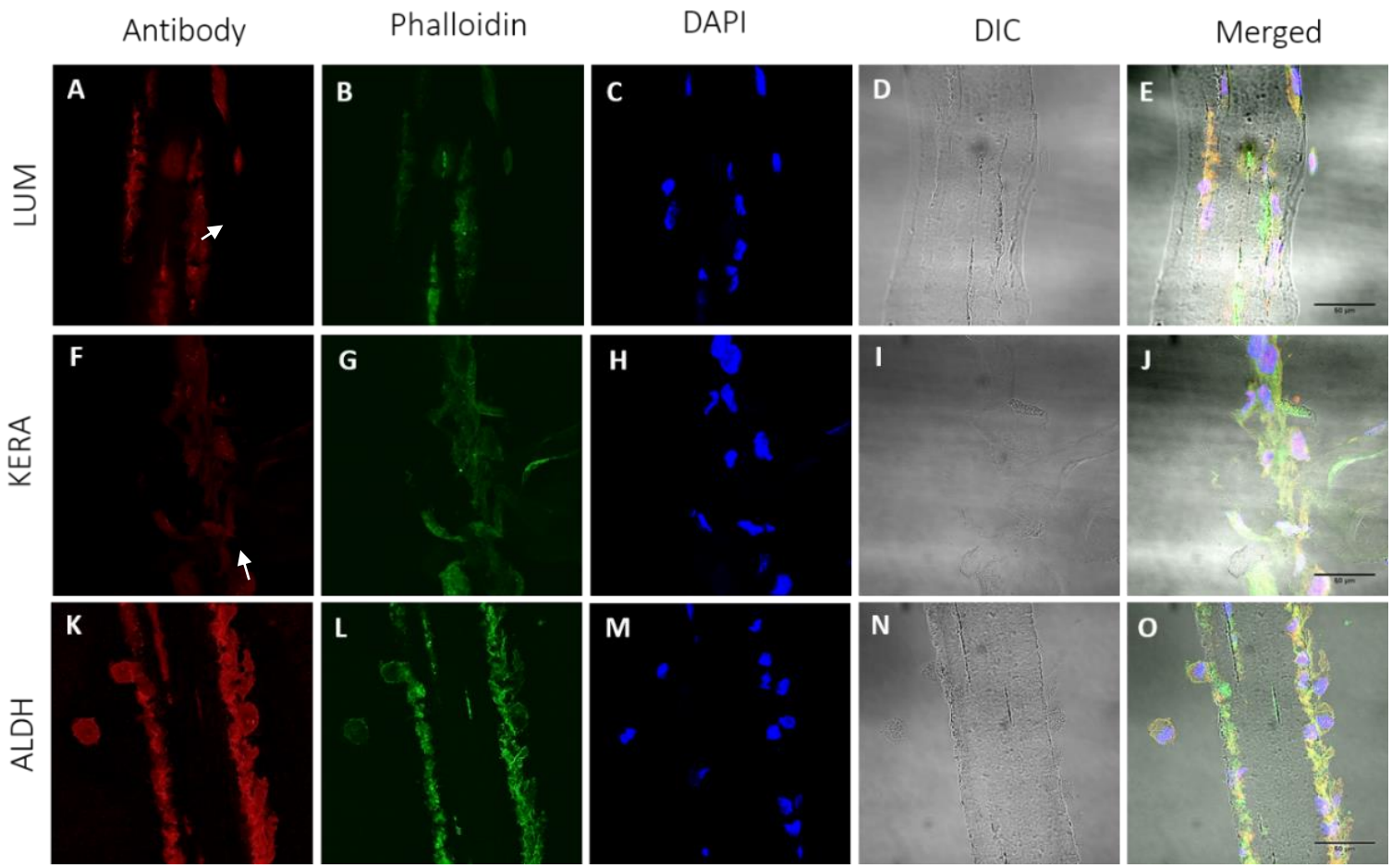

Figure 6.16 – Confocal micrographs of frozen sections of RAFT-TEs cultured with human CSSCs in CSSC media for 3 weeks. Cells are positive for three keratocytes markers, Lumican, Keratocan and ALDH1A1. DAPI staining nuclei in blue, FITC Phalloidin staining cytoplasm in green and differential antibody staining in red. Differential interference contrast (DIC) microscopy (in grey) shows the collagen structure. Arrow points at cell clusters. Scale bars = 50 μm.

Summary of Results:

- The gene expression profile of CSSC changed when exposed to different culture conditions. Taking the basal condition (sparse, in TCP, in CSSC media) as the control, the observed differences were:
    - After 3 weeks in KDM (2D)
        - ✓ CD90 and CD73 – upregulation
        - ✓ LUM, KERA and ALDH1 – upregulation
        - ✓ P63 and ACTA – upregulation
    - After 3 weeks in CSSC medium with spontaneous differentiation (2D)
        - ✓ CD90 – upregulation
        - ✓ LUM and ALDH1 – upregulation
        - ✓ P63 and ACTA – upregulation
    - After 3 weeks in CSSC medium inside RAFT-TE (3D)
        - ✓ LUM and ALDH1 – upregulation
        - ✓ P63 and ACTA – upregulation
    - After 3 weeks in CSSC medium inside Gel (3D)
        - ✓ P63 and ACTA – upregulation

- The protein production profile of CSSC was only assessed in RAFT-TE. Due to the reduced cell numbers, RAFT-TE was chosen as the condition where protein investigation would be more relevant both considering its clinical application, and the visualisation of the position of the cells inside the matrix. This demonstrated that:
    - After 3 weeks in CSSC medium inside RAFT-TE (3D)
        - ✓ PAX6 and CD90- highly expressed
        - ✓ CD73 – absent
        - ✓ LUM and ALDH – highly expressed
        - ✓ KERA – weakly expressed.

- CSSCs migrate to the surface of RAFT-TE.

6.4.3. The effect of culture conditions and spatial arrangement of cells on keratocyte behaviour

Since in the previous section, the cells cultured inside RAFT-TE for 3 weeks showed a differentiation potential that more closely resembled the condition of keratocyte-like cells (KDM), this third section was designed to optimise the differentiation of CSSCs towards the keratocyte phenotype. Figure S6.5 of Appendix presents RNA quality and concentration before and after the cleaning procedure.

6.4.3.1. Gene expression profile of keratocyte-like cells differentiated from CSSCs

The gene expression profiles of keratocyte-like cells differentiated from CSSC cultured under different conditions were characterized by q-PCR. All of the comparisons were made against baseline control expression of genes of interest during 2D differentiation, i.e. CSSCs cultured in KDM (keratocyte differentiation media) for 3 weeks. The results were normalized against 18s levels. The results for each individual donor can be found in Figure S6.6 of Appendix.

The CSSCs were either differentiated in 2D in KDM medium for 3 weeks and then cultured for 1 week in RAFT-TEs (referred as pre-differentiated keratocytes) or directly seeded inside RAFT-TE as CSSCs and then differentiated for 3 weeks in KDM media. The conditions where the cells were pre-differentiated before 3D culture are highlighted with a plus (+), meaning they have experienced differentiation both in 2D and 3D (2D + 3D).

CSSC markers (PAX6, CD90 and CD73) were assessed together with the keratocyte markers (LUM, KERA and ALDH) and alpha-smooth actin (ACTA).

Both PAX6 and KERA did not reach detection levels so are not represented in Figure 6.17. With the exception of the Gel+ condition, all the cell culture conditions experienced a significant downregulation of CD90 (Figure 6.17A) when compared to the baseline (CSSCs cultured for 3wks, in TCP, in KDM

media). CD73 expression (Figure 6.17B) was similar in all the conditions, although not very consistent between donors as shown by the size of the boxplots. However, CD73 was downregulated in the Gel^+ (pre-differentiated keratocytes cultured in non-compressed TE) condition (**p≤0.01).

Lumican (Figure 6.17C) showed similar patterns of expression in 2D, $RAFT^+$ (pre-differentiated keratocytes) and RAFT (differentiated in 3D only) conditions. However, lumican expression was downregulated in both gel conditions (Gel^+ ***p≤0.001 & Gel ****p≤ 0.0001). There was no significant difference with regards to ALDH expression in any of the conditions.

Finally, there was a downregulation of ACTA in most of the conditions except Gel^+ (pre-differentiated keratocytes). The higher downregulation can be observed on the $RAFT^+$ (pre-differentiated keratocytes) condition (****p≤ 0.0001).

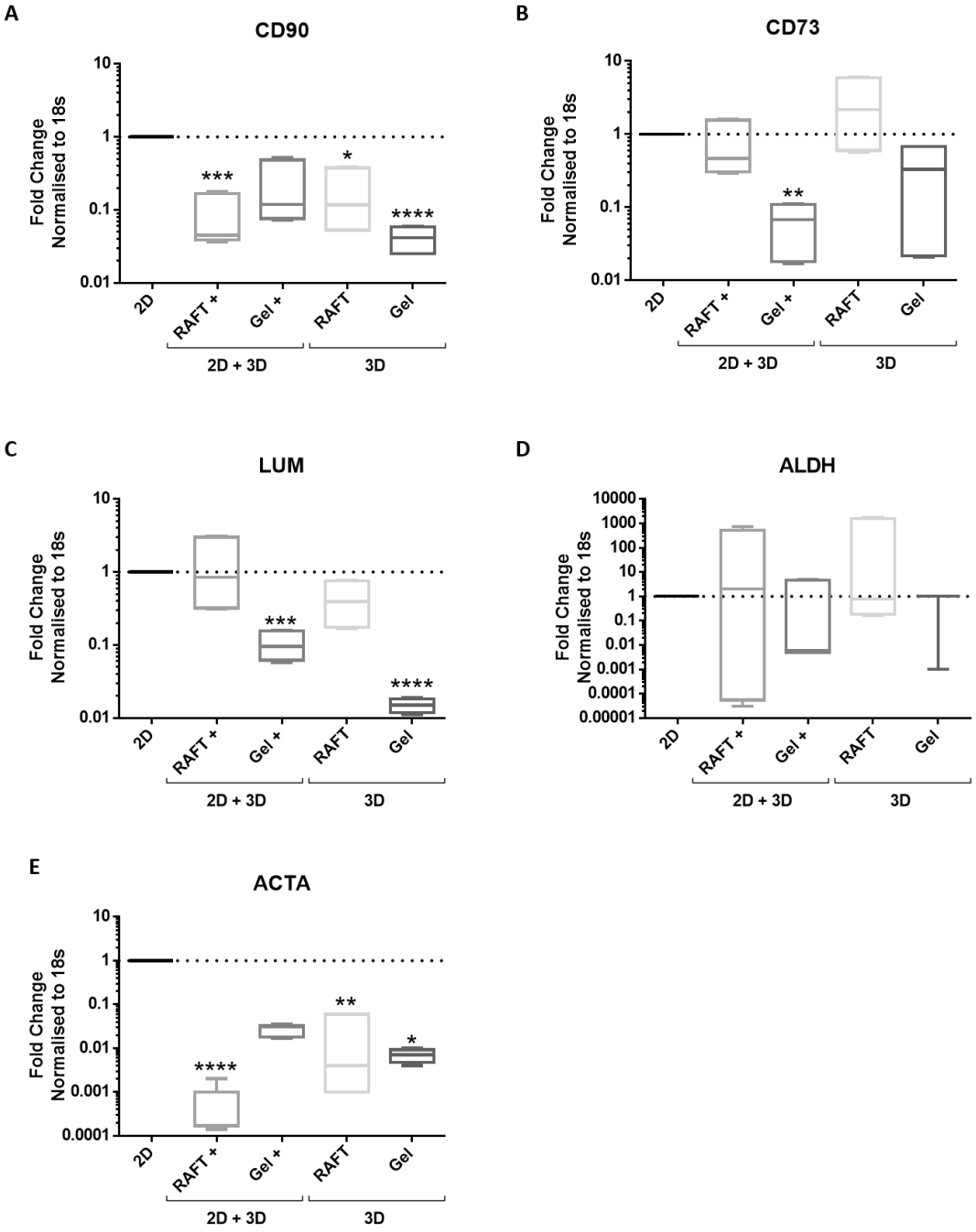

Figure 6.17 – Expression of mesenchymal stem cell markers (CD90 & CD73), keratocyte markers (LUM & ALDH1) and ACTA by: RAFT+ (pre-differentiated keratocytes in 2D for 3wks, and cultured inside RAFT-TE for 1wk in KDM media), Gel+ (pre-differentiated keratocytes in 2D for 3wks, and cultured inside TE for 1wk in KDM media), RAFT (CSSCs cultured inside RAFT-TE and differentiated for 3 wks in KDM media) and Gel (CSSCs cultured inside TE and differentiated for 3 wks in KDM media) assessed by Real-Time qPCR. (Data is represented in a boxplot, n=3, Kruskal-Wallis test followed by Dunn's multiple comparison test where *p≤0.05, **p≤0.01). Dash line represents the basal expression of the markers of interests when cells are cultured in TCP for 3 weeks in KDM media (2D). Abbreviations: (A) CD90- Cluster of Differentiation 90 (also known as Thy-1), (B) CD73 - Cluster of Differentiation 73, (C) LUM- Lumican, (D) ALDH1 - Aldehyde Dehydrogenase 1 Family Member A1 & (E) ACTA- alpha smooth actin.

6.4.3.2. Morphological analysis of CSSCs cultured in KDM inside RAFT-TE and Gel

The morphology of the cells originating from the culture of CSSCs in KDM media after being cultured for three weeks in RAFT-TE and Gel can be observed in Figure 6.18.

In all the 3D culture conditions, very few cells could be observed at the surface of the TEs, unlike when CSSCs were cultured in CSSC media (as shown in Figure 6.9).

Although it was not possible to observe ECM production, the hatching points of the cells (Figure 6.18C & L) from inside the TE to the surface were visible as well as some collagen fibril reorganization (Figure 6.18E).

The cells observed at the surface had a spindle shape and were not organized in any particular direction (Figure 6.18B, H, T). The cells seemed to be less active when cultured in KDM, rather than in CSSC media (Figure 6.9) as suggested by the presence of fewer villi (Figure 6.18D, J, T).

Comparing the pre-differentiated keratocytes (2D+3D, Figure 18 A-J) with the on-site (RAFT-TE only) differentiation (only 3D, Figure 6.18 K-T), it was clear that fewer cells were present on the surface of the TE when the cells were cultured for only one week in the TE.

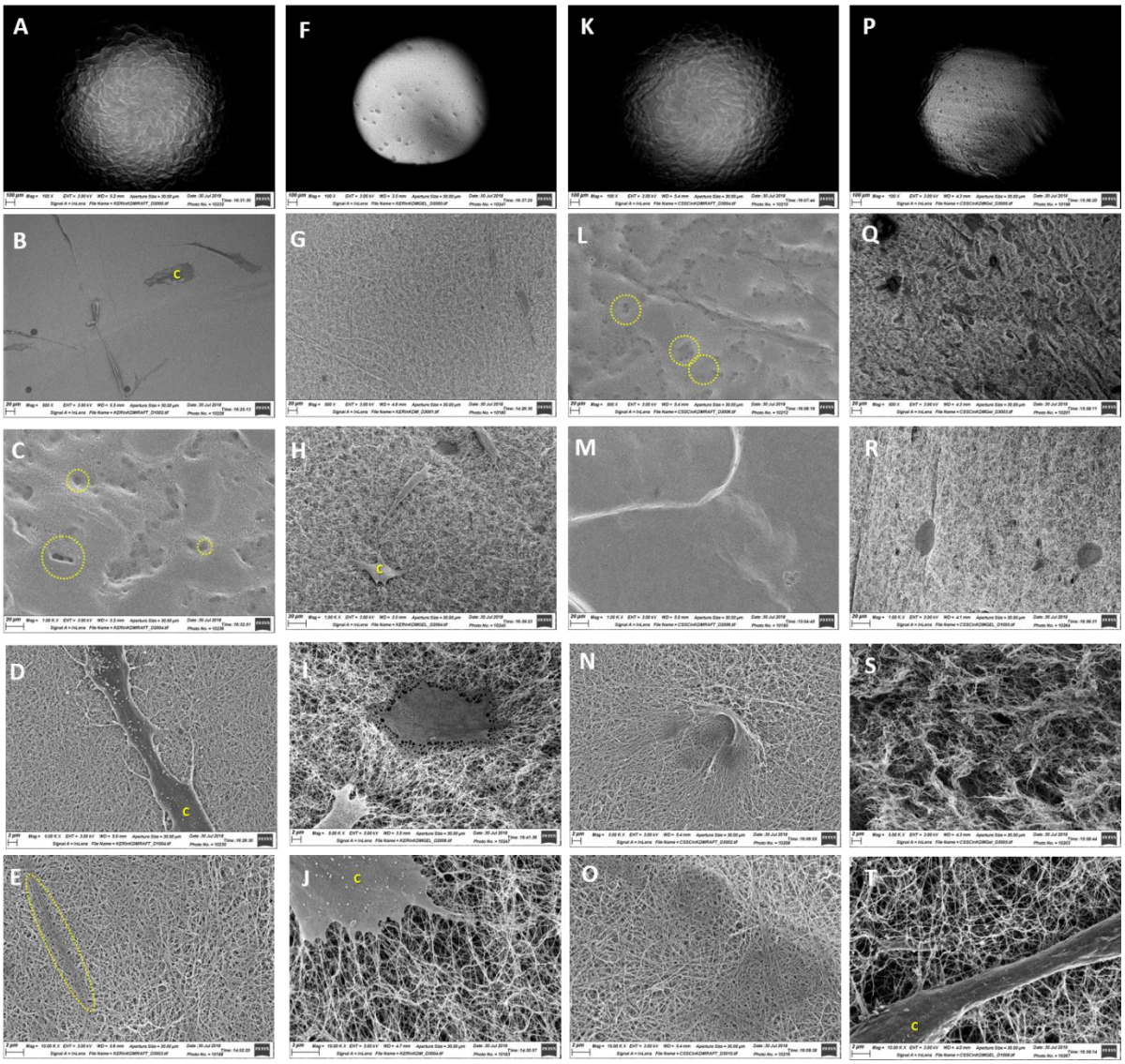

Figure 6.18 – Morphology observation of cells differentiated from CSSC after 3 weeks of culture in KDM media inside RAFT-TE and Gel by SEM: **(A-E)** RAFT+: Pre-differentiated keratocytes in 2D for 3wks, and cultured inside RAFT-TE for 1wk in KDM media; **(F-J)** Gel+: Pre-differentiated keratocytes in 2D for 3wks, and cultured inside TE for 1wk in KDM media; **(K-O)** RAFT: CSSCs cultured inside RAFT-TE and differentiated for 3 wks in KDM media, and **(P-T)** Gel: CSSCs cultured inside TE and differentiated for 3 wks in KDM media. C- cell, dashed circle – hatching points, dashed ellipses – rearranged collagen fibrils

Summary of Results:

- The gene expression profile of keratocytes derived from CSSCs changed depending on the cell culture conditions. Taking the basal condition as the standard to differentiate keratocytes from CSSC cells (sparse CSSC, in TCP and KDM media for 3 wks), the differences observed were:
    - RAFT+ (pre-differentiated keratocytes in 2D for 3wks, and cultured inside RAFT-TE for 1wk in KDM media)
        - ✓ CD90 and CD73 – downregulation
        - ✓ ACTA – downregulation
    - Gel+ (pre-differentiated keratocytes in 2D for 3wks, and cultured inside TE for 1wk in KDM media)
        - ✓ CD73 – downregulation
        - ✓ LUM – downregulation
    - RAFT (CSSCs cultured inside RAFT-TE and differentiated for 3 wks in KDM media)
        - ✓ CD90 – downregulation
        - ✓ ACTA – downregulation
    - Gel (CSSCs cultured inside TE and differentiated for 3 wks in KDM media)
        - ✓ CD90 – downregulation
        - ✓ LUM – downregulation
        - ✓ ACTA – downregulation
- It was possible to differentiate CSSCs into keratocytes inside RAFT-TE using KDM media.
- Cells differentiated inside RAFT-TE showed a downregulation of CSSC marker (CD90), and a downregulation of fibrotic marker (ACTA).
- Non-compressed TE (Gel condition) presented a downregulation of keratocyte marker lumican.

6.4.4. The effect of PDGF on CSSC in RAFT-TE

The fourth and last part of this chapter was designed to understand the role of PDGF in CSSC behaviour inside RAFT-TE and, more specifically, if PDGF affects cell cluster formation.

PDGF promotes cell migration and matrix remodelling [323-325]. Moreover, it can also impact the dispersal of cell clusters in collagen matrices [326]. For this reason, it was investigated as a potential candidate for promoting CSSC clustering inside RAFT-TE.

6.4.4.1. CSSC behaviour overtime when cultured in RAFT-TE with and without PDGF

CSSC behaviour inside RAFT-TE in CSSC media with (Figure 6.19 A-D) and without (Figure 6.19 E-H) PDGF was tracked overtime using light microscopy and live-cell imaging. The live-cell imaging videos can be found in the attached multimedia support (Chapter 6 – PDGF Live imaging videos). The first frame of each video (Figure S6.7) together with a descriptive table of the cell behaviour (Table S6.1) can be found in Appendix 8.4.

In short, the live imaging videos showed that cell activity starts from day 0 with the formation of cell clusters from single cells inside RAFT-TE. From day 2 to day 5, growth was evident, leading to more and larger cell clusters. There was also a lot of cell movement within the clusters, and some cells started to migrate to the surface of the RAFT-TE. Cells seemed to be more motile at the surface, but while some travelled around slowly, others would first touch a neighbouring cell before quickly moving. It was noticeable that cells were less motile when cultured in media without PDGF.

Figure 6.19 supports the findings of the videos where cell cluster growth inside RAFT-TE is faster when PDGF is removed. Furthermore, migration of the cells towards the surface of the RAFT-TE increased in the presence of PDGF.

These data also elucidate cell behaviour with regards to cluster formation. That is, the clusters do not originate from migrating cells coming together but, instead, result mainly from cell proliferation of individual cells *in situ*.

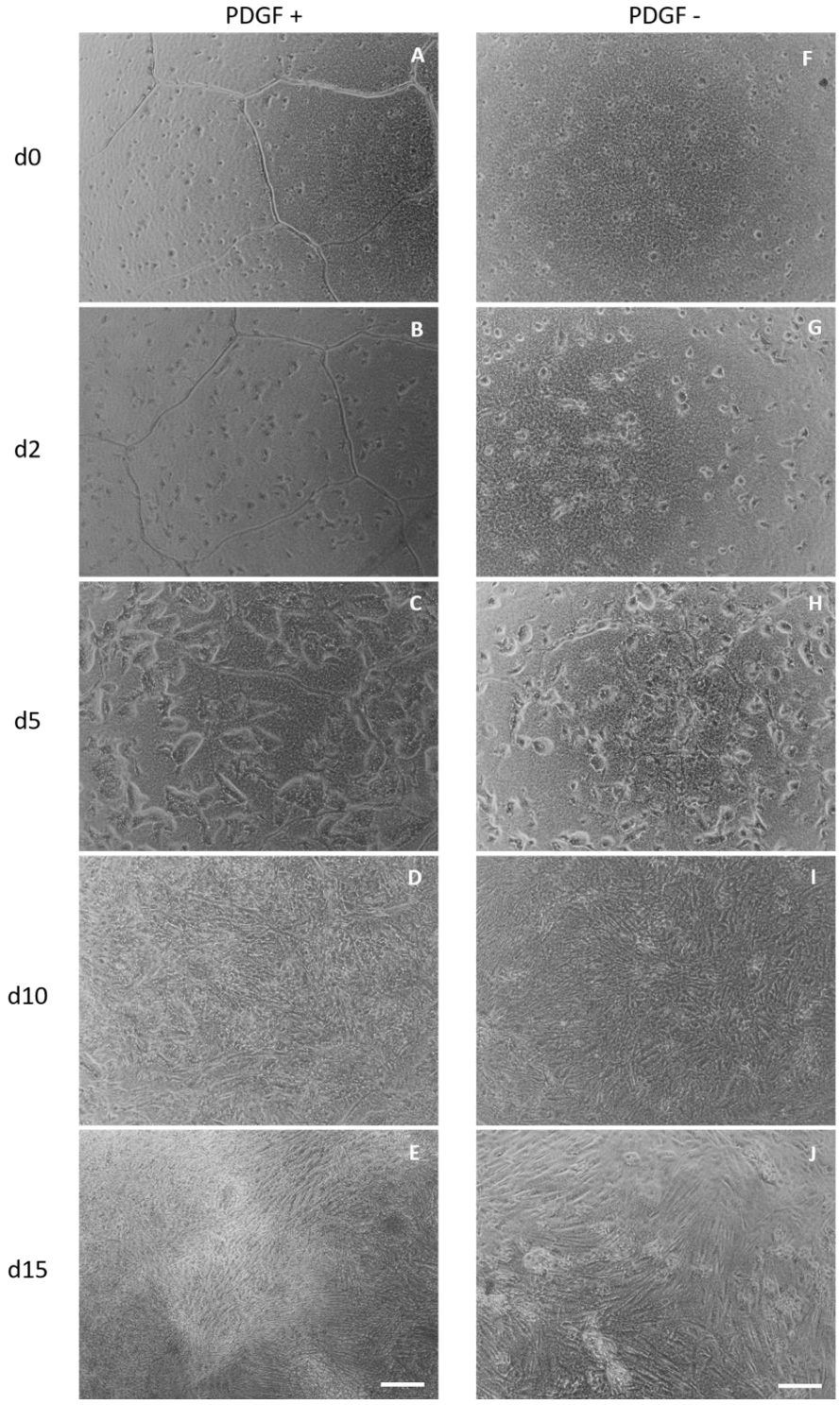

Figure 6.19 – Morphological observation of CSSC inside RAFT-TE with and without PDGF on days 0 **(A, F),** 2 **(B, G)**, 5 **(C, H)**, 10 **(D, I)** and 15 **(D, H)** of culture. (A – D) – CSSC media PDGF+; (E – H) - CSSC media PDGF-.

6.4.4.2. Gene expression profile of CSSC cultured in RAFT-TE in CSSC media with and without PDGF

The expression levels of CSSC markers, keratocyte markers, matrix remodelling and production markers as well as ACTA, ki67, Cdc42 and p63 by CSSC cultured inside RAFT-TE with (PDGF+) and without PDGF (PDGF-) were assessed by Real-Time qPCR, Figure 6.20. The expression was normalized to the 18s levels of CSSCs cultured inside RAFT-TE in CSSC media (PDGF+). Figure S6.8 of appendix 8.4 presents the mean delta Ct and RNA quality of all the samples.

Looking at the CSSC genes (Figure 6.20A), it was clear that PAX6 expression was not detectable in any of the conditions and, for this reason, not plotted. CD90 was upregulated (****p≤ 0.0001) in the absence of PDGF and CD73 remained with similar expression levels. Keratocan expression was not detected in any samples (Figure 6.20B). However, ALDH1 (*p≤0.05) and Lumican (****p≤ 0.0001) were both upregulated in the absence of PDGF (PDGF-). The results for each individual donor can be found in Figure S6.9 of Appendix.

MMPs expression was tested in both conditions of RAFT-TE because they play a crucial role in cell migration, wound healing and tissue/matrix remodelling, which is essential for cluster formation [320]. Matrix remodelling gene expression (MMP1 and MMP2) are presented in Figure 6.20C. There was a significant downregulation of MMP1 (****p≤ 0.0001) in the absence of PDGF (PDGF-) and a slight upregulation of MMP2 (**p≤0.01). Fibronectin and Collagen I production was also assessed (Figure 6.20D). However, none of the conditions displayed any significant difference with regards to the expression of both these matrix proteins. The results for each individual donor can be found in Figure S6.10 of Appendix.

Alpha-smooth actin (ACTA) was assessed to test whether the cells were differentiating towards a fibrotic phenotype. ACTA did not show any statistically significant changes. However, ki67 proliferation marker was downregulated (****p≤ 0.0001) in the absence of PDGF (PGGF-). Cdc42 plays an essential role in cell migration and polarization and was found to be upregulated (****p≤

0.0001) in the absence of PDGF (PDGF-) (****p≤ 0.0001). The results for each individual donor can be found in Figure S6.11 of Appendix. Figure 6.20F presents a heatmap that summarizes all the gene expression profiles side-by-side, highlighting Lumican upregulation and ki67 and MMP1 downregulation as the extreme variations. A detailed heatmap of all the samples can be seen in Figure S6.12 of Appendix.

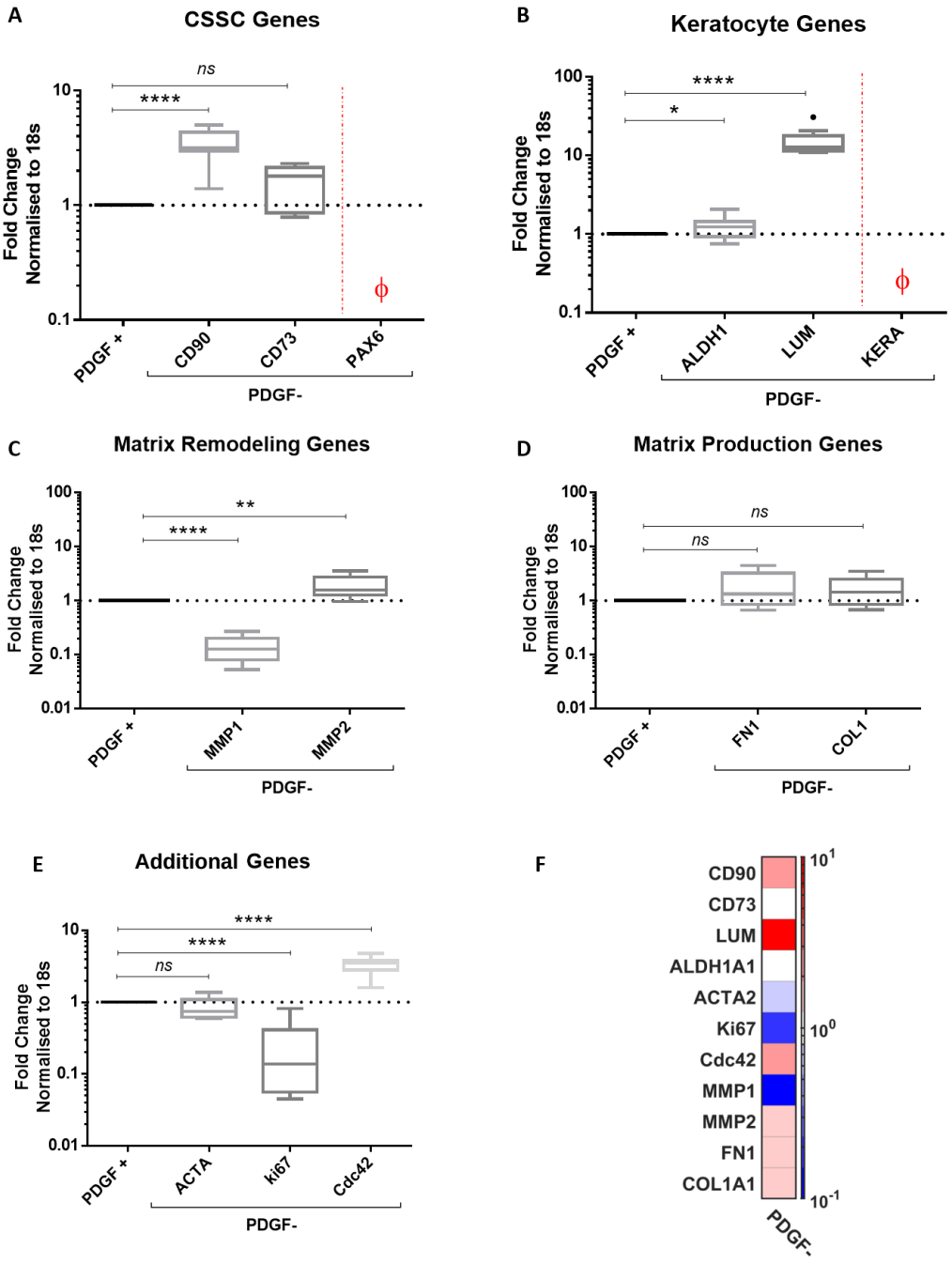

Figure 6.20 – Real-Time qPCR analysis of the expression of: **(A)** mesenchymal stem cell markers (PAX6, CD90 & CD73), **(B)** keratocyte markers (LUM, KERA & ALDH1), **(C)** matrix remodelling genes (MMP1 & MMP2), **(D)** matrix production genes (FN1 & COL1) and **(E)** ACTA, ki67 and Cdc42 on RAFT-TE cultured with and without PDGF for 15 days. (Data is represented in a boxplot, n=3, Kruskal-Wallis test followed by Dunn's multiple comparison test where *p≤0.05, **p≤0.01, ****p≤ 0.0001). Dash line represents the basal expression of the markers of interests when cells are cultured in CSSC media (with PDGF). Abbreviations: ϕ represent gene expression not detectable, (A) PAX6- Paired box protein Pax-6, CD90- Cluster of Differentiation 90 (also known as Thy-1) and CD73 - Cluster of Differentiation 73; (B) LUM- Lumican, KERA – Keratocan, and ALDH1 - Aldehyde Dehydrogenase 1 Family Member A1; (C) MMP1 & MMP2 - Matrix metalloproteinase-1 &2 ; (D) FN1- Fibronectin 1 and COL1- Collagen I ; (E) ACTA- alpha-smooth actin, ki67- proliferation gene, Cdc42- Cell division control protein 42 homolog. **(F)** Heatmap summary showing the upregulation (in red) and downregulation (in blue) of all the analysed genes.

Confocal microscopy was used to confirm marker expression by immunostaining for the genes that showed the biggest expression difference in qPCR. Controls immunostaining images can be found in Figure 6.21.

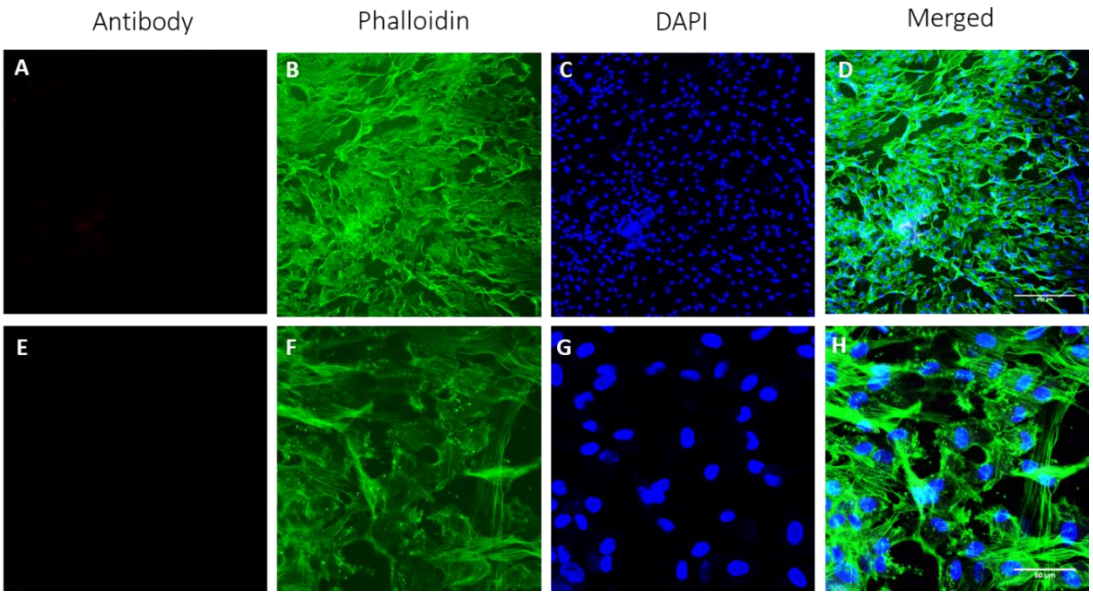

Figure 6.21 – Confocal microscopy control immunostaining of human CSSCs cultured inside RAFT-TE for 15 days in CSSC media. Scale bars: 50 µm (E-H) & 200 µm (A-D).

Lumican production was positive both in the presence and absence of PDGF. However, it was higher in the absence of PDGF (PDGF- Figure 6.22). It was also possible to notice that the signal was stronger (Figure 6.21 M-P), and present in most of the cells at the surface of RAFT-TE cultured without PDGF (PDGF-) when compared to standard CSSC media (PDGF+, Figure 6.22 A-D). It is also noteworthy that only a few cells within the cell cluster were positive for lumican (Figure 6.22 I-L).

Figure 6.23 presents confocal micrographs of ki67 immunostaining (proliferation marker). In the PDGF+ condition, only a few cells at the surface of RAFT-TE (Figure 6.23 A-D) expressed ki67 and about half of the cells within the cell clusters (Figure 6.23 I-L). Yet, ki67 was expressed in most of the cells cultured in CSSC media without PDGF (PDGF-) (Figure 6.23 M-T).

MMP1 (Figure 6.24), a matrix remodelling gene, can be seen in all the cells that are present at the surface of RAFT-TE and only in some cells of the clusters inside the structure (Figure 6.24 Q-T). Contrarily to what was observed with qPCR, the expression of MMP1 seemed to be higher in the condition

without PDGF (PDGF-) since the intensity of the marker is superior (Figure 6.24 I-L).

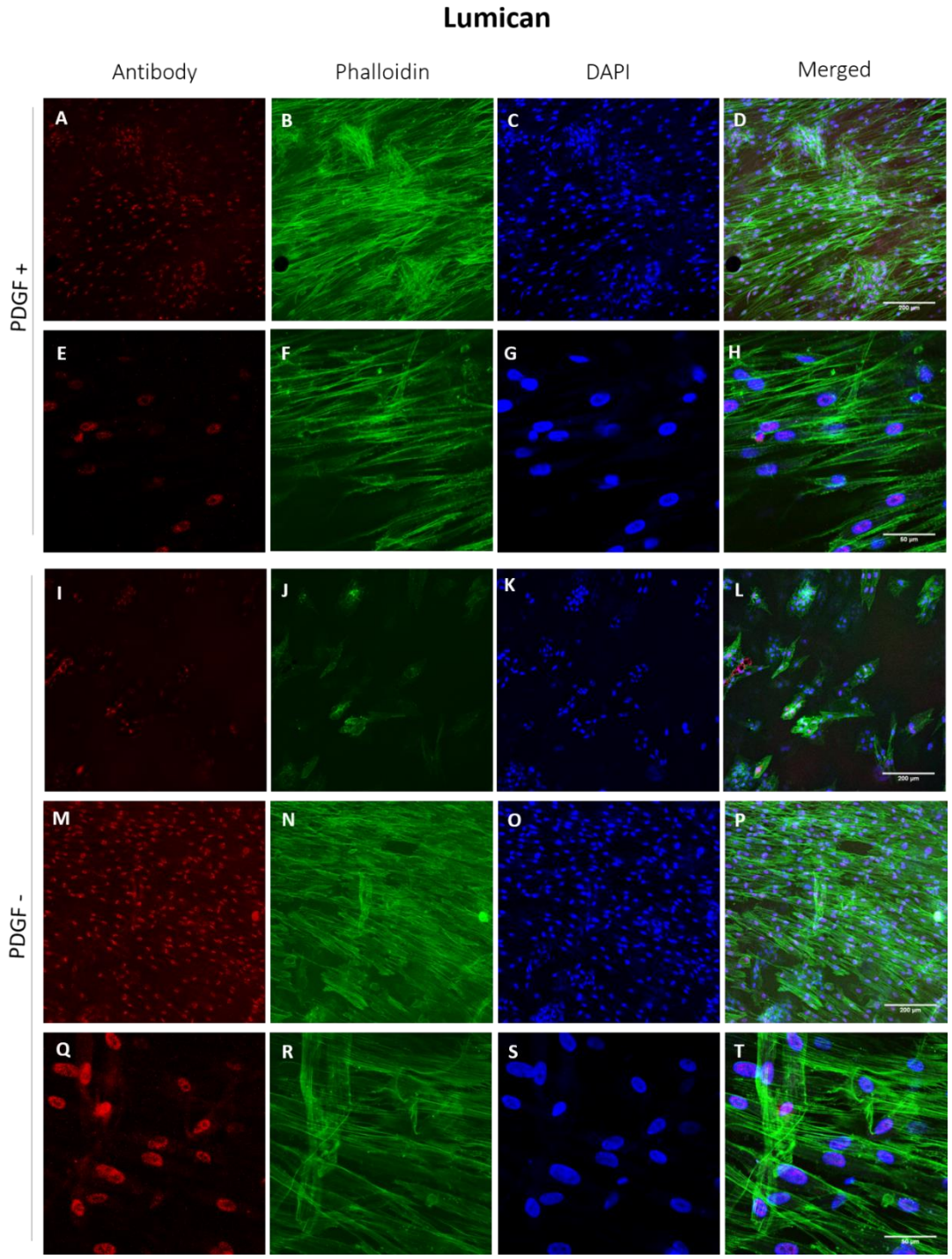

Figure 6.22 – Confocal microscopy of lumican immunostaining of human CSSCs cultured inside RAFT-TE for 15days in CSSC media with **(A-H)** and without **(I-T)** PDGF. Cells displayed positive expression of lumican (keratocyte marker) in both conditions. DAPI staining nuclei in blue, FITC Phalloidin staining cytoplasm in green and differential antibody staining in red. Scale bars: 50 µm (E-H & Q-T) & 200 µm (A-D & I-P).

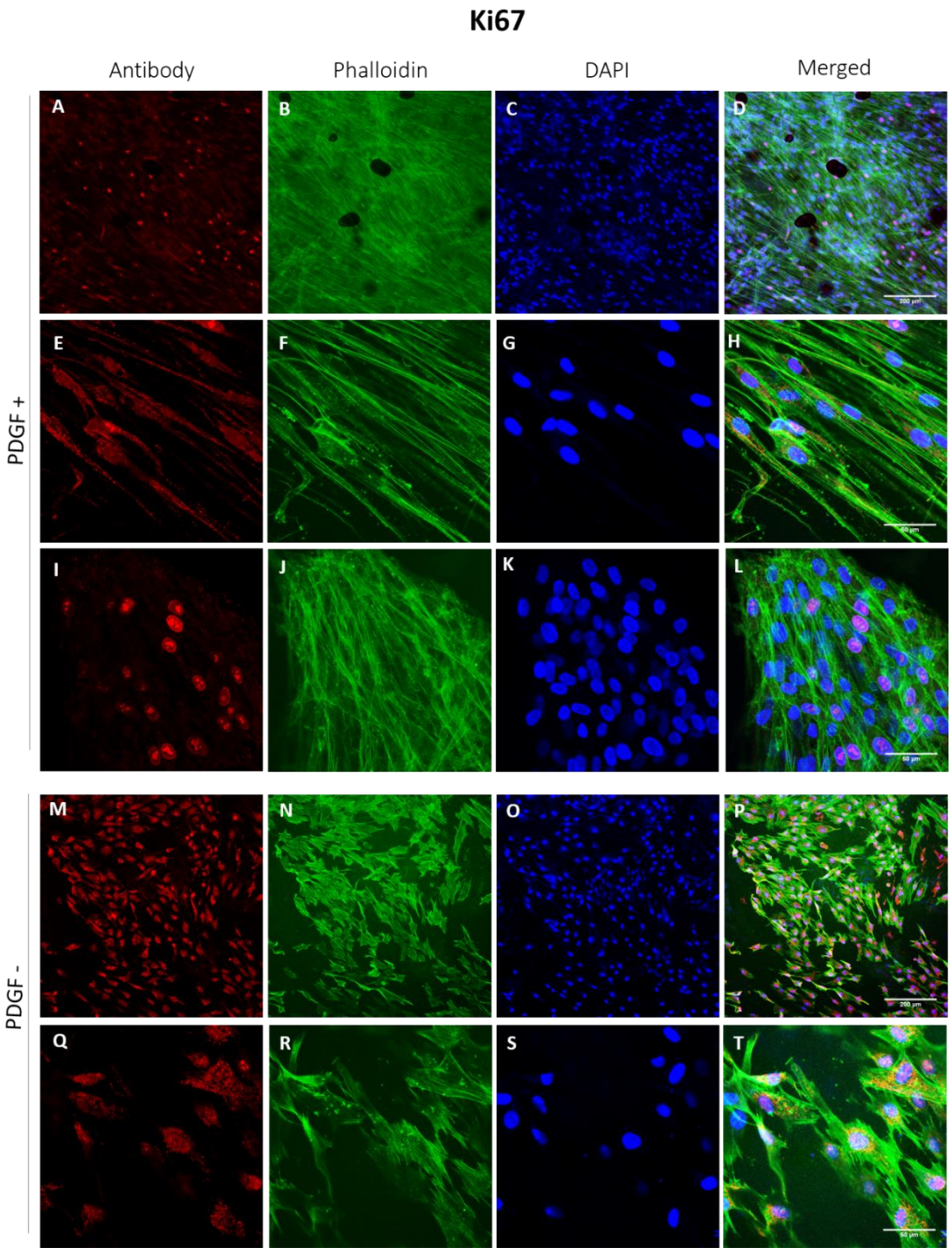

Figure 6.23 – Confocal microscopy of ki67 immunostaining of human CSSCs cultured inside RAFT-TE for 15 days in CSSC media with **(A-L)** and without **(M-T)** PDGF. Cells displayed positive expression of ki67 (proliferation marker) in both conditions. DAPI staining nuclei in blue, FITC Phalloidin staining cytoplasm in green and differential antibody staining in red. Scale bars: 50 µm (E-L & Q-T) & 200 µm (A-D & M-P).

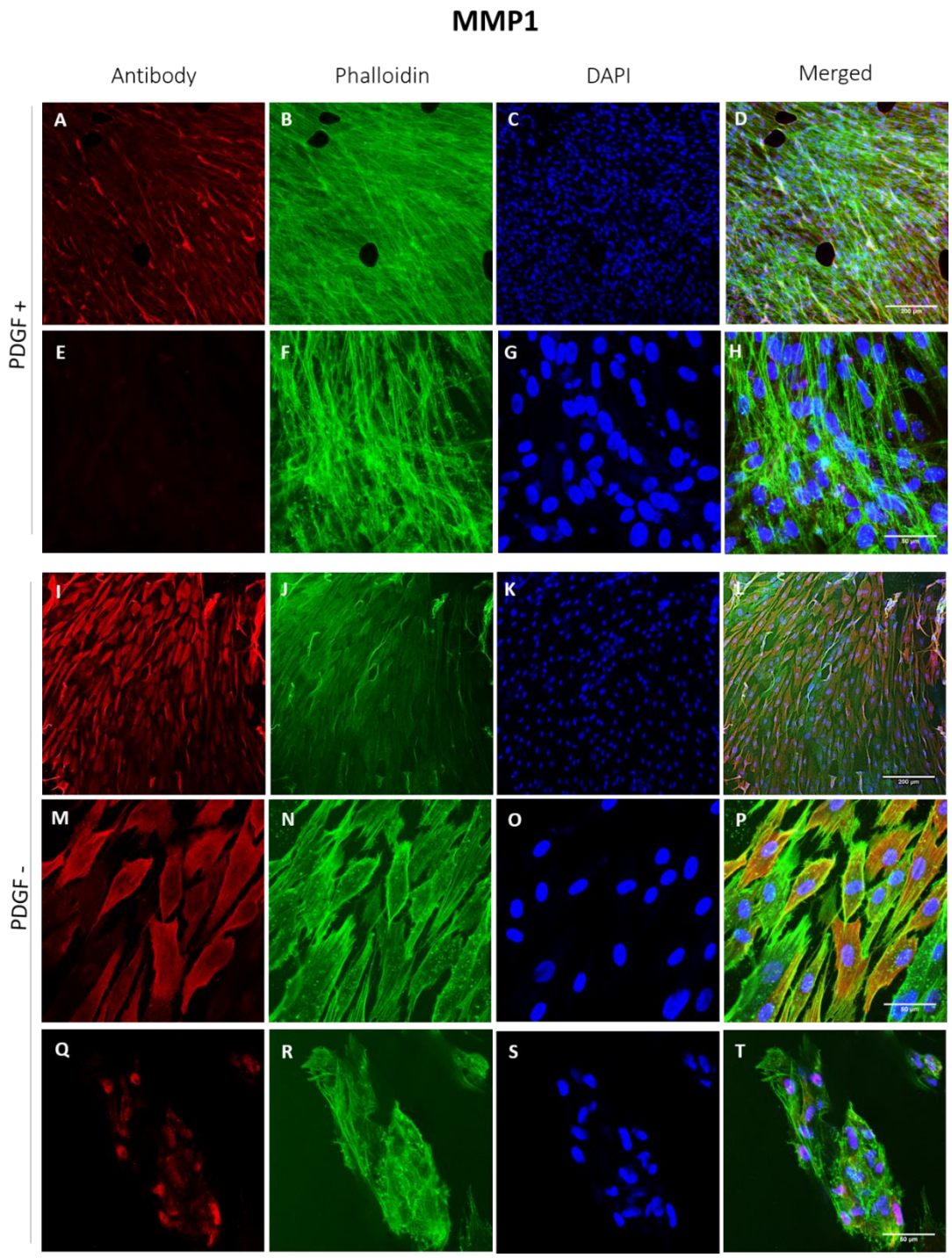

Figure 6.24 – Confocal microscopy of MMP1 immunostaining of human CSSCs cultured inside RAFT-TE for 15 days in CSSC media with **(A-H)** and without **(I-T)** PDGF. Cells displayed positive expression of MMP1 (matrix remodelling marker) in both conditions. DAPI staining nuclei in blue, FITC Phalloidin staining cytoplasm in green and differential antibody staining in red. Scale bars: 50 μm (E-H & M-T) & 200 μm (A-D & I-L).

The morphology of the cells that migrated to the surface of RAFT-TE was evaluated by SEM and is presented in Figure 6.25. CSSC morphology differed when cultured in the presence or absence of PDGF. However, in both

conditions, the surface of the TE was mostly covered with cells. In the absence of PDGF, the cells displayed a flattened shape (Figure 6.25 G-L), while in the presence of PDGF (PDGF+) most of the cells at the surface of the TE acquired a spindle morphology. In both cases, the cells were extremely organized aligning or polarizing in similar directions. Matrix production seemed more evident in the RAFT-TEs cultured with PDGF (Figure 6.25 F). It was also possible to notice that the cells cultured in PDGF+ had more villi (Figure 6.25 E

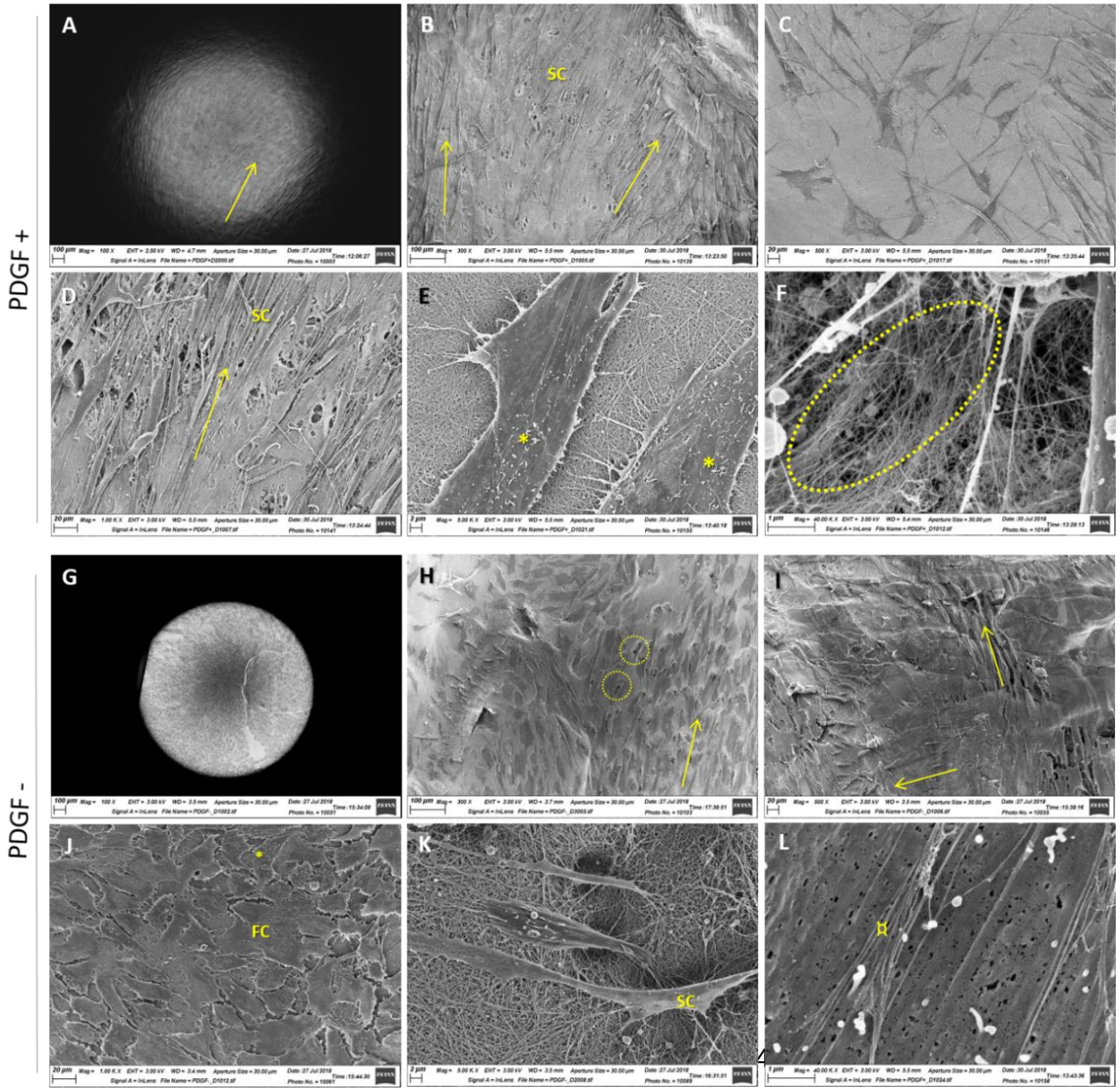

Figure 6.25 – Scanning electron microscopy of cells differentiated from CSSC after 15 days of culture in CSSC media with **(A-F)** and without PDGF **(G-L)** inside RAFT-TE. (SC- spindle-shaped cells, FC- flat-shaped cells, Arrow –cell alignment, ¤ - fibrils on top of cell bodies, * - villi on the cell surface, circle – hatching points, ellipsis – mesh matrix produced by the cells).

Summary of Results:

- PDGF influences CSSC behaviour inside RAFT-TE:
- CSSCs are less motile when cultured without PDGF.
- Cell clusters grow faster in absence of PDGF.
- Cell clusters inside RAFT-TE result from *in situ* proliferation.
- The gene expression profile of CSSCs cultured inside RAFT-TE with and without PDGF was different. In the absence of PDGF, CSSC cultured inside RAFT-TE exhibited:
    - CSSC genes:
        - ✓ CD90– upregulation
    - Keratocyte genes:
        - ✓ ALDH1 – upregulation
        - ✓ LUM – upregulation
    - Matrix remodelling genes:
        - ✓ MMP1 – downregulation
        - ✓ MMP2 – upregulation
    - Other genes:
        - ✓ ki67 – downregulation
        - ✓ Cdc42 – upregulation
- Protein production:
    - Lumican: present in both conditions, but stronger in PDGF-
    - Ki67: present in both conditions, but stronger in PDGF –
    - MMP1: present in both conditions, but stronger in PDGF –
- CSSCs migrate to the surface of RAFT-TE in both conditions.
- In the absence of PDGF the cells had a flattened shape
- In the presence of PDGF the cells had a spindle morphology
- Cells are more active, and matrix production is more evidence in the presence of PDGF.

6.5. Discussion

This chapter focused on the development of a stromal-cell populated RAFT-TE. As discussed in the previous chapter, mixed-population cell seeding of CSSCs and LESCs on top of RAFT-TE did not have the desired outcome, as it resulted in epithelial cell detachment.

Since CSSC might support LESC during their culture (enabling important cell-cell interactions that may be crucial for a successful clinical outcome post-transplantation), this chapter aimed to optimise the culture of CSSCs inside RAFT-TE.

Stem cell microenvironment is crucial in the control of stem cell fate *in vivo*. Further understanding of cell-cell interactions in the stem cell niches is required for the progression of tissue engineering and better control of stem cell fate *in vitro*. The ability to design and engineer artificial stem cell niches allows scientists to study complex environments and segregate individual signals and their impact. Chemical and mechanical properties of artificial ECM have an influence on cell shape, but most importantly on stem cell fate and lineage commitment [327].

Cells use cues from the ECM to tune their mechanical properties by dynamically remodelling their cytoskeletal networks. Consequently, cellular behaviour in artificial matrices like biomaterials is a result of this dual process of interaction. The matrix does affect cell behaviour, but the cells also have an impact on the structure remodelling [327].

This chapter also investigated the possibility of using RAFT-TE to differentiate and deliver keratocyte-like cells differentiated from CSSC, as well as the effect of PDGF in cell clustering inside RAFT-TE.

6.5.1. Identification of the optimum CSSC seeding density inside RAFT-TE

The RAFT manufacturing system aims to reliably recreate the 3D environment/matrix of the cornea. In this chapter, *Koken* collagen was used to produce RAFT-TE with embedded CSSC. For the first time, CSSC were cultured inside *Koken* RAFT-TE, and the outcome was not as expected since CSSC formed cell cluster inside RAFT-TE. In previous works with *First Link* rat tail collagen [255], CSSC differentiated in place towards the keratocyte phenotype, and no cell clusters were observed. However, it is important to note that the TEs presented in this paper were not only produced with a different type of collagen, but also subject to tethering to promote fibril alignment. These differences in experimental settings complicate the comparison of the results presented in the mentioned paper with the ones presented in this thesis.

Here, CSSC inside *Koken* RAFT-TE were shown to form clusters of cells irrespective of the concentration of the cell seeding. Although at the time of this work there was no reference in the literature that could support CSSC cluster formation, recently, Funderburgh's group published a paper where cluster formation inside compressed collagen hydrogels is evident though not extensively discussed [319].

Interestingly, in the present study, cells are not only clustering but also migrating in the z-axis of the RAFT-TE and acquiring different phenotypes. From the available data, two different cell populations could be distinguished after two weeks of culture inside RAFT-TE. The cells that stay inside RAFT-TE and form clusters and the ones that migrate on the z-axis and align at the surface. As observed, both by confocal microscopy and SEM, the cells closer to the surface have an elongated spindle morphology while the middle of the TE is populated with highly aligned cell clusters. Interestingly, it has been shown by Quantock *et al.* that stromal cells in embryonic chick corneas also align in a synchronized way during the course of lamella formation [328].

Another important finding was that the cells showed different marker expression. While most of the cells within the clusters expressed PAX6, the

majority did not show CD90 or CD73 expression, highlighting that CSSCs inside RAFT-TE do not maintain their initial properties. The cells at the surface of the TE were mostly ALDH1A1 positive and thus pointing towards keratocyte differentiation.

Interestingly, some cells at the surface of the RAFT TE expressed p63, an epithelial stem cell marker. There are several possible explanations for this result. CSSCs were isolated from a mixed population of cells containing both CSSC and HLE; therefore, contamination although highly unlikely, cannot be completely discounted. Moreover, one may question if there was a trans-differentiation process. Previous results from Hashmani *et al.* [329] claim that corneal stromal stem cells have the potential for epithelial trans-differentiation. It was shown that the stroma contains a heterogeneous population of cells, and that CD34+ cells have the capacity for epithelial differentiation. Mesenchymal to epithelial lineages differentiation have also been demonstrated in several other studies [330-333]. Intriguingly, the effect of TE depth on MSC differentiation has been studied by other groups. The results suggest that collagen extracellular matrix has an effect on the differentiation of human mesenchymal stem cells towards the epithelial lineage and that this is caused by partial cytoskeletal disruption [334].

Collagen alignment is critical to corneal transparency [335]. The disruption of the native stromal architecture can lead to scar and consequent opacity. Bearing this in mind, the alignment of the collagen fibrils or its reorganization by the cells is of utmost importance. Moreover, the incorporation of aligned topography features in hydrogels, either by tethering, of the collagen hydrogel itself or by the incorporation of aligned electrospun fibres, has shown to influence cell behaviour in the corneal stroma [255, 336, 337]. In this study, RAFT-TE CSSC became highly aligned. That was clear by the cellular remodelling of the matrix, but also by the extremely organized matrix production shown on SEM pictures.

The reduction of the transparency of RAFT-TEs over time can be explained by cell proliferation and cluster formation. Interestingly, transparency was not significantly affected by the initial cell density, thus stressing the importance of

cell behaviour in matrix remodelling and production. Yet, as colleagues previously described, the TE will degrade over time, and so its transparency is only relevant for short-time assessment [184].

The results of this study did not show any negative impact of cell cluster formation inside RAFT-TE on the expansion of HLE using the mixed population culture technique. The cells at the surface had tightly packed cobblestone appearance and were positive for p63, a LESC marker. Furthermore, when compared with the study of Kureshi *et al.* [127], the mixed population expansion was faster and more consistent with the additional presence of CSSC inside RAFT-TE.

In conclusion, CSSCs could successfully be embedded in RAFT-TE.

6.5.2. The effect of culture conditions and spatial arrangement of cells on CSSC behaviour

The first part of this chapter showed that CSSCs could successfully be embedded in RAFT-TE. However, CSSCs behaviour was unexpected, and their morphological and phenotypical changes were not clearly understood by the results discussed above.

The second part of this chapter aimed to study further what happened when CSSCs were embedded in RAFT-TE, by comparing them with multiple differentiation conditions, and the baseline of CSSC in 2D.

To establish the effect of culture conditions and spatial arrangement on CSSC embedded in RAFT-TE, a defined number of CSSCs was used. This number was based on the work previously done in our lab, where the concentration of cells inside TE was compared with their concentration in the native tissue [257, 258]. Hence, 34 800 CSSCs per RAFT-TE were studied for three weeks under various conditions.

In 2D, CSSCs were differentiated using KDM media (KDM condition) and also let to spontaneously differentiate in CSSC media (Diff condition) for three weeks.

In 3D, CSSCs were seeded on non-compressed collagen hydrogels, referred as Gel, and in RAFT-TE (Gel that has been plastic compressed) allowing to test the effect of the compression on cell behaviour.

It was possible to observe, using qPCR, that RAFT-TE maintained a different CSSC gene expression profile when compared to CSSC in 2D culture conditions. Nevertheless, PAX6, CD90 and CD73 remained expressed in CSSC cultured in the 3D matrices showing that despite CSSC differentiation, some cells might still be keeping their original profile and thus resulting in a mixed population inside RAFT-TE (as previously discussed).

When looking at the traditional CSSC markers (PAX6, CD90 and CD73), the current study showed that PAX6 remained stable in all the conditions, CD90 was upregulated in the 2D cultures (KDM & Diff) and CD73 was only upregulated in KDM when compared to the original CSSC profile.

Gene expression quantification of PAX6 remained stable after 3 weeks in culture. Nevertheless, positive staining for PAX6 was observed on the RAFT-TE sections. Although the findings of the current study do not support previous research where PAX6 was downregulated over time, it is important to highlight the differences in the materials and methods that might explain this. In this study, CSSCs were used at later passages, and there is evidence of PAX6 expression decreases over time thus implying that if the CSSCs initially seeded on RAFT already had a lower expression of PAX6 than in the other studies, the downregulation would not be noticeable [242]. Additionally, as referred on Chapter 3, Deng *et al.* had seen a slight upregulation of PAX6 when CSSCs were differentiated towards the keratocyte lineage [237], contrary to the PAX6 downregulation in keratocyte differentiated cells that Funderburgh's group defends [115]. Moreover, a study from our lab reported downregulation of PAX6, as soon as eight hours post seeding, but only in RAFT-TE where the fibrils were aligned through the tethering of the hydrogel [255] which supports the idea that not only time but also the properties of the TE may have an impact on PAX6 expression.

Regarding CD90, gene expression was stable in the 3D cultures (in CSSC media) when compared with the CSSC in 2D but, still positive in the

immunostaining of RAFT-TE sections. In contrast, CD73 was not detected in the immunostaining sections of RAFT-TE after 3 weeks of culture. A potential explanation for these patterns of CD73 and CD90 expression might be the presence of a mixed population of cells, where some still express CSSC markers while others are in a more differentiated state, or that cells pushed towards the keratocyte lineage can express these markers as previously reported in other studies [243].

Keratocyte markers, lumican, keratocan and ALDH1A1 were also assessed to test whether the cells cultured inside RAFT-TE in CSSC medium were differentiating towards a keratocyte phenotype closer to what happens when cultured in 2D in KDM media.

Lumican was upregulated in all the conditions except the Gel and was higher in the KDM than in RAFT-TE although still present and visible on the immunostaining sections. Keratocan was only significantly upregulated in the KDM condition, but only very weak staining could be observed at the protein level. ALDH was significantly upregulated in all the conditions though less than lumican. Its expression was also confirmed at the protein level by immunostaining of RAFT-TE sections. As stated in Chapter 3, the higher upregulation of lumican when compared with the other keratocyte markers has been observed before [237] and is in accordance with previous studies that showed that lumican regulates keratocan and ALDH expression [244, 245]. From this comparison, it was also noticeable that although the cells inside RAFT-TE seem to be differentiating towards a keratocyte phenotype, the differentiation appears to be at an earlier stage than with cells differentiated in 2D in KDM media.

Three additional markers were tested, p63, CK3 (to rule out epithelial cell contamination) and ACTA to evaluate if the cells were differentiating towards a fibrotic phenotype. CK3 did not show significant differences across samples, and presented high Ct values [241], thus leading to the conclusion that no contamination of differentiated epithelial cells happened at the isolation stage. Unexpectedly, p63 was upregulated in all the conditions, although its expression was higher in the 2D cultures (KDM & Diff) than in 3D (RAFT and

Gel conditions). This phenomenon has already been discussed in Chapter 3. Though the expression of p63 by CSSC has not been extensively studied, it was appreciated in the experiments here presented and can relate to other studies where hMSCs and limbal fibroblasts also express this marker [247]. Another possible explanation is the potential of transdifferentiation reported by Dua *et al.* [329]. ACTA was upregulated in all the conditions but especially with the spontaneous differentiation conditions where the CSSC were kept in CSSC medium for 3 weeks in 2D. Although not desirable, a small upregulation of ACTA in CSSC when embedded in compressed collagen hydrogels has also been reported by other groups without impairing the therapy effect, thus not affecting the capacity to prevent scarring and induce regeneration of transparent corneal tissue in wounded mice corneas [319].

Until this point, the chapter focused on understanding the changes in CSSCs when embedded in RAFT-TE, and for this reason, they were used as baseline against which all conditions were compared. Subsequently, all the other conditions tested were also compared against each other. Interestingly, no significant differences were found between the gene expression of the different markers when CSSC were cultured under KDM and Diff conditions. Additionally, when comparing 2D with 3D culture under CSSC media, it was possible to note that markers related to scarring as ACTA, and CD90 were downregulated when cultured inside RAFT-TE (3D). The similarity in gene expression of RAFT and Gel (non-compressed hydrogel) proved that compression has no negative impact on cell behaviour and, the additional upregulation of ALDH on RAFT-TE can be a sign of further cell differentiation towards the keratocyte lineage. Nevertheless, compression is of extreme importance to stabilize the hydrogels and turn them into clinically relevant structures, as discussed in Chapter 4.

An interesting finding was that after three weeks, most of the cells migrated to the surface of RAFT-TE. Although the immunostaining sections still showed that some cell clusters remained within the collagen, most of the cells were at the top, and at the bottom of the TE. This behaviour is different from what was observed in previous studies from our group. Previously, fibroblasts embedded in RAFT-TE stayed mostly in place, did not hatch to the surface, and did not

form cell clusters within the hydrogel [211, 257]. SEM analysis supported the theory that some of the CSSCs ‘hatch’ to the surface of RAFT-TE and proliferate on its surface. This ‘hatching’ phenomenon has been described by Prof. Robert Brown (personal communication). In general, CSSC proved to be more motile and proliferative than fibroblasts when cultured in RAFT-TE.

The cell cluster finding was unexpected and, at the time, had not been reported in CSSCs. However, this may be a useful phenotype because hMSCs that have been previously cultured as spheroids have shown increased anti-inflammatory properties [338] giving some insight into why CSSCs behaved this way. Recently, in accordance with our findings, a study where CSSCs were embedded in collagen compressed hydrogels also reported the assembly of the cells into sphere-like aggregates[319].

On the other hand, in this thesis, after three weeks, most of the cells migrated to the top and bottom of the TE. This surprising finding can partially be explained by the remodelling of the matrix by the cells but is still not fully understood mainly because when *in vivo*, the cells are not found in the compressed collagen structures as soon as 48 hours after being transplanted [319]. The same was found by our group in a rabbit safety study where CSSC were transplanted embedded in RAFT-TE.

6.5.3. The effect of culture conditions and spatial arrangement of cells on keratocyte behaviour

By reviewing the literature, multiple works were found supporting the idea that keratocytes are incredibly challenging to culture *in vitro* as they can easily differentiate into a fibroblastic phenotype and reduce the expression of the typical keratocyte markers [221, 339]. There is some evidence that hydrogels can help to maintain, though not restore, keratocyte phenotype [339, 340].

From the previous experiments, it was possible to observe that CSSC inside RAFT-TE, even when cultured in CSSC media, upregulated keratocyte-

like markers. However, when cultured in 2D in KDM medium, they displayed even higher expression of the typical keratocyte markers.

This part of the work looked at whether it was better to differentiate the cells inside RAFT-TE with KDM media directly, or prior to seeding inside RAFT-TE to demonstrate the capacity of CSSC to differentiate into keratocytes under different conditions. Hence, further confirming their authenticity.

The results of this study showed that it is possible to successfully culture keratocytes inside RAFT-TE. However, low yields and poor RNA quality recovered from RAFT-TE made quantification of gene expression challenging. This was because keratocytes are quiescent, so fewer numbers were available for analysis [112, 224]. The poor quality was speculated to be related to the contamination caused by some sticky components of the matrix produced by the cells. For this reason, the RNA had to be subject to a cleaning step, as described in the methods section, that resulted in an even lower concentration of the sample (Appendix S6.5). The technical replicates had to be pooled (thus reducing the statistical power of this study) and subjected to amplification using the whole transcriptome amplification kit (Qiagen). Due to the technical limitations of the process, the cDNA obtained was of unknown concentration. Although the concentration of cDNA should have been the same in all the samples subject to this process, in order to compare these results with other experiments, the next step involved a series of trials using hMSC samples (of known concentrations) to titrate the new samples before performing qPCR. This was needed to ensure that enough cDNA was present and thus amplification possible, but on the other hand, also to ensure that the concentration of cDNA was not too high since it can affect qPCR performance. The optimal Ct ranges should be between 20 to 30 cycles [341, 342].

Both CSSC markers and keratocyte markers were assessed by qPCR. PAX6 and Keratocan could not be detected in all the samples. PAX6 could only be detected in one sample, and keratocan could be detected in half of the conditions, indicating that the concentration of cDNA was too low due to the process referred above and needs to be further optimized in future experiments.

CD90 was downregulated in most of the conditions except Gel+, while CD73 was only downregulated in Gel+. Nevertheless, it is important to highlight the high variance between samples shown by the high amplitude of the boxplots. These findings are consistent with previous studies that claim that downregulation of CD90 indicates differentiation of CSSC into the keratocyte lineage [114, 121].

Lumican was downregulated in both Gel conditions, implying that non-compressed TEs, in contrary to what was found in the literature, do not support the maintenance of a keratocyte profile when compared to RAFT-TE and 2D cultures [339, 340]. ALDH showed no significant differences. However, the variance between samples in the ALDH gene expression was very high, not allowing any feasible comparisons.

ACTA was assessed to test whether embedding keratocytes in 3D matrices would trigger their activation towards an unwanted scarring phenotype [221, 339]. ACTA was downregulated in all the conditions except Gel+, and the highest reduction of ACTA expression could be observed on the RAFT+ condition.

In general, it was possible to conclude that 3D culture reduces scarring phenotype, does not impact keratocyte marker expression and reduces CSSC marker expression when compared to 2D cultures.

In the current study, SEM was performed to compare the behaviour of CSSC when subject to 2D differentiation followed by 3D culture in RAFT-TE, with direct 3D differentiation inside RAFT-TE. In both cases, very few cells were observed at the surface of the TEs. This was not surprising as keratocytes are quiescent and thus not expected to proliferate and remodel the matrix as much as CSSCs did in the previous section of this chapter. Even the cells that migrated and reached the surface of the TE seemed less active that the cells observed before that were cultured on CSSC since they had far fewer villi on their surface [343]. The pre-differentiated condition (2D+3D) had fewer cells at the surface than the TE where the cells were differentiated for 3 weeks directly inside the matrix. This finding is not unexpected since the cells were CSSC and thus still active when embedded in RAFT-TE, having the

chance to migrate to the surface as opposed to the cells that were pre-differentiated and embedded in RAFT-TE as keratocytes. This idea is supported by the observation of more 'hatching points' at the surface of the TEs where the cells were differentiated only in 3D. One factor that is important to explain this behaviour is the presence of PDGF and EGF in the CSSC media as it has been shown that both promote cell spreading within 3D collagen matrices by inducing matrix deformation [323-325].

CSSC clustering inside RAFT-TE was a largely unreported phenomenon that needed further investigation.

6.5.4. The effect of PDGF on CSSC in RAFT-TE

Although not well understood, the formation of mesenchymal cell spheroids is believed to be linked not only to the cell properties but also to environmental cues. It is a typical behaviour observed during tissue and organ development and has also been reported by hMSCs with enhanced anti-inflammatory properties [338, 344].

Previous works have concluded that cell clustering regulation depends on the balance between the contraction of cells within the clusters and their migration. As reported by Rocha-Azevedo *et al*., fibronectin (FN) matrix assembly can function as a nucleation centre for cell clustering on 3D matrices like collagen hydrogels [345]. This group has also shown that MMP-2 is responsible for FN disruption and thus cell cluster dispersion and that PDGF containing medium promotes individual cell migration [326]. Taking this into account, the final part of this chapter aimed to evaluate if PDGF influences CSSC behaviour inside RAFT-TE. This is because PDGF has been shown to promote cell migration and matrix remodelling in collagen matrices [323-325].

A strong relation between cell clustering and migration has been reported in the literature. Although cell clustering is known to be a typical morphogenic behaviour in tissue and organ development [344], this phenomenon was unexpected and thus not hypothesised for CSSC behaviour inside RAFT-TE. Furthermore, CSSC media contains PDGF, a promigratory growth factor, and

previous studies have demonstrated that PDGF containing medium had an effect on individual cell migration rather than promoting cell clustering [346].

The live-cell imaging performed over two weeks on CSSC embedded in RAFT-TE - cultured both in the presence (+) and absence of PDGF (-) – highlighted two important features: (1) Cells move less in the absence of PDGF and (2) Clusters grow faster in the presence of PDGF (even joining neighbour clusters). Also, more cells migrate towards the surface. These findings support previous research into the area that claim that cell clustering is a dynamic process that results from the balance between migration and contraction of the cell clusters [326].

The effect of PDGF on CSSC differentiation, cell migration and matrix remodelling was further investigated by assessing marker expression under different conditions.

Looking at the traditional CSSC markers, PAX6 was not detectable in any of the conditions, CD73 showed no significant differences, and CD90 was upregulated in CSSC cultured in the absence of PDGF compared to in PDGF containing medium. Again, this marker was controversial, as some papers claim the loss of CD90 with the differentiation of CSSCs into keratocytes [114, 121], while others suggest that keratocytes are able to express CD90 [243]. Comparing this with the results obtained earlier on, this upregulation could be indicative of initial differentiation towards a more differentiated phenotype since this upregulation was observed on the cells pushed towards the keratocyte lineage.

Moreover, keratocyte markers lumican and ALDH were also upregulated in the cells cultured without PDGF further supporting the transition into a more differentiated phenotype. Keratocan was not detectable, but this was not surprising since these cells where only two weeks in culture and keratocan is a later stage differentiation marker [244, 245]. During this study, keratocan was only upregulated after three weeks in culture in KDM media, as described earlier.

MMPs are known to play a crucial role in cell migration, wound healing and tissue/matrix remodelling [320]. In the cornea, it has been shown that MMP1 (interstitial collagenase) and MMP2 (gelatinase A) contribute to epithelial repair and stromal remodelling [321, 322]. MMP1 is required to cleave the collagen triple helix so that MMP2 or -9 can access their respective gelatine substrate cleavage sites [347]. It has also been suggested that, for this reason, they have a long-term function in support of stromal remodelling [348].

In the results here presented, the absence of PDGF in the cell culture media led to a downregulation of MMP1. This was expected since PDGF is known to promote cell migration and matrix remodelling, meaning that in the absence of the growth factor, CSSCs remodel less the matrix [326]. Surprisingly, MMP2 was upregulated in the absence of PDGF. It is important to note the fact that MMP2 has been shown to play a pivotal role in cell cluster dispersion [326] and that the RAFT-TE cultured without PDGF had a slower growth of cell clusters in the first days of culture, indicating that the matrix was being remodelled at a slower pace which may justify this upregulation at a later stage.

Although previous studies found that fibronectin was required for cell clustering by working as a nucleation centre for cell clustering in collagen matrices, no differences were found in this study in FN1 or COL1 production between the two conditions [349, 350].There was also no significant difference in ACTA expression, but there was a clear downregulation of Ki67 proliferative marker when the cells were cultured without PDGF. This difference is justified by other studies that showed that PDGF promotes cell proliferation [351-354].

It is known that two separate forces are needed for cell migration, one at the cell front, to extend lamellipodia or filopodia and establish new adhesion sites, and other to overcome the traction created by the cell-matrix interactions at the rear of the cell [355, 356].

The PDGF receptor affects cell migration and actin cytoskeleton through the small GTPases of the Rho family, which are major candidates in cytoskeletal and mechanical phenotype regulation of cells during migration [357]. RhoA regulates stress fibre formation, Rac controls lamellipodia

formation, and Cdc42 directs the dynamics of filipodia and plays a crucial role in cell polarization [358-362].

Previous studies have shown that Rac activation by PDGF promotes cell spreading and migration in 3D collagen matrices [324, 363]. It has also been reported that Cdc42 is a key regulator of cell-ECM interactions by regulating MMP expression and activation [364-366]. Surprisingly, in this study, Cdc42 was upregulated when the cells were cultured without PDGF. On the contrary, MMP1 expression by CSSC cultured in the absence of PDGF was downregulated. This behaviour has been described in the literature: Cdc42 downregulates MMP1 by suppressing ERK activity and increased cell-cell interactions increase Cdc42 activation (thus reducing MMP-1 expression) [365, 367]. Another important finding was that MMP2 is upregulated when Cdc42 is also upregulated and this can be explained by the reorganization of the actin cytoskeleton that is also possible to observe on the SEM photographs. MMP2 activation has been reported multiple times in response to Cdc42 activation in other cell types [368, 369].

The cells that escaped to the surface of RAFT-TE presented very different morphologies. When in the presence of PDGF, the cells had an elongated spindle shape and more villi. When in its absence, the cells were flatter, even though still polarised in similar directions. One possible explanation is the fact that PDGF is known to promote directional movement in 3D collagen matrices [370] and for promoting a spindle elongated morphology [371]. This cell alignment has also been observed by others on different occasions and experiment setups [172, 372, 373].

Lastly, although it has been shown that PDGF influences cell behaviour inside RAFT-TE, and thus impacts cell clustering, and cell spreading in the collagen matrix, it is not the only factors and further studies would be needed if there is the need to fully control CSSC cluster formation.

6.6. Conclusion

Primarily, this chapter focused on embedding CSSC into the new GMP-compliant version of RAFT-TE. Although CSSC could be successfully embedded, they showed an unexpected behaviour by clustering inside RAFT-TE.

The cells formed highly aligned clusters within the collagen matrix and, in addition to that, after a couple of days, the CSSC moved within the matrix by digesting the collagen (as shown by MMPs expression) and hatched at the surface of the TE. The cells proliferated and rearranged themselves in a highly organized way at the surface of the structures.

From the results, it was also possible to notice that CSSC differentiated into different cell types which leads to the hypotheses that the starting population was not uniform.

Based on the results that showed that the gene expression profile of the cells inside RAFT-TE when cultured on CSSC media was closer to the condition subject to KDM differentiation, this chapter also investigated what would be the best way to differentiate these cells into the keratocyte lineage. However, due to the technical challenges encountered during the analysis, a conclusion could not be achieved.

Further experiments needed to be done to understand the biological mechanisms underlying the clustering phenomenon. PDGF was selected for investigation, and it was shown that its presence or absence in the media impacts CSSC behaviour inside RAFT-TE. Nevertheless, PDGF cannot be presented as the only player of this dynamic process as it could not avoid cluster formation. Nevertheless, this data suggests that there are mechanisms by which PDGF influences cell clustering, and so further studies are needed.

Chapter 7

7. GENERAL DISCUSSION

The cornea on the front surface of the eye is our window to the world. Maintenance of its transparency is essential for focussing light onto the retina at the back of the eye and therefore vision.

This thesis addressed the challenge of corneal scarring, which can be caused by injury, infection or ulceration, and blinds more than 10 million people worldwide [132].

Therapeutic corneal transplantation is limited by the global shortage of suitable donor tissue, high risk of tissue rejection and the type of disorder itself.

Stem cell therapy, together with tissue engineering approaches has the potential to address this significant unmet clinical need. Our team, and others, have successfully transplanted cultured LESC to restore vision in patients with LESC deficiency. However, when scarring of the central cornea also occurs, transplantation of transparent donor corneal stroma is required for vision.

CSSCs reside in the corneal limbus and can be made to differentiate into keratocytes (which maintain healthy transparent corneal stroma). Promisingly, CSSCs are believed to have MSC properties and are especially interesting due to their reported immune-modulatory capacity to delay the host rejection of allogeneic tissue in human recipients.

The work presented on this thesis aimed to develop new strategies for CSSC delivery for ocular surface reconstruction. Five aims were set at the beginning of this thesis in order to optimise the production of clinically-relevant CSSC-populated RAFT-TE. The results answered some of the initial questions, either by supporting the hypotheses, or refuting it. Moreover, the work performed on this thesis also raised new questions which are discussed

below.

The aim on **Chapter 3** was two-fold; firstly, to identify the best anatomical location to maximize CSSC yield by applying a novel tissue clearing technique, and secondly to characterize the CSSC obtained from OC rims in relation to MSC properties, and capacity to differentiate towards the keratocyte lineage.

In the process of designing an ATMP is of uttermost importance to ensure optimization, and reproducibility of the protocols, as well as extensive characterization of the cells being used prior to delivery.

7.1. Optimisation of 3D corneal tissue clearing to support the localisation and isolation of CSSC

Chapter 3 presented a novel imaging technique based on tissue clearing methods for the study of the limbal niche. This is of importance due to the clinical relevance to target future biopsies and obtain maximum CSSC yield.

The results show that it is possible to clear corneal-limbal tissue and visualize anatomical landmarks like the limbal crypts and focal stromal projections. This initial analysis of tissue architecture in iDISCO cleared corneal tissue is supported by previous studies that showed similar features [89, 97]. In line with this, it is possible to state that clearing techniques such as iDISCO can provide an alternative to histological sectioning for volumetric studies. This is a great advantage since the whole niche and corneal rim reconstitution would be possible (if the right technology was available) supporting the understanding of cell-cell interactions, and identification of the best place for CSSC isolation [226].

Due to the lack of availability of the appropriate microscopy setup, it was not possible to address the initial aim of identifying the best location to isolate CSSC. Nevertheless, to the extent of our knowledge, this was the first study that successfully cleared human corneas for the study of the limbal niche.

Although further research is needed to create a full limbal reconstruction and establish the best location from where to obtain the maximum CSSC yield, the isolation and characterization of CSSC was still possible.

7.2. CSSC isolated from the limbal stroma partially confirm MSC properties and differentiation towards the keratocyte lineage

Having in mind the therapeutic use of CSSC in the creation of a corneal tissue equivalent, the second part of **Chapter 3** investigated CSSC behaviour *in vitro* prior to incorporation into RAFT-TE.

CSSC isolated from the limbal stroma were cultured and compared against hMSCs, and the central cornea itself. They were also pushed to differentiate towards the keratocyte lineage, and the phenotype was assessed.

This analysis supports the growing body of literature that highlights the poor or controversial characterisation of CSSC. Contrary to the hypothesized, this study did not fully confirm the phenotype described by Funderburgh JL *et al.* [114, 115], or met all the MSC-definition criteria [107]. CSSCs differentiate into the chondrogenic and the adipogenic lineages. However, these results build on existing evidence that osteogenic differentiation potential correlates negatively with hMSC efficacy to reduce corneal inflammation *in vivo* [239], which could explain the weak differentiation of the CSSC isolated in this thesis into the osteogenic lineage [237].

In line with the hypotheses, CSSCs were successfully pushed towards the keratocyte lineage as shown by the expression of keratocyte markers such as Lumican, Keratocan and ALDH. However, while in previous studies CSSC markers (such as CD90 and CD73) were downregulated [115, 121, 124], here that was not observed. This suggests that there was only partial differentiation of the CSSCs into the keratocyte phenotype, which is in light with previous studies [246].

The generalizability of the results is limited by the differences in culture conditions among the studies. Differences span from the age of donor tissue to time port-mortem, or even the culture media.

7.3. Changes in the manufacturing process affect RAFT-TE properties

Before delving into the delivery of CSSC, a novel and critical study for the progress of RAFT-TE towards the clinic was designed. **Chapter 4** of this thesis presents a head-to-head comparison of *First Link* and *Koken* collagens. This was necessary to access the suitability of replacing a research only grade material (*First Link*) with a GMP compliant product (*Koken*) for the production of RAFT-TE.

While previous bench research focused on RAFT-TE development using *First Link* collagen [127, 206, 211, 254-261], extensive characterisation of RAFT-TE produced with *Koken* collagen was needed to enable the translation and validation of RAFT-TE towards the clinic. The experiments provide new insights for the validation of this product as an ATMP therapy.

Different parameters were tested, from surface topography to hydrophobicity, from thickness to mechanical strength, and also RAFT-TE transparency.

The comparative characterisation data suggests that *Koken* TEs have the potential to be used as an advanced therapy for ocular surface reconstruction due to improved mechanical strength, and ideal thickness when compared with *First Link* TE.

Future studies should consider clinically accepted reagents early in the process of development since translation from bench to clinics is always a challenge. Additionally, this study provides a quantitative comparative dataset against which other collagens can be compared if needed. Moreover, this data also supports the cell culture work that followed with a basis for possible differences in CSSC and LESC behaviour.

7.4. Modifications in RAFT-TE production impact mixed population cell behaviour

One of the prevalent hypotheses regarding CSSCs is that in addition to being the keratocyte progenitors [121], and having anti-scarring properties [114], they also support LESCs [127]. **Chapter 5** initially aimed to design a co-delivery strategy for CSSC with LESCs, by culturing them as a mixed population [292] on top of RAFT-TE to take advantage of their synergic interactions [280].

Contrary to the hypothesized association, over time, the experiments demonstrated that this protocol could not be moved to the clinic. Cell isolation was challenging, cell growth was extremely variable from donor to donor, dependant on the quality of the tissue and, surprisingly, when RAFT-TE was moved out of the well prior to *in vivo* transplantation, the epithelial cell layer detached from the carrier. Since this had not happened before the use of *Koken* RAFT-TE, all the changes implemented in the new clinically relevant manufacturing protocol were explored in order to identify the source of the change in cell behaviour.

Different collagen sources, neutralising solutions, and compression times were tested. Nonetheless, the cells did not remain attached to the TE. It is also important to highlight that both TEs were compared in **Chapter 4**, and that no significant differences were observed at the surface of RAFT-TE apart from fibril diameter, so it was unlikely that cell peeling was only related to the RAFT-TE manufacturing changes.

It is also noteworthy that regardless of the manufacturing changes, the quality of the corneal tissue used for cell isolation was not constant over time. Hypothermic storage is the most common worldwide [282]. However, Moorfields Lions Eye Bank (London, UK), the eye bank from where the UCL Institute of Ophthalmology can access corneal tissue, stores the majority of corneas under OC conditions. In general, it was a challenge to obtain tissue, being only available when it did not meet the necessary requirements to be used for transplant. This meant that the tissue had at least 4 weeks post-mortem. Cell peeling was two times more frequent in mixed population isolated

from OC corneal rims in comparison to OP corneal rims. Nonetheless, the majority of the RAFT-TEs still peeled. In summary, the data suggests that streamlining the cell seeding approach by using the one-step mixed population method was not a good option to use in the clinic.

7.5. Modifications in the cell seeding approach affect RAFT-TE outcomes

In the past few years, there has been growing interest in co-culturing LESC with limbal stromal cells on RAFT-TE, in a closer attempt to recreate the limbal niche for corneal repair [127, 164]. The mix-population direct cell seeding approach is a one-step procedure, and an animal-free derived way for seeding cells on the surface of RAFT-TE [127]. However, contrarily to what is was hypothesized, this method proved not to be the best way to culture CSSC and LESCs on top of RAFT-TE. Numerous seeding strategies for the delivery of CSSC and LESCs on top of RAFT-TE were explored in **Chapter 5**.

The methodological choices were constrained by the available cadaveric tissue for cell isolation, and by the need to develop a GMP-compliant strategy. Despite this, and in order to understand if the mixed population method was the leading cause of cell detachment from RAFT-TE, different seeding approaches were trialled.

It was hypothesized that stromal cells in the mixed population could be overgrowing and impacting epithelial cell layer attachment by extensive remodelling of RAFT-TE [298]. The pre-expansion of the cells in TCP, and selective trypsinisation prior to RAFT-TE seeding showed a slight improvement, but cell peeling was still very high, and so was the presence of stromal cells.

The gold-standard method for LESC isolation is with the dispase, followed by pre-expansion in a growth-arrested 3T3 feeding layer. Since this protocol only requires the scrapping of the superficial limbal area, it isolates LESCs independently of CSSC, and was used to access whether the presence of

stromal cells was causing the cell detachment. However, the described protocols culturing LESCs on 3T3s use fresh tissue, which was not available during this study, and for this reason, the outcomes of this approach were unexpected, resulting in poor epithelium growth.

This method poses a risk of transfer of adventitious agents to the patient due to the pre-expansion of LESCS in 3T3s [127]. To access a seeding alternative that could possibly be used in a clinical setting, and still allowed us to investigate the impact of stromal cells, a new seeding strategy was trialled. LESCs isolated with dispase were directly cultured on top on RAFT-TE, thus eliminating the use of animal-feeder layers [127]. The isolation with dispase, and the superficial scrapping of the limbus, ensured a lower percentage of stromal cells in the cell suspension when compared to the collagenase method that involved the dissection of the superficial corneal limbal region. This method showed a success rate of almost 90%, meaning that only a small percentage of the cultured RAFT-TEs had some areas of cell detachment.

The results might suggest that CSSC negatively impact LESCs. However, based on the findings, a more plausible theory would be that this is not the ideal strategy for co-delivering both cell types. These results build on existing evidence that cell-cell and cell-matrix interactions play a crucial role in the maintenance of the corneal epithelium [300]. The interaction between the epithelial cells and the underlying basement membrane is key in wound healing, which might give some insight on the way the cells attached better when in sole contact with the collagen matrix, rather than when in the presence of stromal cells, that might, for example, compete for adhesion sites [300].

RAFT-TEs culture with the pre-dissociated cell suspension also peeled less than their non-dissociated replicates which adds to the theory that cell differentiation stages might play a role in epithelial cell detachment. Expansion from single cells ensure that colonies sprout at similar times, and thus, the differentiation stage is similar around the entire surface of the TE. This hypothesis builds on the evidence that LESCs putative marker expression is reduced towards the periphery of the colonies, and the cells on the periphery divide more quickly and become more differentiated due to the extensive

number of divisions [314] reducing their attachment to the basement membrane [315].

Further research was needed to establish a way of delivery CSSC with LESCs as a therapy for ocular surface reconstruction. The incorporation of CSSC inside the TE was explored in **Chapter 6** as an alternative to their co-culture on the surface of RAFT-TE.

7.6. CSSC can be successfully cultured inside RAFT-TE

Our previous data showed that the mixed population method is not ideal for co-culture of CSSC with LESCs. Drawing from this learning, CSSC were incorporated inside RAFT-TE and, therefore, **Chapter 6** focused on its manipulation and phenotype assessment for future optimal therapeutic delivery. CSSC, and keratocytes differentiated from CSSC, were cultured under different conditions inside RAFT-TE aiming to develop an organized corneal stromal tissue equivalent.

While previous research has focused on culturing CSSC inside a non-GMP compliant version of RAFT-TE for tissue modelling [255], these results demonstrate that in line with the hypothesis, GMP-compliant RAFT-TE can support the culture of CSSC, and keratocytes derived from CSSC having in mind their therapeutic delivery.

The most striking finding was the formation of cell cluster when CSSC were cultured inside GMP-compliant RAFT-TE which had not been previously reported.

Preliminary studies have also shown that CSSC cultured inside RAFT-TE, even in the presence of cell clusters, does not impair LESCs expansion on the top of RAFT-TE.

7.6.1. CSSC form cell clusters inside RAFT-TE

The results show a consistent formation of cell clusters despite the concentration of CSSC cultured inside RAFT-TE. Although at the time this behaviour had not been reported in CSSC, recently, cluster formation inside compressed collagen hydrogels was evident in a publication, but its implications were not discussed [319].

Mesenchymal cell spheroid formation is a behaviour reported in tissue and organ development but also described in hMSCs with enhanced inflammatory properties [338, 344] which might justify the behaviour of CSSC inside RAFT-TE.

Although this will be discussed at a later stage, it is also important to point out that, after 3 weeks, most of the cells migrated to the surface of RAFT-TE. This behaviour was a surprise, and is not supported by the previous studies where fibroblast embedded in RAFT-TE stayed mostly in place and did not hatch to the surface, neither formed cell cluster inside the hydrogel [211, 257].

7.6.2. CSSC cultured inside RAFT-TE start to differentiate towards the keratocyte lineage

Culturing of CSSC inside RAFT-TE for 3 weeks in CSSC media had an impact on CSSC genotype and phenotype. Contrary to the hypothesized association that CSSC would remain quiescent, they enter a differentiation pathway. The data suggests that CSSC are able to differentiate in different populations: while some still express CSSC markers (like PAX6, CD90 and CD73), others start to express keratocytes markers (as lumican, keratocan and ALDH), thus resulting in a mixed population inside RAFT-TE.

The study supports the correlation between lumican expression and other keratocyte markers, as shown by previous studies [237]. In light with the hypotheses that lumican regulates keratocan and ALDH expression [244, 245], thus explaining why its upregulation happens at earlier stages of differentiation. However, it was also noticeable that differentiation inside RAFT-TE in CSSC is at an earlier stage than the cells differentiated in 2D in

KDM media. For this reason, the effect of the cell culture conditions on keratocyte differentiation was also assessed.

7.7. Culture conditions affect keratocyte differentiation and behaviour in RAFT-TE

Since it was shown that CSSC do not remain quiescent inside RAFT-TE, **Chapter 6** also investigated the best way to culture keratocytes from CSSC inside RAFT-TE.

Keratocytes are known to be difficult to culture *in vitro* due to their potential to differentiate into a fibroblastic phenotype [221, 339]. Nevertheless, as previous studies supported the idea that hydrogels can help to maintain keratocyte phenotype [339, 340], RAFT-TE was accessed as a potentials scaffold for culture and delivery of keratocytes.

It was shown that CSSC differentiated in KDM media inside RAFT-TE for 3 weeks display a more differentiated genotype towards the keratocyte lineage than the ones differentiated in 2D. It was possible to observe a downregulation of CSSC marker (CD90), and a downregulation of fibrotic marker (ACTA) building on previous evidence that downregulation of CD90 signposts differentiation of CSSC into the keratocyte lineage [114, 121], and that ACTA would indicate activation towards a scarring phenotype [221, 339].

In line with the hypotheses, this study showed that it was possible to culture keratocytes inside RAFT-TE. However, the methodological choices, and analysis, were constrained by the fact that keratocytes are quiescent, and in opposition to CSSC, do not have higher proliferation rates [112, 224] which resulted in low concentration and poor quality of the RNA obtained

Reduced keratocyte activity was confirmed by SEM where few cells were observed at the surface of the TEs, presented fewer villi on their surface [343], and less matrix remodelling. A difference in activity was also observed between the cells that were pre-differentiated in 2D, and the cells that were

fully differentiated in 3D (inside RAFT-TE). This was supported by the observation of ‘hatching points’ at the surface of the TEs were the cells were differentiated only in 3D. Nevertheless, the cells observed at the surface were much less than when CSSC were cultured in CSSC media as initially shown. Media composition is an important differentiator that can help to support the different behaviour. The presence of PDGF and EGF has shown to promote cell spreading within 3D collagen matrices by inducing matrix deformation in previous studies [323-325]. Its impact on CSSC behaviour inside RAFT-TE was also assessed in this thesis.

7.8. PDGF plays a role in CSSC cluster formation inside RAFT-TE

Chapter 6 also investigated the role of PDGF in CSSC behaviour inside RAFT-TE, and its impact in cell cluster formation and matrix remodelling. PDGF was chosen as a potential candidate because it has been shown that promotes cell migration and matrix remodelling [323-325], as well as having an impact on the dispersal of cell clusters in collagen matrices [326].

This study demonstrated that CSSCs were less motile and had a high *in situ* proliferation when cultured without PDGF. This resulted in a faster expansion of the cells clusters inside RAFT-TE, rather than matrix disruption and movement towards the surface.

The live-cell imaging performed over two weeks corroborated previous studies where cell clustering is pointed as a dynamic process that results from the balance between migration and contraction of the cell clusters [326].

In addition to contributing to epithelial repair and stromal remodelling [321, 322] in the cornea, MMP1 (interstitial collagenase) and MMP2 (gelatinase A) were accessed due to their central role in cell migration, wound healing and tissue/matrix remodelling [320].

MMP1 was downregulated in the absence of PDGF, indicating that there is less cleavage of the collagen triple helix [347] and that in the absence of the

growth factor, CSSCs remodel the matrix less [326]. However, unexpectedly, MMP2 that has been shown to play an essential role in cell cluster dispersion [326] was upregulated in the absence of PDGF. This upregulation after 2 weeks might be explained by the later remodelling of the matrix, and the slower growth of the cell clusters observed by live microscopy.

This research provides new insights into the role of PDGF, and the process of cell cluster formation of CSSC inside RAFT-TE which could also be used to explain the sphere-like aggregates in collagen compressed gels reported by our collaborators [319].

Finally, the live cell imaging was important to highlight the behaviours of the different cells that support the idea that CSSC might give origin to different cell populations when cultured inside RAFT-TE.

7.9. CSSCs start to remodel the matrix and move toward the surface of RAFT-TE.

Although in the short-term CSSC form cluster inside RAFT-TE, which is corroborated by another study [319], in the long-term, they remodel the collagen and escape the matrix. After only 3 weeks, most of the cells could already be observed at the top and bottom of the TE. This data is a step in the understanding of why, when cultured *in vivo*, the cells are not found in the compressed collagen structures as soon as 48 hours after being transplanted [319]. This has also been described by our group in a rabbit safety study where CSSC were transplanted embedded in RAFT-TE.

7.10. Limitations of this study

One of the biggest limitations of this study was the low availability of fresh corneal tissue from diseased donors. To overcome this limitation, it would be useful to establish a partnership with multiple eye banks, rather than being dependant on the Moorfields Lions Eye bank.

Overall, it is also important to highlight that the methodological and technical choices of this project were limited by the requirements for GMP-compliance, and the fact that the project was already at a translational phase. This meant that reagents were limited to the GMP-grade spectrum, and extensive modifications to the protocol were not allowed at this stage.

Due to the lack of available light-sheet microscopes, the developed protocol for corneal clearing could not confirm the best anatomical location from which to harvest CSSC. Nevertheless, now that technology has evolved, and is available in more microscopy facilities, this is a project that has the potential to broaden the knowledge of limbal niche by exploring cell location and interactions.

There are two other major limitations in this study, and that the results obtained will help to address the design of future research. First, was based on the premise that the mixed population was a good alternative for the delivery of LESCs, as previously shown in our lab under different conditions. However, these RAFT-TEs were never removed from the tissue culture plate before fixation, and thus the issue of cell peeling had not been identified. Second, the formation of cell clusters was a surprise, and before combining the stromal and the epithelial cells, there was the need to understand what was happening inside RAFT-TE. This resulted in an all-new line of research, and time limitations to actually combine the two cell types in a final TE.

7.11. Future work

It is important to consider the results presented herein when considering new lines of research and advancing the current ones.

Further studies should investigate the potential of tissue clearing methods, such as iDISCO, to identify the best location to isolate CSSC, as well as to explore cell-cell interactions within the human corneal limbal niche. Taking this into consideration, a minimum biopsy size to allow CSSC expansion could also be identified to streamline the use of live-patient samples for autologous treatment.

Additional work is certainly required to disentangle the mechanisms underlying epithelial cell peeling. The investigation of cell proportion titration (CSSCs vs LESCs) and its impact of cell attachment to RAFT-TE may constitute the object of future studies.

CSSC clustering inside RAFT-TE is also an interesting topic for future work. In addition to delving into the collagen remodelling process by, for example, confocal reflection microscopy, it would also be interesting to investigate the role of CSSCs embedded in RAFT-TE in immunity and wound healing (using cytokine secretion for example) and their anti-inflammatory properties at different stages of culture.

Finally, it will be important that future research investigates the co-culture (and potentially co-transplantation) of CSSC (inside RAFT-TE) and LESC (on top of RAFT-TE) to access the synergetic effect between these two cell types, and how they support function in the TE.

7.12. Concluding remarks

In conclusion, it was demonstrated that both CSSC and keratocytes derived from CSSC can be cultured inside RAFT-TE. Characterisation of CSSC in 2D and comparison with their culture in 3D has shown differences in phenotypical and genotypical features.

Although isolation with dispase and direct cell seeding proved to significantly reduce cell peeling as an alternative to the one-step mixed population method, this is not the method currently being used in the clinical trial. A step back was taken, and limbal explants are used as a reliable source for the expansion of LESCs on top of RAFT-TE [374].

This work also highlighted that the most simple and innovative methods, do not always result in the best outcomes. Translation from bench to clinics is challenging. This work is novel and contributed to the advancement of an ATMP for ocular surface reconstruction towards the clinic. An adapted version of this therapy has been funded to proceed to clinical trials for partial thickness lamellar corneal transplantation.

8. APPENDIX

8.1. Appendix – Chapter 3

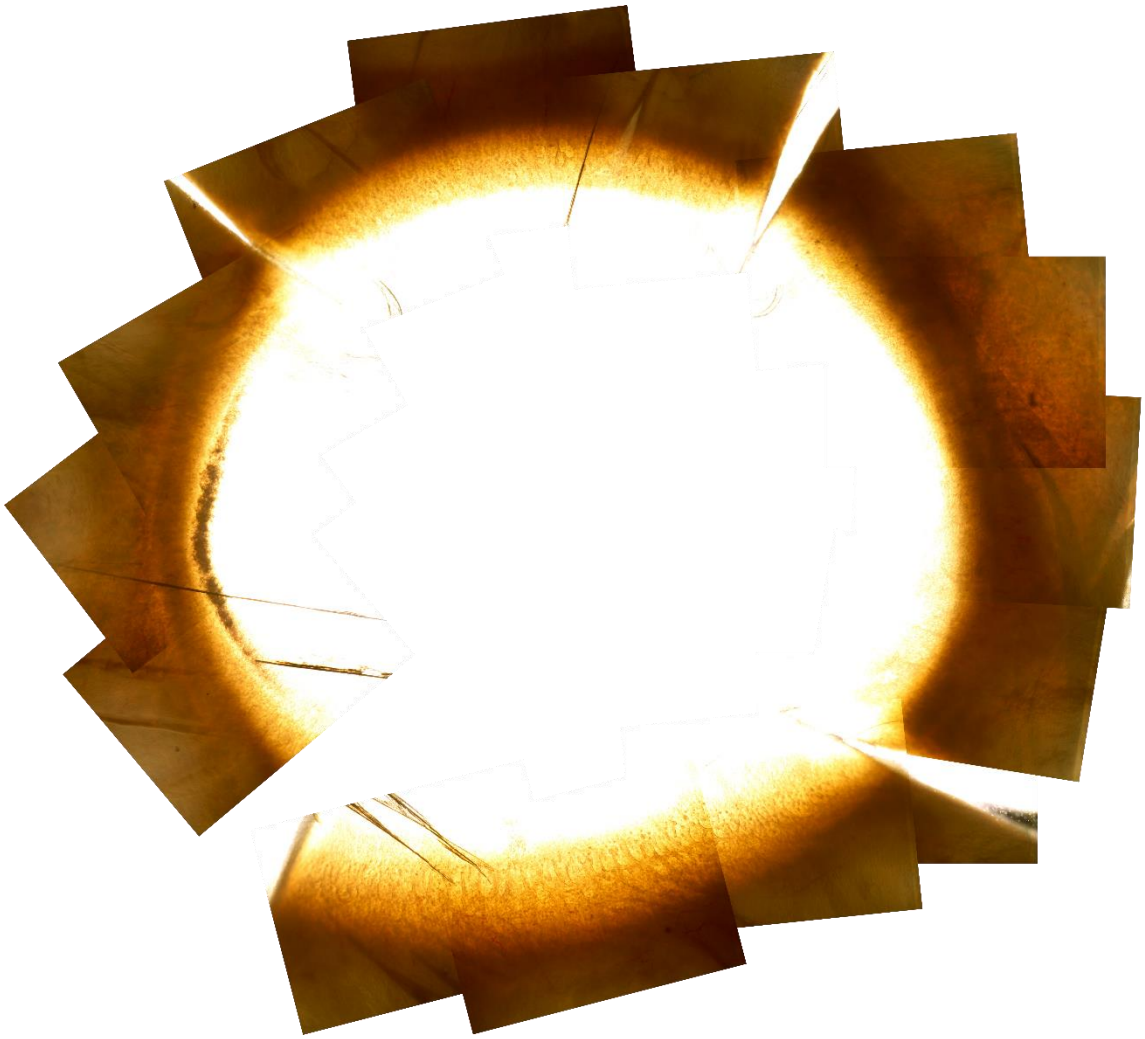

Figure S3.1 – Raw images and montage of optical microscopy tiles showing the presence of crypts.

Table S3.1 – Optimized protocol for corneal tissue clearing based on iDISCO

Day		Protocol
1	I.	Cut corneal rims in half
	II.	Fix 2h or overnight in 4% paraformaldehyde (PFA)
2	I.	Wash fixed samples in 1xPBS/0.2%TritonX-100, RT 1h x2
	II.	Incubate in 1xPBS/0.2%TritonX-100/20%DMSO, 37°C o/n. 1.5mL eppendorf
3	I.	Incubate in 1xPBS/0.1%Tween-20/0.1%TritonX-100/0.1%Deoxycholate/0.1%NP40/20%DMSO, 37°C o/n.
4	I.	Wash in 1xPBS/0.2%TritonX-100, RT 1h x 2
	II.	Incubate pre-treated samples in 1xPBS/0.2%TritonX-100/20%DMSO/0.3Mglycine, 37°C o/n.
5	I.	Block in 1xPBS/0.2%TritonX-100/10%DMSO/6% Goat Serum, 37°, o/n
6	I.	Wash in 1xPBS/0.2%Tween-20 with 10ug/ml heparin (PTwH), RT 1h x 2.
	II.	Incubate with primary antibody in PTwH/5%DMSO/3% Goat Serum, 37°, 4 days. 0.5mLeppendorf
7 **8** **9**	I.	Antibody solutions need to be replaced every day – add x ul of antibody.
10	I.	Wash in PTwH for 10min, 15min, 30min, 1h… then o/n
11	I.	Incubate with secondary antibody in PTwH/3% Goat Serum, 37°, 3 days.
12 **13**	I.	Antibody solutions need to be replaced every day – add x ul of antibody.
14	I.	Wash in PTwH for 10min, 15min, 30min, 1h each; then o/n
15	I.	Incubate the sample overnight in 50% Tetrahydrofuran/H2O (THF, Sigma 186562-12X100ML) in a glass vial with a silicon coated cap (Thermo Scientific C326-0020). It is important to use THF with BHT as inhibitor. -5mL
16	I.	Incubate 1h in 80% THF
	II.	Incubate 2x1h in 100% THF
	III.	Incubate in Dichloromethane (DCM, Sigma 270997-12X100ML) until the sample sinks at the bottom. The sample may not sink if air bubbles are trapped inside.
	IV.	Incubate in DiBenzyl Ether (Sigma 108014-1KG) until the sample is clear. The vial containing DBE should be filled almost completely with DBE to prevent the air inside the vial from oxidizing the sample.
Notes	For the use of THF, DCM and DBE. Work under a hood, collect waste, use glass and not plastics.	

Table S3.2 – Optimized protocol for corneal tissue clearing based on PACT

Day	Protocol
1	I. Cut rims in half II. Fix 2h or overnight in 4% paraformaldehyde (PFA)
2	I. Incubate samples at 4°C overnight in Acrylamide - hydrogel monomer solution A4P0 (4% acrylamide in PBS) supplemented with 0.25% photoinitiator 2,2'-Azobis[2-(2-imidazolin-2-yl)propane] dihydrochloride (VA-044, Wako Chemicals USA). – 15mL tube
3	I. A4P0-infused samples were degassed with nitrogen (Rival R44, gas) for 5 min and then incubated for 2–3 hr at 37°C to initiate tissue-hydrogel hybridization. – Morning II. Remove excess of hydrogel via brief PBS washes III. Leave in PBS overnight
4	I. Tissue-hydrogel matrices were transferred into 50 ml conical tubes containing 8% SDS (Sigma L4509) in 0.1 M PBS (pH 7.5), and depending on tissue size, were incubated for 5 days at 37°C with shaking.
9	I. PACT-processed samples were washed in PBS with 4–5 buffer changes over the course of a day II. Leave in PBS overnight
10	I. Transfer samples to buffer containing primary antibodies (used 1:10 for 1st day and then 1:50, in PBS containing 2% goat serum, 0.1% Triton X-100 and 0.01% sodium azide) for 4 days. – Use 0.5mL eppendorfs
11 **12** **13**	I. Antibody solutions need to be replaced every day – add x ul of antibody.
14	I. Unbound antibody was removed via PBS washes II. Samples were incubated with secondary antibodies (1:100, To-Pro 1:5000, not enough) for 3 days
15 **16**	I. Antibody solutions need to be replaced every day – add x ul of antibody.
17	I. Replace antibody solutions - Morning II. Wash in PBS overnight
18	I. Incubation in imaging media (RIMS)
19	I. Move samples to new Histodenz II. Mount samples in a slide with 2 '1.0mm spacers' (Fastwell, Grace Bio-labs GBL66411350EA), dental cement and a rounded coverslip
Notes	All staining and mounting steps were conducted at room temperature with gentle shaking. **RIMS Imaging Media** with RI 1.46: Forty grams of Sigma D2158 (Histodenz) in 30 ml of 0.02 M PB with 0.1% tween-20 and 0.01% sodium azide (Sigma S2002), pH to 7.5 with NaOH—which results in a final concentration of 88% Histodenz w/v. Samples are incubated in RIMS until transparent (~1 day for PACT samples), followed by mounting in fresh RIMS. **A4PO** - For 200 ml, add 20 ml of 40% (wt/vol) acrylamide to 100 ml of 0.2 M PBS and 80 ml dH2O

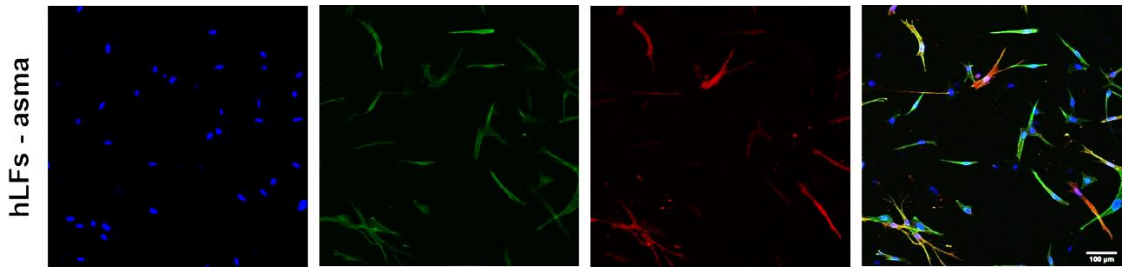

Figure S3.2 – Confocal micrographs of human LFs stimulated with TGFB in 2D. hLFs display positive expression of alpha-smooth actin. DAPI staining nuclei in blue, FITC Phalloidin staining cytoplasm in green and differential antibody staining in red. Scale bars: 100 µm.

8.2. Appendix – Chapter 4

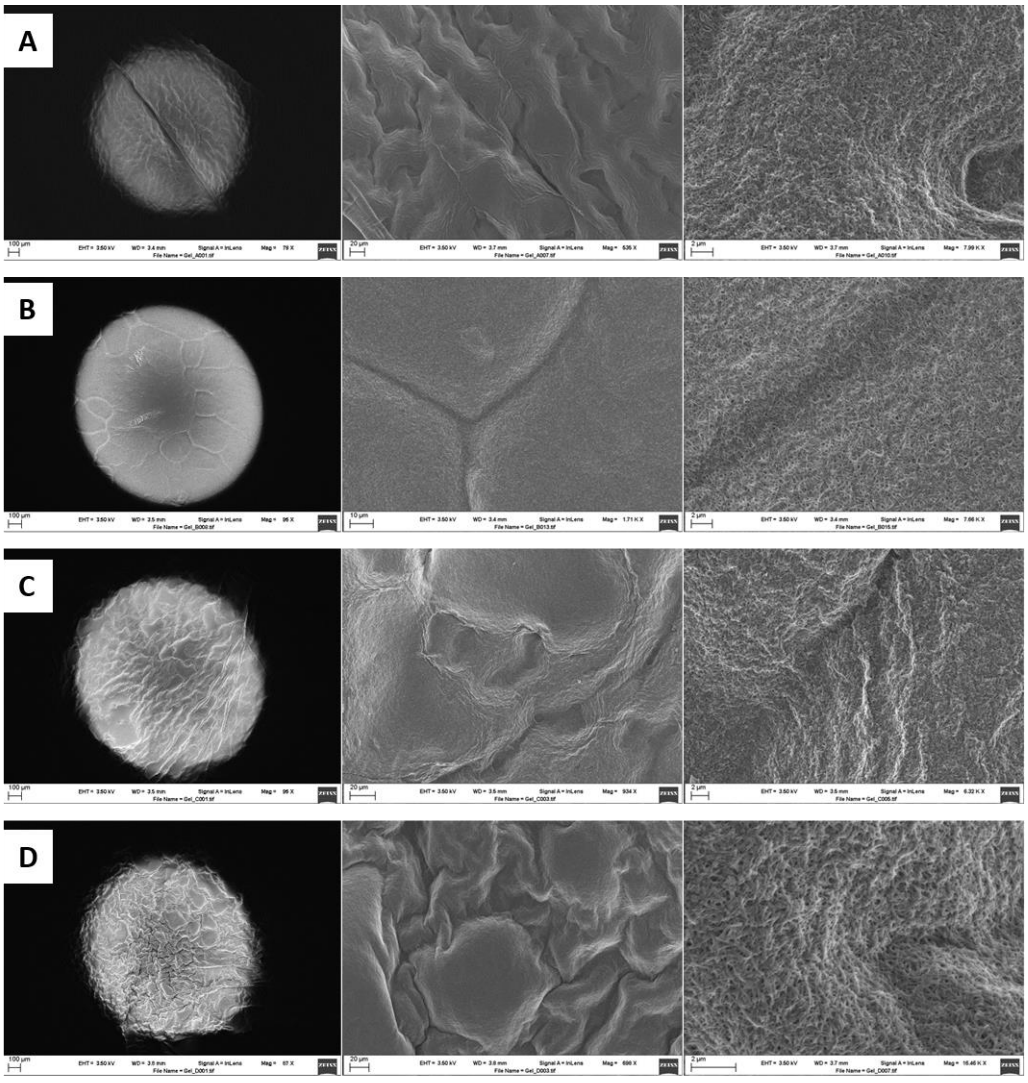

Figure S4.1 – Optimization of the protocol to do SEM on RAFT-TEs: (A) PFA fixed & Osmium treated; (B) PFA fixed & non-Osmium treated; (C) Non-fixed & Osmium treated; (D) Non-fixed & non-Osmium treated.

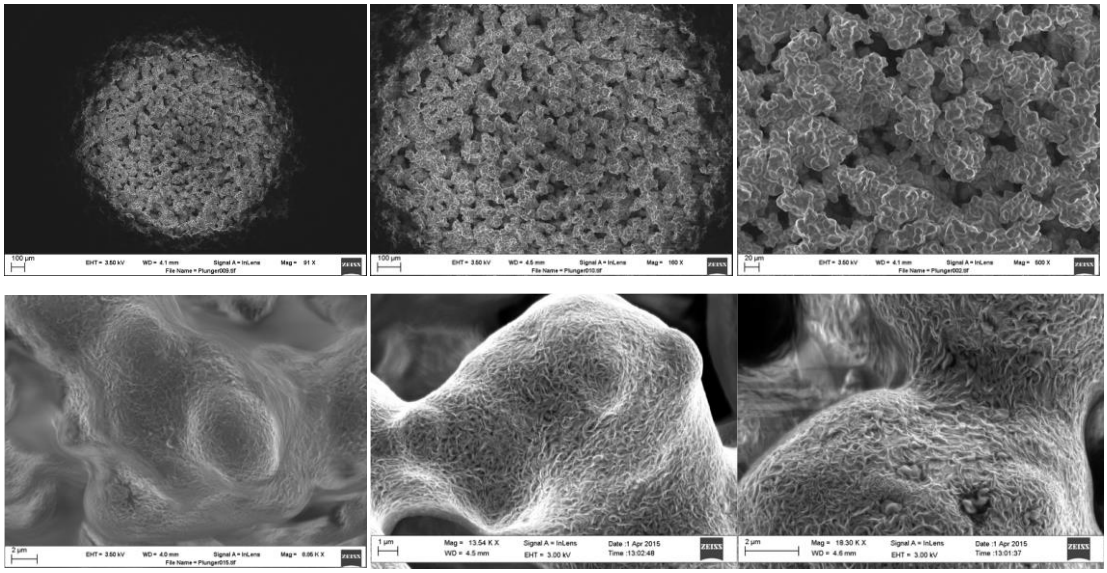

Figure S4.2 – SEM inspection of the surface structure of the hydrophilic porous absorbers (plungers) used for RAF TE production.

8.3. Appendix – Chapter 5

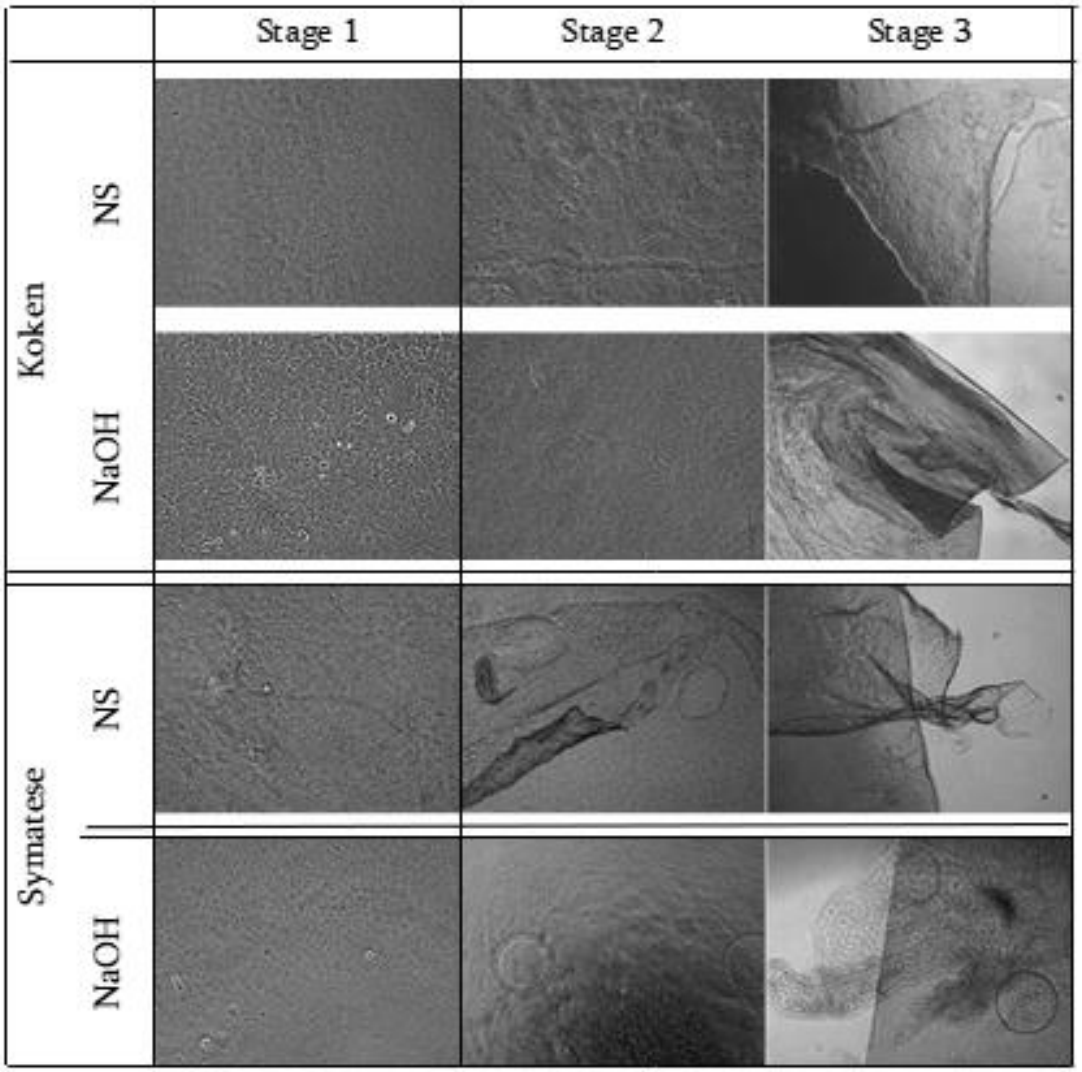

Figure S5.1 – Light microscopy photos of cell morphology on RAFT-TE prepared with *Koken* and *Symatese* collagen as well as with two different neutralisers (NS & NaOH). Focus on cell peeling: Stage 1 - Before FdA (10x); Stage 2 - After FdA & L15 (15min, before shaking, 10x); Stage 3 - Cut in 6 pieces, 15min shaking, fix (10x). Post-this all the RAFT-TEs were analysed as a whole to remove the stress of the cut step.

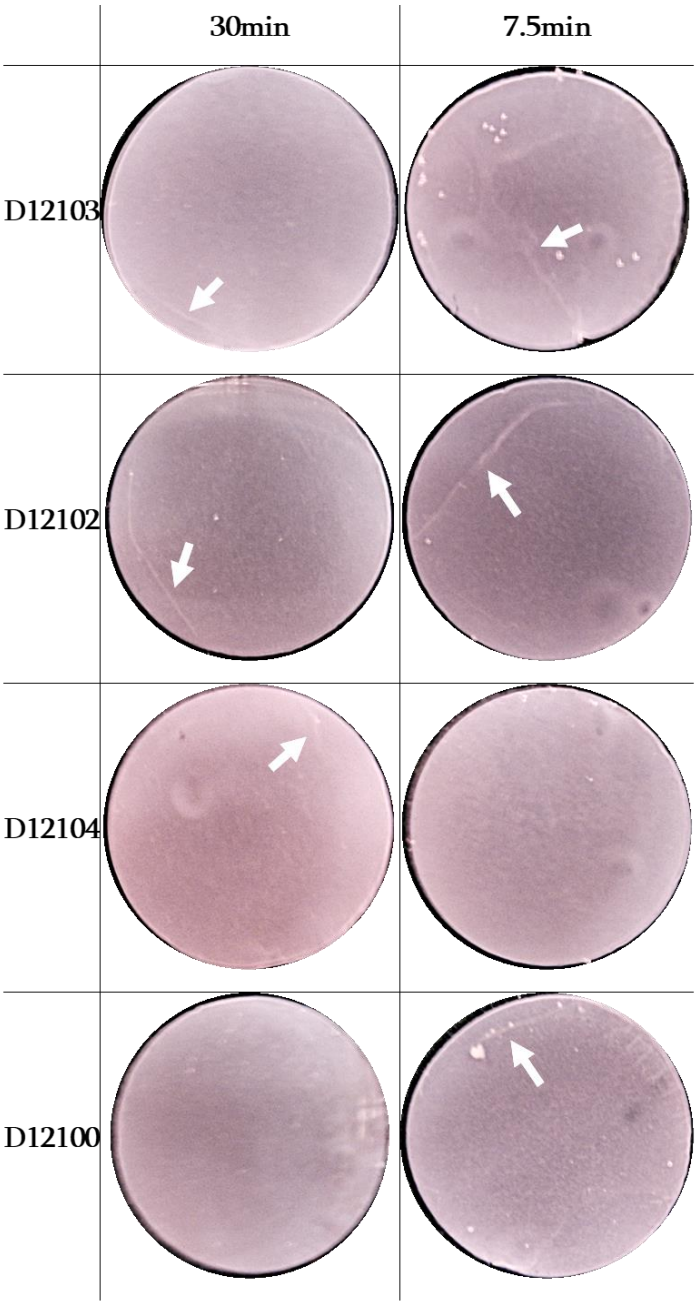

Figure S5.2 – Photo of epithelial cell layer detachment in confluent RAFT-TEs after 15min of shaking (13 days in culture). Comparison between 30min and 7.5min compressed TEs. White arrows point at areas where the cell layer is detaching.

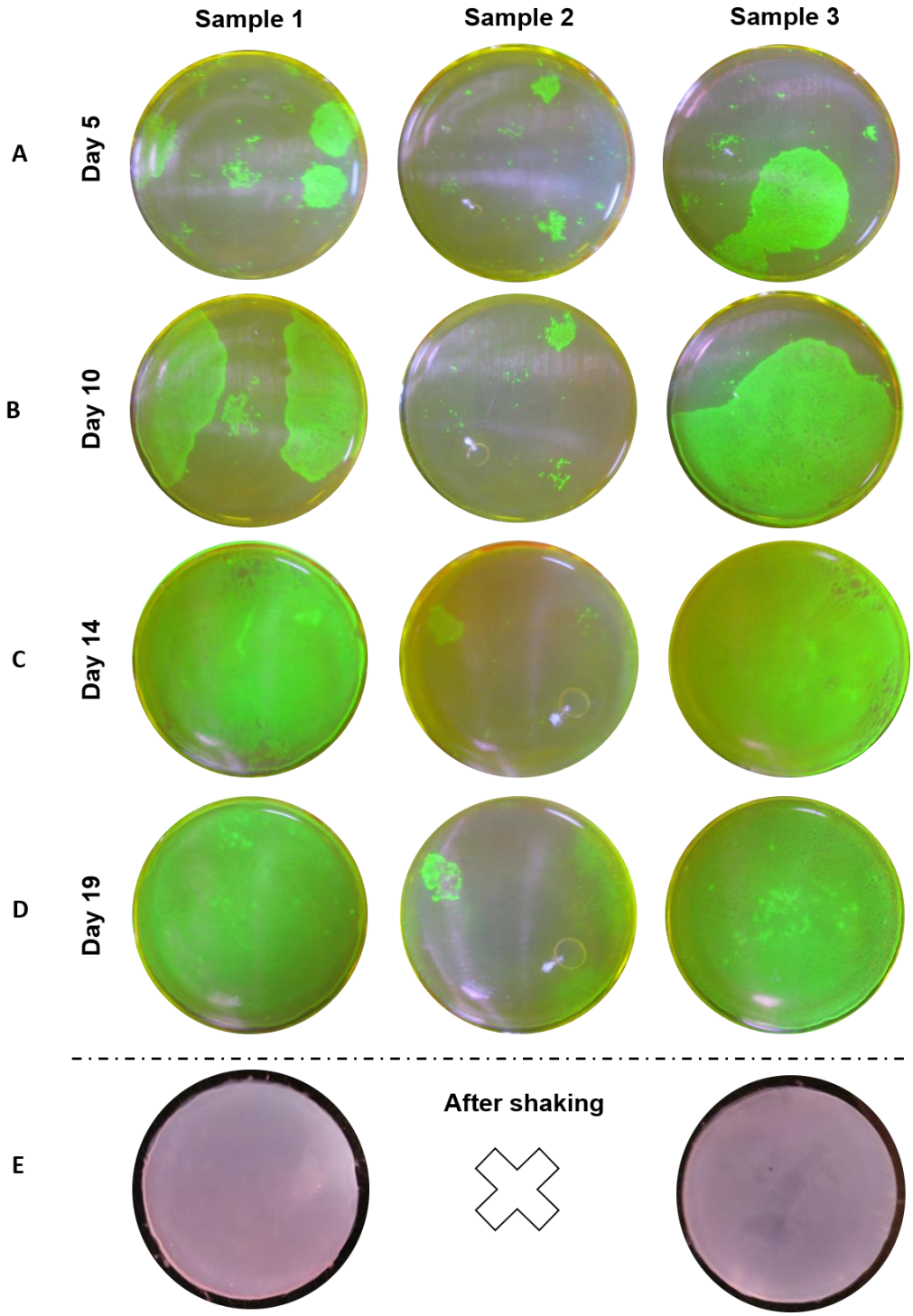

Figure S5.3 – FdA images of RAFT-TEs seeded with Direct dispase method. Growth tack over time (A- d5, B- d10, C-d14 and D-d19). (E) Photo of epithelial cell layer macroscopic appearance in confluent RAFT-TEs after 15min of shaking.

8.4. Appendix – Chapter 6

Videos of z-stacks and 3D projections of CSSC inside (30K, 50K and 100K) RAFT-TE can be found on the attached multimedia support. This data can be found inside Chapter 6 folder under the name "Cell clustering confocal videos".

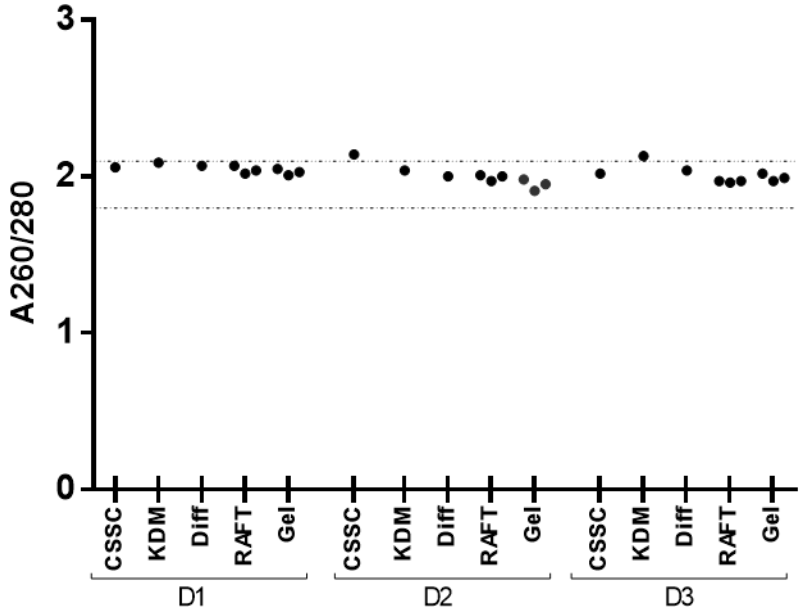

Figure S6.1 – Plot of RNA quality (A260/280) for all the samples analysed on section II by qPCR: CSSC, KDM, Diff, RAFT and Gel of three different donors.

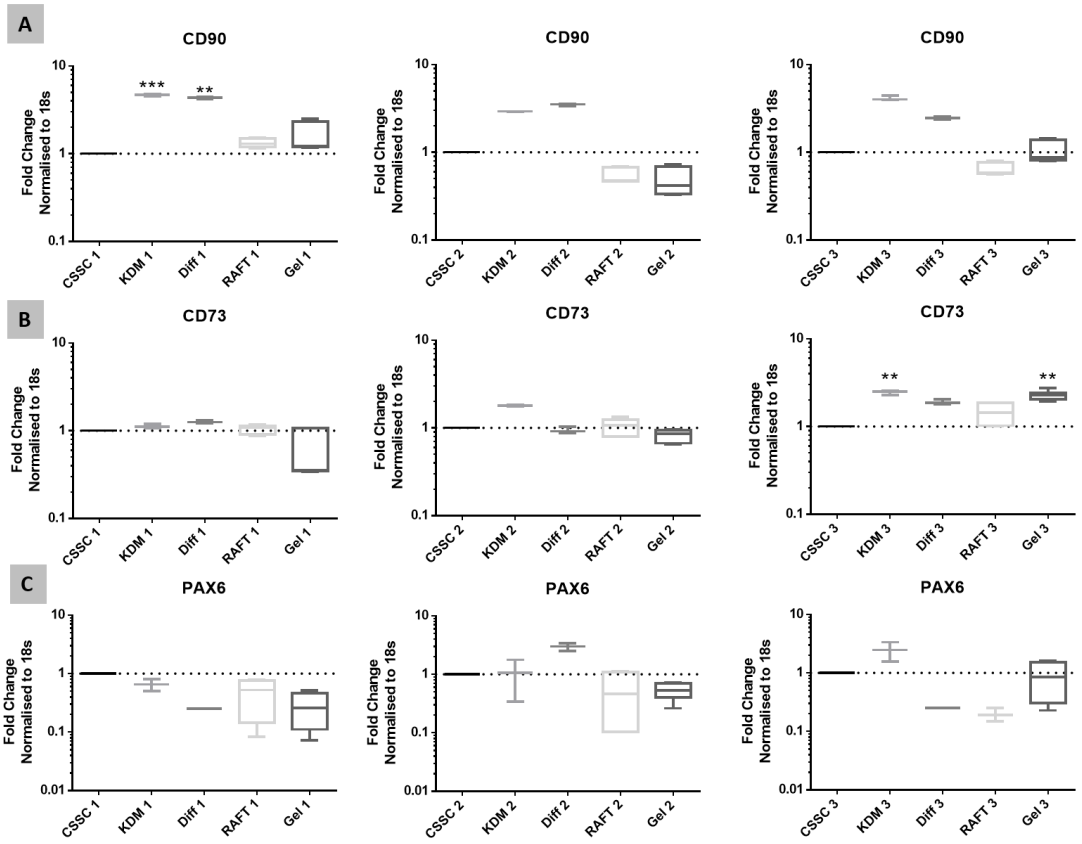

Figure S6.2 – Expression of PAX6 (gene expressed in early eye development) and mesenchymal stem cell markers CD90 and CD73 by: *KDM*- CSSCs differentiated for 3 weeks in KDM (Keratocyte differentiation media), *Diff*- cells spontaneously differentiated for 3 weeks in CSSC media, *RAFT* – CSSCs cultured inside RAFT-TEs for 3 weeks in CSSC media and *Gel* - CSSCs cultured inside non-/compressed RAFT-TEs for 3 weeks in CSSC media in comparison to *CSSC*- CSSCs at P6 cultured on CSSC media assessed by Real Time qPCR. (Data is represented in a boxplot with the technical replicates of each donor, n=3, Kruskal-Wallis test followed by Dunn's multiple comparison test where *p≤0.05, **p≤0.01). Dash line represents the basal expression of the markers of interests when cells are cultured in CSSC media. Abbreviations: (A) CD90- Cluster of Differentiation 90 (also known as Thy-1), (B) CD73 - Cluster of Differentiation 73 & (C) PAX6- Paired box protein Pax-6.

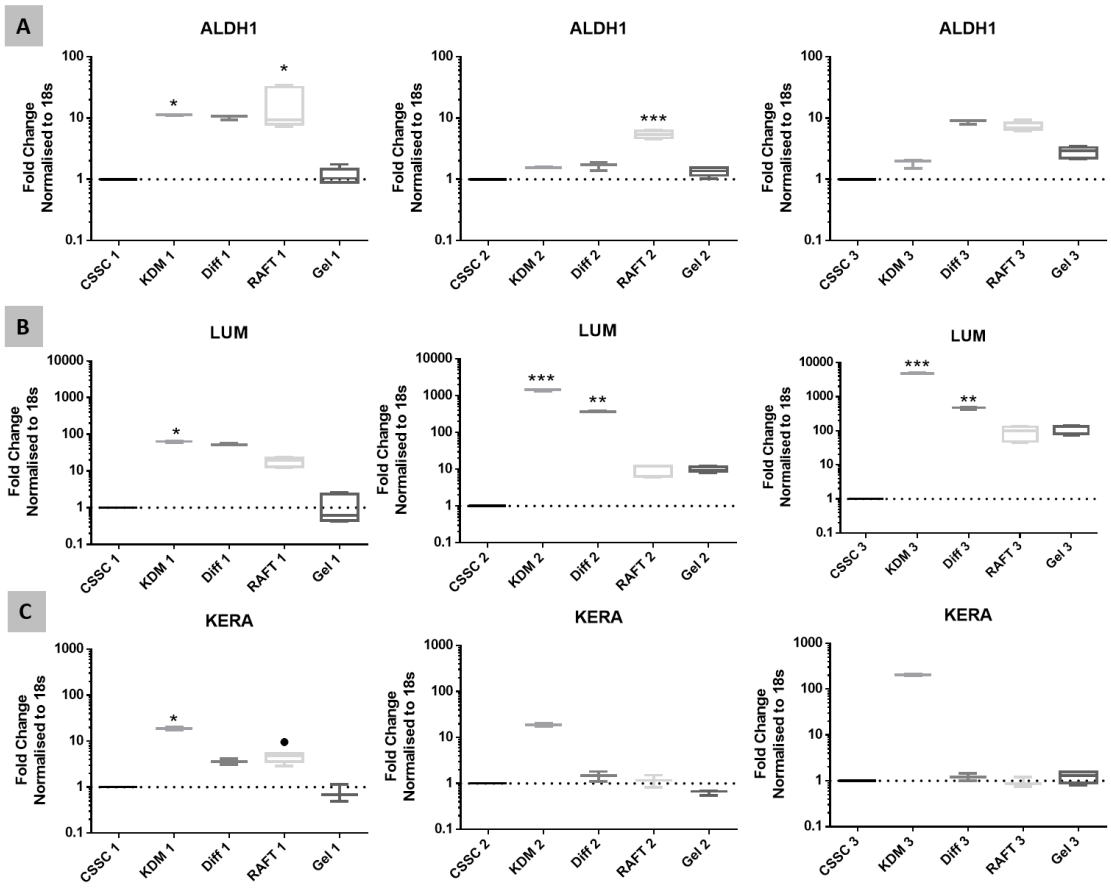

Figure S6.3 – Expression of keratocyte markers LUM, KERA and ALDH1 by: *KDM*- CSSCs differentiated for 3 weeks in KDM (Keratocyte differentiation media), *Diff*- cells spontaneously differentiated for 3 weeks in CSSC media, *RAFT* – CSSCs cultured inside RAFT-TEs for 3 weeks in CSSC media and *Gel* - CSSCs cultured inside non-compressed RAFT-TEs for 3 weeks in CSSC media in comparison to *CSSC*- CSSCs at P6 cultured on CSSC media assessed by Real Time qPCR. (Data is represented in a boxplot with the technical replicates of each donor, n=3, Kruskal-Wallis test followed by Dunn's multiple comparison test where **p≤0.01, ****p≤ 0.0001). Dash line represents the basal expression of the markers of interests when cells are cultured in CSSC media. Abbreviations: (A) ALDH1 - Aldehyde Dehydrogenase 1 Family Member A1, (B) LUM- Lumican & (C) KERA – Keratocan.

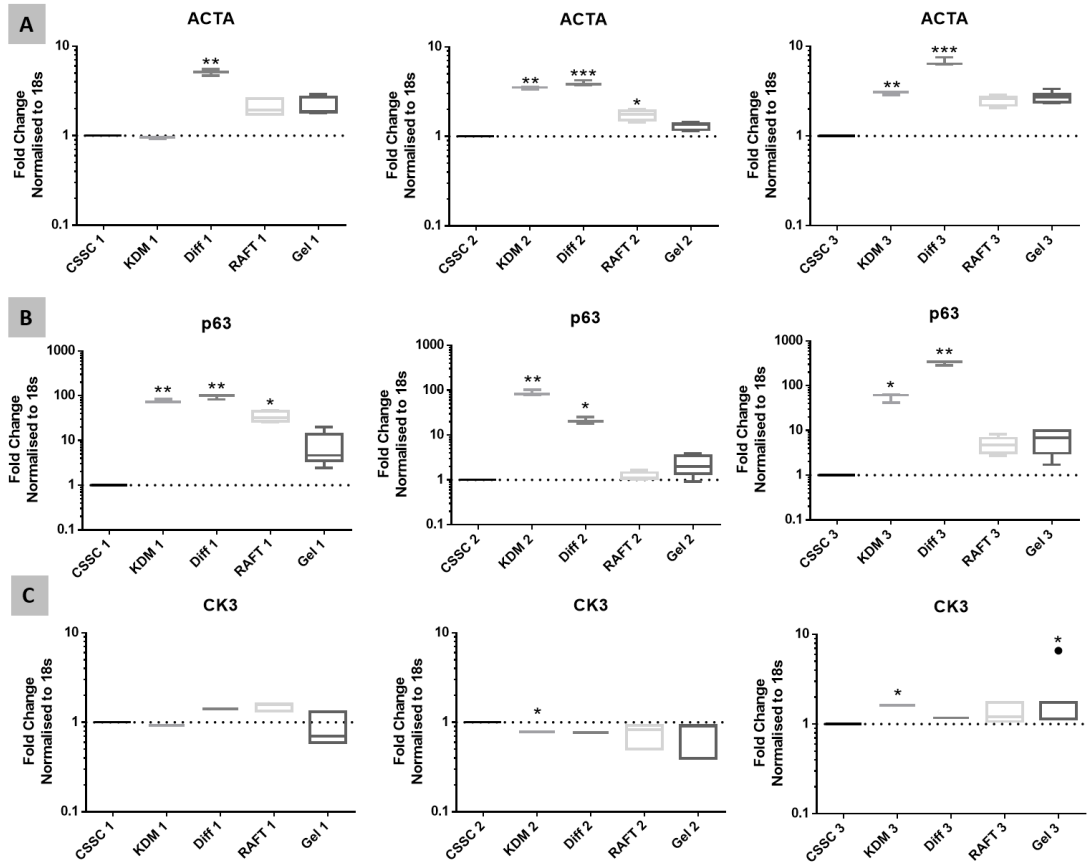

Figure S6.4 – Expression of ΔNp63, CK3 and ACTA by: KDM- CSSCs differentiated for 3 weeks in KDM (Keratocyte differentiation media), Diff- cells spontaneously differentiated for 3 weeks in CSSC media, RAFT – CSSCs cultured inside RAFT-TEs for 3 weeks in CSSC media and Gel - CSSCs cultured inside non-compressed RAFT-TEs for 3 weeks in CSSC media in comparison to CSSC- CSSCs at P6 cultured on CSSC media assessed by Real Time qPCR. (Data is represented in a boxplot with the technical replicates of each donor, n=3, Kruskal-Wallis test followed by Dunn's multiple comparison test where *p≤0.05, **p≤0.01, ****p≤ 0.0001). Dash line represents the basal expression of the markers of interests when cells are cultured in CSSC media. Abbreviations: (A) ACTA- alpha-smooth actin, (B) p63 – ΔNp63 & (C) CK3- Cytokeratin 3.

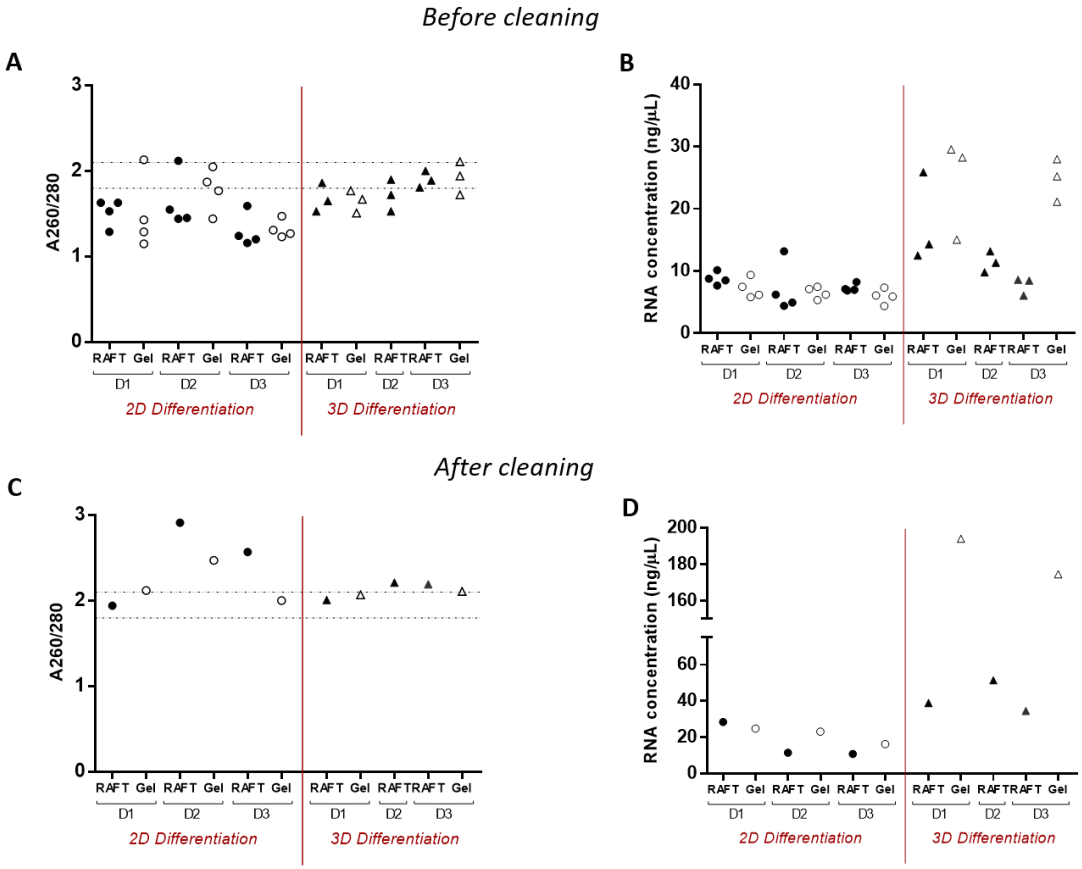

Figure S6.5 – Plot of RNA quality (A260/280) and RNA concentration for all the samples analysed on section III by qPCR before and after the cleaning process: 2D differentiation ('2D+3D' RAFT & Gel – CSSCs differentiated in TCP for 3weeks + 1week in RAFT-TE or Gel in KDM media) and 3D differentiation ('3D' RAFT & Gel – CSSCs directly seeded onto 3D structures and differentiated for 3 weeks in KDM media) of RAFT & Gel of three different donors.

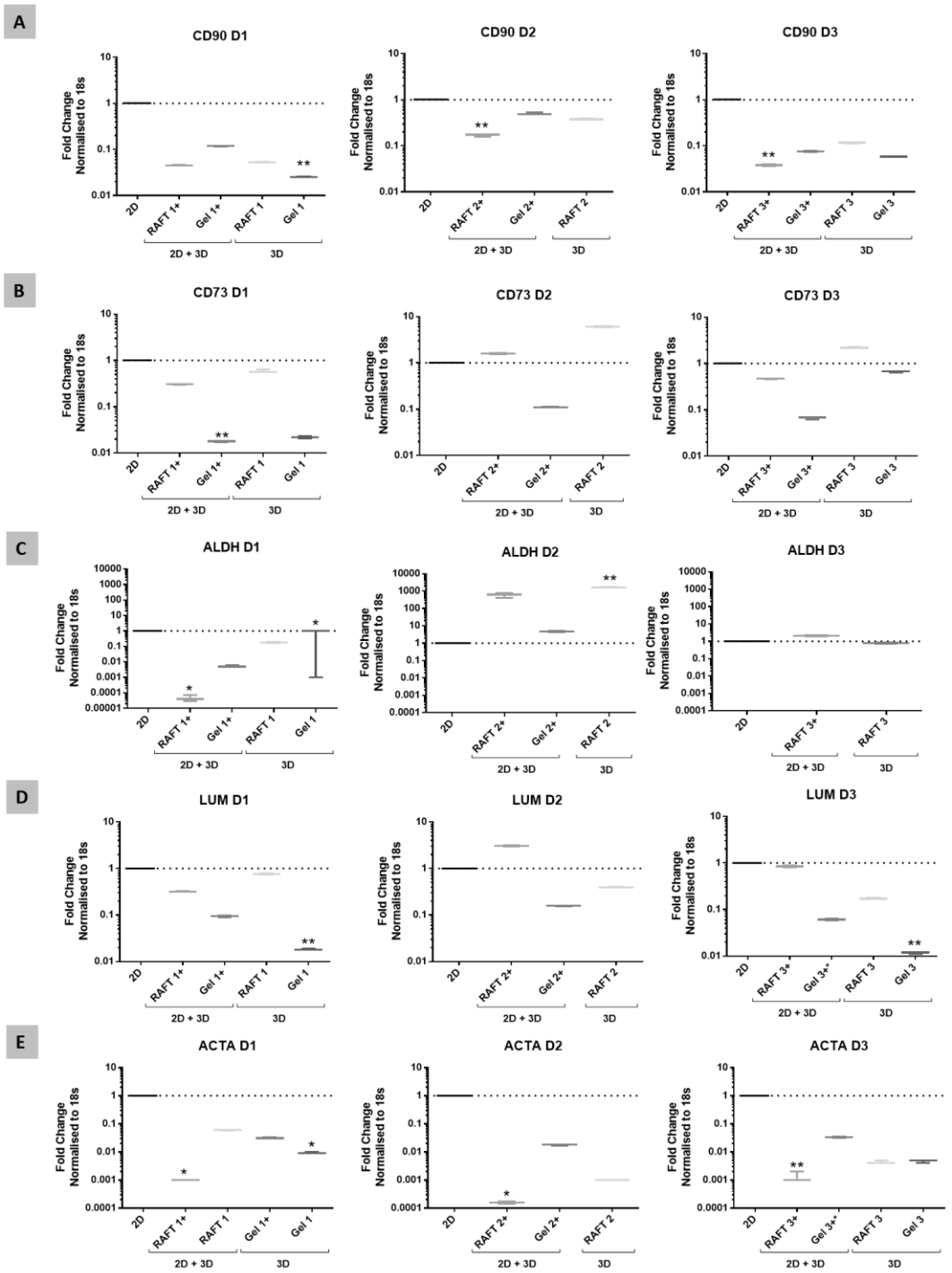

Figure S6.6 – Expression of mesenchymal stem cell markers (CD90 & CD73), keratocyte markers (LUM & ALDH1) and ACTA by: '2D+3D' RAFT & Gel – CSSCs differentiated in TCP for 3weeks + 1week in RAFT-TE or Gel in KDM media and '3D' RAFT & Gel – CSSCs directly seeded onto 3D structures and differentiated for 3 weeks in KDM media assessed by Real Time qPCR. Data is represented in a boxplot with the technical replicates of each donor, n=3, Kruskal-Wallis test followed by Dunn's multiple comparison test where *p≤0.05, **p≤0.01). Dash line represents the basal expression of the markers of interests when cells are cultured in TCP for 3 weeks in KDM media (2D). Abbreviations: (A) CD90- Cluster of Differentiation 90 (also known as Thy-1), (B) CD73 - Cluster of Differentiation 73, (C) ALDH1 - Aldehyde Dehydrogenase 1 Family Member A1, (D) LUM- Lumican & (E) ACTA- alpha-smooth actin.

Live imaging of CSSC cultured for two weeks inside RAFT-TE with and without PDGF can be found on the attached multimedia support. Figure S6.7 is representative of the video timeframes. This data can be found inside Chapter 6 folder under the name "PDGF Live imaging videos".

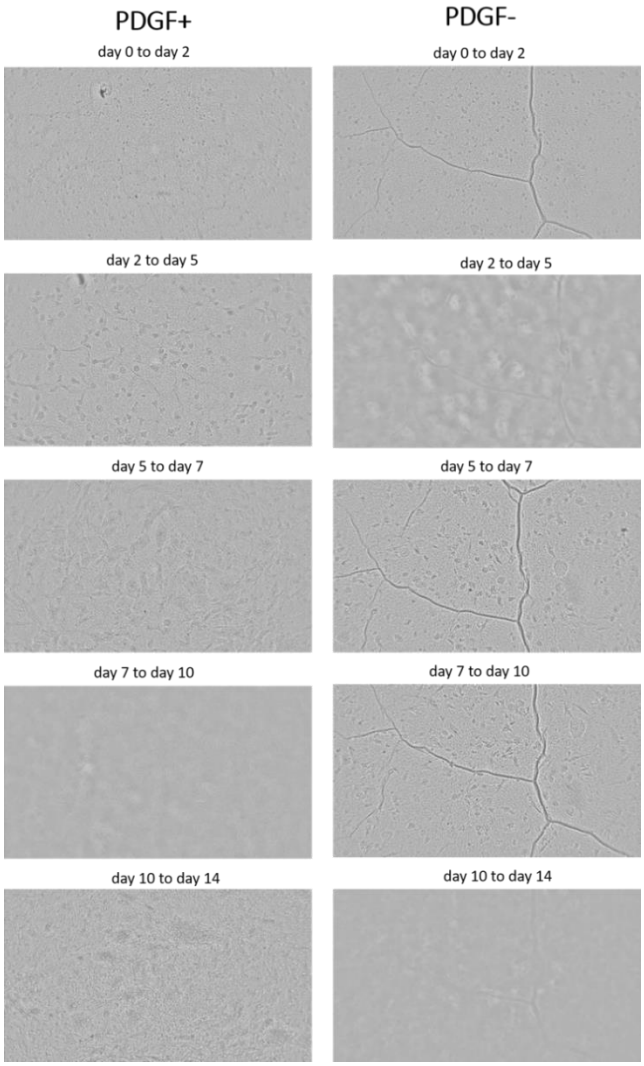

Figure S6.7 – Live imaging of CSSC inside RAFT-TE with and without PDGF over two weeks of culture. Videos can be found on the attached multimedia support.

Table S6.1 – Summary of the differences in CSSC behaviour when cultured for two weeks inside RAFT-TE (with and without PDGF) based on live-cell imaging.

Days of culture	PDGF+	PDGF-
0 to 2	Cells were more active than in PDGF-; Change from single cells to small clusters; Matrix disruption; Few cells at the surface with a kiss & run behaviour.	Cells moved less than when in PDGF+. Clusters started to form and to grow on the spot.
2 to 5	Clusters got more prominent and a lot of movement could be observed within them; Some very motile and elongated cells reached the surface around day 3-4; Some of the clusters started to join by breaking the surrounding matrix.	Some cells started to be observed at the surface, however less elongated, and with shorter movements than when in PDGF+; Clusters got larger but did not join others.
5 to 7	A lot of activity could be observed within the clusters, but also at the surface; Clusters kept enlarging, joining the ones in their surroundings and getting less uniform; Cells at the surface displayed a smaller and less elongated morphology when cell density increased.	Clusters did not grow as much as when in PDGF+, kept the rounded shape and original placement; Fewer cells could be observed at the surface and no areas of confluency could be observed.
7 to 10	The surface of the TE was very confluent and, from day 9, the cells started to reorganize themselves in an oriented way; Cell clusters were very big, joined and almost impossible to be distinguished since day 9.	Some more cells could be observed at the surface, but very few when compared to PDGF+; The ones at the surface had prominent triangular morphology, and slowly moved around by extending filopodia; Clusters grew slightly but kept the uniform rounded shape.
10 to 14	Cells at the surface aligned in parallel and perpendicular directions; Darker regions could be observed in the cluster areas.	More cells could be observed at the surface, but still less than in PDGF+; Clusters could not be observed due to the cells at the surface.

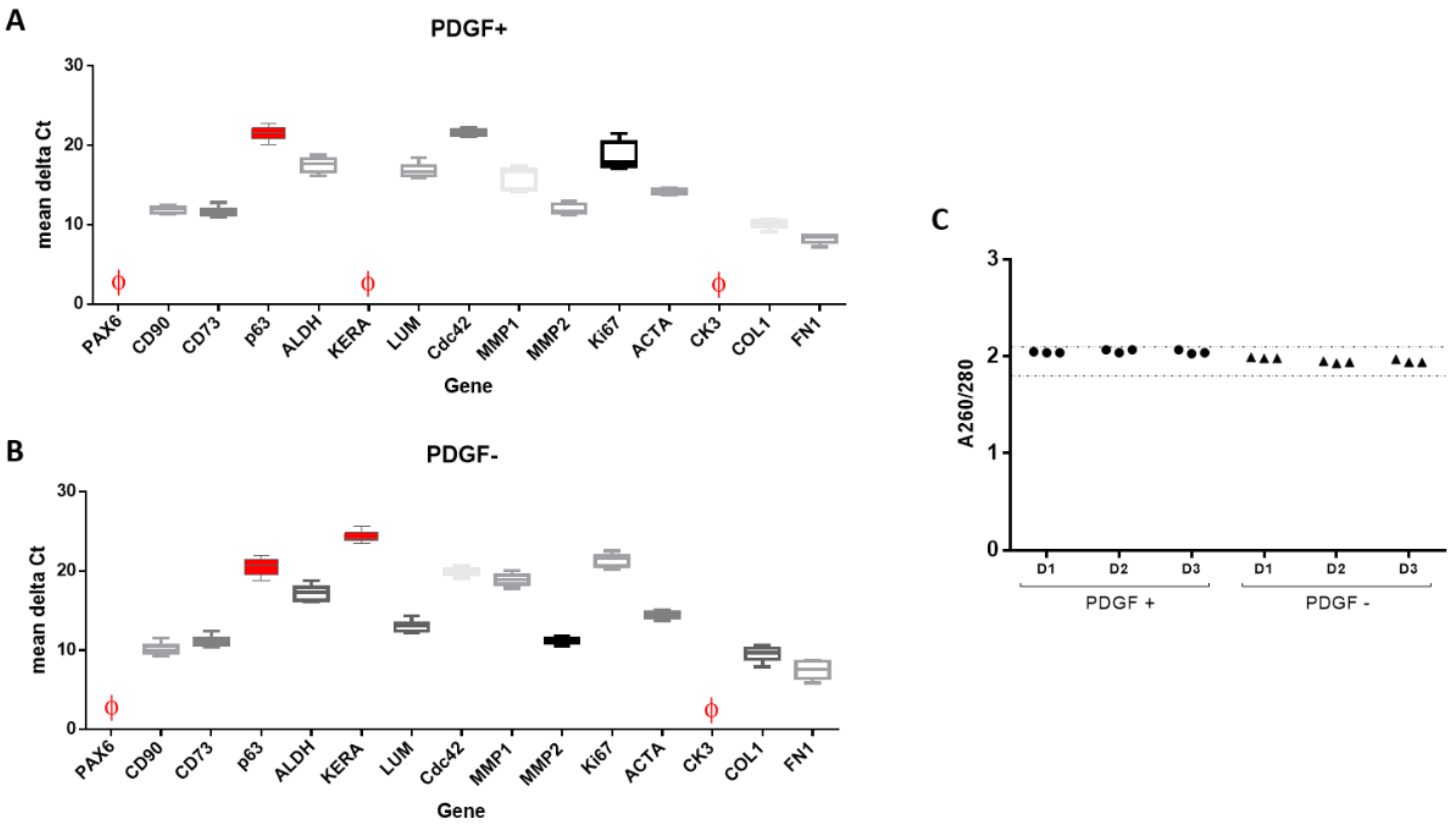

Figure S6.8 – Plot of mean delta Ct of **(A)** PDGF+, **(B)** PDGF – conditions for all the genes and **(C)** RNA quality (A260/280) for all the samples analysed on section IV by qPCR. Red box plots represent genes with mean delta Ct with high variance. Abbreviations: ϕ represents gene expression not detectable, PAX6- Paired box protein Pax-6, CD90- Cluster of Differentiation 90 (also known as Thy-1), CD73 - Cluster of Differentiation 73, LUM- Lumican, KERA – Keratocan, ALDH1 - Aldehyde Dehydrogenase 1 Family Member A1,MMPP1 & MMP2 - Matrix metalloproteinase-1 &2 ; FN1- Fibronectin 1, COL1- Collagen I, ACTA- alpha-smooth actin, ki67- proliferation gene and Cdc42- Cell division control protein 42 homolog.

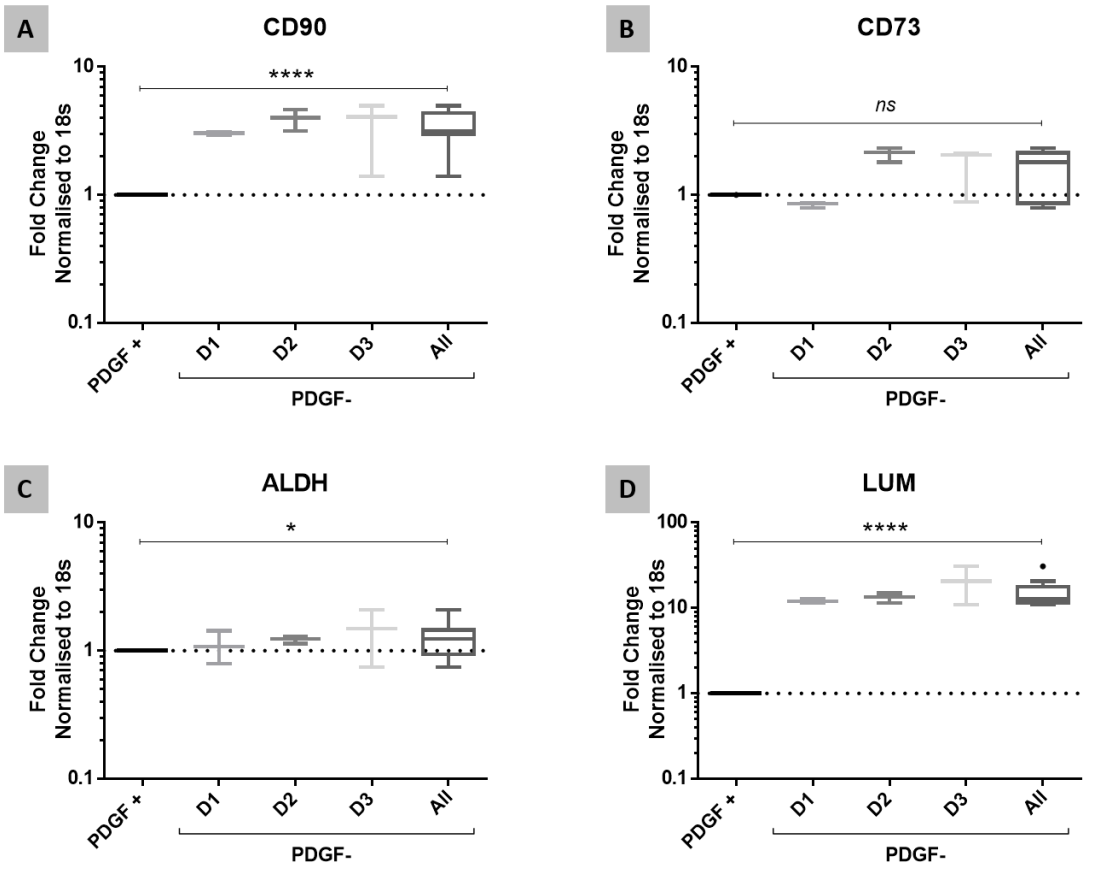

Figure S6.9 – Real Time qPCR analysis of the expression of mesenchymal stem cell markers **(A)** CD90 & **(B)** CD73) and keratocyte markers **(C)** ALDH1 & **(D)** LUM on RAFT-TE cultured with and without PDGF for 15 days. (Data is represented in a boxplot with the technical replicates of each donor, n=3, Kruskal-Wallis test followed by Dunn's multiple comparison test where *p≤0.05, **p≤0.01, ****p≤ 0.0001). Dash line represents the basal expression of the markers of interests when cells are cultured in CSSC media (with PDGF). Abbreviations: (A) CD90- Cluster of Differentiation 90 (also known as Thy-1), (B) CD73 - Cluster of Differentiation 73; (C) ALDH1 - Aldehyde Dehydrogenase 1 Family Member A1 & (D) LUM- Lumican.

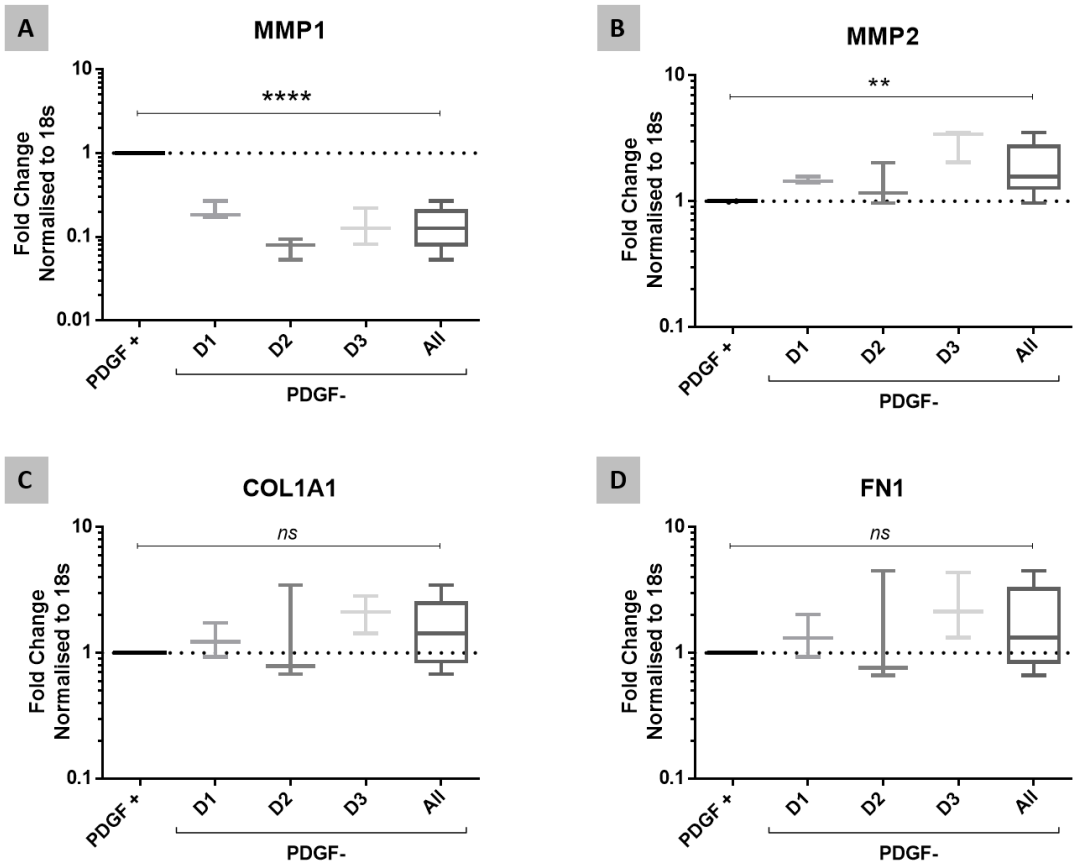

Figure S6.10 – Real Time qPCR analysis of the expression of matrix remodelling genes **(A)** MMP1 & **(B)** MMP2 and matrix production genes **(C)** COL1 & **(D)** FN1 on RAFT-TE cultured with and without PDGF for 15 days. (Data is represented in a boxplot with the technical replicates of each donor, n=3, Kruskal-Wallis test followed by Dunn's multiple comparison test where *p≤0.05, **p≤0.01, ****p≤ 0.0001). Dash line represents the basal expression of the markers of interests when cells are cultured in CSSC media (with PDGF). Abbreviations: (A, B) MMPP1 -2 - Matrix metalloproteinase-1 -2; (C) COL1- Collagen I & (D) FN1- Fibronectin 1.

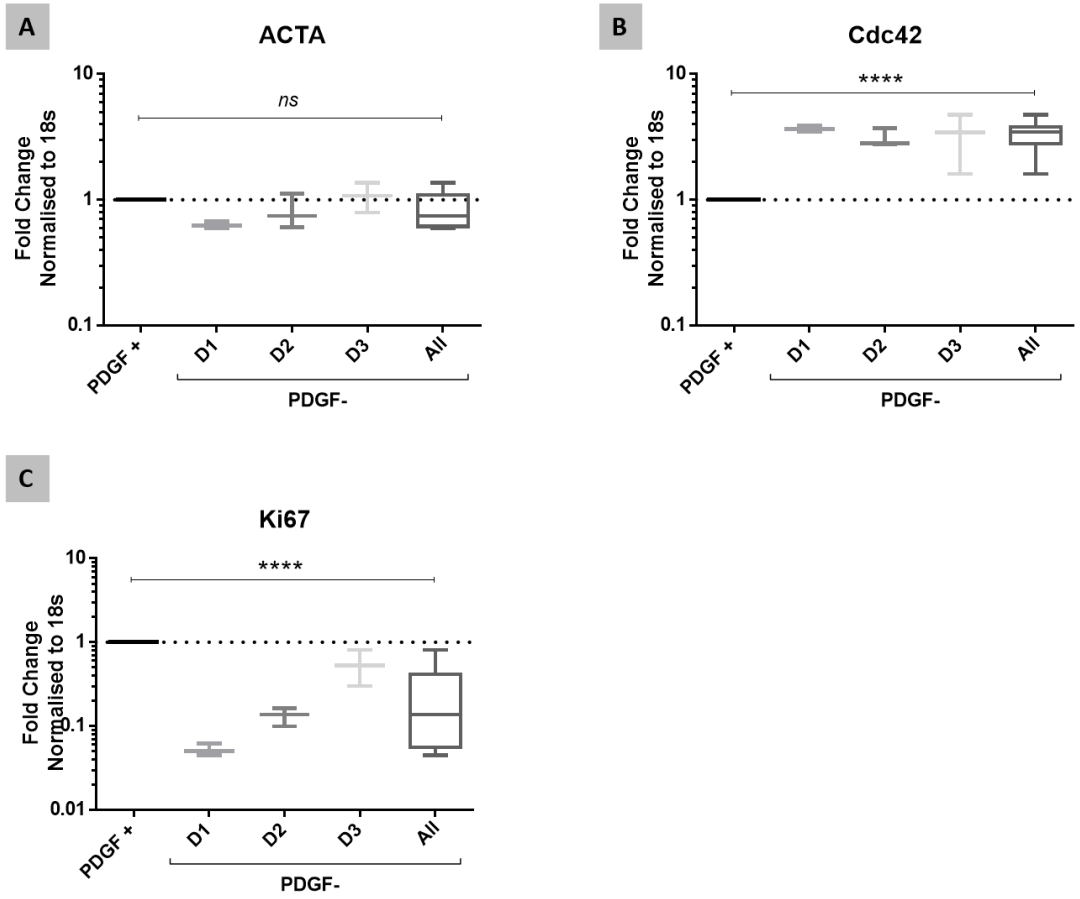

Figure S6.11 – Real Time qPCR analysis of the expression of **(A)** ACTA, **(B)** Cdc42 & **(C)** Ki67 on RAFT-TE cultured with and without PDGF for 15 days. (Data is represented in a boxplot with the technical replicates of each donor, n=3, Kruskal-Wallis test followed by Dunn's multiple comparison test where *p≤0.05, **p≤0.01, ****p≤ 0.0001). Dash line represents the basal expression of the markers of interests when cells are cultured in CSSC media (with PDGF). Abbreviations: (A) ACTA- alpha-smooth actin, (B) Cdc42- Cell division control protein 42 homolog & (C) ki67- proliferation gene.

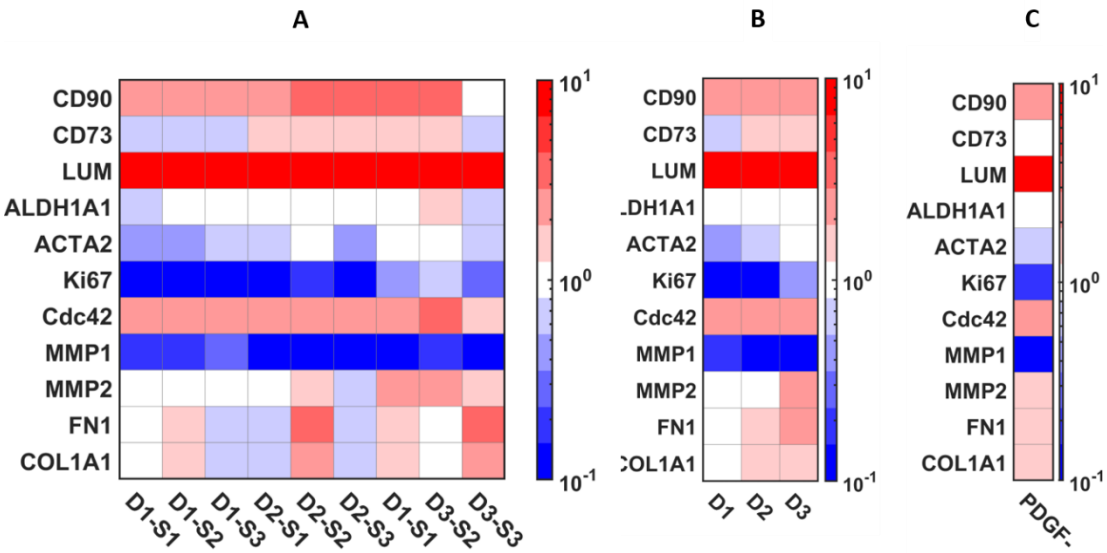

Figure S6.12 –Real Time qPCR analysis of the expression of mesenchymal stem cell markers (CD90 & CD73), keratocyte markers (LUM & ALDH1), matrix remodelling genes (MMP1 & MMP2), matrix production genes (FN1 & COL1) and ACTA, ki67 and Cdc42 on RAFT-TE cultured with and without PDGF for 15 days. Heatmap summary showing the upregulation (in red) and downregulation (in blue) of all the analysed genes on section IV by **(A)** sample, **(B)** donor and **(C)** overall.

9. REFERENCES

[1] J. A. Davis and R. R. Reed, "Role of Olf-1 and Pax-6 Transcription Factors in Neurodevelopment," *The Journal of Neuroscience,* vol. 16, no. 16, pp. 5082-5094, 1996, doi: 10.1523/jneurosci.16-16-05082.1996.

[2] D. Sevel and R. Isaacs, "A re-evaluation of corneal development," (in eng), *Trans Am Ophthalmol Soc,* vol. 86, pp. 178-207, 1988. [Online]. Available: https://www.ncbi.nlm.nih.gov/pubmed/2979018.

[3] J. M. Wolosin, M. T. Budak, and M. A. Akinci, "Ocular surface epithelial and stem cell development," (in eng), *The International journal of developmental biology,* vol. 48, no. 8-9, pp. 981-91, 2004, doi: 10.1387/ijdb.041876jw.

[4] C. E. Ghezzi, J. Rnjak-Kovacina, and D. L. Kaplan, "Corneal tissue engineering: recent advances and future perspectives," *Tissue Eng Part B Rev,* vol. 21, no. 3, pp. 278-87, Jun 2015, doi: 10.1089/ten.TEB.2014.0397.

[5] D. W. DelMonte, and Kim, T. , "Anatomy and physiology of the cornea," *J. Cataract Refract. Surg. ,* vol. 37, pp. 588-598, 2011.

[6] D. Dhouailly, D. J. Pearton, and F. Michon, "The vertebrate corneal epithelium: from early specification to constant renewal," *Dev Dyn,* vol. 243, no. 10, pp. 1226-41, Oct 2014, doi: 10.1002/dvdy.24179.

[7] J. L. Zhang, D. Upadhya, L. Lu, and L. W. Reneker, "Fibroblast Growth Factor Receptor 2 (FGFR2) Is Required for Corneal Epithelial Cell Proliferation and Differentiation during Embryonic Development," (in English), *Plos One,* vol. 10, no. 1, Jan 23 2015, doi: ARTN e0117089 10.1371/journal.pone.0117089.

[8] J. Navaratnam, T. P. Utheim, V. K. Rajasekhar, and A. Shahdadfar, "Substrates for Expansion of Corneal Endothelial Cells towards Bioengineering of Human Corneal Endothelium," *J Funct Biomater,* vol. 6, no. 3, pp. 917-45, Sep 11 2015, doi: 10.3390/jfb6030917.

[9] E. Niemi, "Hydrogels for 3D Culture of Human Corneal Cells aiming for Tissue Engineered Corneal Applicaition," Master, Tampere University of Technology, 2015.

[10] A. A. Torricelli, V. Singh, M. R. Santhiago, and S. E. Wilson, "The corneal epithelial basement membrane: structure, function, and disease," *Invest Ophthalmol Vis Sci,* vol. 54, no. 9, pp. 6390-400, Sep 2013, doi: 10.1167/iovs.13-12547.

[11] J. R. Hassell and D. E. Birk, "The molecular basis of corneal transparency," *Exp Eye Res,* vol. 91, no. 3, pp. 326-35, Sep 2010, doi: 10.1016/j.exer.2010.06.021.

[12] S. Chen, M. J. Mienaltowski, and D. E. Birk, "Regulation of corneal stroma extracellular matrix assembly," *Exp Eye Res,* vol. 133, pp. 69-80, Apr 2015, doi: 10.1016/j.exer.2014.08.001.

[13] K. M. Meek and C. Boote, "The organization of collagen in the corneal stroma," (in English), *Experimental Eye Research,* vol. 78, no. 3, pp. 503-512, Mar 2004, doi: 10.1016/j.exer.2003.07.003.

[14] W. M. Petroll and M. Miron-Mendoza, "Mechanical interactions and crosstalk between corneal keratocytes and the extracellular matrix," (in English), *Experimental Eye Research,* vol. 133, pp. 49-57, Apr 2015, doi: 10.1016/j.exer.2014.09.003.

[15] B. M. Stramer and M. E. Fini, "Uncoupling Keratocyte Loss of Corneal Crystallin from Markers of Fibrotic Repair," *Invest Ophth Vis Sci,* vol. 45, no. 11, pp. 4010-4015, 2004, doi: 10.1167/iovs.03-1057.

[16] T. Estey, J. Piatigorsky, N. Lassen, and V. Vasiliou, "ALDH3A1: a corneal crystallin with diverse functions," *Experimental Eye Research,* vol. 84, no. 1, pp. 3-12, 2007/01/01/ 2007, doi: https://doi.org/10.1016/j.exer.2006.04.010.

[17] M. P. Beales, J. L. Funderburgh, J. V. Jester, and J. R. Hassell, "Proteoglycan Synthesis by Bovine Keratocytes and Corneal Fibroblasts: Maintenance of the Keratocyte Phenotype in Culture," *Invest Ophth Vis Sci,* vol. 40, no. 8, pp. 1658-1663, 1999. [Online]. Available: https://doi.org/.

[18] A. Joseph *et al.*, "Expression of CD34 and L-Selectin on Human Corneal Keratocytes," *Invest Ophth Vis Sci,* vol. 44, no. 11, pp. 4689-4692, 2003, doi: 10.1167/iovs.02-0999.

[19] E. M. Espana, T. Kawakita, C.-Y. Liu, and S. C. G. Tseng, "CD-34 Expression by Cultured Human Keratocytes Is Downregulated during Myofibroblast Differentiation Induced by TGF-β1," *Invest Ophth Vis Sci,* vol. 45, no. 9, pp. 2985-2991, 2004, doi: 10.1167/iovs.04-0201.

[20] A. Bartakova, N. J. Kunzevitzky, and J. L. Goldberg, "Regenerative Cell Therapy for Corneal Endothelium," *Curr Ophthalmol Rep,* vol. 2, no. 3, pp. 81-90, Sep 01 2014, doi: 10.1007/s40135-014-0043-7.

[21] E. M. Espana, M. Sun, and D. E. Birk, "Existence of Corneal Endothelial Slow-Cycling Cells," *Invest Ophthalmol Vis Sci,* vol. 56, no. 6, pp. 3827-37, Jun 2015, doi: 10.1167/iovs.14-16030.

[22] N. Di Girolamo, "Stem cells of the human cornea," *British Medical Bulletin,* vol. 100, no. 1, pp. 191-207, 2011, doi: 10.1093/bmb/ldr026.

[23] M. M. Stiemke, M. D. McCartney, D. Cantu-Crouch, and H. F. Edelhauser, "Maturation of the corneal endothelial tight junction," *Invest Ophth Vis Sci,* vol. 32, no. 10, pp. 2757-2765, 1991. [Online]. Available: https://doi.org/.

[24] R. W. Yee, D. H. Geroski, M. Matsuda, E. J. Champeau, L. A. Meyer, and H. F. Edelhauser, "Correlation of corneal endothelial pump site density, barrier function, and morphology in wound repair," *Invest Ophth Vis Sci,* vol. 26, no. 9, pp. 1191-1201, 1985. [Online]. Available: https://doi.org/.

[25] S. E. Wilson and J. W. Hong, "Bowman's layer structure and function - Critical or dispensable to corneal function? A hypothesis," (in English), *Cornea,* vol. 19, no. 4, pp. 417-420, Jul 2000, doi: Doi 10.1097/00003226-200007000-00001.

[26] M. Pavelka, Roth, J., "Descemet's Membrane " in *Functional Ultrastructure*, 2010, pp. 184-185

[27] W. J. Dupps, Jr. and S. E. Wilson, "Biomechanics and wound healing in the cornea," *Exp Eye Res,* vol. 83, no. 4, pp. 709-20, Oct 2006, doi: 10.1016/j.exer.2006.03.015.

[28] E. R. Mikula, J. V. Jester, and T. Juhasz, "Measurement of an Elasticity Map in the Human Cornea," (in eng), *Investigative ophthalmology & visual science,* vol. 57, no. 7, pp. 3282-3286, 2016, doi: 10.1167/iovs.15-18248.

[29] M. Winkler *et al.*, "Three-dimensional distribution of transverse collagen fibers in the anterior human corneal stroma," (in eng), *Invest Ophthalmol Vis Sci,* vol. 54, no. 12, pp. 7293-301, Nov 5 2013, doi: 10.1167/iovs.13-13150.

[30] J. I. Ahn *et al.*, "Crosslinked collagen hydrogels as corneal implants: Effects of sterically bulky vs. non-bulky carbodiimides as crosslinkers," (in English), *Acta Biomater,* vol. 9, no. 8, pp. 7796-7805, Aug 2013, doi: 10.1016/j.actbio.2013.04.014.

[31] M. Rafat *et al.*, "PEG-stabilized carbodiimide crosslinked collagen-chitosan hydrogels for corneal tissue engineering," (in English), *Biomaterials,* vol. 29, no. 29, pp. 3960-3972, Oct 2008, doi: 10.1016/j.biomaterials.2008.06.017.

[32] Y. J. Zeng, J. Yang, K. Huang, Z. H. Lee, and X. Y. Lee, "A comparison of biomechanical properties between human and porcine cornea," (in English), *J Biomech,* vol. 34, no. 4, pp. 533-537, Apr 2001, doi: Doi 10.1016/S0021-9290(00)00219-0.

[33] G. Lepert, R. M. Gouveia, C. J. Connon, and C. Paterson, "Assessing corneal biomechanics with Brillouin spectro-microscopy," (in English), *Faraday Discuss,* vol. 187, pp. 415-428, 2016, doi: 10.1039/c5fd00152h.

[34] F. Bao, B. Geraghty, Q. Wang, and A. Elsheikh, "Consideration of corneal biomechanics in the diagnosis and management of keratoconus: is it important?," (in eng), *Eye and vision (London, England),* vol. 3, pp. 18-18, 2016, doi: 10.1186/s40662-016-0048-4.

[35] J. A. Thomson *et al.*, "Embryonic Stem Cell Lines Derived from Human Blastocysts," *Science,* vol. 282, no. 5391, p. 1145, 1998, doi: 10.1126/science.282.5391.1145.

[36] D. Ilic and J. M. Polak, "Stem cells in regenerative medicine: introduction," *British Medical Bulletin,* vol. 98, no. 1, pp. 117-126, 2011, doi: 10.1093/bmb/ldr012.

[37] V. K. Singh, M. Kalsan, N. Kumar, A. Saini, and R. Chandra, "Induced pluripotent stem cells: applications in regenerative medicine, disease modeling, and drug discovery," (in eng), *Front Cell Dev Biol,* vol. 3, pp. 2-2, 2015, doi: 10.3389/fcell.2015.00002.

[38] M. L. Lan *et al.*, "Characterizing the radioresponse of pluripotent and multipotent human stem cells," (in eng), *PloS one,* vol. 7, no. 12, pp. e50048-e50048, 2012, doi: 10.1371/journal.pone.0050048.

[39] A. P. Beltrami *et al.*, "Adult cardiac stem cells are multipotent and support myocardial regeneration," (in eng), *Cell,* vol. 114, no. 6, pp. 763-76, Sep 19 2003, doi: 10.1016/s0092-8674(03)00687-1.

[40] P. A. Zuk *et al.*, "Human adipose tissue is a source of multipotent stem cells," (in eng), *Mol Biol Cell,* vol. 13, no. 12, pp. 4279-95, Dec 2002, doi: 10.1091/mbc.e02-02-0105.

[41] N. Polisetty, A. Fatima, S. L. Madhira, V. S. Sangwan, and G. K. Vemuganti, "Mesenchymal cells from limbal stroma of human eye," (in eng), *Mol Vis,* vol. 14, pp. 431-42, Mar 4 2008.

[42] I. Ullah, R. B. Subbarao, and G. J. Rho, "Human mesenchymal stem cells - current trends and future prospective," (in eng), *Biosci Rep,* vol. 35, no. 2, p. e00191, 2015, doi: 10.1042/BSR20150025.

[43] M. Berdasco and M. Esteller, "DNA methylation in stem cell renewal and multipotency," (in eng), *Stem Cell Res Ther,* vol. 2, no. 5, pp. 42-42, 2011, doi: 10.1186/scrt83.

[44] Y. Li *et al.*, "Differences Between Niche Cells and Limbal Stromal Cells in Maintenance of Corneal Limbal Stem Cells," *Investigative Ophthalmology & Visual Science,* vol. 55, no. 3, pp. 1453-1462, 2014, doi: 10.1167/iovs.13-13698.

[45] W. Li, Y. Hayashida, Y. T. Chen, and S. C. G. Tseng, "Niche regulation of corneal epithelial stem cells at the limbus," (in English), *Cell Res,* vol. 17, no. 1, pp. 26-36, Jan 2007, doi: 10.1038/sj.cr.7310137.

[46] A. C. Romano, E. M. Espana, S. H. Yoo, M. T. Budak, J. M. Wolosin, and S. C. G. Tseng, "Different Cell Sizes in Human Limbal and Central Corneal Basal Epithelia Measured by Confocal Microscopy and Flow Cytometry," *Investigative Ophthalmology & Visual Science,* vol. 44, no. 12, pp. 5125-5129, 2003, doi: 10.1167/iovs.03-0628.

[47] Y. Barrandon and H. Green, "Three clonal types of keratinocyte with different capacities for multiplication," *Proc Natl Acad Sci U S A,* vol. 84, no. 8, pp. 2302-6, Apr 1987. [Online]. Available: https://www.ncbi.nlm.nih.gov/pubmed/2436229.

[48] S. Kawasaki, H. Tanioka, K. Yamasaki, C. J. Connon, and S. Kinoshita, "Expression and tissue distribution of p63 isoforms in human ocular surface epithelia," *Exp Eye Res,* vol. 82, no. 2, pp. 293-9, Feb 2006, doi: 10.1016/j.exer.2005.07.001.

[49] R. Hayashi *et al.*, "N-cadherin is expressed by putative stem/progenitor cells and melanocytes in the human limbal epithelial stem cell niche," (in English), *Stem Cells,* vol. 25, no. 2, pp. 289-296, Feb 2007, doi: 10.1634/stemcells.2006-0167.

[50] Z. Chen, C. S. De Paiva, L. H. Luo, F. L. Kretzer, S. C. Pflugfelder, and D. Q. Li, "Characterization of putative stem cell phenotype in human limbal epithelia," (in English), *Stem Cells,* vol. 22, no. 3, pp. 355-366, 2004, doi: DOI 10.1634/stemcells.22-3-355.

[51] K. Watanabe *et al.*, "Human limbal epithelium contains side population cells expressing the ATP-binding cassette transporter ABCG2," *FEBS Lett,* vol. 565, no. 1-3, pp. 6-10, May 07 2004, doi: 10.1016/j.febslet.2004.03.064.

[52] B. R. Ksander *et al.*, "ABCB5 is a limbal stem cell gene required for corneal development and repair," (in English), *Nature,* vol. 511, no. 7509, pp. 353-+, Jul 17 2014, doi: 10.1038/nature13426.

[53] G. Pellegrini *et al.*, "p63 identifies keratinocyte stem cells," (in English), *P Natl Acad Sci USA,* vol. 98, no. 6, pp. 3156-3161, Mar 13 2001, doi: DOI 10.1073/pnas.061032098.

[54] D. G. Harkin, Z. Barnard, P. Gillies, S. L. Ainscough, and A. J. Apel, "Analysis of p63 and cytokeratin expression in a cultivated limbal autograft used in the treatment of limbal stem cell deficiency," (in eng), *Br J Ophthalmol,* vol. 88, no. 9, pp. 1154-8, Sep 2004, doi: 10.1136/bjo.2003.037853.

[55] Y. Du, J. Chen, J. L. Funderburgh, X. Zhu, and L. Li, "Functional reconstruction of rabbit corneal epithelium by human limbal cells cultured on amniotic membrane," (in eng), *Molecular vision,* vol. 9, pp. 635-643, 2003. [Online]. Available: https://pubmed.ncbi.nlm.nih.gov/14685149.

[56] E. Di Iorio, V. Barbaro, S. Ferrari, C. Ortolani, M. De Luca, and G. Pellegrini, "Q-FIHC: quantification of fluorescence immunohistochemistry to analyse p63 isoforms and cell cycle phases in human limbal stem cells," (in eng), *Microsc Res Tech,* vol. 69, no. 12, pp. 983-91, Dec 2006, doi: 10.1002/jemt.20375.

[57] E. Di Iorio, V. Barbaro, A. Ruzza, D. Ponzin, G. Pellegrini, and M. De Luca, "Isoforms of DeltaNp63 and the migration of ocular limbal cells in human corneal regeneration," (in eng), *Proc Natl Acad Sci U S A,* vol. 102, no. 27, pp. 9523-8, Jul 5 2005, doi: 10.1073/pnas.0503437102.

[58] B. M. Koroma, J. M. Yang, and O. H. Sundin, "The Pax-6 homeobox gene is expressed throughout the corneal and conjunctival epithelia," (in English), *Invest Ophth Vis Sci,* vol. 38, no. 1, pp. 108-120, Jan 1997. [Online]. Available: <Go to ISI>://WOS:A1997WC89700013.

[59] M. Matic, I. N. Petrov, S. H. Chen, C. Wang, S. D. Dimitrijevich, and J. M. Wolosin, "Stem cells of the corneal epithelium lack connexins and metabolite transfer capacity," (in English), *Differentiation,* vol. 61, no. 4, pp. 251-260, May 1997, doi: DOI 10.1046/j.1432-0436.1997.6140251.x.

[60] A. Schermer, S. Galvin, and T. T. Sun, "Differentiation-related expression of a major 64K corneal keratin in vivo and in culture suggests limbal location of corneal epithelial stem cells," *J Cell Biol,* vol. 103, no. 1, pp. 49-62, Jul 1986. [Online]. Available: https://www.ncbi.nlm.nih.gov/pubmed/2424919.

[61] M. T. Budak, O. S. Alpdogan, M. Zhou, R. M. Lavker, M. A. Akinci, and J. M. Wolosin, "Ocular surface epithelia contain ABCG2-dependent side population cells exhibiting features associated with stem cells," (in eng), *J Cell Sci,* vol. 118, no. Pt 8, pp. 1715-24, Apr 15 2005, doi: 10.1242/jcs.02279.

[62] V. Barbaro, A. Testa, E. Di Iorio, F. Mavilio, G. Pellegrini, and M. De Luca, "C/EBPdelta regulates cell cycle and self-renewal of human limbal stem cells," (in eng), *The Journal of cell biology,* vol. 177, no. 6, pp. 1037-1049, 2007, doi: 10.1083/jcb.200703003.

[63] N. Nagai *et al.*, "Instillation of Sericin Enhances Corneal Wound Healing through the ERK Pathway in Rat Debrided Corneal Epithelium," (in eng), *International journal of molecular sciences,* vol. 19, no. 4, p. 1123, 2018, doi: 10.3390/ijms19041123.

[64] U. Schlotzer-Schrehardt and F. E. Kruse, "Identification and characterization of limbal stem cells," *Exp Eye Res,* vol. 81, no. 3, pp. 247-64, Sep 2005, doi: 10.1016/j.exer.2005.02.016.

[65] S. Yoshida *et al.*, "Cytokeratin 15 can be used to identify the limbal phenotype in normal and diseased ocular surfaces," (in eng), *Invest Ophthalmol Vis Sci,* vol. 47, no. 11, pp. 4780-6, Nov 2006, doi: 10.1167/iovs.06-0574.

[66] A. Ramirez-Miranda, M. N. Nakatsu, S. Zarei-Ghanavati, C. V. Nguyen, and S. X. Deng, "Keratin 13 is a more specific marker of conjunctival epithelium than keratin 19," (in eng), *Molecular vision,* vol. 17, pp. 1652-1661, 2011. [Online]. Available: https://pubmed.ncbi.nlm.nih.gov/21738394.

[67] A. Schermer, S. Galvin, and T. T. Sun, "Differentiation-related expression of a major 64K corneal keratin in vivo and in culture suggests limbal location of corneal epithelial stem cells," *Journal of Cell Biology,* vol. 103, no. 1, pp. 49-62, 1986, doi: 10.1083/jcb.103.1.49.

[68] A. M.-H. Yeung, U. Schlötzer-Schrehardt, B. Kulkarni, N. L. Tint, A. Hopkinson, and H. S. Dua, "Limbal Epithelial Crypt: A Model for Corneal Epithelial Maintenance and Novel Limbal Regional Variations," *JAMA Ophthalmology,* vol. 126, no. 5, pp. 665-669, 2008, doi: 10.1001/archopht.126.5.665.

[69] N. C. Joyce, B. Meklir, S. J. Joyce, and J. D. Zieske, "Cell cycle protein expression and proliferative status in human corneal cells," *Investigative Ophthalmology & Visual Science,* vol. 37, no. 4, pp. 645-655, 1996.

[70] P. B. Thomas *et al.*, "Identification of Notch-1 expression in the limbal basal epithelium," (in eng), *Molecular vision,* vol. 13, pp. 337-344, 2007. [Online]. Available: https://pubmed.ncbi.nlm.nih.gov/17392684.

[71] E. C. Figueira, N. Di Girolamo, M. T. Coroneo, and D. Wakefield, "The phenotype of limbal epithelial stem cells," *Invest Ophthalmol Vis Sci,* vol. 48, no. 1, pp. 144-56, Jan 2007, doi: 10.1167/iovs.06-0346.

[72] G. Li *et al.*, "Transcription Factor PAX6 (Paired Box 6) Controls Limbal Stem Cell Lineage in Development and Disease," (in eng), *J Biol Chem,* vol. 290, no. 33, pp. 20448-54, Aug 14 2015, doi: 10.1074/jbc.M115.662940.

[73] Y. Qu *et al.*, "Unique expression pattern and functional role of periostin in human limbal stem cells," *PLoS One,* vol. 10, no. 2, p. e0117139, 2015, doi: 10.1371/journal.pone.0117139.

[74] M. Lyngholm, H. Vorum, K. Nielsen, M. Ostergaard, B. Honore, and N. Ehlers, "Differences in the protein expression in limbal versus central human corneal epithelium--a search for stem cell markers," *Exp Eye Res,* vol. 87, no. 2, pp. 96-105, Aug 2008, doi: 10.1016/j.exer.2008.05.001.

[75] R. Lu *et al.*, "Transcription Factor TCF4 Maintains the Properties of Human Corneal Epithelial Stem Cells," *STEM CELLS,* vol. 30, no. 4, pp. 753-761, 2012, doi: 10.1002/stem.1032.

[76] J. D. Zieske, G. Bukusoglu, M. A. Yankauckas, M. E. Wasson, and H. T. Keutmann, "Alpha-enolase is restricted to basal cells of stratified squamous epithelium," (in eng), *Dev Biol,* vol. 151, no. 1, pp. 18-26, May 1992, doi: 10.1016/0012-1606(92)90209-y.

[77] R. M. Gouveia, G. Lepert, S. Gupta, R. R. Mohan, C. Paterson, and C. J. Connon, "Assessment of corneal substrate biomechanics and its effect on epithelial stem cell maintenance and differentiation," (in eng), *Nat Commun,* vol. 10, no. 1, pp. 1496-1496, 2019, doi: 10.1038/s41467-019-09331-6.

[78] R. A. Thoft and J. Friend, "The X, Y, Z hypothesis of corneal epithelial maintenance," *Invest Ophthalmol Vis Sci,* vol. 24, no. 10, pp. 1442-3, Oct 1983. [Online]. Available: https://www.ncbi.nlm.nih.gov/pubmed/6618809.

[79] G. Pellegrini, O. Golisano, A. Lambiase, S. Bonini, P. Rama, and M. De Luca, "Location and clonal analysis of stem cells and their differentiated progeny in the human ocular

surface," (in English), *Invest Ophth Vis Sci,* vol. 40, no. 4, pp. S323-S323, Mar 15 1999. [Online]. Available: <Go to ISI>://WOS:000079269201713.

[80] G. Pellegrini *et al.*, "Biological parameters determining the clinical outcome of autologous cultures of limbal stem cells," (in English), *Regen Med,* vol. 8, no. 5, pp. 553-567, Sep 2013, doi: 10.2217/rme.13.43.

[81] H. S. Dua, A. Miri, T. Alomar, A. M. Yeung, and D. G. Said, "The Role of Limbal Stem Cells in Corneal Epithelial Maintenance: Testing the Dogma," *Ophthalmology,* vol. 116, no. 5, pp. 856-863, 2009/05/01/ 2009, doi: https://doi.org/10.1016/j.ophtha.2008.12.017.

[82] F. Majo, A. Rochat, M. Nicolas, G. A. Jaoudé, and Y. Barrandon, "Oligopotent stem cells are distributed throughout the mammalian ocular surface," *Nature,* vol. 456, p. 250, 10/01/online 2008, doi: 10.1038/nature07406.

[83] J. D. West, N. J. Dorà, and J. M. Collinson, "Evaluating alternative stem cell hypotheses for adult corneal epithelial maintenance," (in eng), *World journal of stem cells,* vol. 7, no. 2, pp. 281-299, 2015, doi: 10.4252/wjsc.v7.i2.281.

[84] J. J. Yoon, S. Ismail, and T. Sherwin, "Limbal stem cells: Central concepts of corneal epithelial homeostasis," *World J Stem Cells,* vol. 6, no. 4, pp. 391-403, Sep 26 2014, doi: 10.4252/wjsc.v6.i4.391.

[85] N. Di Girolamo *et al.*, "Tracing the fate of limbal epithelial progenitor cells in the murine cornea," (in eng), *Stem Cells,* vol. 33, no. 1, pp. 157-69, Jan 2015, doi: 10.1002/stem.1769.

[86] A. Amitai-Lange, A. Altshuler, J. Bubley, N. Dbayat, B. Tiosano, and R. Shalom-Feuerstein, "Lineage tracing of stem and progenitor cells of the murine corneal epithelium," (in eng), *Stem Cells,* vol. 33, no. 1, pp. 230-9, Jan 2015, doi: 10.1002/stem.1840.

[87] P. Eberwein and T. Reinhard, "Concise Reviews: The Role of Biomechanics in the Limbal Stem Cell Niche: New Insights for Our Understanding of This Structure," *STEM CELLS,* vol. 33, no. 3, pp. 916-924, 2015, doi: 10.1002/stem.1886.

[88] H. S. Dua, V. A. Shanmuganathan, A. O. Powell-Richards, P. J. Tighe, and A. Joseph, "Limbal epithelial crypts: a novel anatomical structure and a putative limbal stem cell niche," (in eng), *Br J Ophthalmol,* vol. 89, no. 5, pp. 529-532, 2005, doi: 10.1136/bjo.2004.049742.

[89] K. Grieve *et al.*, "Three-dimensional structure of the mammalian limbal stem cell niche," *Experimental Eye Research,* vol. 140, pp. 75-84, 2015/11/01/ 2015, doi: https://doi.org/10.1016/j.exer.2015.08.003.

[90] M. F. Goldberg and A. J. Bron, "Limbal palisades of Vogt," *Trans Am Ophthalmol Soc,* Article vol. Vol. 80, pp. 155-171, 1982. [Online]. Available: https://www.scopus.com/inward/record.uri?eid=2-s2.0-0020331522&partnerID=40&md5=8c965c0c8b3b5626c3ace8c1b12ab25e.

[91] W. M. Townsend, "The limbal palisades of Vogt," *Trans Am Ophthalmol Soc,* Conference Paper vol. 89, pp. 721-756, 1991. [Online]. Available: https://www.scopus.com/inward/record.uri?eid=2-s2.0-0026329897&partnerID=40&md5=2b95e1ddc13569605a90c8955cfe571a.

[92] V. A. Shanmuganathan *et al.*, "Morphological characteristics of the limbal epithelial crypt," *Brit J Ophthalmol,* vol. 91, no. 4, p. 514, 2007, doi: 10.1136/bjo.2006.102640.

[93] M. Nubile *et al.*, "Pathological changes of the anatomical structure and markers of the limbal stem cell niche due to inflammation," *Molecular Vision,* Article vol. 19, pp. 516-525, 2013. [Online]. Available: https://www.scopus.com/inward/record.uri?eid=2-s2.0-84874437325&partnerID=40&md5=b01e372ad30c305e67fbe96c83d6f196.

[94] R. K. Molvær *et al.*, "Interactive 3D computer model of the human corneolimbal region: crypts, projections and stem cells," *Acta Ophthalmol,* vol. 91, no. 5, pp. 457-462, 2013, doi: 10.1111/j.1755-3768.2012.02446.x.

[95] K. Bizheva, N. Hutchings, L. Sorbara, A. A. Moayed, and T. Simpson, "In vivo volumetric imaging of the human corneo-scleral limbus with spectral domain OCT," *Biomed. Opt. Express,* vol. 2, no. 7, pp. 1794-1802, 2011/07/01 2011, doi: 10.1364/BOE.2.001794.

[96] K. L. Lathrop, D. Gupta, L. Kagemann, J. S. Schuman, and N. SundarRaj, "Optical Coherence Tomography as a Rapid, Accurate, Noncontact Method of Visualizing the Palisades of Vogt," *Invest Ophth Vis Sci,* vol. 53, no. 3, pp. 1381-1387, 2012, doi: 10.1167/iovs.11-8524.

[97] A. J. Shortt, G. A. Secker, P. M. Munro, P. T. Khaw, S. J. Tuft, and J. T. Daniels, "Characterization of the Limbal Epithelial Stem Cell Niche: Novel Imaging Techniques Permit In Vivo Observation and Targeted Biopsy of Limbal Epithelial Stem Cells," *STEM CELLS,* vol. 25, no. 6, pp. 1402-1409, 2007, doi: 10.1634/stemcells.2006-0580.

[98] M. A. Dziasko, H. E. Armer, H. J. Levis, A. J. Shortt, S. Tuft, and J. T. Daniels, "Localisation of epithelial cells capable of holoclone formation in vitro and direct interaction with stromal cells in the native human limbal crypt," *PLoS One,* vol. 9, no. 4, p. e94283, 2014, doi: 10.1371/journal.pone.0094283.

[99] A. Miri *et al.*, "In vivo confocal microscopic features of normal limbus," *Brit J Ophthalmol,* vol. 96, no. 4, pp. 530-536, 2012, doi: 10.1136/bjophthalmol-2011-300550.

[100] S. X. Deng, K. D. Sejpal, Q. Tang, A. J. Aldave, O. L. Lee, and F. Yu, "Characterization of limbal stem cell deficiency by in vivo laser scanning confocal microscopy: a microstructural approach," (in eng), *Arch Ophthalmol,* vol. 130, no. 4, pp. 440-445, 2012, doi: 10.1001/archophthalmol.2011.378.

[101] S. Fujisawa *et al.*, "Understanding the three-dimensional world from two-dimensional immunofluorescent adjacent sections," (in eng), *Journal of pathology informatics,* vol. 6, pp. 27-27, 2015, doi: 10.4103/2153-3539.158052.

[102] D. S. Richardson and J. W. Lichtman, "Clarifying Tissue Clearing," *Cell,* vol. 162, no. 2, pp. 246-257, 2015, doi: 10.1016/j.cell.2015.06.067.

[103] Y. Henning, C. Osadnik, and E. P. Malkemper, "EyeCi: Optical clearing and imaging of immunolabeled mouse eyes using light-sheet fluorescence microscopy," *Experimental Eye Research,* vol. 180, pp. 137-145, 2019/03/01/ 2019, doi: https://doi.org/10.1016/j.exer.2018.12.001.

[104] B. Hohberger, C. Baumgart, and A. Bergua, "Optical clearing of the eye using the See Deep Brain technique," *Eye,* vol. 31, no. 10, pp. 1496-1502, 2017/10/01 2017, doi: 10.1038/eye.2017.83.

[105] C. Prahst *et al.*, "Mouse retinal cell behaviour in space and time using light sheet fluorescence microscopy," *eLife,* vol. 9, p. e49779, 2020/02/19 2020, doi: 10.7554/eLife.49779.

[106] S. Zhao *et al.*, "Cellular and Molecular Probing of Intact Transparent Human Organs," *bioRxiv,* p. 643908, 2019, doi: 10.1101/643908.

[107] M. Dominici *et al.*, "Minimal criteria for defining multipotent mesenchymal stromal cells. The International Society for Cellular Therapy position statement," *Cytotherapy,* vol. 8, no. 4, pp. 315-317, 2006/01/01/ 2006, doi: https://doi.org/10.1080/14653240600855905.

[108] A. I. Caplan, "Mesenchymal Stem Cells: Time to Change the Name!," (in eng), *Stem Cells Transl Med,* vol. 6, no. 6, pp. 1445-1451, Jun 2017, doi: 10.1002/sctm.17-0051.

[109] D. Sipp, P. G. Robey, and L. Turner, "Clear up this stem-cell mess," (in eng), *Nature,* vol. 561, no. 7724, pp. 455-457, Sep 2018, doi: 10.1038/d41586-018-06756-9.

[110] M. L. Orozco Morales, N. M. Marsit, O. D. McIntosh, A. Hopkinson, and L. E. Sidney, "Anti-inflammatory potential of human corneal stroma-derived stem cells determined by a novel in vitro corneal epithelial injury model," (in eng), *World journal of stem cells,* vol. 11, no. 2, pp. 84-99, 2019, doi: 10.4252/wjsc.v11.i2.84.

[111] A. J. Hertsenberg, G. Shojaati, M. L. Funderburgh, M. M. Mann, Y. Du, and J. L. Funderburgh, "Corneal stromal stem cells reduce corneal scarring by mediating neutrophil infiltration after wounding," (in eng), *PloS one,* vol. 12, no. 3, pp. e0171712-e0171712, 2017, doi: 10.1371/journal.pone.0171712.

[112] N. Pinnamaneni and J. L. Funderburgh, "Concise review: Stem cells in the corneal stroma," (in eng), *Stem cells (Dayton, Ohio),* vol. 30, no. 6, pp. 1059-1063, 2012, doi: 10.1002/stem.1100.

[113] S. Basu *et al.*, "Human limbal biopsy-derived stromal stem cells prevent corneal scarring," (in eng), *Sci Transl Med,* vol. 6, no. 266, p. 266ra172, Dec 10 2014, doi: 10.1126/scitranslmed.3009644.

[114] Y. Du, M. L. Funderburgh, M. M. Mann, N. SundarRaj, and J. L. Funderburgh, "Multipotent stem cells in human corneal stroma," *Stem Cells,* vol. 23, no. 9, pp. 1266-75, Oct 2005, doi: 10.1634/stemcells.2004-0256.

[115] M. L. Funderburgh, Y. Du, M. M. Mann, N. SundarRaj, and J. L. Funderburgh, "PAX6 expression identifies progenitor cells for corneal keratocytes," (in eng), *FASEB J,* vol. 19, no. 10, pp. 1371-1373, 2005, doi: 10.1096/fj.04-2770fje.

[116] Y. Du *et al.*, "Stem cell therapy restores transparency to defective murine corneas," (in eng), *Stem cells (Dayton, Ohio),* vol. 27, no. 7, pp. 1635-1642, 2009, doi: 10.1002/stem.91.

[117] V. S. Sangwan, N. Gupta, A. Singh, and S. MacNeil, "Cutting corners, or simplifying technology to reach more patients; using the body as its own incubator for epithelial regeneration," *Indian Journal of Ophthalmology,* vol. 67, no. 8, pp. 1261-1263, 2019, doi: 10.4103/ijo.IJO_632_19.

[118] D. J. Prockop and J. Y. Oh, "Mesenchymal stem/stromal cells (MSCs): role as guardians of inflammation," (in eng), *Mol Ther,* vol. 20, no. 1, pp. 14-20, Jan 2012, doi: 10.1038/mt.2011.211.

[119] W. T. Tse, J. D. Pendleton, W. M. Beyer, M. C. Egalka, and E. C. Guinan, "Suppression of allogeneic T-cell proliferation by human marrow stromal cells: implications in transplantation," (in eng), *Transplantation,* vol. 75, no. 3, pp. 389-97, Feb 15 2003, doi: 10.1097/01.Tp.0000045055.63901.A9.

[120] A. I. Caplan and J. E. Dennis, "Mesenchymal stem cells as trophic mediators," (in eng), *J Cell Biochem,* vol. 98, no. 5, pp. 1076-84, Aug 1 2006, doi: 10.1002/jcb.20886.

[121] A. K. Kureshi, J. L. Funderburgh, and J. T. Daniels, "Human corneal stromal stem cells exhibit survival capacity following isolation from stored organ-culture corneas," *Invest Ophthalmol Vis Sci,* vol. 55, no. 11, pp. 7583-8, Oct 21 2014, doi: 10.1167/iovs.14-14448.

[122] S. H. Park, K. W. Kim, Y. S. Chun, and J. C. Kim, "Human mesenchymal stem cells differentiate into keratocyte-like cells in keratocyte-conditioned medium," (in English), *Experimental Eye Research,* vol. 101, pp. 16-26, Aug 2012, doi: 10.1016/j.exer.2012.05.009.

[123] J. Wu, Y. Du, S. C. Watkins, J. L. Funderburgh, and W. R. Wagner, "The engineering of organized human corneal tissue through the spatial guidance of corneal stromal stem cells," (in eng), *Biomaterials,* vol. 33, no. 5, pp. 1343-1352, 2012, doi: 10.1016/j.biomaterials.2011.10.055.

[124] G. H. F. Yam, A. K. Riau, M. L. Funderburgh, J. S. Mehta, and V. Jhanji, "Keratocyte biology," *Experimental Eye Research,* p. 108062, 2020/05/19/ 2020, doi: https://doi.org/10.1016/j.exer.2020.108062.

[125] K. Higa, S. Shimmura, H. Miyashita, J. Shimazaki, and K. Tsubota, "Melanocytes in the corneal limbus interact with K19-positive basal epithelial cells," (in eng), *Exp Eye Res,* vol. 81, no. 2, pp. 218-23, Aug 2005, doi: 10.1016/j.exer.2005.01.023.

[126] M. A. Dziasko, S. J. Tuft, and J. T. Daniels, "Limbal melanocytes support limbal epithelial stem cells in 2D and 3D microenvironments," (in eng), *Exp Eye Res,* vol. 138, pp. 70-9, Sep 2015, doi: 10.1016/j.exer.2015.06.026.

[127] A. K. Kureshi, M. Dziasko, J. L. Funderburgh, and J. T. Daniels, "Human corneal stromal stem cells support limbal epithelial cells cultured on RAFT tissue equivalents," *Sci Rep,* vol. 5, p. 16186, 2015, doi: 10.1038/srep16186.

[128] M. N. Nakatsu, S. González, H. Mei, and S. X. Deng, "Human limbal mesenchymal cells support the growth of human corneal epithelial stem/progenitor cells," (in eng), *Invest Ophthalmol Vis Sci,* vol. 55, no. 10, pp. 6953-9, Oct 2 2014, doi: 10.1167/iovs.14-14999.

[129] S. Y. Chen, Y. Hayashida, M. Y. Chen, H. T. Xie, and S. C. Tseng, "A new isolation method of human limbal progenitor cells by maintaining close association with their niche cells," (in eng), *Tissue Eng Part C Methods,* vol. 17, no. 5, pp. 537-48, May 2011, doi: 10.1089/ten.TEC.2010.0609.

[130] D. G. Phinney and M. F. Pittenger, "Concise Review: MSC-Derived Exosomes for Cell-Free Therapy," (in eng), *Stem Cells,* vol. 35, no. 4, pp. 851-858, Apr 2017, doi: 10.1002/stem.2575.

[131] G. Shojaati *et al.*, "Mesenchymal Stem Cells Reduce Corneal Fibrosis and Inflammation via Extracellular Vesicle-Mediated Delivery of miRNA," (in eng), *Stem Cells Transl Med,* vol. 8, no. 11, pp. 1192-1201, Nov 2019, doi: 10.1002/sctm.18-0297.

[132] W. H. Organization. "Prevention of blindness and visual impairment: priority eye diseases. ." (accessed 2016).

[133] A. V. Ljubimov and M. Saghizadeh, "Progress in corneal wound healing," *Prog Retin Eye Res,* vol. 49, pp. 17-45, Nov 2015, doi: 10.1016/j.preteyeres.2015.07.002.

[134] I. L. Tsai, C. C. Hsu, K. H. Hung, C. W. Chang, and Y. H. Cheng, "Applications of biomaterials in corneal wound healing," *J Chin Med Assoc,* vol. 78, no. 4, pp. 212-7, Apr 2015, doi: 10.1016/j.jcma.2014.09.011.

[135] K. M. Meek and C. Knupp, "Corneal structure and transparency," *Prog Retin Eye Res,* vol. 49, pp. 1-16, Nov 2015, doi: 10.1016/j.preteyeres.2015.07.001.

[136] C. Osei-Bempong, F. C. Figueiredo, and M. Lako, "The limbal epithelium of the eye--a review of limbal stem cell biology, disease and treatment," *Bioessays,* vol. 35, no. 3, pp. 211-9, Mar 2013, doi: 10.1002/bies.201200086.

[137] S. Ahmad, S. Kolli, M. Lako, F. Figueiredo, and J. T. Daniels, "Stem cell therapies for ocular surface disease," *Drug Discovery Today,* vol. 15, no. 7, pp. 306-313, 2010/04/01/ 2010, doi: https://doi.org/10.1016/j.drudis.2010.02.001.

[138] H. S. Dua and A. Azuara-Blanco, "Limbal stem cells of the corneal epithelium," (in English), *Surv Ophthalmol,* vol. 44, no. 5, pp. 415-425, Mar-Apr 2000, doi: Doi 10.1016/S0039-6257(00)00109-0.

[139] M. Haagdorens *et al.*, "Limbal Stem Cell Deficiency: Current Treatment Options and Emerging Therapies," (in English), *Stem Cells Int,* 2016, doi: Artn 9798374 10.1155/2016/9798374.

[140] S. Ahmad, "Concise Review: Limbal Stem Cell Deficiency, Dysfunction, and Distress," (in English), *Stem Cell Transl Med,* vol. 1, no. 2, pp. 110-115, Feb 2012, doi: 10.5966/sctm.2011-0037.

[141] T. E. Clinch, K. M. Goins, and L. M. Cobo, "Treatment of Contact Lens-related Ocular Surface Disorders with Autologous Conjunctival Transplantation," *Ophthalmology,* vol. 99, no. 4, pp. 634-638, 1992/04/01/ 1992, doi: https://doi.org/10.1016/S0161-6420(92)31925-6.

[142] K. Sejpal, P. Bakhtiari, and S. X. Deng, "Presentation, diagnosis and management of limbal stem cell deficiency," (in eng), *Middle East Afr J Ophthalmol,* vol. 20, no. 1, pp. 5-10, Jan-Mar 2013, doi: 10.4103/0974-9233.106381.

[143] A. Fatima, G. Iftekhar, V. S. Sangwan, and G. K. Vemuganti, "Ocular surface changes in limbal stem cell deficiency caused by chemical injury: a histologic study of excised pannus from recipients of cultured corneal epithelium," *Eye,* Clinical Study vol. 22, p. 1161, 06/08/online 2007, doi: 10.1038/sj.eye.6702895.

[144] J. Hong *et al.*, "In vivo confocal microscopy of conjunctival goblet cells in patients with Sjögren's syndrome dry eye," *Brit J Ophthalmol,* vol. 94, no. 11, p. 1454, 2010, doi: 10.1136/bjo.2009.161059.

[145] N. Efron, M. Al-Dossari, and N. Pritchard, "In vivo confocal microscopy of the bulbar conjunctiva," *Clinical & Experimental Ophthalmology,* vol. 37, no. 4, pp. 335-344, 2009/05/01 2009, doi: 10.1111/j.1442-9071.2009.02065.x.

[146] V. S. Sangwan, S. Basu, S. MacNeil, and D. Balasubramanian, "Simple limbal epithelial transplantation (SLET): a novel surgical technique for the treatment of unilateral limbal stem cell deficiency," (in eng), *Br J Ophthalmol,* vol. 96, no. 7, pp. 931-4, Jul 2012, doi: 10.1136/bjophthalmol-2011-301164.

[147] C. Sotozono *et al.*, "Visual improvement after cultivated oral mucosal epithelial transplantation," (in eng), *Ophthalmology,* vol. 120, no. 1, pp. 193-200, Jan 2013, doi: 10.1016/j.ophtha.2012.07.053.

[148] P. Gain *et al.*, "Global Survey of Corneal Transplantation and Eye Banking," (in eng), *JAMA Ophthalmol,* vol. 134, no. 2, pp. 167-73, Feb 2016, doi: 10.1001/jamaophthalmol.2015.4776.

[149] V. Romano, M. Dinsdale, and S. Kaye, "Compensating for a shortage of corneal donors after Brexit," *The Lancet,* vol. 394, no. 10200, p. 732, 2019/08/31/ 2019, doi: https://doi.org/10.1016/S0140-6736(19)31099-2.

[150] A. M. Williams and K. W. Muir, "Awareness and attitudes toward corneal donation: challenges and opportunities," (in eng), *Clin Ophthalmol,* vol. 12, pp. 1049-1059, 2018, doi: 10.2147/opth.S142702.

[151] D. Pascolini and S. P. Mariotti, "Global estimates of visual impairment: 2010," (in English), *Brit J Ophthalmol,* vol. 96, no. 5, pp. 614-618, May 2012, doi: 10.1136/bjophthalmol-2011-300539.

[152] W. J. Dupps, Jr. and S. E. Wilson, "Biomechanics and wound healing in the cornea," (in eng), *Experimental eye research,* vol. 83, no. 4, pp. 709-720, 2006, doi: 10.1016/j.exer.2006.03.015.

[153] B. Salvador-Culla and P. E. Kolovou, "Keratoprosthesis: A Review of Recent Advances in the Field," (in eng), *Journal of functional biomaterials,* vol. 7, no. 2, p. 13, 2016, doi: 10.3390/jfb7020013.

[154] M. Ahearne, J. Fernández-Pérez, S. Masterton, P. W. Madden, and P. Bhattacharjee, "Designing Scaffolds for Corneal Regeneration," *Advanced Functional Materials,* vol. n/a, no. n/a, p. 1908996, 2020/02/18 2020, doi: 10.1002/adfm.201908996.

[155] N. P. Singh, D. G. Said, and H. S. Dua, "Lamellar keratoplasty techniques," (in eng), *Indian journal of ophthalmology,* vol. 66, no. 9, pp. 1239-1250, 2018, doi: 10.4103/ijo.IJO_95_18.

[156] T. D. Keenan, F. Carley, D. Yeates, M. N. Jones, S. Rushton, and M. J. Goldacre, "Trends in corneal graft surgery in the UK," (in eng), *Br J Ophthalmol,* vol. 95, no. 4, pp. 468-72, Apr 2011, doi: 10.1136/bjo.2010.182329.

[157] M. W. Grinstaff, "Designing hydrogel adhesives for corneal wound repair," (in English), *Biomaterials,* vol. 28, no. 35, pp. 5205-5214, Dec 2007, doi: 10.1016/j.biomaterials.2007.08.041.

[158] J. Menzel-Severing, F. E. Kruse, and U. Schlotzer-Schrehardt, "Stem cell-based therapy for corneal epithelial reconstruction: present and future," (in English), *Can J Ophthalmol,* vol. 48, no. 1, pp. 13-21, Feb 2013, doi: 10.1016/j.jcjo.2012.11.009.

[159] E. J. Tocce, V. K. Smirnov, D. S. Kibalov, S. J. Liliensiek, C. J. Murphy, and P. F. Nealey, "The ability of corneal epithelial cells to recognize high aspect ratio nanostructures," (in English), *Biomaterials,* vol. 31, no. 14, pp. 4064-4072, May 2010, doi: 10.1016/j.biomaterials.2010.01.101.

[160] P. B. Malafaya, G. A. Silva, and R. L. Reis, "Natural-origin polymers as carriers and scaffolds for biomolecules and cell delivery in tissue engineering applications," (in English), *Adv Drug Deliver Rev,* vol. 59, no. 4-5, pp. 207-233, May 30 2007, doi: 10.1016/j.addr.2007.03.012.

[161] A. S. Hoffman, "Hydrogels for biomedical applications," (in English), *Adv Drug Deliver Rev,* vol. 54, no. 1, pp. 3-12, Jan 17 2002, doi: Doi 10.1016/S0169-409x(01)00239-3.

[162] N. Annabi *et al.*, "25th Anniversary Article: Rational Design and Applications of Hydrogels in Regenerative Medicine," (in English), *Adv Mater,* vol. 26, no. 1, pp. 85-124, Jan 2014, doi: 10.1002/adma.201303233.

[163] K. Gelse, E. Poschl, and T. Aigner, "Collagens - structure, function, and biosynthesis," (in English), *Adv Drug Deliver Rev,* vol. 55, no. 12, pp. 1531-1546, Nov 28 2003, doi: 10.1016/j.addr.2003.08.002.

[164] H. J. Levis, R. A. Brown, and J. T. Daniels, "Plastic compressed collagen as a biomimetic substrate for human limbal epithelial cell culture," (in English), *Biomaterials,* vol. 31, no. 30, pp. 7726-7737, Oct 2010, doi: 10.1016/j.biomaterials.2010.07.012.

[165] M. Koulikovska *et al.*, "Enhanced Regeneration of Corneal Tissue via a Bioengineered Collagen Construct Implanted by a Nondisruptive Surgical Technique," (in English), *Tissue Eng Pt A,* vol. 21, no. 5-6, pp. 1116-1130, Mar 1 2015, doi: 10.1089/ten.tea.2014.0562.

[166] W. Liu *et al.*, "Recombinant human collagen for tissue engineered corneal substitutes," (in eng), *Biomaterials,* vol. 29, no. 9, pp. 1147-58, Mar 2008, doi: 10.1016/j.biomaterials.2007.11.011.

[167] B. Wright, P. A. De Bank, K. A. Luetchford, F. R. Acosta, and C. J. Connon, "Oxidized alginate hydrogels as niche environments for corneal epithelial cells," (in English), *Journal of Biomedical Materials Research Part A,* vol. 102, no. 10, pp. 3393-3400, Oct 2014, doi: 10.1002/jbm.a.35011.

[168] A. de la Mata *et al.*, "Chitosan-gelatin biopolymers as carrier substrata for limbal epithelial stem cells," (in English), *J Mater Sci-Mater M,* vol. 24, no. 12, pp. 2819-2829, Dec 2013, doi: 10.1007/s10856-013-5013-3.

[169] P. Rama, S. Matuska, G. Paganoni, A. Spinelli, M. De Luca, and G. Pellegrini, "Limbal Stem-Cell Therapy and Long-Term Corneal Regeneration," (in English), *Hum Gene Ther,* vol. 21, no. 10, pp. 1393-1394, Oct 2010.

[170] M. Grolik *et al.*, "Hydrogel membranes based on genipin-cross-linked chitosan blends for corneal epithelium tissue engineering," (in English), *J Mater Sci-Mater M,* vol. 23, no. 8, pp. 1991-2000, Aug 2012, doi: 10.1007/s10856-012-4666-7.

[171] S. Koo, S. J. Ahn, H. Zhang, J. C. Wang, and E. K. F. Yim, "Human Corneal Keratocyte Response to Micro- and Nano-Gratings on Chitosan and PDMS," (in English), *Cell Mol Bioeng,* vol. 4, no. 3, pp. 399-410, Sep 2011, doi: 10.1007/s12195-011-0186-7.

[172] J. Wu, Y. Q. Du, M. M. Mann, J. L. Funderburgh, and W. R. Wagner, "Corneal stromal stem cells versus corneal fibroblasts in generating structurally appropriate corneal stromal tissue," (in English), *Experimental Eye Research,* vol. 120, pp. 71-81, Mar 2014, doi: 10.1016/j.exer.2014.01.005.

[173] Y. Q. Feng, M. Borrelli, T. Meyer-ter-Vehn, S. Reichl, S. Schrader, and G. Geerling, "Epithelial Wound Healing on Keratin Film, Amniotic Membrane and Polystyrene In

Vitro," (in English), *Curr Eye Res,* vol. 39, no. 6, pp. 561-570, Jun 2014, doi: 10.3109/02713683.2013.853804.

[174] G. Uzunalli *et al.*, "Bioactive self-assembled peptide nanofibers for corneal stroma regeneration," (in English), *Acta Biomater,* vol. 10, no. 3, pp. 1156-1166, Mar 2014, doi: 10.1016/j.actbio.2013.12.002.

[175] J. Wu, J. Rnjak-Kovacina, Y. Q. Du, M. L. Funderburgh, D. L. Kaplan, and J. L. Funderburgh, "Corneal stromal bioequivalents secreted on patterned silk substrates," (in English), *Biomaterials,* vol. 35, no. 12, pp. 3744-3755, Apr 2014, doi: 10.1016/j.biomaterials.2013.12.078.

[176] S. Sharma, D. Gupta, S. Mohanty, M. Jassal, A. K. Agrawal, and R. Tandon, "Surface-modified electrospun poly(epsilon-caprolactone) scaffold with improved optical transparency and bioactivity for damaged ocular surface reconstruction," *Invest Ophthalmol Vis Sci,* vol. 55, no. 2, pp. 899-907, Feb 12 2014, doi: 10.1167/iovs.13-12727.

[177] P. Deshpande *et al.*, "Simplifying corneal surface regeneration using a biodegradable synthetic membrane and limbal tissue explants," (in English), *Biomaterials,* vol. 34, no. 21, pp. 5088-5106, Jul 2013, doi: 10.1016/j.biomaterials.2013.03.064.

[178] E. S. Gil, B. B. Mandal, S. H. Park, J. K. Marchant, F. G. Omenetto, and D. L. Kaplan, "Helicoidal multi-lamellar features of RGD-functionalized silk biomaterials for corneal tissue engineering," (in English), *Biomaterials,* vol. 31, no. 34, pp. 8953-8963, Dec 2010, doi: 10.1016/j.biomaterials.2010.08.017.

[179] S. Bobba, S. Chow, S. Watson, and N. Di Girolamo, "Clinical outcomes of xeno-free expansion and transplantation of autologous ocular surface epithelial stem cells via contact lens delivery: a prospective case series," (in English), *Stem Cell Res Ther,* vol. 6, Mar 12 2015, doi: ARTN 23 10.1186/s13287-015-0009-1.

[180] L. J. Bray, K. A. George, D. W. Hutmacher, T. V. Chirila, and D. G. Harkin, "A dual-layer silk fibroin scaffold for reconstructing the human corneal limbus," (in English), *Biomaterials,* vol. 33, no. 13, pp. 3529-3538, May 2012, doi: 10.1016/j.biomaterials.2012.01.045.

[181] C. R. McLaughlin *et al.*, "Regeneration of functional nerves within full thickness collagen-phosphorylcholine corneal substitute implants in guinea pigs," (in eng), *Biomaterials,* vol. 31, no. 10, pp. 2770-8, Apr 2010, doi: 10.1016/j.biomaterials.2009.12.031.

[182] C. Petsch, U. Schlötzer-Schrehardt, E. Meyer-Blazejewska, M. Frey, F. E. Kruse, and B. O. Bachmann, "Novel collagen membranes for the reconstruction of the corneal surface," (in eng), *Tissue Eng Part A,* vol. 20, no. 17-18, pp. 2378-89, Sep 2014, doi: 10.1089/ten.TEA.2013.0552.

[183] A. Tidu *et al.*, "Development of human corneal epithelium on organized fibrillated transparent collagen matrices synthesized at high concentration," (in English), *Acta Biomaterialia,* vol. 22, pp. 50-58, Aug 2015, doi: 10.1016/j.actbio.2015.04.018.

[184] I. Massie, A. K. Kureshi, S. Schrader, A. J. Shortt, and J. T. Daniels, "Optimization of optical and mechanical properties of real architecture for 3-dimensional tissue equivalents: Towards treatment of limbal epithelial stem cell deficiency," (in English), *Acta Biomater,* vol. 24, pp. 241-250, Sep 15 2015, doi: 10.1016/j.actbio.2015.06.007.

[185] J. J. Chae *et al.*, "Regeneration of corneal epithelium utilizing a collagen vitrigel membrane in rabbit models for corneal stromal wound and limbal stem cell deficiency," (in eng), *Acta Ophthalmol,* vol. 93, no. 1, pp. e57-66, Feb 2015, doi: 10.1111/aos.12503.

[186] N. Builles *et al.*, "Use of magnetically oriented orthogonal collagen scaffolds for hemi-corneal reconstruction and regeneration," (in eng), *Biomaterials,* vol. 31, no. 32, pp. 8313-22, Nov 2010, doi: 10.1016/j.biomaterials.2010.07.066.

[187] M. Koulikovska *et al.*, "Enhanced regeneration of corneal tissue via a bioengineered collagen construct implanted by a nondisruptive surgical technique," (in eng), *Tissue Eng Part A,* vol. 21, no. 5-6, pp. 1116-30, Mar 2015, doi: 10.1089/ten.TEA.2014.0562.

[188] V. Kishore, R. Iyer, A. Frandsen, and T.-U. Nguyen, "In vitro characterization of electrochemically compacted collagen matrices for corneal applications," *Biomedical Materials,* vol. 11, no. 5, p. 055008, 2016/10/06 2016, doi: 10.1088/1748-6041/11/5/055008.

[189] R. A. Crabb and A. Hubel, "Influence of matrix processing on the optical and biomechanical properties of a corneal stroma equivalent," (in eng), *Tissue Eng Part A,* vol. 14, no. 1, pp. 173-82, Jan 2008, doi: 10.1089/ten.a.2007.0139.

[190] X. Xiao *et al.*, "In vivo study of the biocompatibility of a novel compressed collagen hydrogel scaffold for artificial corneas," (in eng), *J Biomed Mater Res A,* vol. 102, no. 6, pp. 1782-7, Jun 2014, doi: 10.1002/jbm.a.34848.

[191] P. Fagerholm *et al.*, "Stable corneal regeneration four years after implantation of a cell-free recombinant human collagen scaffold," (in eng), *Biomaterials,* vol. 35, no. 8, pp. 2420-7, Mar 2014, doi: 10.1016/j.biomaterials.2013.11.079.

[192] O. Buznyk, N. Pasyechnikova, M. M. Islam, S. Iakymenko, P. Fagerholm, and M. Griffith, "Bioengineered Corneas Grafted as Alternatives to Human Donor Corneas in Three High-Risk Patients," (in eng), *Clin Transl Sci,* vol. 8, no. 5, pp. 558-62, Oct 2015, doi: 10.1111/cts.12293.

[193] M. Miotto, R. M. Gouveia, A. M. Ionescu, F. Figueiredo, I. W. Hamley, and C. J. Connon, "4D Corneal Tissue Engineering: Achieving Time-Dependent Tissue Self-Curvature through Localized Control of Cell Actuators," *Advanced Functional Materials,* vol. 29, no. 8, p. 1807334, 2019, doi: 10.1002/adfm.201807334.

[194] T. Mimura *et al.*, "Cultured human corneal endothelial cell transplantation with a collagen sheet in a rabbit model," (in eng), *Invest Ophthalmol Vis Sci,* vol. 45, no. 9, pp. 2992-7, Sep 2004, doi: 10.1167/iovs.03-1174.

[195] H. J. Levis *et al.*, "Plastic Compressed Collagen as a Novel Carrier for Expanded Human Corneal Endothelial Cells for Transplantation," (in English), *Plos One,* vol. 7, no. 11, Nov 30 2012, doi: ARTN e50993 10.1371/journal.pone.0050993.

[196] N. Vázquez *et al.*, "Human Bone Derived Collagen for the Development of an Artificial Corneal Endothelial Graft. In Vivo Results in a Rabbit Model," (in eng), *PLoS One,* vol. 11, no. 12, p. e0167578, 2016, doi: 10.1371/journal.pone.0167578.

[197] R. N. Palchesko, J. L. Funderburgh, and A. W. Feinberg, "Engineered Basement Membranes for Regenerating the Corneal Endothelium," (in eng), *Adv Healthc Mater,* vol. 5, no. 22, pp. 2942-2950, Nov 2016, doi: 10.1002/adhm.201600488.

[198] J. Yoshida, S. Yokoo, A. Oshikata-Miyazaki, S. Amano, T. Takezawa, and S. Yamagami, "Transplantation of Human Corneal Endothelial Cells Cultured on Bio-Engineered Collagen Vitrigel in a Rabbit Model of Corneal Endothelial Dysfunction," (in eng), *Curr Eye Res,* vol. 42, no. 11, pp. 1420-1425, Nov 2017, doi: 10.1080/02713683.2017.1351568.

[199] R. M. T. ten Ham, J. Hoekman, A. M. Hövels, A. W. Broekmans, H. G. M. Leufkens, and O. H. Klungel, "Challenges in Advanced Therapy Medicinal Product Development: A Survey among Companies in Europe," *Molecular Therapy - Methods & Clinical Development,* vol. 11, pp. 121-130, 2018/12/14/ 2018, doi: https://doi.org/10.1016/j.omtm.2018.10.003.

[200] R. Sheth-Shah, A. J. Vernon, S. Seetharaman, M. H. Neale, and J. T. Daniels, "Regulatory requirements in the good manufacturing practice production of an epithelial cell graft for ocular surface reconstruction," *Regen Med,* vol. 11, no. 3, pp. 307-320, 2016, doi: 10.2217/rme-2015-0020.

[201] *Directive 2001/83/EC of the European parliament and of the council of 6 November 2001 on the community code relating to medicinal products for human USE 67–128* [Online] Available: www.ema.europa.eu/docs/en_GB/document_library/Regulatory_and_procedural_guideline/2009/10/WC500004481.pdf.

[202] *Directive 2004/23/EC of the European parliament and of the council of 31 March 2004 on setting standards of quality and safety for the donation, procurement, testing, processing, preservation, storage and distribution of human tissues and cells, 48–58*. [Online] Available: http://eur-lex.europa.eu/LexUriServ/LexUriServ.do?uri=OJ:L:2004:102:0048:0058:en:PDF

[203] *Commission Directive 2003/94/EC of 8 October 2003 laying down the principles and guidelines of good manufacturing practice in respect of medicinal products for human use and investigational medicinal products for human use, 222–226*. [Online] Available: http://ec.europa.eu/health/files/eudralex/vol-1/dir_2003_94/dir_2003_94_en.pdf.

[204] *Commission Directive 2009/120/EC of 14 September 2009 amending Directive 2001/83/EC of the European Parliament and of the Council on the Community code relating to medicinal products for human use as regards advanced therapy medicinal products. 3–12*. [Online] Available: http://eur-lex.europa.eu/LexUriServ/LexUriServ.do?uri=OJ:L:2009:242:0003:0012:EN:PDF

[205] R. A. Brown, M. Wiseman, C. B. Chuo, U. Cheema, and S. N. Nazhat, "Ultrarapid engineering of biomimetic materials and tissues: Fabrication of nano- and microstructures by plastic compression," (in English), *Adv Funct Mater,* vol. 15, no. 11, pp. 1762-1770, Nov 2005, doi: 10.1002/adfm.200500042.

[206] H. J. Levis, A. K. Kureshi, I. Massie, L. Morgan, A. J. Vernon, and J. T. Daniels, "Tissue Engineering the Cornea: The Evolution of RAFT," *J Funct Biomater,* vol. 6, no. 1, pp. 50-65, Jan 22 2015, doi: 10.3390/jfb6010050.

[207] M. V. Brown RA, "Plastic compaction of a collagen gel, Patent WO2012004564, 12," 2012.

[208] E. Hadjipanayi, V. Mudera, and R. A. Brown, "Guiding cell migration in 3D: A collagen matrix with graded directional stiffness," *Cell Motility,* vol. 66, no. 3, pp. 121-128, 2009/03/01 2009, doi: 10.1002/cm.20331.

[209] E. A. Abou Neel, U. Cheema, J. C. Knowles, R. A. Brown, and S. N. Nazhat, "Use of multiple unconfined compression for control of collagen gel scaffold density and mechanical properties," *Soft Matter,* 10.1039/B609784G vol. 2, no. 11, pp. 986-992, 2006, doi: 10.1039/B609784G.

[210] U. Cheema and R. A. Brown, "Rapid Fabrication of Living Tissue Models by Collagen Plastic Compression: Understanding Three-Dimensional Cell Matrix Repair In Vitro," (in eng), *Adv Wound Care (New Rochelle),* vol. 2, no. 4, pp. 176-184, 2013, doi: 10.1089/wound.2012.0392.

[211] H. J. Levis, J. Menzel-Severing, R. A. Drake, and J. T. Daniels, "Plastic compressed collagen constructs for ocular cell culture and transplantation: a new and improved technique of confined fluid loss," (in eng), *Curr Eye Res,* vol. 38, no. 1, pp. 41-52, Jan 2013, doi: 10.3109/02713683.2012.725799.

[212] K. J. Livak and T. D. Schmittgen, "Analysis of Relative Gene Expression Data Using Real-Time Quantitative PCR and the 2−ΔΔCT Method," *Methods,* vol. 25, no. 4, pp. 402-408, 2001/12/01/ 2001, doi: https://doi.org/10.1006/meth.2001.1262.

[213] H. J. Lewerenz, *Photons in natural and life sciences : an interdisciplinary approach* (Springer series in optical sciences 157). Heldelberg ; London: Springer (in English), 2012, pp. xvii, 288 : ill. (some col.) ; 25 cm.

[214] L. Salasnich, *Quantum physics of light and matter : a modern introduction to photons, atoms and many-body systems* (UNITEXT for physics). Cham: Springer (in English), 2014, pp. ix, 195 pages : illustrations ; 24 cm.
[215] N. Kango, "Instrumentation," in *Textbook of Microbiology*. New Delhi: I.K. International Publishing House Pvt. Limited, 2010, pp. 182–229.
[216] N. Renier, Z. Wu, David J. Simon, J. Yang, P. Ariel, and M. Tessier-Lavigne, "iDISCO: A Simple, Rapid Method to Immunolabel Large Tissue Samples for Volume Imaging," *Cell,* vol. 159, no. 4, pp. 896-910, 2014, doi: 10.1016/j.cell.2014.10.010.
[217] B. Yang *et al.*, "Single-cell phenotyping within transparent intact tissue through whole-body clearing," (in eng), *Cell,* vol. 158, no. 4, pp. 945-958, 2014, doi: 10.1016/j.cell.2014.07.017.
[218] F. Li and S. Z. Zhao, "Mesenchymal stem cells: Potential role in corneal wound repair and transplantation," (in eng), *World J Stem Cells,* vol. 6, no. 3, pp. 296-304, Jul 26 2014, doi: 10.4252/wjsc.v6.i3.296.
[219] F. Arnalich-Montiel *et al.*, "Adipose-derived stem cells are a source for cell therapy of the corneal stroma," (in eng), *Stem Cells,* vol. 26, no. 2, pp. 570-9, Feb 2008, doi: 10.1634/stemcells.2007-0653.
[220] Y. Du *et al.*, "Adipose-derived stem cells differentiate to keratocytes in vitro," (in eng), *Molecular vision,* vol. 16, pp. 2680-2689, 2010. [Online]. Available: https://www.ncbi.nlm.nih.gov/pubmed/21179234.
[221] J. L. Funderburgh, M. M. Mann, and M. L. Funderburgh, "Keratocyte phenotype mediates proteoglycan structure: a role for fibroblasts in corneal fibrosis," (in eng), *The Journal of biological chemistry,* vol. 278, no. 46, pp. 45629-45637, 2003, doi: 10.1074/jbc.M303292200.
[222] J. V. Jester, P. A. Barry-Lane, W. M. Petroll, D. R. Olsen, and H. D. Cavanagh, "Inhibition of Corneal Fibrosis by Topical Application of Blocking Antibodies to TGFβ in the Rabbit," *Cornea,* vol. 16, no. 2, pp. 177-187, 1997. [Online]. Available: https://journals.lww.com/corneajrnl/Fulltext/1997/03000/Inhibition_of_Corneal_Fibrosis_by_Topical.10.aspx.
[223] A. A. M. Torricelli, A. Santhanam, J. Wu, V. Singh, and S. E. Wilson, "The corneal fibrosis response to epithelial-stromal injury," (in eng), *Experimental eye research,* vol. 142, pp. 110-118, 2016, doi: 10.1016/j.exer.2014.09.012.
[224] J. A. West-Mays and D. J. Dwivedi, "The keratocyte: corneal stromal cell with variable repair phenotypes," (in eng), *The international journal of biochemistry & cell biology,* vol. 38, no. 10, pp. 1625-1631, 2006, doi: 10.1016/j.biocel.2006.03.010.
[225] K. Higa *et al.*, "Aquaporin 1-positive stromal niche-like cells directly interact with N-cadherin-positive clusters in the basal limbal epithelium," *Stem Cell Research,* vol. 10, no. 2, pp. 147-155, 2013/03/01/ 2013, doi: https://doi.org/10.1016/j.scr.2012.11.001.
[226] M. A. Dziasko and J. T. Daniels, "Anatomical features and cell-cell interactions in the human limbal epithelial stem cell niche," *Ocul Surf,* May 2 2016, doi: 10.1016/j.jtos.2016.04.002.
[227] J. Mertz, "Optical sectioning microscopy with planar or structured illumination," *Nat Methods,* Review Article vol. 8, p. 811, 09/29/online 2011, doi: 10.1038/nmeth.1709.
[228] E. G. Reynaud, U. Krzic, K. Greger, and E. H. K. Stelzer, "Light sheet-based fluorescence microscopy: more dimensions, more photons, and less photodamage," (in eng), *HFSP J,* vol. 2, no. 5, pp. 266-275, 2008, doi: 10.2976/1.2974980.
[229] K. H. R. Jensen and R. W. Berg, "Advances and perspectives in tissue clearing using CLARITY," *Journal of Chemical Neuroanatomy,* vol. 86, pp. 19-34, 2017/12/01/ 2017, doi: https://doi.org/10.1016/j.jchemneu.2017.07.005.

[230] R. Tomer, L. Ye, B. Hsueh, and K. Deisseroth, "Advanced CLARITY for rapid and high-resolution imaging of intact tissues," (in eng), *Nature protocols,* vol. 9, no. 7, pp. 1682-1697, 2014, doi: 10.1038/nprot.2014.123.

[231] J. Icha, C. Schmied, J. Sidhaye, P. Tomancak, S. Preibisch, and C. Norden, "Using Light Sheet Fluorescence Microscopy to Image Zebrafish Eye Development," (in eng), *J Vis Exp,* no. 110, pp. e53966-e53966, 2016, doi: 10.3791/53966.

[232] S. HELL, G. REINER, C. CREMER, and E. H. K. STELZER, "Aberrations in confocal fluorescence microscopy induced by mismatches in refractive index," *Journal of Microscopy,* vol. 169, no. 3, pp. 391-405, 1993, doi: 10.1111/j.1365-2818.1993.tb03315.x.

[233] A. Ertürk *et al.*, "Three-dimensional imaging of solvent-cleared organs using 3DISCO," *Nature Protocols,* vol. 7, p. 1983, 10/11/online 2012, doi: 10.1038/nprot.2012.119

.[234] T. Laroche, O. Burri, L. K. Dubey, and A. Seitz, "Development of Sample-Adaptable Holders for Lightsheet Microscopy," (in English), *Frontiers in Neuroanatomy,* Protocols vol. 13, no. 26, 2019-March-08 2019, doi: 10.3389/fnana.2019.00026.

[235] K. Chatterjee, F. W. Pratiwi, F. C. M. Wu, P. Chen, and B.-C. Chen, "Recent Progress in Light Sheet Microscopy for Biological Applications," *Applied Spectroscopy,* vol. 72, no. 8, pp. 1137-1169, 2018, doi: 10.1177/0003702818778851.

[236] Y. Wan, K. McDole, and P. J. Keller, "Light-Sheet Microscopy and Its Potential for Understanding Developmental Processes," *Annual Review of Cell and Developmental Biology,* vol. 35, no. 1, pp. 655-681, 2019, doi: 10.1146/annurev-cellbio-100818-125311.

[237] A. Dos Santos, A. Balayan, M. L. Funderburgh, J. Ngo, J. L. Funderburgh, and S. X. Deng, "Differentiation Capacity of Human Mesenchymal Stem Cells into Keratocyte Lineage," (in eng), *Invest Ophth Vis Sci,* vol. 60, no. 8, pp. 3013-3023, 2019, doi: 10.1167/iovs.19-27008.

[238] E. E. Golub and K. Boesze-Battaglia, "The role of alkaline phosphatase in mineralization," *Current Opinion in Orthopaedics,* vol. 18, no. 5, pp. 444-448, 2007, doi: 10.1097/BCO.0b013e3282630851.

[239] R. H. Lee *et al.*, "TSG-6 as a biomarker to predict efficacy of human mesenchymal stem/progenitor cells (hMSCs) in modulating sterile inflammation in vivo," (in eng), *Proc Natl Acad Sci U S A,* vol. 111, no. 47, pp. 16766-71, Nov 25 2014, doi: 10.1073/pnas.1416121111.

[240] R. Parsa, A. Yang, F. McKeon, and H. Green, "Association of p63 with Proliferative Potential in Normal and Neoplastic Human Keratinocytes," *Journal of Investigative Dermatology,* vol. 113, no. 6, pp. 1099-1105, 1999/12/01/ 1999, doi: https://doi.org/10.1046/j.1523-1747.1999.00780.x.

[241] M. N. McCall, H. R. McMurray, H. Land, and A. Almudevar, "On non-detects in qPCR data," (in eng), *Bioinformatics,* vol. 30, no. 16, pp. 2310-2316, 2014, doi: 10.1093/bioinformatics/btu239.

[242] S.-Y. Chen *et al.*, "Pax 6 Controls Neural Crest Potential of Limbal Niche Cells to Support Self-Renewal of Limbal Epithelial Stem Cells," *Scientific Reports,* vol. 9, no. 1, p. 9763, 2019/07/05 2019, doi: 10.1038/s41598-019-45100-7.

[243] L. E. Sidney, M. J. Branch, S. E. Dunphy, H. S. Dua, and A. Hopkinson, "Concise review: evidence for CD34 as a common marker for diverse progenitors," (in eng), *Stem cells (Dayton, Ohio),* vol. 32, no. 6, pp. 1380-1389, 2014, doi: 10.1002/stem.1661.

[244] W. W. Kao and C. Y. Liu, "Roles of lumican and keratocan on corneal transparency," (in eng), *Glycoconj J,* vol. 19, no. 4-5, pp. 275-85, May-Jun 2002, doi: 10.1023/a:1025396316169.

[245] W. W. Kao, J. L. Funderburgh, Y. Xia, C. Y. Liu, and G. W. Conrad, "Focus on molecules: lumican," (in eng), *Exp Eye Res,* vol. 82, no. 1, pp. 3-4, Jan 2006, doi: 10.1016/j.exer.2005.08.012.

[246] L. E. Sidney and A. Hopkinson, "Corneal keratocyte transition to mesenchymal stem cell phenotype and reversal using serum-free medium supplemented with fibroblast growth factor-2, transforming growth factor-β3 and retinoic acid," *J Tissue Eng Regen M,* vol. 12, no. 1, pp. e203-e215, 2018, doi: 10.1002/term.2316.

[247] K. R. Katikireddy, R. Dana, and U. V. Jurkunas, "Differentiation Potential of Limbal Fibroblasts and Bone Marrow Mesenchymal Stem Cells to Corneal Epithelial Cells," *STEM CELLS,* vol. 32, no. 3, pp. 717-729, 2014, doi: 10.1002/stem.1541.

[248] M. M. Schmidt *et al.*, "Collagen extraction process," vol. 23, pp. 913-922, 01/01 2016.

[249] R. Holmes, S. Kirk, G. Tronci, X. Yang, and D. Wood, "Influence of telopeptides on the structural and physical properties of polymeric and monomeric acid-soluble type I collagen," (in eng), *Mater Sci Eng C Mater Biol Appl,* vol. 77, pp. 823-827, Aug 1 2017, doi: 10.1016/j.msec.2017.03.267.

[250] C. B. Raub *et al.*, "Noninvasive assessment of collagen gel microstructure and mechanics using multiphoton microscopy," (in eng), *Biophysical journal,* vol. 92, no. 6, pp. 2212-2222, 2007, doi: 10.1529/biophysj.106.097998.

[251] C. B. Raub *et al.*, "Image correlation spectroscopy of multiphoton images correlates with collagen mechanical properties," (in eng), *Biophysical journal,* vol. 94, no. 6, pp. 2361-2373, 2008, doi: 10.1529/biophysj.107.120006.

[252] F. Gobeaux *et al.*, "Fibrillogenesis in dense collagen solutions: a physicochemical study," (in eng), *J Mol Biol,* vol. 376, no. 5, pp. 1509-22, Mar 7 2008, doi: 10.1016/j.jmb.2007.12.047.

[253] M. Naciri, D. Kuystermans, and M. Al-Rubeai, "Monitoring pH and dissolved oxygen in mammalian cell culture using optical sensors," (in eng), *Cytotechnology,* vol. 57, no. 3, pp. 245-250, 2008, doi: 10.1007/s10616-008-9160-1.

[254] A. R. O'Callaghan, M. A. Dziasko, R. Sheth-Shah, M. P. Lewis, and J. T. Daniels, "Oral Mucosa Tissue Equivalents for the Treatment of Limbal Stem Cell Deficiency," *Advanced Biosystems,* vol. 4, no. 7, p. 1900265, 2020, doi: 10.1002/adbi.201900265.

[255] D. Mukhey, J. B. Phillips, J. T. Daniels, and A. K. Kureshi, "Controlling human corneal stromal stem cell contraction to mediate rapid cell and matrix organization of real architecture for 3-dimensional tissue equivalents," *Acta Biomaterialia,* vol. 67, pp. 229-237, 2018/02/01/ 2018, doi: https://doi.org/10.1016/j.actbio.2017.11.047.

[256] H. J. Levis and J. T. Daniels, "Recreating the Human Limbal Epithelial Stem Cell Niche with Bioengineered Limbal Crypts," (in eng), *Curr Eye Res,* vol. 41, no. 9, pp. 1153-60, Sep 2016, doi: 10.3109/02713683.2015.1095932.

[257] I. Massie, S. B. Dale, and J. T. Daniels, "Limbal Fibroblasts Maintain Normal Phenotype in 3D RAFT Tissue Equivalents Suggesting Potential for Safe Clinical Use in Treatment of Ocular Surface Failure," (in eng), *Tissue engineering. Part C, Methods,* vol. 21, no. 6, pp. 576-584, 2015, doi: 10.1089/ten.TEC.2014.0458.

[258] I. Massie, H. J. Levis, and J. T. Daniels, "Response of human limbal epithelial cells to wounding on 3D RAFT tissue equivalents: Effect of airlifting and human limbal fibroblasts," *Experimental Eye Research,* vol. 127, pp. 196-205, 2014/10/01/ 2014, doi: https://doi.org/10.1016/j.exer.2014.07.024.

[259] A. K. Kureshi, R. A. Drake, and J. T. Daniels, "Challenges in the development of a reference standard and potency assay for the clinical production of RAFT tissue equivalents for the cornea," *Regenerative Medicine,* vol. 9, no. 2, pp. 167-177, 2014, doi: 10.2217/rme.13.92.

[260] H. J. Levis, I. Massie, M. A. Dziasko, A. Kaasi, and J. T. Daniels, "Rapid tissue engineering of biomimetic human corneal limbal crypts with 3D niche architecture,"

(in eng), *Biomaterials,* vol. 34, no. 35, pp. 8860-8, Nov 2013, doi: 10.1016/j.biomaterials.2013.08.002.

[261] H. J. Levis *et al.*, "Plastic compressed collagen as a novel carrier for expanded human corneal endothelial cells for transplantation," (in eng), *PLoS One,* vol. 7, no. 11, p. e50993, 2012, doi: 10.1371/journal.pone.0050993.

[262] R. Parenteau-Bareil, R. Gauvin, and F. Berthod, "Collagen-Based Biomaterials for Tissue Engineering Applications," (in English), *Materials,* vol. 3, no. 3, pp. 1863-1887, Mar 2010, doi: 10.3390/ma3031863.

[263] D. W. DelMonte and T. Kim, "Anatomy and physiology of the cornea," (in eng), *J Cataract Refract Surg,* vol. 37, no. 3, pp. 588-98, Mar 2011, doi: 10.1016/j.jcrs.2010.12.037.

[264] D. J. Munoz-Pinto, B. Grigoryan, J. Long, M. Grunlan, and M. S. Hahn, "An approach for assessing hydrogel hydrophobicity," *J Biomed Mater Res A,* vol. 100, no. 10, pp. 2855-60, Oct 2012, doi: 10.1002/jbm.a.34289.

[265] J. B. Phillips and R. Brown, "Micro-structured Materials and Mechanical Cues in 3D Collagen Gels," (in English), *Methods Mol Biol,* vol. 695, pp. 183-196, 2011, doi: 10.1007/978-1-60761-984-0_12.

[266] L. Casares *et al.*, "Hydraulic fracture during epithelial stretching," *Nat Mater,* vol. 14, no. 3, pp. 343-51, Mar 2015, doi: 10.1038/nmat4206.

[267] L. C. Abraham, E. Zuena, B. Perez-Ramirez, and D. L. Kaplan, "Guide to collagen characterization for biomaterial studies," *J Biomed Mater Res B Appl Biomater,* vol. 87, no. 1, pp. 264-85, Oct 2008, doi: 10.1002/jbm.b.31078.

[268] E. E. Antoine, P. P. Vlachos, and M. N. Rylander, "Review of collagen I hydrogels for bioengineered tissue microenvironments: characterization of mechanics, structure, and transport," *Tissue Eng Part B Rev,* vol. 20, no. 6, pp. 683-96, Dec 2014, doi: 10.1089/ten.TEB.2014.0086.

[269] E. E. Antoine, P. P. Vlachos, and M. N. Rylander, "Tunable collagen I hydrogels for engineered physiological tissue micro-environments," *PLoS One,* vol. 10, no. 3, p. e0122500, 2015, doi: 10.1371/journal.pone.0122500.

[270] L. M. L. Ya-li Yang, Laura J. Kaufman, "Elastic Moduli of Collagen Gels Can Be Predicted from Two-Dimensional Confocal Microscopy," *Biophys J,* vol. 97, pp. 2051–2060, 2009.

[271] K. E. Sung *et al.*, "Control of 3-dimensional collagen matrix polymerization for reproducible human mammary fibroblast cell culture in microfluidic devices," *Biomaterials,* vol. 30, no. 27, pp. 4833-41, Sep 2009, doi: 10.1016/j.biomaterials.2009.05.043.

[272] D. E. Birk, J. M. Fitch, J. P. Babiarz, K. J. Doane, and T. F. Linsenmayer, "Collagen fibrillogenesis in vitro: interaction of types I and V collagen regulates fibril diameter," (in eng), *J Cell Sci,* vol. 95 (Pt 4), pp. 649-57, Apr 1990.

[273] M. Shayegan and N. R. Forde, "Microrheological characterization of collagen systems: from molecular solutions to fibrillar gels," *PLoS One,* vol. 8, no. 8, p. e70590, 2013, doi: 10.1371/journal.pone.0070590.

[274] V. E. Tovell, I. Massie, A. K. Kureshi, and J. T. Daniels, "Functional Limbal Epithelial Cells Can Be Successfully Isolated From Organ Culture Rims Following Long-Term Storage," (in English), *Investigative Ophthalmology & Visual Science,* vol. 56, no. 6, pp. 3531-3540, Jun 2015, doi: 10.1167/iovs.14-15429.

[275] M. S. Sridhar, "Anatomy of cornea and ocular surface," (in eng), *Indian J Ophthalmol,* vol. 66, no. 2, pp. 190-194, 2018, doi: 10.4103/ijo.IJO_646_17.

[276] L. Liang, H. Sheha, J. Li, and S. C. G. Tseng, "Limbal stem cell transplantation: new progresses and challenges," *Eye,* vol. 23, no. 10, pp. 1946-1953, 2009/10/01 2009, doi: 10.1038/eye.2008.379.

[277] P. Prabhasawat, P. Ekpo, M. Uiprasertkul, S. Chotikavanich, and N. Tesavibul, "Efficacy of cultivated corneal epithelial stem cells for ocular surface reconstruction," (in eng), *Clin Ophthalmol,* vol. 6, pp. 1483-1492, 2012, doi: 10.2147/OPTH.S33951.

[278] M. Grueterich, E. M. Espana, and S. C. G. Tseng, "Ex vivo expansion of limbal epithelial stem cells: amniotic membrane serving as a stem cell niche," *Surv Ophthalmol,* vol. 48, no. 6, pp. 631-646, 2003/11/01/ 2003, doi: https://doi.org/10.1016/j.survophthal.2003.08.003.

[279] A. J. Shortt *et al.*, "Transplantation of Ex Vivo Cultured Limbal Epithelial Stem Cells: A Review of Techniques and Clinical Results," *Surv Ophthalmol,* vol. 52, no. 5, pp. 483-502, 2007/09/01/ 2007, doi: https://doi.org/10.1016/j.survophthal.2007.06.013.

[280] M. Notara, A. J. Shortt, G. Galatowicz, V. Calder, and J. T. Daniels, "IL6 and the human limbal stem cell niche: a mediator of epithelial-stromal interaction," *Stem Cell Res,* vol. 5, no. 3, pp. 188-200, Nov 2010, doi: 10.1016/j.scr.2010.07.002.

[281] E. Pels, H. Beele, and I. Claerhout, "Eye bank issues: II. Preservation techniques: warm versus cold storage," (in eng), *Int Ophthalmol,* vol. 28, no. 3, pp. 155-63, Jun 2008, doi: 10.1007/s10792-007-9086-1.

[282] W. J. Armitage, "Preservation of Human Cornea," (in eng), *Transfus Med Hemother,* vol. 38, no. 2, pp. 143-147, 2011, doi: 10.1159/000326632.

[283] G. L. A. Jones, D. Ponzin, E. Pels, H. Maas, A. B. Tullo, and I. Claerhout, *European Eye Bank Association*.

[284] J. L. Lepe-Zuniga, J. S. Zigler, Jr., and I. Gery, "Toxicity of light-exposed Hepes media," *J Immunol Methods,* vol. 103, no. 1, p. 145, Oct 23 1987. [Online]. Available: http://www.ncbi.nlm.nih.gov/pubmed/3655381.

[285] J. S. Zigler, Jr., J. L. Lepe-Zuniga, B. Vistica, and I. Gery, "Analysis of the cytotoxic effects of light-exposed HEPES-containing culture medium," *In Vitro Cell Dev Biol,* vol. 21, no. 5, pp. 282-7, May 1985. [Online]. Available: http://www.ncbi.nlm.nih.gov/pubmed/4019356.

[286] S. R. Caliari and J. A. Burdick, "A practical guide to hydrogels for cell culture," (in English), *Nat Methods,* vol. 13, no. 5, pp. 405-414, May 2016. [Online]. Available: <Go to ISI>://WOS:000374981900012.

[287] S. Molladavoodi, H. J. Kwon, J. Medley, and M. Gorbet, "Human corneal epithelial cell response to substrate stiffness," (in English), *Acta Biomater,* vol. 11, pp. 324-332, Jan 1 2015, doi: 10.1016/j.actbio.2014.10.005.

[288] M. Ahearne, "Introduction to cell-hydrogel mechanosensing," (in English), *Interface Focus,* vol. 4, no. 2, Apr 6 2014, doi: ARTN 20130038 10.1098/rsfs.2013.0038.

[289] R. Garcia-Villegas *et al.*, "Pax-6 Is Expressed Early in the Differentiation of a Corneal Epithelial Model System," (in English), *J Cell Physiol,* vol. 220, no. 2, pp. 348-356, Aug 2009, doi: 10.1002/jcp.21771.

[290] D. Q. Li, Z. Chen, X. J. Song, C. S. de Paiva, H. S. Kim, and S. C. Pflugfelder, "Partial enrichment of a population of human limbal epithelial cells with putative stem cell properties based on collagen type IV adhesiveness," (in eng), *Exp Eye Res,* vol. 80, no. 4, pp. 581-90, Apr 2005, doi: 10.1016/j.exer.2004.11.011.

[291] P. Ordonez and N. Di Girolamo, "Limbal Epithelial Stem Cells: Role of the Niche Microenvironment," *STEM CELLS,* vol. 30, no. 2, pp. 100-107, 2012, doi: 10.1002/stem.794.

[292] S.-Y. Chen, Y. Hayashida, M.-Y. Chen, H. T. Xie, and S. C. G. Tseng, "A new isolation method of human limbal progenitor cells by maintaining close association with their niche cells," (in eng), *Tissue Eng Part C Methods,* vol. 17, no. 5, pp. 537-548, 2011, doi: 10.1089/ten.TEC.2010.0609.

[293] I. Mariappan, S. Kacham, J. Purushotham, S. Maddileti, J. Siamwala, and V. S. Sangwan, "Spatial distribution of niche and stem cells in ex vivo human limbal

cultures," (in eng), *Stem Cell Transl Med,* vol. 3, no. 11, pp. 1331-1341, 2014, doi: 10.5966/sctm.2014-0120.

[294] H.-T. Xie, S.-Y. Chen, G.-G. Li, and S. C. G. Tseng, "Isolation and expansion of human limbal stromal niche cells," (in eng), *Invest Ophth Vis Sci,* vol. 53, no. 1, pp. 279-286, 2012, doi: 10.1167/iovs.11-8441.

[295] K. Duval *et al.*, "Modeling Physiological Events in 2D vs. 3D Cell Culture," (in eng), *Physiology (Bethesda),* vol. 32, no. 4, pp. 266-277, 2017, doi: 10.1152/physiol.00036.2016.

[296] B. M. Baker and C. S. Chen, "Deconstructing the third dimension: how 3D culture microenvironments alter cellular cues," (in eng), *Journal of cell science,* vol. 125, no. Pt 13, pp. 3015-3024, 2012, doi: 10.1242/jcs.079509.

[297] K. Chitcholtan, E. Asselin, S. Parent, P. H. Sykes, and J. J. Evans, "Differences in growth properties of endometrial cancer in three dimensional (3D) culture and 2D cell monolayer," (in eng), *Exp Cell Res,* vol. 319, no. 1, pp. 75-87, Jan 1 2013, doi: 10.1016/j.yexcr.2012.09.012.

[298] K. Bott *et al.*, "The effect of matrix characteristics on fibroblast proliferation in 3D gels," *Biomaterials,* vol. 31, no. 32, pp. 8454-8464, 2010/11/01/ 2010, doi: https://doi.org/10.1016/j.biomaterials.2010.07.046.

[299] N. Gjorevski, A. S. Piotrowski, V. D. Varner, and C. M. Nelson, "Dynamic tensile forces drive collective cell migration through three-dimensional extracellular matrices," (in eng), *Scientific reports,* vol. 5, pp. 11458-11458, 2015, doi: 10.1038/srep11458.

[300] K. Suzuki, T. Tanaka, M. Enoki, and T. Nishida, "Coordinated Reassembly of the Basement Membrane and Junctional Proteins during Corneal Epithelial Wound Healing," *Investigative Ophthalmology & Visual Science,* vol. 41, no. 9, pp. 2495-2500, 2000.

[301] P. Arpitha, N. V. Prajna, M. Srinivasan, and V. Muthukkaruppan, "High expression of p63 combined with a large N/C ratio defines a subset of human limbal epithelial cells: Implications on epithelial stem cells," *Investigative Ophthalmology and Visual Science,* Article vol. 46, no. 10, pp. 3631-3636, 2005, doi: 10.1167/iovs.05-0343.

[302] F. Majo, A. Rochat, M. Nicolas, G. A. Jaoudé, and Y. Barrandon, "Oligopotent stem cells are distributed throughout the mammalian ocular surface," *Nature,* vol. 456, no. 7219, pp. 250-254, 2008/11/01 2008, doi: 10.1038/nature07406.

[303] E. Di Iorio, V. Barbaro, A. Ruzza, D. Ponzin, G. Pellegrini, and M. De Luca, "Isoforms of ΔNp63 and the migration of ocular limbal cells in human corneal regeneration," *Proceedings of the National Academy of Sciences of the United States of America,* vol. 102, no. 27, pp. 9523-9528, 2005, doi: 10.1073/pnas.0503437102.

[304] A. A. M. Torricelli, V. Singh, M. R. Santhiago, and S. E. Wilson, "The corneal epithelial basement membrane: structure, function, and disease," (in eng), *Investigative ophthalmology & visual science,* vol. 54, no. 9, pp. 6390-6400, 2013, doi: 10.1167/iovs.13-12547.

[305] A. Tuori, H. Uusitalo, R. E. Burgeson, J. Terttunen, and I. Virtanen, "The Immunohistochemical Composition of the Human Corneal Basement Membrane," *Cornea,* vol. 15, no. 3, 1996. [Online]. Available: https://journals.lww.com/corneajrnl/Fulltext/1996/05000/The_Immunohistochemical_Composition_of_the_Human.10.aspx.

[306] W. Li, H. He, C. L. Kuo, Y. Gao, T. Kawakita, and S. C. Tseng, "Basement membrane dissolution and reassembly by limbal corneal epithelial cells expanded on amniotic membrane," (in eng), *Invest Ophthalmol Vis Sci,* vol. 47, no. 6, pp. 2381-9, Jun 2006, doi: 10.1167/iovs.05-1491.

[307] L. Y. Sakai, D. R. Keene, N. P. Morris, and R. E. Burgeson, "Type VII collagen is a major structural component of anchoring fibrils," (in eng), *J Cell Biol,* vol. 103, no. 4, pp. 1577-86, Oct 1986, doi: 10.1083/jcb.103.4.1577.

[308] J. H. Miner and P. D. Yurchenco, "Laminin functions in tissue morphogenesis," (in eng), *Annu Rev Cell Dev Biol,* vol. 20, pp. 255-84, 2004, doi: 10.1146/annurev.cellbio.20.010403.094555.

[309] B. Bystrom, I. Virtanen, P. Rousselle, K. Miyazaki, C. Linden, and F. Pedrosa Domellof, "Laminins in normal, keratoconus, bullous keratopathy and scarred human corneas," (in eng), *Histochem Cell Biol,* vol. 127, no. 6, pp. 657-67, Jun 2007, doi: 10.1007/s00418-007-0288-4.

[310] P. D. Yurchenco, "Basement membranes: cell scaffoldings and signaling platforms," (in eng), *Cold Spring Harbor perspectives in biology,* vol. 3, no. 2, p. a004911, 2011, doi: 10.1101/cshperspect.a004911.

[311] M. Notara *et al.*, "In sickness and in health: Corneal epithelial stem cell biology, pathology and therapy," (in eng), *Exp Eye Res,* vol. 90, no. 2, pp. 188-95, Feb 2010, doi: 10.1016/j.exer.2009.09.023.

[312] A. R. O'Callaghan and J. T. Daniels, "Concise review: limbal epithelial stem cell therapy: controversies and challenges," (in eng), *Stem Cells,* vol. 29, no. 12, pp. 1923-32, Dec 2011, doi: 10.1002/stem.756.

[313] S. L. Mason *et al.*, "Yield and Viability of Human Limbal Stem Cells From Fresh and Stored Tissue," *Investigative Ophthalmology & Visual Science,* vol. 57, no. 8, pp. 3708-3713, 2016, doi: 10.1167/iovs.16-19354.

[314] S. Kolli, M. Lako, F. Figueiredo, H. Mudhar, and S. Ahmad, "Loss of corneal epithelial stem cell properties in outgrowths from human limbal explants cultured on intact amniotic membrane," (in eng), *Regen Med,* vol. 3, no. 3, pp. 329-42, May 2008, doi: 10.2217/17460751.3.3.329.

[315] F. Castro-Munozledo and E. Gomez-Flores, "Challenges to the study of asymmetric cell division in corneal and limbal epithelia," (in eng), *Exp Eye Res,* vol. 92, no. 1, pp. 4-9, Jan 2011, doi: 10.1016/j.exer.2010.11.002.

[316] I. K. Gipson, "The epithelial basement membrane zone of the limbus," (in eng), *Eye (Lond),* vol. 3 (Pt 2), pp. 132-40, 1989, doi: 10.1038/eye.1989.21.

[317] K. Le Blanc *et al.*, "Treatment of severe acute graft-versus-host disease with third party haploidentical mesenchymal stem cells," *Lancet,* vol. 363, no. 9419, pp. 1439-41, May 1 2004, doi: 10.1016/S0140-6736(04)16104-7.

[318] A. K. Kureshi, R. A. L. Drake, and J. T. Daniels, "Challenges in the development of a reference standard and potency assay for the clinical production of RAFT tissue equivalents for the cornea," *Regen Med,* vol. 9, no. 2, pp. 167-177, 2014/03/01 2014, doi: 10.2217/rme.13.92.

[319] G. Shojaati, I. Khandaker, K. Sylakowski, M. L. Funderburgh, Y. Du, and J. L. Funderburgh, "Compressed Collagen Enhances Stem Cell Therapy for Corneal Scarring," (in eng), *Stem Cell Transl Med,* vol. 7, no. 6, pp. 487-494, 2018, doi: 10.1002/sctm.17-0258.

[320] A. Page-McCaw, A. J. Ewald, and Z. Werb, "Matrix metalloproteinases and the regulation of tissue remodelling," (in eng), *Nat Rev Mol Cell Biol,* vol. 8, no. 3, pp. 221-33, Mar 2007, doi: 10.1038/nrm2125.

[321] M. Matsubara, M. T. Girard, C. L. Kublin, C. Cintron, and M. E. Fini, "Differential roles for two gelatinolytic enzymes of the matrix metalloproteinase family in the remodelling cornea," *Developmental Biology,* vol. 147, no. 2, pp. 425-439, 1991/10/01/ 1991, doi: https://doi.org/10.1016/0012-1606(91)90300-R.

[322] M. T. Girard, M. Matsubara, C. Kublin, M. J. Tessier, C. Cintron, and M. E. Fini, "Stromal fibroblasts synthesize collagenase and stromelysin during long-term tissue remodeling," (in eng), *J Cell Sci,* vol. 104 (Pt 4), pp. 1001-11, Apr 1993.

[323] W. M. Petroll, L. Ma, A. Kim, L. Ly, and M. Vishwanath, "Dynamic assessment of fibroblast mechanical activity during Rac-induced cell spreading in 3-D culture," (in eng), *J Cell Physiol,* vol. 217, no. 1, pp. 162-171, 2008, doi: 10.1002/jcp.21487.

[324] F. Grinnell, L. B. Rocha, C. Iucu, S. Rhee, and H. Jiang, "Nested collagen matrices: A new model to study migration of human fibroblast populations in three dimensions," *Exp Cell Res,* vol. 312, no. 1, pp. 86-94, 2006/01/01/ 2006, doi: https://doi.org/10.1016/j.yexcr.2005.10.001.

[325] J. Lundgaard Andresen, T. Ledet, and N. Ehlers, "Keratocyte migration and peptide growth factors: the effect of PDGF, bFGF, EGF, IGF-I, aFGF and TGF-ß on human keratocyte migration in a collagen gel," *Curr Eye Res,* vol. 16, no. 6, pp. 605-613, 1997/01/01 1997, doi: 10.1076/ceyr.16.6.605.5081.

[326] B. da Rocha-Azevedo, C.-H. Ho, and F. Grinnell, "PDGF-stimulated dispersal of cell clusters and disruption of fibronectin matrix on three-dimensional collagen matrices requires matrix metalloproteinase-2," (in eng), *Mol Biol Cell,* vol. 26, no. 6, pp. 1098-1105, 2015, doi: 10.1091/mbc.E14-09-1396.

[327] F. Guilak, D. M. Cohen, B. T. Estes, J. M. Gimble, W. Liedtke, and C. S. Chen, "Control of Stem Cell Fate by Physical Interactions with the Extracellular Matrix," (in English), *Cell Stem Cell,* vol. 5, no. 1, pp. 17-26, Jul 2 2009, doi: 10.1016/j.stem.2009.06.016.

[328] R. D. Young *et al.*, "Three-dimensional aspects of matrix assembly by cells in the developing cornea," *Proceedings of the National Academy of Sciences,* vol. 111, no. 2, pp. 687-692, 2014, doi: 10.1073/pnas.1313561110.

[329] K. Hashmani *et al.*, "Characterization of corneal stromal stem cells with the potential for epithelial transdifferentiation," (in English), *Stem Cell Res Ther,* vol. 4, Jun 24 2013, doi: ARTN 22610.1186/scrt226.

[330] V. Paunescu *et al.*, "In vitro differentiation of human mesenchymal stem cells to epithelial lineage," (in English), *J Cell Mol Med,* vol. 11, no. 3, pp. 502-508, May-Jun 2007, doi: 10.1111/j.1582-4934.2007.00041.x.

[331] G. S. Wang *et al.*, "Adult stem cells from bone marrow stroma differentiate into airway epithelial cells: Potential therapy for cystic fibrosis," (in English), *P Natl Acad Sci USA,* vol. 102, no. 1, pp. 186-191, Jan 4 2005, doi: 10.1073/pnas.0406266102.

[332] M. Ohyama *et al.*, "Characterization and isolation of stem cell-enriched human hair follicle bulge cells," (in English), *J Clin Invest,* vol. 116, no. 1, pp. 249-260, Jan 2006, doi: 10.1172/Jci26043.

[333] Y. Sasahara *et al.*, "Human keratinocytes derived from the bulge region of hair follicles are refractory to differentiation," (in English), *Int J Oncol,* vol. 34, no. 5, pp. 1191-1199, May 2009, doi: 10.3892/ijo_00000247.

[334] T. Takebayashi *et al.*, "Human mesenchymal stem cells differentiate to epithelial cells when cultured on thick collagen gel," (in English), *Bio-Med Mater Eng,* vol. 23, no. 1-2, pp. 143-153, 2013, doi: 10.3233/Bme-120739.

[335] D. M. Maurice, "The Structure and Transparency of the Cornea," (in English), *J Physiol-London,* vol. 136, no. 2, pp. 263-&, 1957. [Online]. Available: <Go to ISI>://WOS:A1957WC30300004.

[336] S. L. Wilson, I. Wimpenny, M. Ahearne, S. Rauz, A. J. El Haj, and Y. Yang, "Chemical and Topographical Effects on Cell Differentiation and Matrix Elasticity in a Corneal Stromal Layer Model," (in English), *Adv Funct Mater,* vol. 22, no. 17, pp. 3641-3649, Sep 11 2012, doi: 10.1002/adfm.201200655.

[337] J. Wu, Y. Q. Du, S. C. Watkins, J. L. Funderburgh, and W. R. Wagner, "The engineering of organized human corneal tissue through the spatial guidance of corneal stromal

stem cells," (in English), *Biomaterials,* vol. 33, no. 5, pp. 1343-1352, Feb 2012, doi: 10.1016/j.biomaterials.2011.10.055.

[338] J. H. Ylostalo, T. J. Bartosh, K. Coble, and D. J. Prockop, "Human mesenchymal stem/stromal cells cultured as spheroids are self-activated to produce prostaglandin E2 that directs stimulated macrophages into an anti-inflammatory phenotype," (in eng), *Stem Cells,* vol. 30, no. 10, pp. 2283-96, Oct 2012, doi: 10.1002/stem.1191.

[339] P. Kumar, A. Pandit, and D. I. Zeugolis, "Progress in Corneal Stromal Repair: From Tissue Grafts and Biomaterials to Modular Supramolecular Tissue-Like Assemblies," *Adv Mater,* vol. 28, no. 27, pp. 5381-5399, 2016, doi: 10.1002/adma.201503986.

[340] N. Garagorri *et al.*, "Keratocyte behavior in three-dimensional photopolymerizable poly(ethylene glycol) hydrogels," (in eng), *Acta Biomater,* vol. 4, no. 5, pp. 1139-1147, 2008, doi: 10.1016/j.actbio.2008.05.007.

[341] J. Kuang, X. Yan, A. J. Genders, C. Granata, and D. J. Bishop, "An overview of technical considerations when using quantitative real-time PCR analysis of gene expression in human exercise research," (in eng), *PloS one,* vol. 13, no. 5, pp. e0196438-e0196438, 2018, doi: 10.1371/journal.pone.0196438.

[342] T. Nolan, R. E. Hands, and S. A. Bustin, "Quantification of mRNA using real-time RT-PCR," (in eng), *Nat Protoc,* vol. 1, no. 3, pp. 1559-82, 2006, doi: 10.1038/nprot.2006.236.

[343] L. Huang *et al.*, "Dynamic culture of a thermosensitive collagen hydrogel as an extracellular matrix improves the construction of tissue-engineered peripheral nerve," (in eng), *Neural Regen Res,* vol. 9, no. 14, pp. 1371-1378, 2014, doi: 10.4103/1673-5374.137590.

[344] B. da Rocha-Azevedo and F. Grinnell, "Fibroblast morphogenesis on 3D collagen matrices: the balance between cell clustering and cell migration," (in eng), *Exp Cell Res,* vol. 319, no. 16, pp. 2440-2446, 2013, doi: 10.1016/j.yexcr.2013.05.003.

[345] B. da Rocha-Azevedo, C.-H. Ho, and F. Grinnell, "Fibroblast cluster formation on 3D collagen matrices requires cell contraction dependent fibronectin matrix organization," (in eng), *Exp Cell Res,* vol. 319, no. 4, pp. 546-555, 2013, doi: 10.1016/j.yexcr.2012.10.005.

[346] S. Rhee, C. H. Ho, and F. Grinnell, "Promigratory and procontractile growth factor environments differentially regulate cell morphogenesis," (in eng), *Exp Cell Res,* vol. 316, no. 2, pp. 232-44, Jan 15 2010, doi: 10.1016/j.yexcr.2009.09.021.

[347] J. T. Daniels *et al.*, "Matrix Metalloproteinase Inhibition Modulates Fibroblast-Mediated Matrix Contraction and Collagen Production In Vitro," *Invest Ophth Vis Sci,* vol. 44, no. 3, pp. 1104-1110, 2003, doi: 10.1167/iovs.02-0412.

[348] J. M. Sivak and M. E. Fini, "MMPs in the eye: emerging roles for matrix metalloproteinases in ocular physiology," *Progress in Retinal and Eye Research,* vol. 21, no. 1, pp. 1-14, 2002/01/01/ 2002, doi: https://doi.org/10.1016/S1350-9462(01)00015-5.

[349] C. A. Sevilla, D. Dalecki, and D. C. Hocking, "Extracellular Matrix Fibronectin Stimulates the Self-Assembly of Microtissues on Native Collagen Gels," *Tissue Eng Pt A,* vol. 16, no. 12, pp. 3805-3819, 2010/12/01 2010, doi: 10.1089/ten.tea.2010.0316.

[350] C. A. Sevilla, D. Dalecki, and D. C. Hocking, "Regional fibronectin and collagen fibril co-assembly directs cell proliferation and microtissue morphology," (in eng), *PLoS One,* vol. 8, no. 10, p. e77316, 2013, doi: 10.1371/journal.pone.0077316.

[351] W. J. Kim, R. R. Mohan, R. R. Mohan, and S. E. Wilson, "Effect of PDGF, IL-1alpha, and BMP2/4 on corneal fibroblast chemotaxis: expression of the platelet-derived growth factor system in the cornea," (in eng), *Invest Ophthalmol Vis Sci,* vol. 40, no. 7, pp. 1364-72, Jun 1999.

[352] V. P. Hoppenreijs, E. Pels, G. F. Vrensen, P. C. Felten, and W. F. Treffers, "Platelet-derived growth factor: receptor expression in corneas and effects on corneal cells," (in eng), *Invest Ophthalmol Vis Sci,* vol. 34, no. 3, pp. 637-49, Mar 1993.

[353] J. V. Jester and J. Ho-Chang, "Modulation of cultured corneal keratocyte phenotype by growth factors/cytokines control in vitro contractility and extracellular matrix contraction," *Experimental Eye Research,* vol. 77, no. 5, pp. 581-592, 2003/11/01/ 2003, doi: https://doi.org/10.1016/S0014-4835(03)00188-X.

[354] P. Gallego-Muñoz, L. Ibares-Frías, M. C. Valsero-Blanco, R. Cantalapiedra-Rodriguez, J. Merayo-Lloves, and M. C. Martínez-García, "Effects of TGFβ1, PDGF-BB, and bFGF, on human corneal fibroblasts proliferation and differentiation during stromal repair," *Cytokine,* vol. 96, pp. 94-101, 2017/08/01/ 2017, doi: https://doi.org/10.1016/j.cyto.2017.03.011.

[355] D. A. Lauffenburger and A. F. Horwitz, "Cell migration: a physically integrated molecular process," (in eng), *Cell,* vol. 84, no. 3, pp. 359-69, Feb 9 1996, doi: 10.1016/s0092-8674(00)81280-5.

[356] M. Raftopoulou and A. Hall, "Cell migration: Rho GTPases lead the way," (in eng), *Dev Biol,* vol. 265, no. 1, pp. 23-32, Jan 1 2004, doi: 10.1016/j.ydbio.2003.06.003.

[357] A. Kim, N. Lakshman, D. Karamichos, and W. M. Petroll, "Growth factor regulation of corneal keratocyte differentiation and migration in compressed collagen matrices," (in eng), *Invest Ophth Vis Sci,* vol. 51, no. 2, pp. 864-875, 2010, doi: 10.1167/iovs.09-4200.

[358] M. Huang, L. Satchell, J. B. Duhadaway, G. C. Prendergast, and L. D. Laury-Kleintop, "RhoB links PDGF signaling to cell migration by coordinating activation and localization of Cdc42 and Rac," (in eng), *J Cell Biochem,* vol. 112, no. 6, pp. 1572-84, Jun 2011, doi: 10.1002/jcb.23069.

[359] A. J. Ridley and A. Hall, "The small GTP-binding protein rho regulates the assembly of focal adhesions and actin stress fibers in response to growth factors," *Cell,* vol. 70, no. 3, pp. 389-399, 1992/08/07/ 1992, doi: https://doi.org/10.1016/0092-8674(92)90163-7.

[360] C. D. Nobes and A. Hall, "Rho, Rac, and Cdc42 GTPases regulate the assembly of multimolecular focal complexes associated with actin stress fibers, lamellipodia, and filopodia," *Cell,* vol. 81, no. 1, pp. 53-62, 1995/04/07/ 1995, doi: https://doi.org/10.1016/0092-8674(95)90370-4.

[361] S. J. Heasman and A. J. Ridley, "Mammalian Rho GTPases: new insights into their functions from in vivo studies," (in eng), *Nat Rev Mol Cell Biol,* vol. 9, no. 9, pp. 690-701, Sep 2008, doi: 10.1038/nrm2476.

[362] S. Etienne-Manneville, "Cdc42--the centre of polarity," (in eng), *J Cell Sci,* vol. 117, no. Pt 8, pp. 1291-300, Mar 15 2004, doi: 10.1242/jcs.01115.

[363] J. L. Andresen, T. Ledet, and N. Ehlers, "Keratocyte migration and peptide growth factors: the effect of PDGF, bFGF, EGF, IGF-I, aFGF and TGF-beta on human keratocyte migration in a collagen gel," (in eng), *Curr Eye Res,* vol. 16, no. 6, pp. 605-13, Jun 1997, doi: 10.1076/ceyr.16.6.605.5081.

[364] N. S. Sipes *et al.*, "Cdc42 regulates extracellular matrix remodeling in three dimensions," (in eng), *The Journal of biological chemistry,* vol. 286, no. 42, pp. 36469-36477, 2011, doi: 10.1074/jbc.M111.283176.

[365] C. F. Deroanne *et al.*, "Cdc42 downregulates MMP-1 expression by inhibiting the ERK1/2 pathway," (in eng), *J Cell Sci,* vol. 118, no. Pt 6, pp. 1173-83, Mar 15 2005, doi: 10.1242/jcs.01707.

[366] Y. Zhuge and J. Xu, "Rac1 mediates type I collagen-dependent MMP-2 activation. role in cell invasion across collagen barrier," (in eng), *J Biol Chem,* vol. 276, no. 19, pp. 16248-56, May 11 2001, doi: 10.1074/jbc.m010190200.

[367] M. G. Rohani, B. K. Pilcher, P. Chen, and W. C. Parks, "Cdc42 Inhibits ERK-Mediated Collagenase-1 (MMP-1) Expression in Collagen-Activated Human Keratinocytes," *Journal of Investigative Dermatology,* vol. 134, no. 5, pp. 1230-1237, 2014/05/01/ 2014, doi: https://doi.org/10.1038/jid.2013.499.

[368] E. Ispanovic, D. Serio, and T. L. Haas, "Cdc42 and RhoA have opposing roles in regulating membrane type 1-matrix metalloproteinase localization and matrix metalloproteinase-2 activation," *American Journal of Physiology-Cell Physiology,* vol. 295, no. 3, pp. C600-C610, 2008, doi: 10.1152/ajpcell.00460.2007.

[369] D. Serio, E. Ispanovic, and T. L. Haas, "Cdc42 increases activation of MMP-2 in endothelial cells," *The FASEB Journal,* vol. 22, no. 1_supplement, pp. 925.9-925.9, 2008, doi: 10.1096/fasebj.22.1_supplement.925.9.

[370] A. Kim, C. Zhou, N. Lakshman, and W. M. Petroll, "Corneal stromal cells use both high- and low-contractility migration mechanisms in 3-D collagen matrices," (in eng), *Exp Cell Res,* vol. 318, no. 6, pp. 741-752, 2012, doi: 10.1016/j.yexcr.2011.12.018.

[371] J. Fernández-Pérez and M. Ahearne, "Influence of Biochemical Cues in Human Corneal Stromal Cell Phenotype," *Curr Eye Res,* vol. 44, no. 2, pp. 135-146, 2019/02/01 2019, doi: 10.1080/02713683.2018.1536216.

[372] W. Zhang, J. Chen, L. J. Backman, A. D. Malm, and P. Danielson, "Surface Topography and Mechanical Strain Promote Keratocyte Phenotype and Extracellular Matrix Formation in a Biomimetic 3D Corneal Model," (in eng), *Adv Healthc Mater,* vol. 6, no. 5, Mar 2017, doi: 10.1002/adhm.201601238.

[373] F. N. Syed-Picard *et al.*, "Scaffold-free tissue engineering of functional corneal stromal tissue," (in eng), *J Tissue Eng Regen Med,* vol. 12, no. 1, pp. 59-69, Jan 2018, doi: 10.1002/term.2363.

[374] L. Morgan and J. T. Daniels, "A simple method to culture limbal epithelial stem cells from cryopreserved corneal limbal explants," *Investigative Ophthalmology & Visual Science,* vol. 55, no. 13, pp. 5164-5164, 2014.